東北大学

TOHOKU UNIVERSITY

Analysis of the Blood Flow Behavior through Microchannels by a Confocal Micro-PIV/PTV System

(共焦点マイクロ PIV-PTV システムによる微小流路内の血流動態の解析)

A dissertation submitted for the degree of Doctor of Philosophy (Engineering)

Graduate School of Engineering

Department of Bioengineering and Robotics

by

Rui Alberto Madeira Macedo de **LIMA**

July 17, 2007

ABSTRACT

Over the years, various experimental methods have been applied in an effort to understand the blood flow behavior in microcirculation. Most of our current knowledge in microcirculation is based on macroscopic flow phenomena such as Fahraeus effect and Fahraeus-Linqvist effect. The development of optical experimental techniques has contributed to obtain explanations on the way the blood flows through microvessels. Although the past results have been encouraging, detailed studies on the flow properties of blood in the microcirculation has been limited by several technical factors such as poor spatial resolution and difficulty to obtain quantitative detailed measurements at such small scales. Therefore, there is still a lack of knowledge on the microscale flow behavior of blood cells through microvessels.

In recent years, due to advances in computers, optics, and digital image processing techniques, it has become possible to combine a particle image velocimetry (PIV) system with a conventional microscope. As a result, this combination, known as a micro-PIV, has greatly increased the resolution of the conventional PIV. Although the conventional micro-PIV technique has proven to be useful in measuring the flow behavior in microfluidics devices, the entire flow field is illuminated and consequently the out-of-focus emitted light can result in high levels of background noise, which degrades the measured velocity fields. More recently, considerable progress in the development of confocal microscopy and the advantages of this technique over conventional microscopy have led to a new technique known as confocal micro-PIV. This technique combines the conventional PIV system with a spinning disk confocal microscope (SDCM), which has the ability to obtain in-focus images with an optical thickness less than 1 μm (optical sectioning effect) and also to improve the particle image contrast, definition, and spatial resolution. This emerging technique has been successfully applied to measure homogenous fluids, however the question whether a confocal micro-PIV system is a suitable technique to study the blood flow behavior through microchannels remains.

In our work, a confocal micro-PIV system and also a confocal micro-particle tracking velocimetry (PTV) system are used, for the first time, to investigate *in vitro* blood flow through microchannels. By using these systems we have aimed to obtain further insights into the complex flow properties of blood in the microcirculation with the expectation that a better understanding on the blood flow phenomena will make a contribution to the prevention, diagnosis, and treatment of vascular diseases.

The validity of our confocal micro-PIV system is performed by comparing the experimental results of pure water seeded with tracer particles with an established analytical solution for a steady flow in a long straight microchannel. Good agreement was obtained, especially around the centre of the microchannel, with errors on the order of 5% or less. Furthermore, we have also demonstrated, for the first time, the ability of the

confocal micro-PIV to generate 3D velocity profiles of a blood cell suspension fluid (~ 4% haematocrit (Hct)).

The confocal system is used to determine both ensemble and instantaneous velocity profiles for *in vitro* blood (haematocrit up to 17%), flowing through a 100-μm square glass microchannel at a constant flow rate and low Reynolds number (Re = 0.025). It was observed small fluctuations in the instantaneous velocity profiles which were found to be closely related to the increase with the Hct. Although the micro-PIV community tend to ignore these fluctuations, this study shows that the root mean square (RMS) values increase with the haematocrit implying that the presence of RBCs within the plasma flow strongly influences the measurements of the instantaneous velocity fields. Consequently, information provided by instantaneous velocities should be taken into account. Furthermore, by measuring the velocity profiles *in vitro* blood (20% Hct) in a rectangular (300 μm wide, 45 μm deep) polydimethysiloxane (PDMS) microchannel, small fluctuations were also found in the velocity profiles. Therefore, our results clearly show evidence that the encountered fluctuations are closely related to the motion and interaction of RBCs when flowing in a crowded environment.

We show that the confocal micro-PIV system is able to measure with good accuracy the blood plasma flow with Hct up to 9%, in a 100 μm square microchannel. However, for Hct bigger than 9%, the light absorbed and scattered by the RBCs contributes to diminish the concentration of tracer particles in the acquired confocal images. Hence, a novel approach was implemented to the confocal system in order to obtain more reliable quantitative measurements on the motion of blood cells at high suspensions of RBCs. By using labeled RBCs and Dextran-40, a confocal micro-PTV system was employed, for the first time, in an effort to track individual tracer cells at high concentration suspensions of RBCs. The ability of the confocal system to generate thin in-focus planes has allowed both qualitative and quantitative measurements in flowing blood at concentrated suspensions (up to 35% Hct) of cell-cell hydrodynamic interaction, RBC orientation and RBC radial dispersion at different depths. Such data is thought to be extremely relevant to elucidate the blood transport mechanisms and associated diseases such as thrombosis and atherosclerosis.

By using the confocal micro-PTV system, the RBCs radial dispersion coefficient (D_{yy}) was measured in the middle plane of a 50μm and 100 μm glass capillaries in both diluted and concentrated suspensions (Hcts up to 35%) at low Reynolds numbers (Re from 0.003 to 0.005). There is evidence that the RBCs D_{yy} tends to increase with the Hct but, at Hct of about 25%, it tends to level off. This finding suggests that, at moderate Hcts, the development of the plasma layer and the consequent decrease of the local cell density, surrounding the RBCs, may enhance the radial dispersion of RBCs. In addition, we have also found that D_{yy} is greatest at radial positions between 0.4R to 0.8R, whereas at locations adjacent to wall (0.8R to 1R) and around the middle of the capillary (0R to 0.2R) the paths of the tracer RBCs tend to exhibit lower radial displacements. Furthermore, our results also provide evidence that RBCs D_{yy} tends to decrease with the diameter. This phenomenon is believed to be due to Hct reduction with the diameter (Faharaeus effect) and

also to geometry constrictions which limit the amplitude of the RBCs radial displacements. Hence, this finding seems to indicate that the reduction of RBC radial dispersion may be linked to the decrease in apparent viscosity with decreasing diameter (Faharaeus-Lindqvist effect).

The work reported in this thesis represents the first application of a confocal micro-PIV/PTV system to study the blood flow behavior through microchannels. The confocal system proves to be able to eliminate the problems and concerns of the experimental techniques used in the past and provide additional detailed description on the RBC motion not obtainable by other conventional methods. Finally, the research carried out throughout this thesis provides the basis not only to obtain further insights on the blood mass transport mechanisms under both physiological and pathological conditions but also to improve the existing theories, models, and computer simulations on the blood flow at both micro and macroscale levels.

ACKNOWLEDGMENTS

I am really fortunate to have encountered so many extraordinary people during my time in Japan and there are many to whom I am indebted for their kind support and friendship. Hence, I would like to express my sincere gratitude to the following people and organizations:

Professor Takami Yamaguchi, for his continuous guidance and support through-out this thesis. His tremendous knowledge in both medical science and bioengineering has been a continuous source of inspiration to me, and helped me to grow both academically and personally. It has been a privilege to have him as my PhD supervisor. I was extremely impressed by his extraordinary dedication to the best interests of his students.

Professor Shigeo Wada, for supporting and advising me in the first two years of my PhD and teaching me much about both experimental and computational biomechanics. The enthusiastic discussions gave me confidence in my research and helped me to pursue my own goals. It was an honor to work with such a talented researcher.

Dr. Takuji Ishikawa, for supporting and advising me in the last year of my PhD I am deeply indebted for all the stimulating discussions and his valuable advices. I have learned a lot about biofluid mechanics from him.

Dr. Ken-ichi Tsubota and Dr. Yohsuke Imai, for their valuable advices and support to the progress of this research.

Dr. Motohiro Takeda, for teaching and providing me extremely valuable advices in the preparation of the blood samples. I would also like to thank all the members of the Ohuchi laboratory (Surgical Oncology Division) for all their valuable assistance.

All members of Esashi, Ono and Tanaka laboratory (Dept. of Nanomechanics), for all their support in fabricating the PDMS microchannels. In particular, I would like to thank Dr. Shuji

Tanaka for his valuable advices on microfabrication and for introducing me to the world of BioMEMS.

Dr. Toshiro Ohashi, Dr. Naoya Sakamoto and Mr. Kazushi Ito (Cell Biomechanics Division), for their advices in labeling RBCs and culturing endothelial cells.

Professor Matsuhiko Nishizawa and Dr. Hirokazu Kaji, for providing me many advices related to culture endothelial cells in PDMS microchannels. I look forward to working with them to solve some of the mysteries of the microcirculation.

Professor Toshiyuki Hayase and Dr. Noriaki Matsuki, for their valuable comments and advices about this study.

All the members of the PFSL laboratory, for all their outstanding assistance with myriad issues. In particular, I would like to express my sincere gratitude to Dr. Masanori Nakamura for his support and comments for this study. I would also like to thank Ms. Alexandra Mannai and Mr. Hiroki Fujiwara for many lively discussions and advices about the confocal micro-PIV. I expect great work from them in the years to come. I really had an unforgettable time with such talented people. I believe that this laboratory is one of the best in the world. To all the PFSL members … "*BANZAI*".

To the secretaries of PFSL laboratory, 21st Century COE Program, REDEEM and ESTEEM for their unconditional assistance and encouragement with innumerable issues. I am extremely indebted for all their support to me, my wife and son.

Ms. Uiko Yamaguchi, for her kind and tremendous assistance to me and my family. I would never forget her generous help to me, my wife, son and parents. I wish also to thank Ms. Sachiyo Wada for her support to me and my family.

To all my friends around the world, for giving me motivation and making my life and work more enjoyable. In particular, I would like to thank Angela and Ana, two Portuguese girls studying in Japan, for helping me to remember Portugal with "*saudade*" (Portuguese word meaning "*a melancholic longing for people and experiences lingering on as treasured memories*").

To all my family in Japan and Portugal, for their unconditional support, love and encouragement. In particular, I would like to express my sincere gratitude to my mother-in-low, Yoko, for her kind and extraordinary assistance to me and my family. When not working in my research, I spent much of my time in her house in Utsunomiya, where I have relaxed and got strength to my research.

To my lovely parents Elvira and Custodio Lima, for all their outstanding education, advices, encouragement and love. I am eternally grateful for their continuous encouragement to me in pursuing a research carrier and also for supporting me on my many adventures in my life. Their understanding and help made this work possible. My parents were and will be a continuous source of inspiration to me. I would also like to thank my lovely grandmother Maria da Paixao Madeira for showing to me that nothing is impossible in this material world. I am very proud of her.

To my lovely wife Tomoko Yaginuma and my son Mario Lima Yaginuma, for the unconditional support and love provided to me during this research. They have assisted and encouraged me in innumerable ways. I could not have done this work without their understanding and assistance. I hope to return this help and love for years to come.

To the Ministry of Education, Culture, Sports, Science and Technology of Japan (MEXT), for supporting me financially. I would also like to express my gratitude to Instituto Politecnico de Braganca, Portugal, for releasing me from my teaching duties and also for giving me the opportunity to do my Ph.D. in Japan. I hope to foster the relationship between Portugal and Japan for years to come.

Last but not least, I would like to express my sincere gratitude to my father-in-law Professor Toshio Yaginuma. I am internally grateful for introducing me to Professor Takami Yamaguchi and also to the world of cardiovascular mechanics. This thesis is dedicated to him.

Rui Lima

July, 2007.

Dedicated to my father-in-law, Toshio Yaginuma.

――― 星の光は今の光ではない。
何千、何万光年前かの光である。
若い皆さんの輝きは人生の最後の時に輝くはずであり、
またそうあらねばならないと思う。

柳沼　淑夫
平成 14 年 6 月　静岡にて

"… The light of a star is not its present light.
It is the light emitted tens of thousands of light-years ago.
The light of a young person is sure to shine in the last part of their life, and that is how it should be."

Toshio Yaginuma
June 2002 in Shizuoka, Japan.

LIST OF PAPERS

This thesis consists of two introductory parts (Chapter 1 and 2) and five appended papers (Chapter 3 to 7), which are listed below.

PAPER I (Chapter 3)

Lima, R., Wada, S., Tsubota, K., and Yamaguchi, T., 2006. Confocal micro-PIV measurements of three dimensional profiles of cell suspension flow in a square microchannel. Measurement Science and Technology 17, 797-808.

PAPER II (Chapter 4)

Lima, R., Wada, S., Takeda, M., Tsubota, K., and Yamaguchi, T., 2007. *In vitro* confocal micro-PIV measurements of blood flow in a square microchannel: the effect of the haematocrit on instantaneous velocity profiles. Journal of Biomechanics 40, 2752-2757.

PAPER III (Chapter 5)

Lima, R., Wada, S., Tanaka, S., Takeda, M., Ishikawa T., Tsubota, K., Imai, Y., and Yamaguchi, T., 2008. *In vitro* blood flow in a rectangular PDMS microchannel: experimental observations using a confocal micro-PIV system. Biomedical Microdevices, (in press).

Lima, R., Wada, S., Tanaka, S., Takeda, M., Tsubota, K., Ishikawa, T., and Yamaguchi, T., 2006. Velocity measurements of blood flow in a rectangular PDMS microchannel assessed by confocal micro-PIV system. In: Proceedings of the World Congress on Medical Physics and Biomedical Engineering. Seoul, pp. 278-281.

PAPER IV (Chapter 6)

Lima, R., Ishikawa, T., Imai, Y., Takeda, M., Wada, S., and Yamaguchi, T., Measurements of individual red blood cell motions under high hematocrit conditions using a confocal micro-PTV system. (submitted to Annals of Biomedical Engineering).

PAPER V (Chapter 7)

Lima, R., Ishikawa, T., Takeda, M., Imai, Y., Tsubota, K., Wada, S., and Yamaguchi, T., 2008. Radial dispersion of red blood cells in blood flowing through glass capillaries: role of heamatocrit and geometry. Journal of Biomechanics, (in press).

CONTENTS

APPENDIXES

CHAPTER 1

INTRODUCTION

Blood in large arteries may be treated as a homogenous fluid from a macroscopic perspective. However, in reality blood is a suspension of deformable cells in a viscous fluid plasma. In microcirculation, which comprises the smallest arteries and veins, the flow behavior of individual blood cells and their interactions provide the microrheological basis of flow properties of blood at a macroscopic level. As a result, in microcirculation it is fundamental to study the flow behavior of blood at cellular level.

Over the years, various experimental methods have been applied in an effort to understand the blood flow behavior in microcirculation. Most of our current knowledge in microcirculation is based on macroscopic flow phenomena such as Fahraeus effect and Fahraeus-Linqvist effect. The development of optical experimental techniques has contributed to obtain possible explanations on the way the blood flows through microvessels. Although the past results have been encouraging, detailed studies on blood flow behavior at a microscopic level has been limited by several factors such as poor spatial resolution, difficulty to obtain accurate measurements at such small scales, optical errors arisen from walls of the microvessels and high concentration of blood cells, and difficulty in visualization of results due to insufficient computing power and absence of reliable image analysis techniques. Therefore, at the present we have lack of understanding on the microscale flow behavior of blood cells through microvessels.

The aim of this study is to provide further insights into the microscale blood flow behaviour through microchannels, by applying an emerging optical technique known as confocal micro-PIV/PTV. In the following sections, first we provide some basic information on the blood composition and then we provide the most significant contributions on the microcirculation field with emphasis on the *in-vitro* experiments and optical measuring techniques. Finally, the main objectives of this thesis are presented and an outline of the work is given in section 1.5.

1.1 Blood flow behavior in microchannels

1.1.1 Haemodynamics of the circulatory system

The primary function of the circulating blood is to transport oxygen, nutrients, waste products and heat throughout the body. The oxygenated blood leaves the heart, with high pressure and velocity (Reynolds number (Re) > 2000), through the aorta and moves into other large arteries, then into arterioles and, finally, into the capillaries. On its way back from the capillaries the blood moves into venules and then into veins in order to return to the heart and to begin the same journey all over again (see Figure 1.1a).

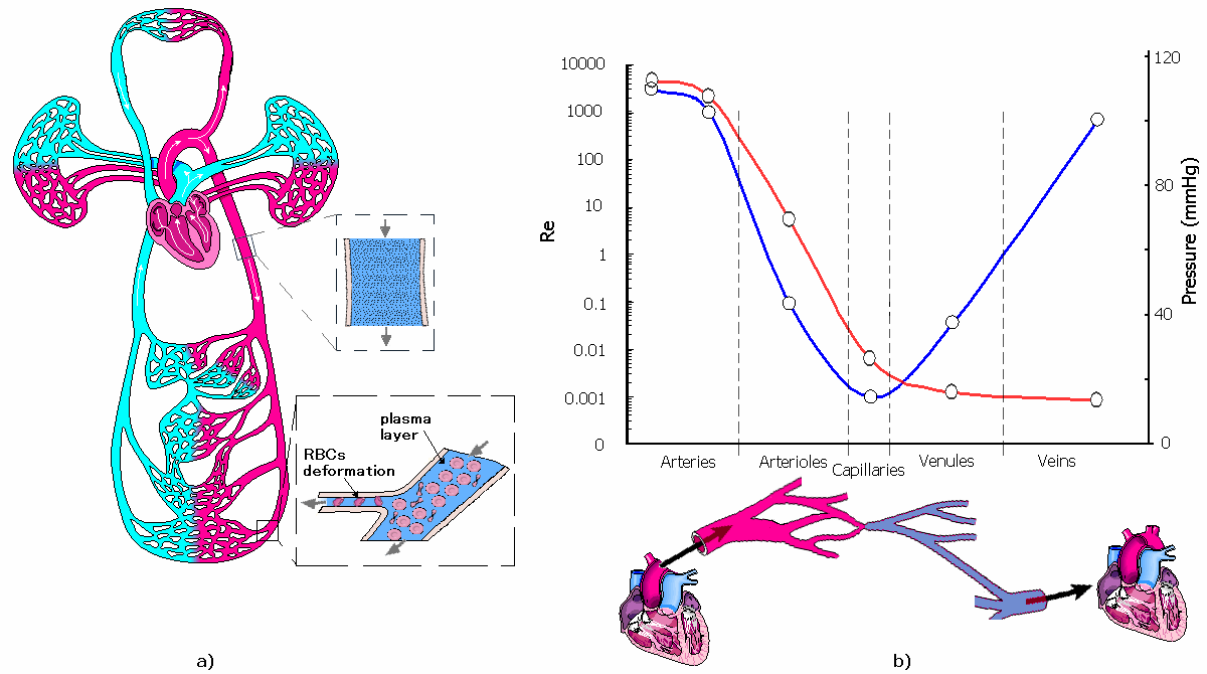

Figure 1.1 a) Schematic diagram of the circulatory system. b) Schematic diagram showing the changes in blood pressure and Re on the large arteries, capillaries and veins (Burton 1966, Caro et al. 1979, Levick 2003).

In large arteries, where the diameter of the blood vessels is large enough compared to individual cells, it has been proved adequate to consider blood as a Newtonian fluid (Caro et al. 1979, Fung 1997, Yamaguchi et al. 2006). Accordingly, blood in large arteries may be treated as a homogeneous fluid (continuous viscous fluid) where its particulate nature is ignored. Moreover, due to the large Reynolds number (Re) in arteries, blood flow is governed by inertial forces. However, arteries divide into successive smaller arteries and consequently the cross-sectional area of the vascular bed increases. As a result both pressure and velocity decrease as the blood flows into the smaller vessels. When the blood reaches the arterioles and capillaries the Re became less than 1, where viscous force dominates over inertial forces

(see diagram in Figure 1.1b). At this microscale it is fundamental to take into account the effects of the non-Newtonian properties of the blood on its flow behavior (Caro et al. 1979, Fung 1993, Burt 1966). A clear example of the non-Newtonian nature of the blood, illustrated in Figure 1.1a, is the formation of a plasma layer at microvessels less than 300 μm, known as Fahraeus-Lindqvist effect (Fahraeus and Lindqvist 1931). It is based on the Fahraeus-Lindqvist effect we define microcirculation as the one including all microvessels or microchannels with a diameter smaller than 300 μm.

1.1.2 Blood composition

Blood is not a homogeneous fluid, but one composed of a suspension of cells, proteins and ions in plasma. In normal blood, three types of cells comprise about 46% of its volume (see Table 1.1). These cells are the red blood cells (also known as erythrocytes), white blood cells (also known as leukocytes) and platelets (also known as thrombocytes) (see Figure 1.2).

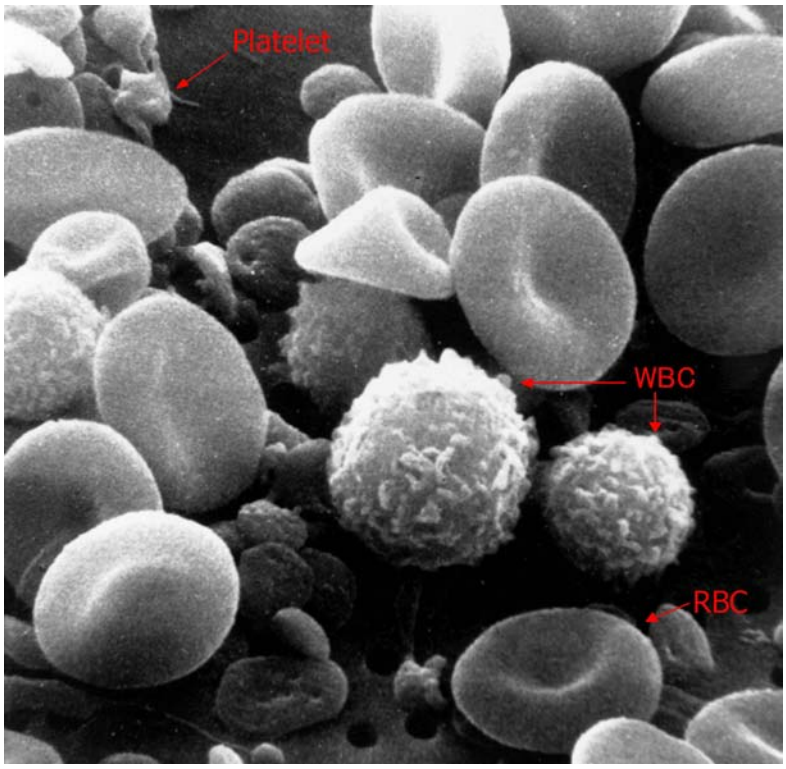

Figure 1.2 Scanning electron microscope image of human blood cells (adapted from National Cancer Institute, USA)

Table 1.1 – Blood cells composition (Caro et al. 1979).

Cell	Unstressed shape and dimensions (μm)	Volume concentration (%) in blood
Red blood cell (RBC)	Biconcave shape (8×1-3)	45
White blood cell (WBC)	Roughly spherical (7-22)	1
Platelets	Round or oval (1-4)	

Red blood cells (RBCs)

Blood flow behavior in microcirculation is strongly influenced by the red blood cells (RBCs), since they occupy almost half of whole blood volume. RBCs are formed in the bone marrow and during maturation they lose their nuclei before entering the circulatory system. When suspended in an isotonic medium (such as plasma or physiological saline) RBCs has a biconcave discoid shape, with a major diameter of about 8 μm. The dimensions and shape of a typical human RBC is shown in Figure 1.3.

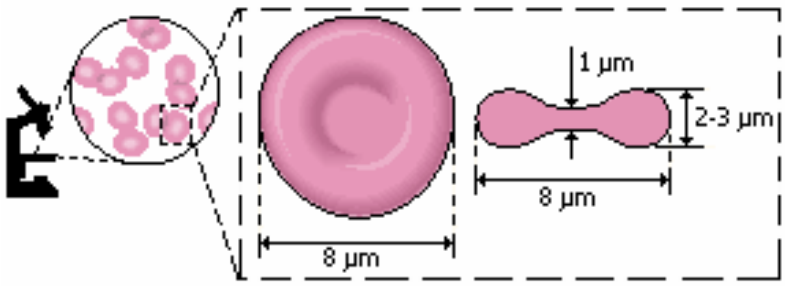

Figure 1.3 Dimensions and shape of an unstressed human RBC (adapted from Caro et al. 1979).

The RBC density is about 1.08×10^{3} $kg.m^{-3}$ and its major cellular components are the cytoplasm and a thin membrane composed of lipid bilayer and protein molecules. The internal fluid (cytoplasm) is essentially a concentrated hemoglobin (Hb) solution which as the ability to transport oxygen and carbon dioxide. In addition the internal viscosity provided by the intracellular Hb contributes to the rheological properties of the RBC. The protein matrix, usually known as cytoskeleton, plays an important role on its mechanical properties and in maintaining its biconcave disk shape. As a result the ability of RBCs to deform is greatly influenced by its cell membrane and shape and also by the Hb concentration. There is experimental evidence that normal RBCs are extremely deformable into a variety of shapes in flowing blood in response to hydrodynamic stresses acting on them. Figure 1.4 shows several examples of RBCs deformation in capillaries and in extremely narrow microchannels (Caro et al. 1979, Chien et al. 1984, Shiga et al. 1990, Fung 1993)

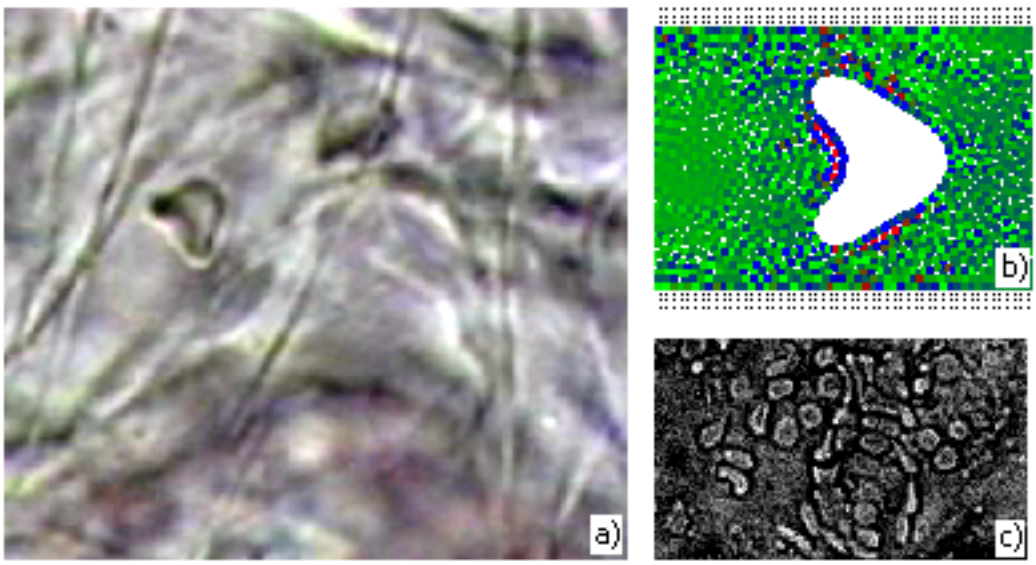

Figure 1.4 RBCs deformation a) *in vivo* capillaries (www.ne.jp/asahi/minamiya/medicine), b) by computational simulation (Tsubota et al. 2006a), c) through narrow microchannels.

White blood cells (WBCs)

White blood cells (WBCs) are nucleated cells that represent the major defence mechanism against infections. Their shape is, in general, roughly spherical but their surface is not normally smooth (see Figure 1.2). The diameter of WBCs ranges from about 7 up to 22 μm, depending on its type. Healthy blood contains normally less than 1% of WBCs of the total volume of blood cells. (Caro et al. 1979, Chien et al. 1984)

It has been argued that WBCs are less deformable than RBCs however WBCs can pass through the capillaries vessels walls. Thus the mechanical properties of WBCs are not clearly understood and need further research. Little is also known about the effect of the WBCs on the blood flow behavior in microcirculation. The blood flow under pathological conditions may promote the amount of WBCs within the flow and consequently they may disturb the blood flow behavior in microvessels.

Platelets

Platelets are cells with no nuclei, round or oval discoid shape, in general, and with diameters from about 1 to 2 μm. The number of platelets is usually less than the WBCs and they may have little effect on the blood flow behavior. Although platelets play an important role in blood coagulation and thrombus formation, this topic is beyond the scope of the present work (Caro et al. 1979, Chien et al. 1984).

Plasma

Plasma is a yellowish fluid which contains 90% of water by volume and 10% of proteins (such as albumin and fibrinogen), inorganic substances (such as sodium ions and chloride ions), vitamins, dissolved gases, etc. The proteins within the plasma flow, due to their large molecular size, usually do not pass through the capillary wall, thus generating an osmotic pressure. In *in vitro* experiments the osmotic pressure is an important parameter that needs special attention. For example, when RBCs are suspended in an isotonic solution, like physiological saline, their shape does not change. However, if the RBCs are suspended in a hypotonic solution (NaCl less than 0.9%) the water diffuses into the cells interior and as a result they swell and may undergo hemolysis (Burton 1966, Waite 2005).

1.1.3 Blood rheology

Rheological properties from rotational viscometers

When the blood plasma was investigated with a viscometer, it was found that it behaves as a Newtonian fluid. However, it was demonstrated that for a haematocrit (Hct) of 45% (percentage of the total blood volume occupied by the cells) the viscosity varies with the shear rate ($\dot{\gamma} = \partial v / \partial y$), implying that the blood at high Hcts behaves as non-Newtonian fluid (see Figure 1.5). Moreover, it was also shown that blood viscosity also varies with the temperature and disease state (Chien et al. 1984, Fung 1993).

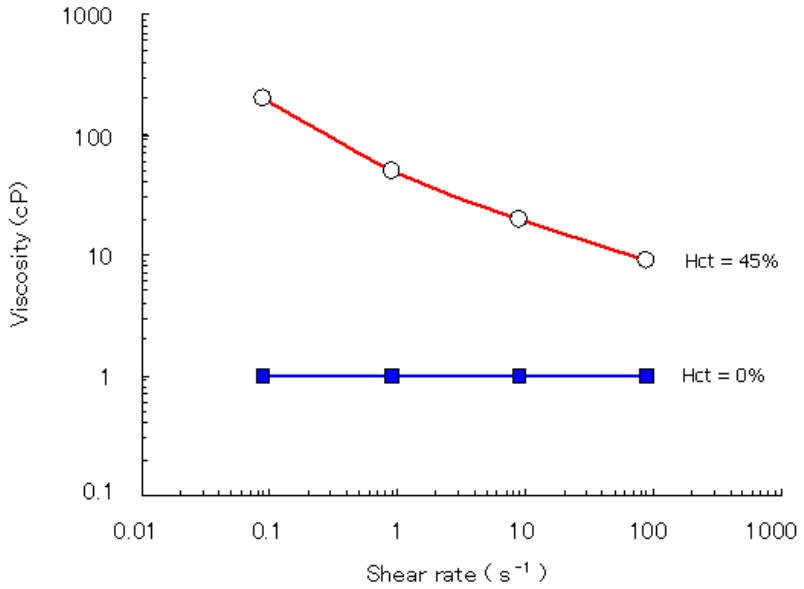

Figure 1.5 Relation between viscosity and shear rate ($\dot{\gamma}$) of normal blood (45% Hct) and plasma (0% Hct) (adapted from Fung 1993).

Several experiments have examined the variation of viscosity with shear rate by using different kinds of fluids such as water, normal RBCs (45% Hct) suspended in plasma, washed RBCs (45% Hct) suspended in albumin-ringer solution and glutaraldehyde-hardened RBCs (45% Hct) in albumin-ringer solution. From Figure 1.6., it is very clear that the normal blood has a rheological behavior significantly different from water. In fact, for the case of normal RBCs suspended in plasma, at low shear rates ($\dot{\gamma}$<1s^{-1}) the cells tend to aggregate to form rouleaux, where the presence of proteins (fibrinogen and globulin) in the plasma are believed to contribute to the RBCs aggregation. When the shear rate increases the rouleaux tend to break-up and the viscosity to decrease due to the deformation of the RBCs and the alignment with the flow. In the case of RBCs suspended in albumin-ringer solution, without fibrinogen and globulin, the results have shown that the RBCs do not have tendency to form rouleaux, a fact that reflects the lower viscosity at low $\dot{\gamma}$. These RBCs at high shear rate also deform and align with the flow. In contrast, hardened RBCs by losing their ability to deform they tend to increase the viscosity, especially at $\dot{\gamma}$ > 1 s^{-1} (Chien 1970, Goldsmith and Turitto 1986, Fung 1993).

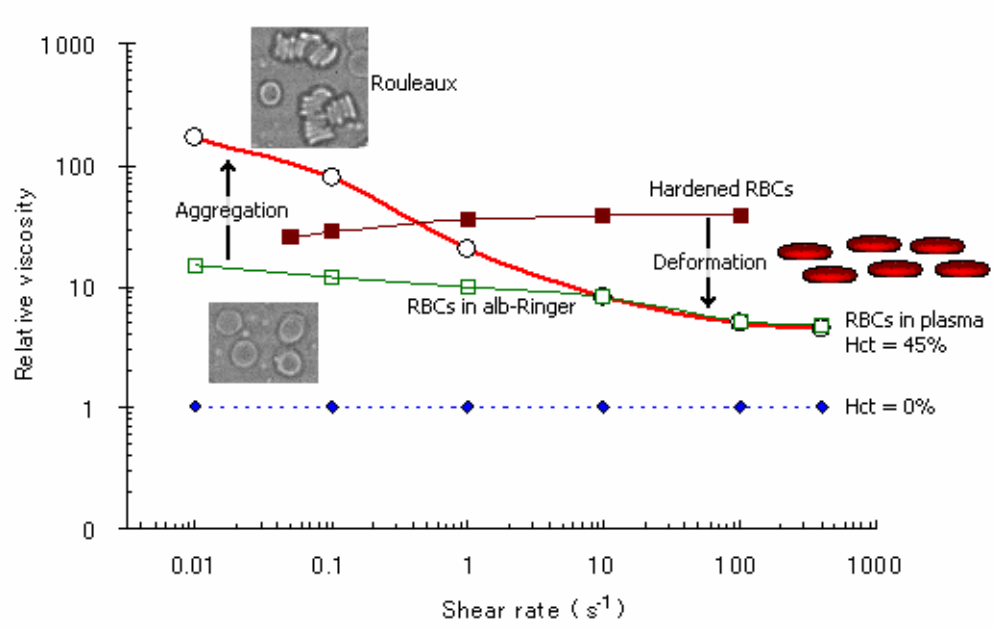

Figure 1.6 Relation between viscosity and shear rate ($\dot{\gamma}$) of water (0% Hct), normal RBCs (45% Hct) suspended in plasma, washed RBCs (45% Hct) in albumin-ringer solution and hardened RBCs (45% Hct) in albumin-ringer solution (adapted from Chien 1970, Goldsmith and Turitto 1986, Levick 2003, Fujiwara 2007).

Another interesting experiment, revealing the remarkable fluidity of normal blood, was performed by Goldsmith and Mason. Figure 1.7 shows that in the suspension of rigid spheres, at 50% concentration, the viscosity increases exponentially making them difficult to flow.

However, in the case of normal blood, even at 80% Hct, it has the ability to behave as a fluid (Goldsmith and Turitto 1986, Fung 1993).

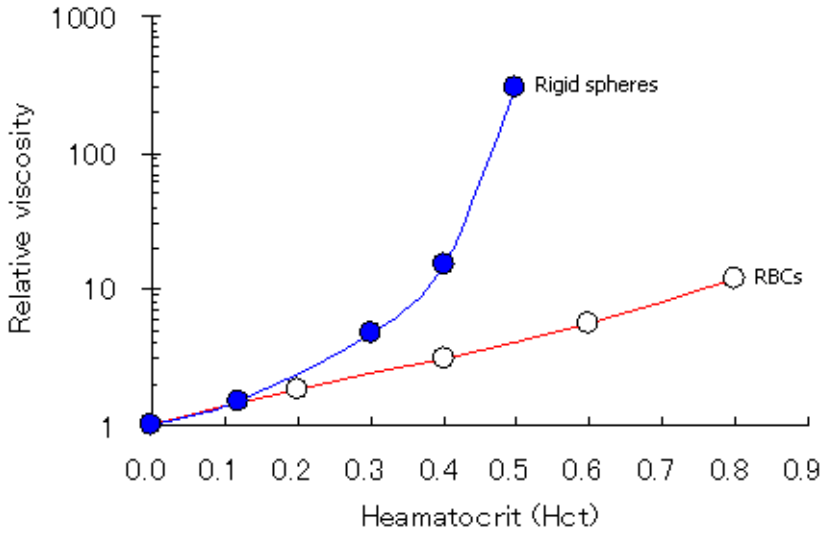

Figure 1.7 Relative viscosity of blood at 25°C as a function of Hct compared to that of suspensions of rigid spheres (adapted from Goldsmith and Turitto 1986).

Although rotational viscometers have provided important findings on the blood rheological behavior, it should be emphasized that the actual rheological behavior of blood through microchannels may be different from some of the results above.

Rheological behavior in microchannels

The most astonishing flow characteristics of blood are known as Faharaeus effect and Faharaeus-Lindqvist effect. These two effects are strongly related to the microtube diameter and they were also observed *in vivo* experiments. Obviously in rotational viscometers these effects were never observed.

In the classical work of Robin Faharaeus, he observed that blood flow behavior and its heamatocrit are strongly affected by microtubes diameters less than 300 μm. The Fahareus effect indicates that the Hct in the glass capillaries (< 300 μm) is lower than the feed Hct, which suggests that the Hct decreases as the blood proceeds through narrower microvessels (see Figure 1.8). This phenomenon results from the axial migration of the RBCs to the centre of the microtube and consequent faster motion of the cells when compared with the suspending medium, such as plasma or dextran (Faharaeus and Lindqvist 1931, Chien et al. 1984, Fung 1993, Maeda 1996).

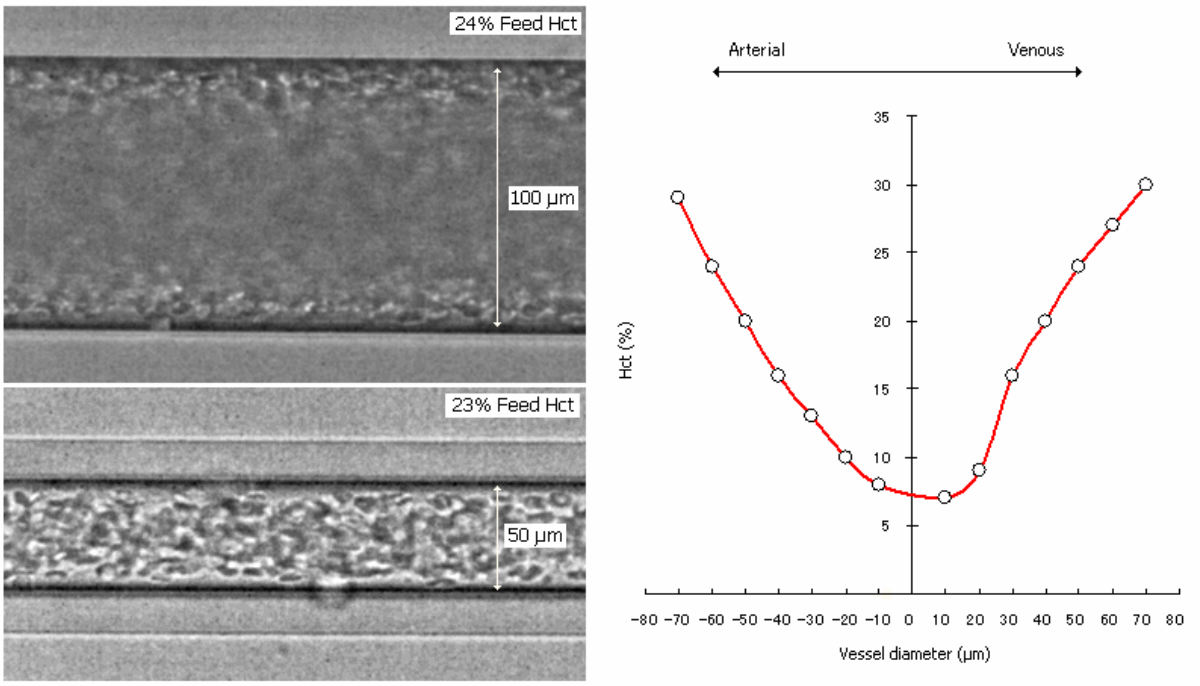

a) b)

Figure 1.8 (a) Fahareus effect in glass capillaries (Lima et al.) (b) Arteriovenous distribution of heamatocrit in mesenteric microvasculature of the cat (adapted from Fung 1997).

The Faharaeus-Lindqvist effect is somehow related to the above phenomenon. Again for microtubes diameters less than 300 µm, Faharaeus and Lindqvist observed that the apparent blood viscosity decreases as the microtube diameter became smaller (Faharaeus and Lindqvist 1931). After them, several works have extended their experiment down to diameters of about 3 µm and they have observed that the decrease of the apparent viscosity continues down to diameters of about 10 µm. However, the Faharaeus-Lindqvist effect is reversed at diameters 5 to 7 µm (see Figure 1.9). This phenomenon indicates that the tube Hct is not the only parameter affecting the apparent viscosity. Thus, it is believed that the plasma layer and also the microscopic motions of RBCs play an important role on the apparent blood viscosity (Chien et al. 1984, Fung , Pries et al. 1992, Maeda 1996, Pries and Secomb 2003).

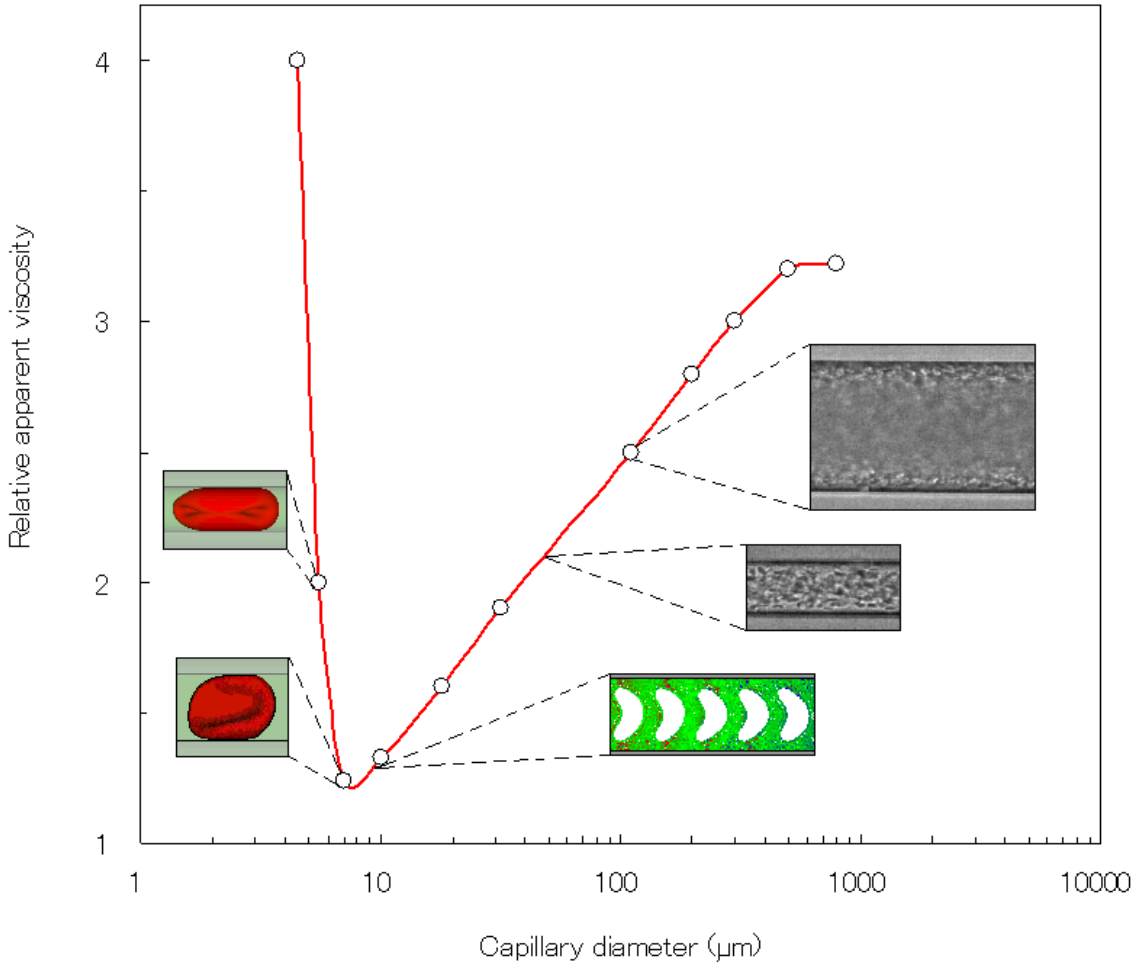

Figure 1.9 Relative apparent viscosity of *in vitro* blood through glass capillaries with diameters between 3.3μm and 800μm (adapted from Pries et al. 1992, Wada and Kobayashi 2002, Tsubota et al. 2006b).

An obvious explanation for the Faharaeus-Lindqvist effect is the decrease of the dynamic Hct (Hct in the microtube) with decreasing microtube or microvessel diameter and the consequent decrease of the apparent viscosity. This effect can also be explained by the formation of a marginal plasma layer near the wall of the microchannel. This plasma-rich layer located between the RBC core and wall (where the shear forces are maximal) contributes to the reduction of apparent blood viscosity. In microcirculation the plasma layer is believed to reduce the friction between RBCs and endothelial cells and consequent flow resistance. However, the complex formation of the plasma layer has not yet convincingly demonstrated mainly due to multi-physical and hemorheological factors that affect the plasma layer. Currently, the most acceptable explanation is due to the tendency of the RBCs to migrate toward the microtube axis enhanced by the RBCs deformation and interations (see Figure 1.10) (Schmid-Schonbein and Wells 1969, Goldsmith 1971, 1984, Caro et al. 1979, Fung 1993, Maeda 1996).

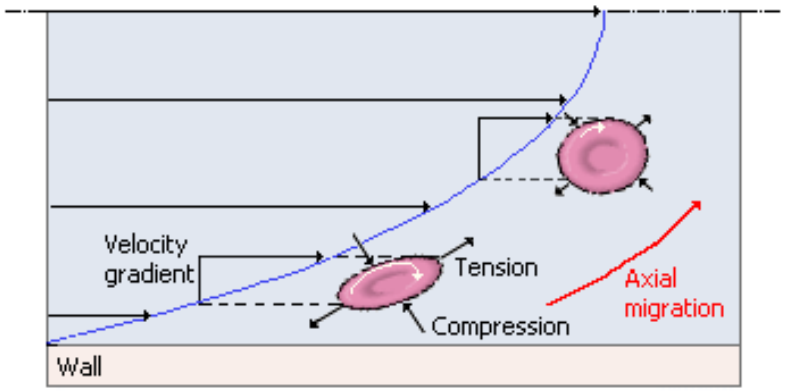

Figure 1.10 The RBCs axial migration may be explained by the tank-tread motion of the RBC membrane due to the velocity gradient ($\dot{\gamma}$) of the flow (Mchedlishvili and Maeda 2001).

The rheological behavior of blood in microcirculation can not be directly estimated from rotational viscometers, since it is strongly influenced by several combined effects of the plasma layer, RBC deformability or aggregation and RBC radial distribution. In fact several researchers have observed that the viscosity fails to increase with decreasing shear rate or increasing RBCs aggregation tendency (Reinke et al. 1987, Cokelet and Goldsmith 1991, Alonso et al. 1995). This observation does not corroborate with the findings provided from rotational viscometers. Cokelet and Goldsmith 1991, have measured the hydrodynamic resistance of normal RBCs suspended in dextran 110 and albumin-saline flowing through vertical microtubes at low flow rates. In Figure 1.11 it is possible to observe that when RBCs were suspended in dextran 110 the hydrodynamic resistance decreased at low flow rates due to the RBCs aggregation. This surprising phenomenon is maybe due to the increase of the thickness of the plasma layer enhanced by RBCs aggregation. In contrast when RBCs were suspended in albumin-saline the hydrodynamic resistance has increased linearly mainly because there was not any aggregation of RBCs and plasma layer. It should be noted that in horizontal tubes an increase of the apparent viscosity may happen at low shear rate only if sedimentation of RBCs occurs (Gaehtgens 1987, Alonso et al. 1995). Despite the significance of the role of RBCs aggregation on the blood viscosity, some controversies related to the chemicals used to enhance the aggregation of cells still remain.

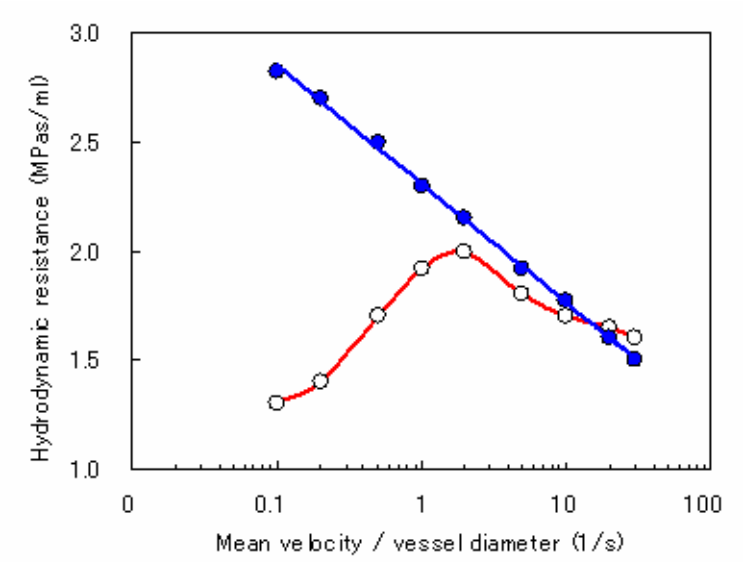

Figure 1.11 Hydrodynamic resistance (R) as a function of mean tube velocity ($\overline{U}$) (adapted from Cokelet and Goldsmith 1990).

1.1.4 Microscopic flow behavior in microchannels

In order to obtain further insight into the blood rheological behavior, Goldsmith and his colleagues (Goldsmith 1971a, Goldsmith 1971b, Goldsmith and Karino 1977, Goldsmith and Marlow 1979, Goldsmith and Turitto 1986) have performed series of experiments with diluted and concentrated suspensions of various types of particles and RBCs through a glass capillaries. In their experiments they used a conventional microscope in order to obtain detailed information about the blood flow behavior at a microscopic level.

Particles and RBCs in diluted suspensions

In Poiseuille flow, the behavior of suspended particles depends on several factors such as shear rate, particle deformability, size and shape. Generally, at low shear rates and diluted suspensions, rigid spherical particles and hardened RBCs (HRBCs) tend to move axially without any radial migration. On the other hand, deformable bodies tend to migrate towards the tube axis due to a radial hydrodynamic force. For higher Re (>1) where the inertial forces become important, both deformable bodies and rigid spheres have axial migration, however the spheres not always migrate toward the centre. The spheres near the wall moves towards the centre whereas the ones in the centre moves towards the wall. At the end they reach an equilibrium radial position of 0.6R, where R is the tube radius. This effect is known as tubular pinch effect. Figure 1.12 shows typical motions for rigid and deformable particles (Goldsmith 1971, Caro et al. 1978).

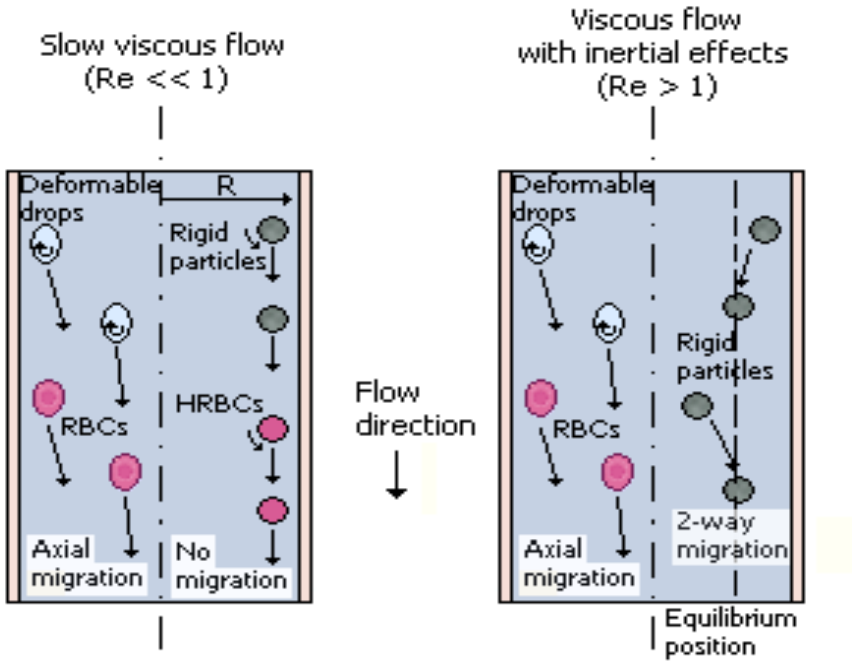

Figure 1.12 Schematic representation of migration differences of rigid, deformable particles and HRBCs in the median plane of the microtube (adapted from Goldsmith 1971).

The motion of a single RBC in plasma undergoing Poiseuille flow reflects the behavior of both rigid and deformable particles. When the shear rate ($\dot{\gamma}$) is less than approximately 20s^{-1}, the cell seems to rotate in orbits similar to rigid discs where they flip and rotate with a periodically varying angular velocity (rotational and tumbling motion). At low shear rates it was observed that its biconcave shape retains while rotating, however it was also observed that the RBCs tended to migrate away from the walls suggesting that small deformations may also occur. At $\dot{\gamma} \gtrsim 20$ s^{-1} the rotation progressively deviates from that of rigid disks and tend to be aligned with the direction of the flow. At $\dot{\gamma}$ around 33 s^{-1}, the RBCs cease to rotate as a whole and instead deform and rotate around the interior of cell, the so-called "tank-tread" motion. Although there is no experimental evidence, it is suggested that the membrane motion is transmitted into the interior of cell (cytoplasm) and may enhance the circulation of the hemoglobin (Hb) solution and consequently it may play an important role in the oxygen release from RBCs to tissues. At very high shear rates ($\dot{\gamma}$ > 5000 s^{-1}), RBCs are subjected to the tubular pinch effect with an equilibrium position nearer to the centre of the microtube (Goldsmith 1971b, Caro et al. 1978, Chien et al. 1984).

In turn, hardened RBCs behave like rigid particles at all shear rates. At Re<<1, they do not exhibit radial migrations, however at Re > 1 they experience the tubular pinch phenomenon. (Caro et al. 1978, Goldsmith and Turitto 1986).

RBCs in concentrated suspensions

Although the flow properties of RBCs in diluted suspensions were extensively studied for many the years, such is not the case when the RBCs flow within a crowded environment. The reason is mainly related to technical limitations of optical systems to obtain reliable measurements at Hct bigger than 10%. However, Goldsmith and coworkers (Goldsmith 1971a, Goldsmith and Karino 1977, Goldsmith and Marlow 1979, Goldsmith and Turitto 1986) have overcome this technical difficulty by using transparent RBCs (known as ghost cells) as the suspension medium. By using ghost cells they were able to study the behavior of individual RBC flowing in concentrated suspension of RBC ghosts. Although there are controversies whether ghost cells have the same rheological properties of normal RBCs (Goldsmith and Marlow 1979, Nash and Meiselman 1983), to our knowledge their work have provided the best insight into the complex behavior of RBCs flowing in the interior of concentrated suspensions.

The motion of RBCs in concentrated suspensions is appreciably different from those observed in very diluted suspensions (Hct < 1 %). At concentrated suspensions the motion of RBCs is disturbed not only by the collisions with neighboring cells but also by the plasma layer near the wall. In this way, the cell paths exhibit continuous erratic displacements with the largest ones occurring in the region between 0.5 and 0.8 of the tube radius from the axis. At a given microtube, the magnitude of radial displacements tends to increase with the concentration of RBC ghost cells. However, at concentrations bigger than 50%, the displacement decreases. At Hct > 50%, although the crowded environment leads to an increase of the cell deformation, it also limits the magnitude of the RBC radial dispersion (Goldsmith and Karino 1977, Goldsmith and Marlow 1979, Goldsmith and Turitto 1986).

The RBCs flowing at Hct bigger than 30% are deformed into a variety of shapes and rotate irregularly. Qualitative observations indicate that the degree of deformation increases with the concentration of ghost cells. It was also observed that at the centre of microtube some RBCs have retained their biconcave shape (Goldsmith and Karino 1977, Goldsmith and Marlow 1979, Goldsmith 1984). Although the work of Goldsmith has provided important qualitative observations on the microscale behavior of RBCs flowing through microtubes, this research field remains relatively unexplored.

Velocity profiles

Blood flow velocity in microvessels and microchannels have been measured during the years by several measurements techniques such as: double-slit photometric (Gaehtgens et al. 1970, Baker and Wayland 1974), video microscopy and image analysis (Bugliarello et al. 1963, Goldsmith 1971a, Goldsmith and Marlow 1979, Tangelder et al. 1986; Parthasarathi et al.1999), laser-Doppler anemometer (Einav et al., 1975, Born et al. 1978, Cochrane et al. 1981; Uijttewaal et al. 1994, Golster et al. 1999) and particle-measuring methods (Suggi et al. 2005, Nakano et al. 2003, Olsen et al. 2006). From all these studies there is no general consensus about the actual velocity profile in microvessels. Although some results reported parabolic profiles (Baker and Wayland 1974, Golster et al. 1999, Suggi et al. 2005), others suggested blunt profiles (Bugliarello et al. 1963, Goldsmith 1971a, Goldsmith and Marlow 1979, Tangelder et al. 1986, Nakano et al. 2003, Olsen et al. 2006) and even others reported blunt profiles at extremely low velocities and diameters and parabolic profiles at diameters bigger than about 100μm (Gaehtgens et al. 1970, Cochrane et al. 1981). The large scatter of results reflects the complexity of the phenomena happening in microcirculation. However, it is clear from the past researches that the flow velocity profiles are strongly affected by several combined parameters such as : Hct, microtube diameter, shear rate, flow rate, suspension fluid (plasma, PS or dextran), experimental errors, concentration of trace particles, etc. Despite the great amount of research on this area, experimental evidence remains scarce and controversies still remain.

An important work on this field was performed by Goldsmith and his co-workers (Goldsmith 1971a, Goldsmith and Marlow 1979, Goldsmith and Turitto 1986). Again by using suspensions of ghost cells, they have obtained velocity profiles based on the microscopic flow behavior of RBCs. Their results suggested that at diluted solutions (~1% Hct) the velocity profile is close to parabolic. At higher Hct, the profile becomes flat around the axis of the microtube (see Figure 1.13). The degree of blunting increases with the Hct and decreases with the flow rate. The main reason for the former phenomena seems to be related to the interactions of the suspended RBCs in shear flow whereas the latter may be associated with the decrease of blood viscosity due to cell disaggregation and deformation (Goldsmith 1971a, Caro et al. 1978, Goldsmith and Marlow 1979, Goldsmith and Turitto 1986).

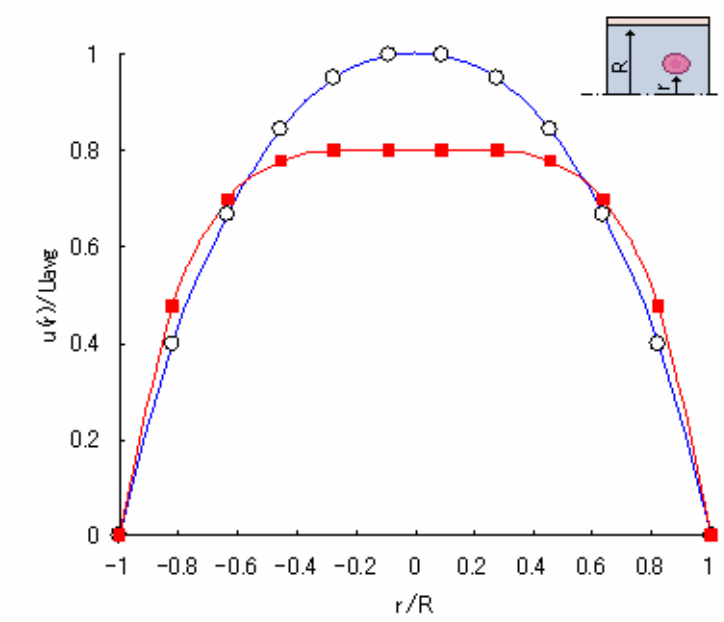

Figure 1.13 Schematic representation of the velocity profiles at Re <1 in capillaries for RBCs suspended in diluted (<1% Hct) and concentrated (32% Hct) suspensions. Local velocities (u(r)) are plotted as ratios of the centre line velocity (Uavg) (adapted from Caro et al. 1978 and Goldsmith and Turitto 1986).

Although qualitatively these results may provide a good basis of actual flow behavior of blood through microchannels, careful interpretation of the results should be considered due not only to the use of ghost cells but also unknown temporal and spatial resolution of the measurement technique.

1.1.5 Relevance of blood flow in microchannels

The complexity to control and obtain reliable measurements of the blood flow behavior through the *in vivo* microvascular system has led several researchers to perform their studies by using narrow glass tubes with simple geometries. By using *in vitro* models it allow a more precise control over the experimental variables of interest and extract detailed information of the flow behavior of individual blood cells. In fact, much of the understanding of the haemodynamics phenomena observed in microcirculation was obtained from studies on the both macro and microrheology properties of blood flowing through glass microtubes. Although glass microchannels present certain similarities to *in vivo* microcirculation, it is also clear that these kind of static *in vitro* experiments differ from microvessels in several respects, such as: elasticity of microvessels, role of the irregularly shaped endothelial surface and effect of the branches and asymmetrical structure of microvessels. Thus it was not surprising that several studies on blood flow in glass microtubes and in microvessels have yielded conflicting results with respect to flow resistance (Pries et al. 1994) and deformability of RBCs (Suzuki et al. 1996). In the former case, they reported that the apparent viscosity was higher *in vivo*

than in glass tubes whereas in the latter they have found that RBCs deform less in microvessels. However, the observed *in vivo/in vitro* discrepancies have not yet been convincingly explained. As a result, further work is clearly needed in this research field.

1.1.6 BioMEMS – the new generation of microchannels

It is obvious that the conflicting results arisen from *in vivo/in vitro* can not be explained by using the research done in straight rigid glass microchannels. One possible way to overcome the limitations of the glass capillaries is by using microelectromechanical systems (MEMS) technology to manufacture microdevices to study *in vitro* blood flow in an environment closer to *in vivo* conditions, know as BioMEMS devices or simply biochips. By using a soft lithographic technique it is possible to fabricate polydimethysiloxane (PDMS) microchannels with complex geometries similar to human blood arterioles and capillary networks (see Figure 1.14). Besides the ability to mimic complex geometries this kind of microchannels have others remarkable properties such as good optical transparency, biocompatibility and permeability to gases. This latter property makes these microchannels adequate to culture living cells on their surfaces and consequently they provide a powerful way to study several phenomena in the microcirculation (Kaji et al., 2006, 2007). However, to our knowledge the current MEMS technology can not manufacturer accurately microchannels with circular cross section. Instead they usually fabricate microchannels with rectangular cross section. Despite the great significance of this limitation, research on this field remains extremely scarce. A simple technique to overcome this limitation is presented in Appendix C.

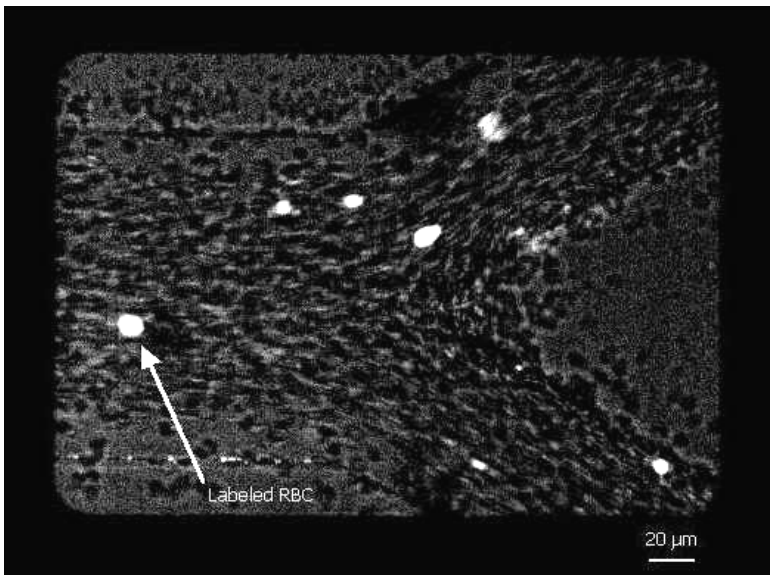

Figure 1.14 *In vitro* blood flowing through a bifurcation fabricated by soft lithography.

1.2 Flow visualization techniques in microcirculation

In large blood vessels, the conventional non-invasive medical instruments to measure the blood flow are the Doppler ultrasound and magnetic resonance imaging (MRI) techniques. Although, both techniques have revolutionized cardiovascular diagnosis, these *in vivo* diagnostic techniques have several limitations. Among them is the inability to obtain quantitative detailed information at a microscale level due to the relatively poor spatial resolution (Giddens et al. 1993, Stanton 1999). Accordingly, these techniques did not gain popularity among the microcirculation research community.

In the past, blood flow in both microvessels and microchannels has been measured by several measurements techniques such as: double-slit photometric (Gaehtgens et al. 1970, Baker and Wayland 1974), laser-Doppler anemometer (Einav et al., 1975, Born et al. 1978, Cochrane et al. 1981; Uijttewaal et al. 1994, Golster et al. 1999). These techniques used direct photometric information obtained without image information (Slaaf et al. 1984). However, most successful techniques are the video-based methods (Goldsmith 1971a, Goldsmith and Marlow 1979, Tangelder et al. 1986; Parthasarathi et al.1999). Generally, these methods record video microscopy images in order to be analyzed off-line by using image processing techniques.

A very recent video-approach to study the flow properties of blood in microcirculation is the micro-particle image velocimetry (PIV) (Sugii et al. 2002, 2005, Chiu et al. 2003, Nakano et al. 2003, Bitsch et al. 2005, Vennemann et al. 2006, Kim and Lee 2006). Due to its high spatial and temporal resolution, this method is gaining widespread use for studying several phenomena in microcirculation. However, micro-PIV systems by using conventional microscopes, the entire flow field is illuminated and consequently, the out-of-focus emitted light can result in high levels of background noise, which degrades the measured velocity fields (Meinhart et al. 1999, 2000, Nguyen and Wereley 2002). This limitation can be overcome by using a spinning disk confocal microscope (SDCM) (Ichihara et al. 1996, Tanaami et al. 2002, Inoue and Inoue 2002) instead of the conventional microscope. Very recently Park and his co-workers (Park et al. 2004) have applied successfully this technique to measure pure water, seeded with tracer particles, through a glass microchannel. However, to our knowledge, no study has evaluated the ability of a confocal micro-PIV system to measure blood flow through microchannels.

The present work applies for the first time a confocal micro-PIV/PTV system to study blood flow behavior through microchannels. By using this system we expect to obtain further insights into the complex flow properties of blood in the microcirculation.

1.3 Objectives of the present study

The numerous physical and biological effects happening at a microscale level, together with the absence of adequate techniques to obtain detailed information at a microscale level, are the main reasons for lack of understanding on the flow properties of blood in the microcirculation. Therefore, it is clear that precise and reliable measurement approaches to study the blood flow at a microscale level are essential to obtain further insights on blood flow behavior and also to provide information for the validation and development of theoretical models and computer simulations.

From the preceding review on the available measuring flow techniques, it is clear that the confocal video-based technique is the most reliable method in microfluidics. However, the question whether a confocal system is a suitable technique to study blood flow in microchannels still remains. The answer to this question is one of the main topics addressed by this dissertation.

The main objectives of the present dissertation can be summarized as follows:

1. To evaluate the performance of a confocal micro-PIV system to study the behavior of a blood cell suspension fluid through a square microchannel and also to investigate its ability to obtain 3D profiles of the fluid flow.
2. To investigate the ability of the confocal micro-PIV system to obtain detailed information on the blood flow behavior through both glass and polydimethysiloxane (PDMS) microchannels.
3. To identify the advantages and limitations of the confocal micro-PIV system and perform the necessary modifications in order to obtain accurate quantitative information on the blood flow behavior in microchannels.
4. To obtain direct and quantitative detailed description of the mechanical properties of the individual red blood cells and of cell-cell interactions occurring during flow.

5. To obtain reliable information on the microscale flow behavior of RBCs in microchannels in order to validate and develop both theoretical and numerical models.
6. To obtain macroscopic properties of a RBC suspension flow in order to construct a better continuum model for large scale blood flow.

1.4 Outline

The remainder of this thesis is organized in the following manner: Chapter 2 presents the most relevant theoretical and technical issues related to both conventional and confocal micro-PIV and also a comparison between both methods. Chapter 3 presents validation studies to evaluate the performance of a confocal micro-PIV system to measure both pure water and diluted suspensions of RBCs (~ 4% Hct) through a 100 μm square microchannel in several horizontal planes. Chapter 4 presents both ensemble and instantaneous velocity profiles for *in vitro* blood with haematocrit (Hct) up to 17%, flowing through a 100 μm square microchannel. Chapter 5 shows the ability of our confocal micro-PIV system to measure the velocity profiles of both physiological saline (PS) and *in vitro* blood (20% Hct) in a rectangular polydimethysiloxane (PDMS) microchannel. Chapter 6 presents a new approach, based on a low-image-density PIV technique (confocal micro-PTV), to obtain detailed quantitative measurements on the motion of blood cells at both diluted and high suspensions of RBCs, flowing through a 100 μm glass capillary. Chapter 7 presents the application of the confocal micro-PTV system to calculate the RBCs radial dispersion coefficient (D_{yy}) in the middle plane of a 50μm and 100 μm glass capillaries at low Reynolds numbers (Re from 0.003 to 0.005). Finally, Chapter 8 presents the main conclusions and recommendations for future research.

CHAPTER 2

CONVENTIONAL AND CONFOCAL MICRO-PIV: AN OVERVIEW

2.1 Introduction

Over the last 20 years, particle image velocimetry (PIV) has matured from its developmental stage to a reliable technique for macroscopic flows and is continuously expanding to a broad range of applications such as aeronautics, environmental and biomedical sciences (Adrian 1991, Raffel et al. 1998). Recently, this technique has been successfully extended to microscale flows by combining the conventional PIV system with an inverted epifluorescent microscope (Santiago et al. 1998). This combination, known as micro-PIV, has greatly increased the resolution of conventional PIV; as a result, this technique has gained widespread use in investigating the flow behaviour in microchannels (Koutsiaris et al. 1999, Meinhart et al. 1999, Klank et al. 2002, Sugii et al. 2002, Chiu et al.2003, Devasenathipathy et al. 2003, Shinohara et al. 2004). Very recently, considerable progress in the development of confocal microscopy and the advantages of this technique over conventional microscopy (Pawley 1990, Inoue and Inoue 2002, Wright and Wright 2002, Amos and White 2003) has led to a new technique known as confocal micro-PIV (Tanaami et al. 2002, Kinoshita et al. 2005, Lima et al. 2005, 2006) or confocal laser scanning microscopy (CLSM) micro-PIV (Park et al. 2004). In this chapter the most relevant theoretical and technical issues related to both conventional and confocal micro-PIV are discussed. In addition, a comparison between conventional and confocal micro-PIV is also presented. More detailed information on PIV and micro-PIV can be found in Adrian 1991, Raffel et al. 1998, Mielnik 2005.

2.2 Basic principle of PIV/PTV

2.2.1. Calculation methodology

The basic principle to calculate several physical parameters (displacement, velocity, etc) related to fluid mechanics is common for both PIV and micro-PIV. Generally, this technique consists in measuring the displacement of tracer particles flowing within the working fluid.

The classical way is to seed fluorescent microspheres that match the density of the working fluid. However, to measure blood flow, it is also common to use natural tracer particles such as RBCs and platelets. In order to obtain a reliable signal for image analysis, the blood cells are labelled with a fluorescent dye. It is worth saying that caution must be taken when labelling blood cells because it is a complex process which involves multiple physical and biochemical phenomena. By applying a powerful light source, the flow field of interest is illuminated and as a result particles separated by a known time interval (Δt) are recorded by high speed camera. By using a short Δt, it can be assumed that the magnitude and direction of the particles velocity are constant. As a result, the location of a particle on two consecutive images (x_i^t and $x_i^{t+\Delta t}$) can be used to estimate the particle instantaneous velocity as:

$$\vec{u} = \frac{x_i^{t+\Delta t} - x_i^t}{\Delta t} \quad (2.1)\,; \quad \vec{v} = \frac{y_i^{t+\Delta t} - y_i^t}{\Delta t} \quad (2.2); \quad V_p = \left(|\vec{u}|^2 + |\vec{v}|^2 \right)^{1/2} \quad (2.3);$$

where *u* and *v* are respectively the velocity components of the particle in the x and y direction, whereas Vp is the total velocity magnitude of the particle. The PIV conceptual principle is summarised in Figure 2.1.

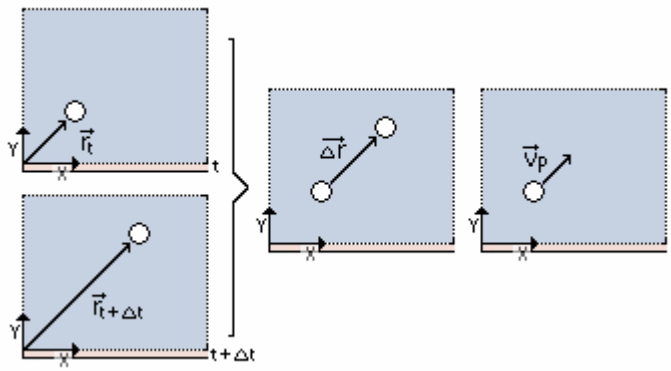

Figure 2.1 Conceptual principle for both PIV and PTV.

The methodology used to calculate the velocity of one particle can be extended to the entire flow field of interest. Although instantaneous velocities are crucial to study phenomenon at high Re and two-phase flows, in microfluidics it is common practice to average the instantaneous velocities over a large number of recorded image pairs (N usually bigger than 20). Hence, the time-average mean velocity vector of the flow can be defined as

$$\vec{U} = \frac{1}{N}\sum_{t=1}^{N} u_t \quad (2.4), \qquad \vec{V} = \frac{1}{N}\sum_{t=1}^{N} v_t \quad (2.5),$$

where N is the number of valid instantaneous velocity measurements, u and v are the time-average mean velocity components of the particle in the x and y directions, respectively

2.2.2 PIV vs PTV

The density of particles in the recorded images determines the most adequate PIV methodology to obtain the velocity fields. When the concentration of particles is high enough that every interrogation window contains at least three particles, this method is called high-image-density PIV mode (see Figure 2.2) (Adrian 1991). Because this is the most reliable way to calculate the velocity fields, this method is known as PIV cross-correlation or simply PIV. The velocity field is estimated by using a statistical technique known as cross-correlation (see Figure 2.5). The cross-correlation method is described in section 2.3.2.

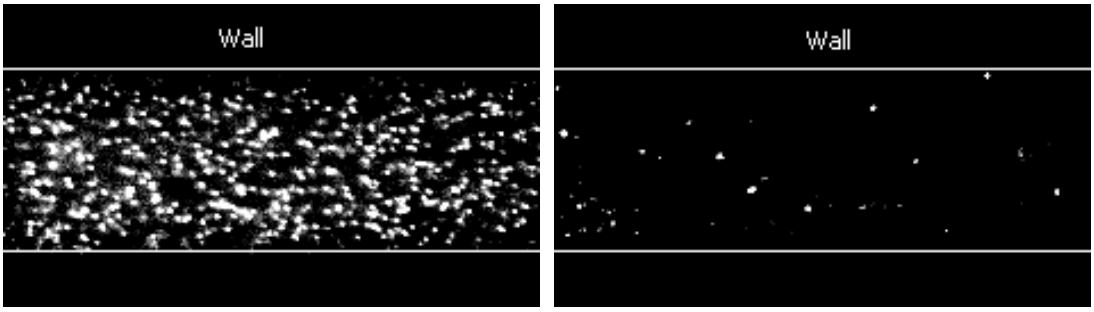

a) b)

Figure 2.2 Confocal a) high density image (pure water) and b) low density image (blood 30% Hct).

In some specific situations such as physiological fluids with high concentrations of cells, the amount of tracer particles captured within the fluid is often very low. If the number of particles within the interrogation area is small ($\lesssim 3$), it is recommended to measure the displacements by tracking individual particles in a Lagrangian way (see Figure 2.3). This kind of PIV mode (low-image-density PIV mode) is often referred as particle tracking velocimetry (PTV) or as single particle tracking (SPT) (Adrian 1991, Sbalzarini and Koumoutsakos 2005). The main advantage of this method is the ability to obtain detailed quantitative information on the motion of particles and cells flowing within the working fluid. This method is becoming indispensable in several biomedical fields such as cell biology and microcirculation. The main limitation of the PTV is to compute automatically multiple particles trajectories specially when there are continuous collisions of particles. In order to overcome this limitation manual tracking methods are often employed.

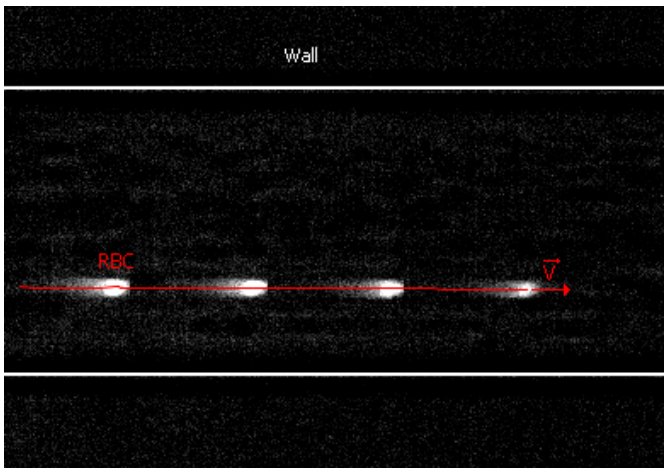

Figure 2.3 Trajectory of RBC flowing in a microchannel by using a particle tracking technique (MTj).

2.3 Conventional micro-PIV system

The main components of a conventional micro-PIV system consists of a microscope, a high resolution objective lens, optical filters, a high power light source for flow illumination (usually laser or mercury arc lamp) and a high speed camera.. A schematic illustration of a conventional micro-PIV is shown in Figure 2.4. In brief, the light enters the inverted microscope and is reflected 90° upwards by a dichromatic mirror to be transmitted through the objective lens which illuminates the entire flow volume. The objective lens collects the light emitted from fluorescent particles which travels back to the dichromatic mirror. This mirror filters out all reflected light (noise) only allowing to pass the emitted light from the tracer particles. Finally, the signals from the particles are recorded onto a high speed camera to be transferred to a computer for post-processing and image analysis.

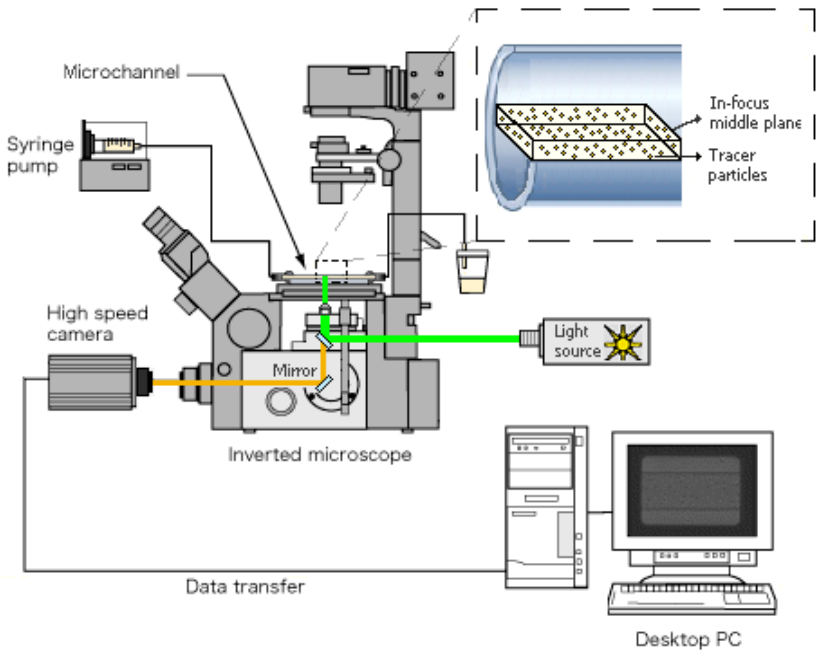

Figure 2.4. Experimental setup of a typical conventional micro-PIV system.

The resolution of a micro-PIV system is influenced by many factors such as out-of-focus particle images from volume illumination, density and size of the tracer particles, size and optical characteristics of the microchannel and image quality.

2.3.1 Volume illumination and depth of field

In liquid fluids two fundamental aspects differentiate micro-PIV from macroscopic PIV: as the tracer particles are reduced (usually from 1 μm to 0.1 μm), the Brownian motion of the particles may become significant and the flow is usually volume illuminated rather than a thin sheet of laser light (Sinton 2004). However, the errors due to Brownian motion can be significantly decreased by using particles bigger than 0.5 μm (Nguyen and Wereley 2002, Devasenathipathy et al. 2003). Hence, if we use particles diameters of 1 μm, the major error comes from the out-of-focus particles originated from the volume illumination of the fluid flow. The consequence of volume illumination is the fact that all the particles in the illuminated fluid volume (both in-focus and out-of-focus particles) will contribute for high background noise and consequent degradation of the velocity fields.

The depth of field is a very controversial parameter in conventional microscopy mainly because there are several definitions of when an object is considered to be unfocused. In the micro-PIV community the most accepted way to estimate the total depth of field was proposed by Meinhart and his co-workers (Meinhart et al. 2000a). By considering the contributions of diffraction, geometrical optics and finite size of the particle, they derived the following equation :

$$\delta z_m = \frac{3n\lambda_0}{NA^2} + \frac{2.16\, d_p}{\tan\theta} + d_p \qquad (2.6)$$

where δz_m is the measurement plane thickness, n is the refractive index of the imaging medium, λ_0 is the wavelength of light in a vacuum, NA is the numerical aperture of the objective lens, θ is the collection angle of the objective and d_p is the diameter of the tracer particles. From equation (2.6), it is clear that the numerical aperture of the objective lens and also the size of the particles strongly affect the δz_m .

The volume illumination leads to serious restrictions on both temporal and spatial resolution of conventional micro-PIV. This limitation is often overcome by using special image-processing techniques (Nguyen and Wereley 2002), ensemble correlation methods (Meinhart

et al. 2000b, Nguyen and Wereley 2002), power filter techniques (Bourdon et al. 2004) and a confocal micro-PIV system (Tanaami et al. 2002, Park et al. 2004, Kinoshita et al. 2005, Lima et al. 2005, 2006).

2.3.2 Cross-correlation methods

The PIV cross-correlation method is known as the most accurate way to obtain velocity fields and as a result it is the most popular method among the PIV research community. In brief, the PIV cross-correlation method is a statistical analysis that determines the average displacement by comparing the positions of the tracer particles within an interrogation area (image divided into a fine grid, usually less than 32 × 32 pixels) in two consecutive images. The cross-correlation function $R_{fg}(x, y)$ can be defined as (Rafael et al. 1998, Nguyen and Wereley 2002):

$$R_{fg}(x,y) = \sum_{i=1}^{p}\sum_{j=1}^{q} f(i,j)g(i+x, j+y), \qquad (2.7)$$

where p and q are the dimensions (in pixels) of the interrogation area, and $f(i,j)$ and $g(i,j)$ represent the grey value distribution of the first and second image, respectively. The cross-correlation function correlates images of particles in two consecutive interrogation areas (particle image pair). The displacement of a particle image pair corresponds to the highest peak in the correlation plane. This correlation peak consists of a series of peaks where the highest one usually corresponds to average particle displacement. Finally, by dividing this displacement by the known interval time between the images, the average velocity within the interrogation area is calculated (see Figure 2.5).

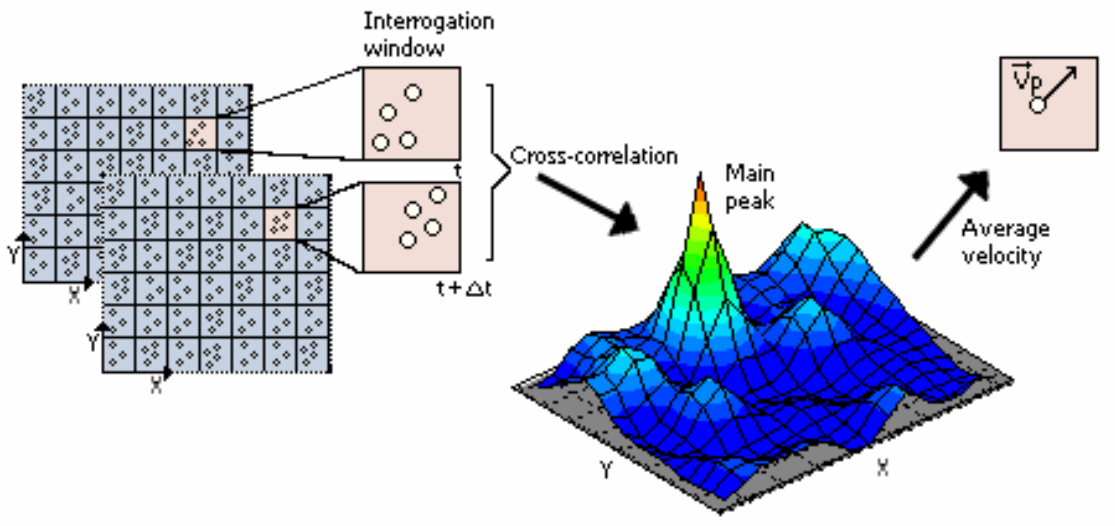

Figure 2.5 Cross-correlation PIV.

However, when small interrogation areas (usually less then 32 × 32 pixels) are used, random correlations can result in noisy peaks and can generate an erroneous velocity vector (outlier). To reduce measurement uncertainty and also to improve the signal-to-noise ratio, a multi-grid interrogation technique can be applied to the cross-correlation analysis (Rafael et al. 1998). The evaluation procedure of this advanced correlation technique is first based on a cross-correlation analysis at a relatively high correlation area (usually 32 × 32 pixels or more) in order to obtain an accurate estimation of the displacement and then the process is repeated at each pass by refining the interrogation area. By using this procedure, the displacement at a smaller interrogation area can be estimated with high accuracy and consequently high-resolution velocity vectors can be generated.

Another interrogation technique to reduce measurement uncertainty and the signal-to-noise ratio (SNR) is the multi-pass interrogation technique (Willert et al. 1996, Westerweel et al. 1997). The evaluation procedure is based on iterative cross-correlation analysis in which a multiple-pass algorithm is used to offset the interrogation area by the integer part of the particle image displacement (in pixel units) determined in a previous pass. Convergence is achieved when the residual displacement was less than one pixel, and as a result, reevaluation is not needed. Between each interrogation pass, an outlier search algorithm is used to filter intermediate results (Willert et al. 1996, Westerweel et al. 1997).

2.3.3 Signal-to-noise ratio (SNR)

The SNR can be defined as the highest peak image intensity divided by average peak intensity in the predefined interrogation window, and gives an indication of the quality of the correlation. Several parameters can influence the SNR such as the time between images, the size of the interrogation area, depth of field, the particle concentration and the test section depth.

Besides the influence of the depth of field, the concentration of tracer particles within the fluid and also the depth of the microchannel can significantly influence the SNR. Meinhart and his colleagues (Meinhart et al. 2000a) have demonstrated that the SNR can be improved by decreasing either the microchannel depth or the particle concentration. Another way to improve SNR is by using ensemble correlation methods.

2.3.4 Ensemble correlation methods

In PIV and micro-PIV, the classical way to obtain average velocity fields is by first measuring the instantaneous velocities and then averaging them in time. This approach is known as the average velocity method and has the advantage to calculate both instantaneous and average velocity fields (Willert et al. 1996, Meinhart et al. 2000b). The information provided by the instantaneous velocity measurements is extremely important to study transient phenomena that often happen in two-phase flows, such as blood flow in microcirculation.

In conventional micro-PIV, the volume illumination generates high background noise that can lead to inaccurate and unreliable velocity fields. In order to overcome this limitation, two methods were proposed: the average image method and the average correlation method (Meinhart et al. 2000b, Nguyen and Wereley 2002). These last two methods are frequently implemented in conventional micro-PIV as they improve the signal-to-noise ratio and consequently generate more accurate average velocity fields. However, by using these methods, the microscale phenomena often encountered in two-phase flows are lost through the averaging process. Although these methods may be appropriate to measure homogenous microfluidic flows to study more complex fluids, such as blood, the average velocity method seems to be most suitable.

2.4 Confocal micro-PIV system

The main components of a confocal micro-PIV system consists of a microscope combined with a confocal scanning unit (microlens-Nipkow disk confocal unit, CSU22), a high resolution objective lens, a high power light source for flow illumination (usually laser) and a high speed camera. A schematic illustration of a confocal micro-PIV is shown in Figure 2.6. In brief, the light emitted by the laser enters the confocal scanning unit (CSU22) and then is conducted to the inverted microscope to illuminate the microchannel from below the microscope stage. The light emitted from the flowing fluorescent particles travels back into the CSU22 scanning unit, where a dichromatic mirror reflects it onto a high-speed camera to record the confocal images.

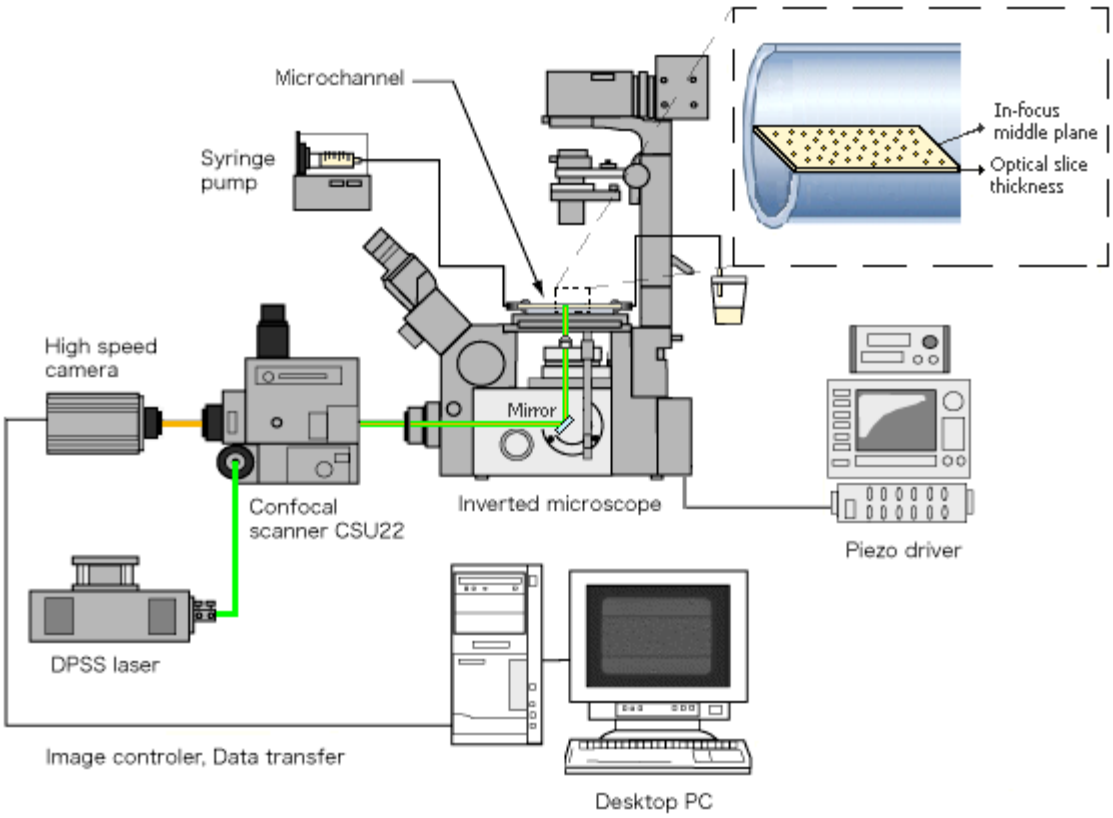

Figure 2.6 Experimental setup of our confocal micro-PIV system.

2.4.1 Confocal scanning unit (CSU-22)

In a conventional microscope, the entire depth or volume of the sample is illuminated continuously, which leads to the detection of out-of-focus emitted light, as well as light from the focal plane of interest. By contrast, with a confocal microscope, the sample is scanned using one or more very small spots that illuminate only the plane of focus at one time. In this way, the presence of suitably positioned confocal pinholes that act as a spatial filter, removes out-of-focus emitted light, improving the lateral and axial spatial resolution. This spatial filter is the key to create optical sectioning planes along the depth of the microchannel. Typically, the confocal microscope is combined with a laser light source and scanning system in order to generate the entire field. By repeating a series of scans for multiple focal planes, we can obtain a 3D image of the specimen (Pawley 1989, Inoue 2002, Wright 2002, Lima et al. 2006). However, conventional confocal microscopes use a point-scanning confocal system, which requires several seconds to generate a full-frame image. This is sufficient for scanning static specimens, but is very slow for studying microfluidics phenomena, such as blood flow. One way to overcome this speed limitation is to use a spinning disk confocal microscope, which uses a spinning disk or a Nipkow disk with several thousand pinholes usually arranged in a helical pattern. Since the disk spins very rapidly (1,800–5,000 rpm), it is possible to capture images in real time, which can be viewed directly or captured using a high-speed camera. In

brief, the scanning method in the CSU units developed by Yokogawa Electric consists of two disks connected axially: the upper disk has 20,000 micro-lenses and the lower one, known as a Nipkow disk, has 20,000 matching pinholes 50 μm in diameter. The excitation light that first passes through the micro-lenses is focused onto the corresponding pinhole and then illuminates the focal plane. Fluorescent light emitted from the focal plane is captured by the objective lens and focused back along the same path onto the Nipkow disk containing the pinhole array. The pinholes remove the out-of-focus light and a dichromatic mirror located between the two disks reflects the treated emitted light from the focal plane onto a high-speed camera to build the image (see Figure 2.7). As the disks spin very rapidly, thousands of spots of light are scanned simultaneously across the focal plane within a very short time. This produces a very clean image for every video frame and can be viewed directly by eye (Inoue 2002, Tanaami et al. 2002, Wright 2002). The first CSU unit developed by Yokogawa was the CSU10, which operates with a fixed disk speed of 1,800 rpm and can acquire up to 120 full frame images every second (Inoue 2002, Tanaami et al. 2002, Park et al. 2004). However, this scanning rate limits the application of this type of confocal microscope to study high-speed flows. To overcome this temporal resolution limitation, Yokogawa recently developed a new scanning unit known as the CSU22, in which the rotation speed of the Nipkow disk can be set from 1,800 to 5,000 rpm, making it possible to acquire confocal images at up to 2,000 frames per second (Inoue 2002, Tanaami et al. 2002). Another remarkable innovation is the incorporation of a high-speed objective lens actuator (piezo-driver) allowing the accurate capture of full-frame optical sectioned images along the depth of the microchannel (z-axis). Note that this system has submicron z-direction resolution and can be controlled via computer.

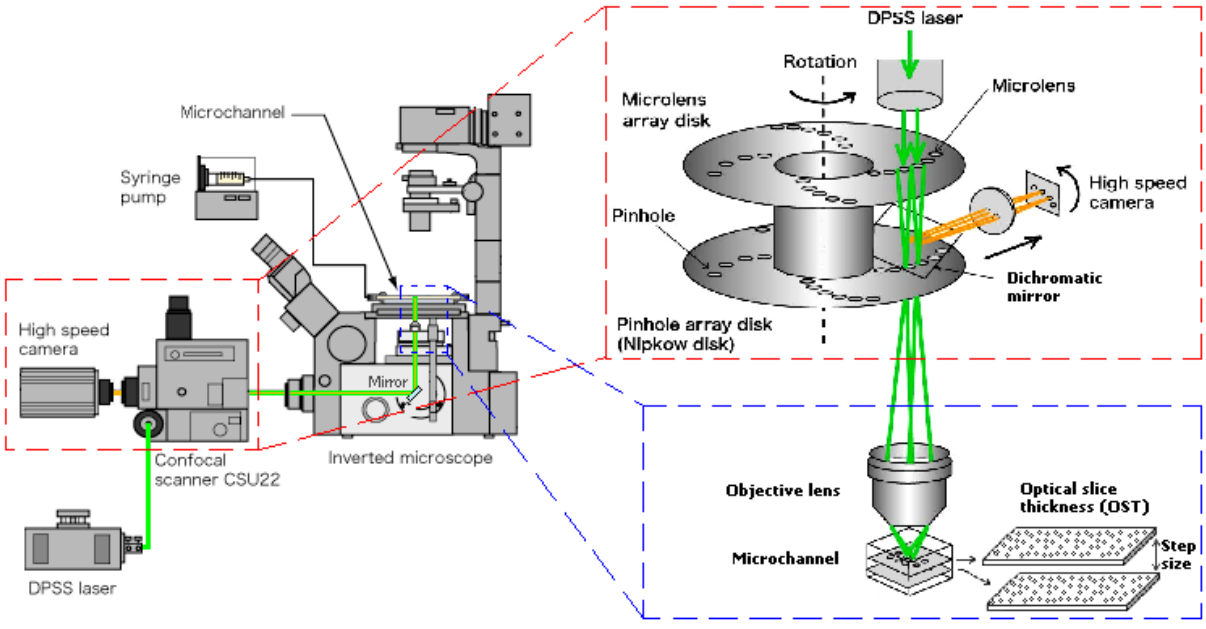

Figure 2.7 Principle of the Confocal scanning unit (CSU-22).

2.4.2 Spatial resolution and optical slice thickness (OST)

Confocal microscopy is a well established technique for many biomedical research applications mainly because of its unique optical sectioning capability. As a result, several researchers have developed analytical expressions for spatial resolution using confocal microscopes, including Inoue (1989), Webb (1996), and Willhelm et al. (2003). One way to obtain lateral resolution, axial resolution, and optical slide thickness is to use the concept of resolution probability proposed by Willhelm et al. (2003).

The image formed by a point of light in the focal plane is not an ideal point object because the point is always distributed over a possible area within the image plane. As a result, the image properties of an optical system can be described using the point spread function (PSF), which represents the light intensity distribution on the image plane. This distribution has a higher probability at the centre (higher light intensity) and a lower probability at the outside (lower light intensity) (Willhelm et al. 2003).

Resolution can be defined as the ability to distinguish two point objects from each other (Wright and Wright 2002). In confocal microscopy, the pinhole plays an important role in calculating spatial resolution. Since the modified pinhole diameter (MPD = PD/M) can be defined as the pinhole diameter (PD in μm) divided by the magnification (M), the airy unit (AU) can be obtained using the following equation (Willhelm et al. 2003, Park et al. 2004)

$$AU = \frac{1.22\lambda_{ex}}{NA} \qquad (2.8)$$

where λ_{ex} is the wavelength of the illuminating laser light and NA is the numerical aperture of the microscopic objective lens. It is possible to determine the spatial resolution of the confocal system by applying the following criteria:

if MPD > 1.0 AU, apply geometric-optical analysis;
if MPD < 0.25 AU, apply wave-optical analysis (Willhelm et al. 2003).

By using the CSU-22, the diameter of each pinhole was optimized to 50 μm, which implies that by using magnification up to 60× and NA>0.75, the geometric–optical analysis should be followed. Hence, by using the geometric–optical analysis, it is possible to calculate the spatial resolution of the confocal system by applying the following equations (Willhelm et al. 2003):

$$R_l = \frac{0.51\lambda_{ex}}{NA} \tag{2.9}$$

$$R_a = \frac{0.88\lambda_{ex}}{n - \sqrt{n^2 - NA^2}} \tag{2.10}$$

$$OST = \sqrt{\left(\frac{0.88\lambda_{em}}{n - \sqrt{n^2 - NA^2}}\right)^2 + \left(\frac{\sqrt{2}n \cdot MPD}{NA}\right)^2} \tag{2.11}$$

where R_l is the lateral resolution, R_a is the axial resolution, OST is the optical slice thickness, λ_{em} is the emission wavelength, and n the refractive index of the immersion liquid. A full description of these equations can be found in Willhelm et al. (2003).

In the present work, we have used two kinds of dry objective lenses: 20×–0.75 NA and 40×–0.9 NA. Generally, by increasing the magnification (M), both spatial resolution and OST can be significantly improved however parameters such as the working distance and the field of view will be reduced. Hence, the selection of the objective lens requires careful considerations regarding the design of the microchannel and flow rate.

2.4.3 Consequences of using the CSU-22

The main advantage of using a confocal spinning disk (CSD) is its ability to obtain thin in-focus images. As a result confocal micro-PIV systems have potential to obtain three-dimensional information about the fluid flow and also to obtain detailed flow-field measurements. In this way it is possible to study transient phenomena that often occurs in two-phase flows (such as blood flow) by using the information provided by the instantaneous velocities.

Although the advantages of using the CSU-22 are evident, the fraction of illuminating light that makes through to moving pinholes to the tracer particles is reduced to about 60% (Conchello and Lichtman 2005) which decreases the temporal resolution of the confocal systems. In addition several other factors may also contribute to the reduction of the temporal resolution: rotation speed limit of the Nipkow disk, type of working fluid and microchannel.

The scanning unit CSU-22 from Yokogawa allows the acquisition of images at up to 2,000 frames/s, which corresponds to a time interval of 0.5 ms between a pair of images. Although this temporal resolution can be achieved using pure water, the images recorded using in vitro

blood were too dark to be processed. However, by decreasing the temporal resolution to 200 frames/s, the incident illumination light that passes through the pinholes was enough to successfully measure velocities up to 0.52 mm/s.

2.5 Comparison between conventional and confocal micro-PIV

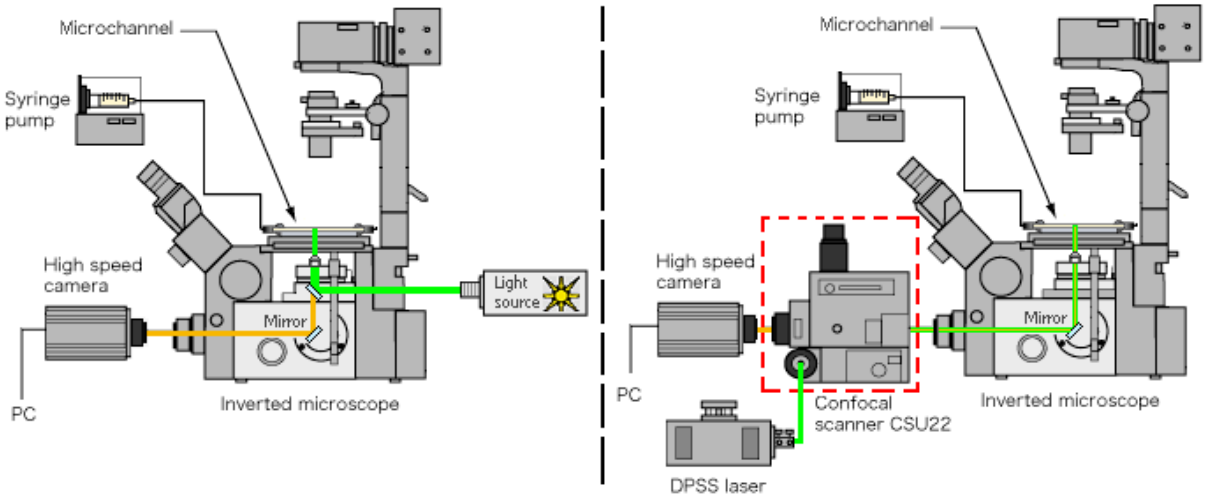

a) b)

Figure 2.8 Main components of a) conventional micro-PIV, b) confocal micro-PIV system.

Figure 2.8 shows the main components of both conventional and confocal micro-PIV. It is clear that main difference between the two systems is the inclusion of the CSU-22 in the confocal system. A study to compare both systems was performed under the same flow conditions. The flow measurements were performed in a 100 μm glass square microchannel where pure water (PW) seeded with 0.15% tracer particles was pressure driven by means of syringe pump (Re ~ 0.014). The contribution of CSU-22 on the flow measurements is clearly demonstrated in Figure 2.9. Note that for the case of the conventional micro-PIV the measurements were obtained by using epi-fluorescent microscope equipped with a mercury lamp and color filters.

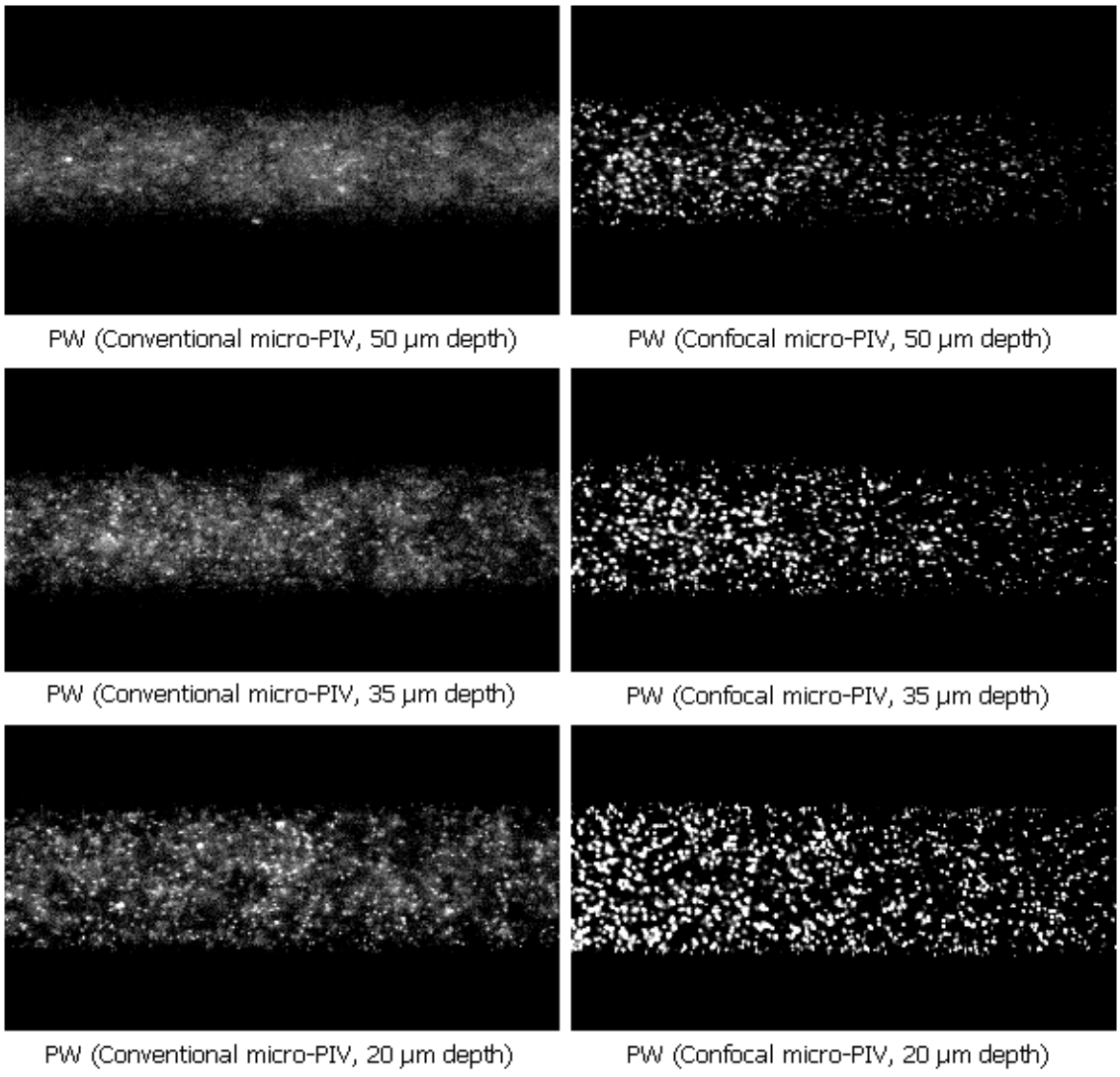

Figure 2.9 Comparison of particle images from both conventional and confocal micro-PIV at several depths for pure water (PW).

From Figure 2.9, it is evident that by using the CSU-22 it is possible to obtain much clearer image definition of the individual particles located within the in-focus plane of interest. Hence, the confocal system reduces blurring and eliminates most of the out-of-focus background noise and as a result increases the contrast and information capacity of an image. In contrast, the images recorded by the conventional system were largely blurred, since the out-focus-light reduces contrast and decreases resolution making difficult to discern the tracer particles within the flow. It is worth saying that the conventional microscopic images may be improved by using a more powerful light source, i. e., laser. In addition, it is also possible to observe that the resolution of images has tendency to be improved by decreasing the depth of the measurement plane. These observations are in close agreement with the results obtained by Meinhart et al. (2000a).

The signal-to-noise ratio (SNR) from the images recorded in middle plane of the microchannel was also calculated (see Figure 2.10). The results show higher SNR for the confocal images which reflects the high-quality images produced by the confocal system.

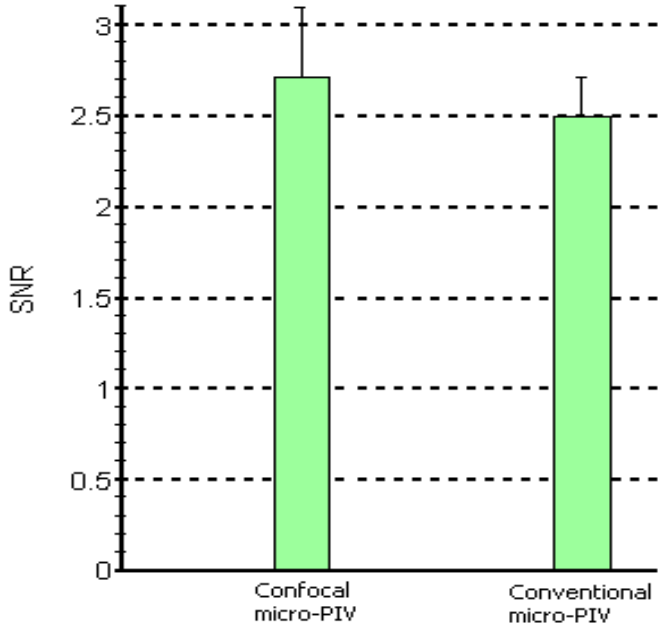

Figure 2.10 SNR from both confocal and conventional micro-PIV.

2.5.1 Background noise rejection

Figure 2.11 shows clearly the ability of both spinning disk confocal microscope (SDCM) and single aperture confocal microscope (SACM) to reduce the background noise from the out-of-focus planes. By using a conventional microscope the intensity of the particles within the out-of-focus planes does not change with the distance from the in-focus plane. In contrast, for the case of SDCM the brightness of tracer particles decreases dramatically, specially at distances very close (1 μm) to the in-focus plane. This dramatic improvement on the background noise rejection can be seen in Figure 2.9. As a result, the removal of the unwanted light provides greater contrast of the tracer particles and permits the generation of true thin optical sections.

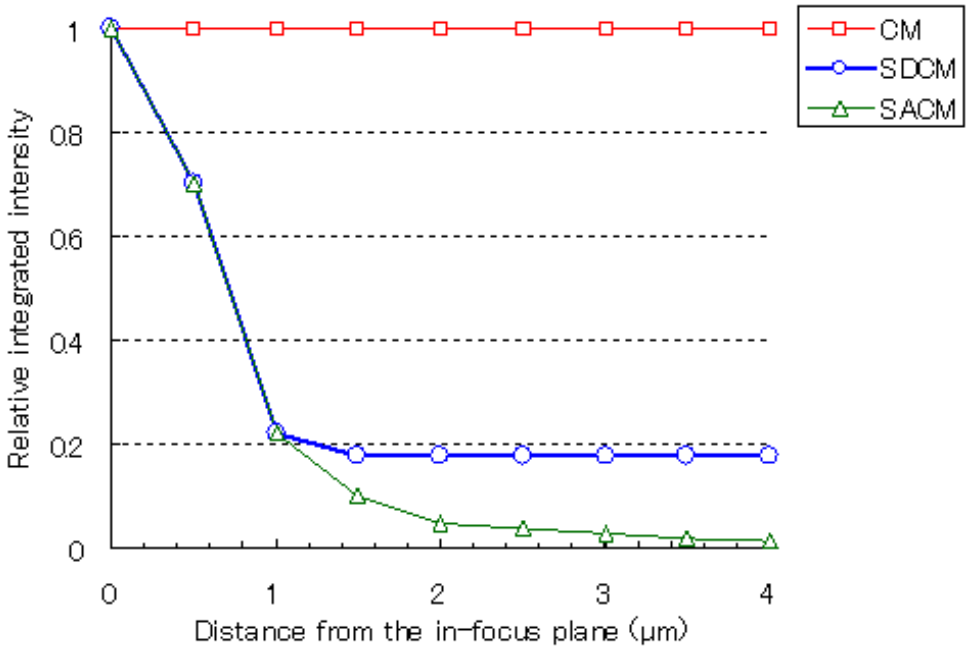

Figure 2.11 Comparison of the background noise rejection of the spinning disk confocal microscope (SDCM) with a conventional microscope (CM) and single aperture confocal microscope (SACM) (adapted from Conchello and Lichtman 2005).

2.5.2 Optical resolutions, depth of field and optical slice thickness (OST)

Table 2.1 and Figure 2.12 compare the theoretical optical resolutions and volume depth from both conventional and confocal micro-PIV systems. Generally, it is possible to observe that the resolution improves by using a confocal system. The improvement is more pronounced in the measurement volume depth. Under the same experimental conditions, the effective measurement volume depth (from equation 2.6) is strongly influenced by the tracer particle size. As a result, when using conventional micro-PIV, it is recommended to use particles less than 1μm. When using RBCs as tracer particles, the depth of field is estimated to be around 37.66 μm which makes this option not to be most suitable technique to study blood flow at low Re. In contrast, by using a confocal system, as already mentioned, it is possible to obtain true optical sections which are not affected by the tracer particle size. Hence, we believe that a confocal micro-PIV system is the best suitable technique to study the flow behaviour of blood in microcirculation.

Table 2.1. The optical resolutions, depth of field and optical slice thickness (OST) for 40× objective lens, NA = 0.9, n = 1, λ_{ex} = 532 nm and λ_{em} = 612 nm (Willhelm et al. 2003, Park et al. 2004).

	Conventional micro-PIV equations	Conventional micro-PIV Tracer Particle diameter (μm) 0.2	1	4	8	Confocal micro-PIV
Lateral resolution (μm)	$\frac{0.61\lambda_{em}}{NA}$	0.42				0.35
Axial resolution (μm)	$\frac{2n\lambda_{em}}{NA^2}$	1.51				0.83
OST (μm) (Eq. 2.11)	---	---	---	---	---	2.1
Depth of field (μm)	Equation 2.6	2.86	6.43	19.82	37.66	---

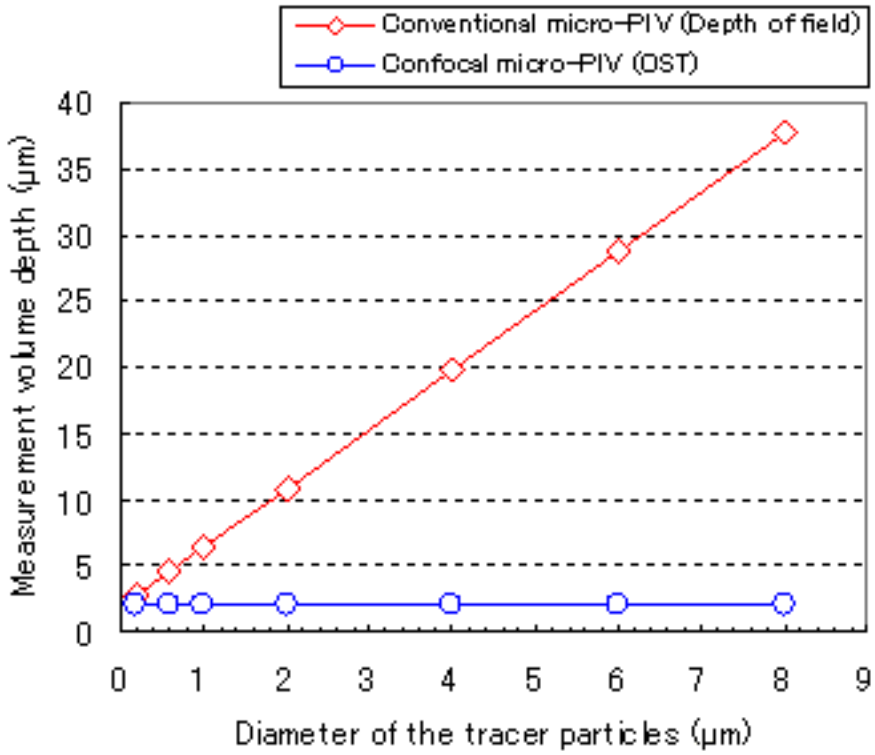

Figure 2.12. Theoretical measurements of the volume depth as function of tracer particles diameter.

2.6 Applications of micro-PIV in microcirculation

Since the first successful applications of PIV to microscale flows (Santiago et al. 1998, Koutsiaris et al. 1999, Meinhart et al. 1999), this technique has gained widespread use for studying the flow behaviour in several research fields in science and engineering. In the biomedical field, Sugii and his co-workers, by using a conventional micro-PIV system, they have used red blood cells (RBCs) as tracer markers to measure their velocities in both straight

(Sugii et al. 2002) and bifurcated arterioles (Nakano et al. 2003) and they found that the velocity profiles were markedly blunt in the central region. However, later they measured both tracer particles and RBCs through a 100 μm glass capillary and they reported that by using in vitro blood with about 20% Hct the velocity profiles were parabolic (Sugii et al. 2005). By using a microchannel close to a rectangular shape, Bitsch and his co-workers (Bitsch et al. 2005) have reported blunt profiles. More recently, by using liposomes tracer particles the blood-plasma velocity was measured in the beating heart of a chicken embryo (Vennemann et al. 2006). Kim and Lee (2006) have analysed the flow behaviour of blood through a circular opaque microchannel by using an X-ray PIV technique. Their measurements have shown typical non-Newtonian flow characteristics of blood such as yield stress and shear-thinning effects. In addition, Chiu et al. (2003) have also applied the conventional micro-PIV system to analyse the effect of flow in monocyte adhesion to endothelial cells cultured in a vertical step flow chamber.

In conclusion, most of the findings related to the blood flow dynamics by using conventional micro-PIV, have yielded conflicting results. In addition, presently we have no detailed information on the microscale flow behavior of RBCs in microvessels. The present work applies for the first time a confocal micro-PIV/PTV system to study blood flow behavior through microchannels.

CHAPTER 3

CONFOCAL MICRO-PIV MEASUREMENTS OF THREE-DIMENSIONAL PROFILES OF CELL SUSPENSION FLOW IN A SQUARE MICROCHANNEL

3.1 Introduction

The flow of blood in the microcirculation (microvessels less than 300 μm in diameter) is characterized mainly by the flow of red blood cells (RBC), which may be normal or pathological. Despite the large amount of microcirculation research, there is no detailed experimental information on flow velocity profiles, RBC deformability, or aggregation in microvascular networks (Lee 2000, Mchedlishvili and Maeda 2001, Lipowsky 2005). This lack of knowledge is mainly due to the absence of an adequate technique with high spatial and temporal resolution to measure fluid mechanics effects at the microscopic level.

Most research in this area has involved experimental studies using optical techniques mainly because they are less invasive for measuring the flow field. One of the most popular optical techniques is particle-based flow velocimetry, in which the flow is seeded with trace particles. Several techniques are used to acquire particle data, such as laser Doppler velocimetry (LDV), particle streak velocity (PSV), and particle image velocimetry (PIV) (Sinton 2004). The most widely used method is PIV, which is a well established technique for measuring macroscopic fluidics (Raffel et al. 1998). Recently, this technique has been successfully extended to microscale flows by combining the conventional PIV system with an inverted epifluorescent microscope (Santiago et al. 1998). This combination, known as micro-PIV, has greatly increased the resolution of conventional PIV; as a result, this technique has gained widespread use in investigating the flow behavior in microfluidic devices (Koutsiaris et al. 1999, Meinhart et al. 1999, Klank et al. 2002, Sugii et al. 2002, Chiu et al.2003, Devasenathipathy et al. 2003, Shinohara et al. 2004). However, using conventional microscopes, the entire flow field is illuminated. Consequently, the out-of-focus emitted light can result in high levels of background noise, which degrades the measured velocity fields (Meinhart et al. 1999, 2000, Nguyen and Wereley 2002).

Recently, considerable progress in the development of confocal microscopy and the advantages of this technique over conventional microscopy (Pawley 1990, Inoue and Inoue 2002, Wright and Wright 2002, Amos and White 2003) has led to a new technique known as confocal micro-PIV (Tanaami et al. 2002, Kinoshita et al. 2005, Lima et al. 2005) or confocal laser scanning microscopy (CLSM) micro-PIV (Park et al. 2004). This method combines the conventional PIV system with a spinning disk confocal microscope (SDCM). By combining its outstanding spatial filtering technique with a multipoint illumination system, this microscope has the ability to obtain in-focus images with optical thickness less than 1 μm (optical sectioning effect), which is extremely difficult to achieve using conventional microscopy. By combining SDCM with the conventional PIV system, it is possible to achieve a PIV system with an extremely high spatial resolution able to generate 3D velocity profiles. Very recently, Park et al. (2004) compared confocal micro-PIV with conventional micro-PIV and demonstrated that the former has improved particle image contrast and definition, allowing more accurate velocity measurements. However, they did not explore its optical sectioning capability for generating 3D velocity profiles, and more importantly, all their experiments used homogeneous fluids. To our knowledge, no study has evaluated the ability of a confocal micro-PIV system to investigate phenomena in nonhomogeneous fluids, such as a cell suspension. Moreover, the system Park et al. (2004) used had a high spatial accuracy, but a low temporal resolution (up to 120 frames per second), which limited the applicability of their system for studying microcirculation phenomena.

The aim of the present study is to evaluate the performance of our confocal micro-PIV system in order to investigate its ability to study the behavior of a blood cell suspension fluid within a square microchannel. In addition, this is the first attempt to obtain 3D profiles using the optical sectioning capability of a confocal micro-PIV system.

3.2 Materials and Methods

3.2.1 Working fluids

It is general practice to use a well known Newtonian fluid to evaluate the performance of a new measurement technique. In this study, pure water (PW) was used as our working reference fluid to analyse the performance of the confocal micro-PIV system. The flow through the microchannel was measured by seeding the flow with particles. These particles should scatter light efficiently and be sufficiently small compared to the dimensions of the

microchannel. To avoid Brownian motion, the particles should be bigger than 500 nm (Santiago et al. 1998, Nguyen and Wereley 2002, Devasenathipathy et al. 2003). By selecting particles with a nominal diameter of 1 μm, we expected to reduce the effect of Brownian motion substantially.

This study examined two working fluids (see Table 3.1): PW and Hanks solution (HS) containing about 4% (by volume) human red blood cells (RBCs). Both fluids were seeded with 0.1% (by volume) 1 μm diameter red fluorescent solid polymer microspheres (R0100; Duke Scientific, Palo Alto, CA, USA). The blood used was collected from a healthy adult, heparin was added to prevent coagulation, and it was stored hermetical at 4ºC until the experiment was performed at room temperature (25± 2ºC).

3.2.2 Square microchannel

Rectangular microchannels have become popular for studying blood flow phenomena *in vitro* under physiological flow conditions. Laminar flow through such channels generates a purely axial flow. As a result, the performance of a new measurement flow technique is commonly evaluated using rectangular microchannels (Kroll et al. 1996, Meinhart et al. 1999, Brown 2000). In this study, we used a 100 × 100 μm borosilicate glass microchannel fabricated by Vitrocom (Mountain Lakes, NJ, USA), in which the flow behavior is very similar to the flow through capillaries. A schematic of the square microchannel is shown in Figure 3.1. The microchannel was mounted on a slide glass approximately 120 μm thick, which was immersed in pure water to minimise the refraction from the walls of the microchannel.

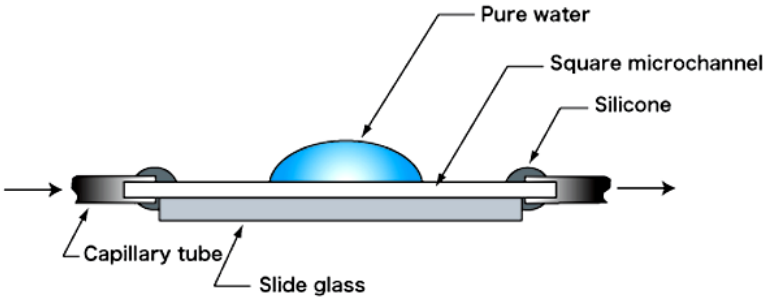

Figure 3.1 The components of the square microchannel device.

3.2.3 Confocal micro-PIV system and experimental setup

The system combines a confocal spinning disk microscope with the conventional PIV technique. For simplicity, we call our system confocal micro-PIV. Some researchers also call it confocal laser scanning microscopy (CLSM) micro-PIV (Park et al. 2004). The confocal

micro-PIV system we used consists of an inverted microscope (IX71; Olympus, Tokyo, Japan) combined with a confocal scanning unit (CSU22; Yokogawa, Tokyo, Japan) and a diode-pumped solid-state (DPSS) laser (Laser Quantum, Cheshire, UK) with an excitation wavelength of 532 nm. A high-speed camera (Phantom v7.1; Vision Research, New Jersey, USA) was connected to the outlet port of the CSU22 (see Figure 3.2). The microchannel was placed on the stage of the inverted microscope and the flow rate of the working fluid was kept constant at 0.15 μl/min using a syringe pump (KD Scientific, Holliston, MA, USA). The Reynolds number used in our experiment was 0.025, and the entrance length (*Le*) was 65 μm, since $Le = 1.3 \times (\text{width}/2)$ (Fung 1997). By making the measurements in the middle of the microchannel, we assured that the velocity profiles were fully developed at the site of recording.

The laser beam illuminated the microchannel from below the microscope stage through a dry 20× objective lens with a numerical aperture (NA) of 0.75. Satisfactory illumination was achieved by seeding 1 μm diameter fluorescent particles, which absorb green light (absorbance peak 542 nm) and emit red light (emission peak 612 nm). The light emitted from the flowing fluorescent particles passes through a colour filter into the CSU22 scanning unit, where a dichromatic mirror reflects it onto a high-speed camera to record the PIV images. Although the camera we used can record images at a rate of 2,000 frames/s, these images were too dark to process because of the low exposure time of the particles. For this reason and because of the complex fluid (HS with 4% RBCs) used in our study, we decided to capture images with a resolution of 640 × 480 pixels and 12-bit greyscale, at a rate of 200 frames/s with an exposure time of 4,995 μs. By recording the images for a period of approximately 0.5 s at a rate of 200 frames/s, the temporal resolution of the measurements was 5 ms. After recording the images, they were digitized and transferred to a computer for evaluation using Phantom camera control software (PH607). The PIV images of the flowing particles were processed and the flow velocity was determined using PivView version 2.3 (PivTec GmbH, Goettingen, Germany) (Rafael et al. 1998). The images were evaluated using a cross-correlation method, where the time between two images was set to 20 and 5 ms for pure water and the blood suspension, respectively. By using a multiple-pass interrogation algorithm with 24 × 16 pixel interrogation window (vertical and horizontal overlap of 50%), which corresponds to a spatial resolution of 28.24 × 18.83 μm, it was possible to obtain the corresponding velocity vector fields.

The confocal micro-PIV system has the unique capability to acquire a series of optical sections along the *z*-axis. To obtain optical sectioned images, we used a 3D system (RT3D; Yokogawa), consisting of a RT3D signal and a low-voltage piezoelectric translator (LVPZT) controller. By combining the RT3D system with the CSU22, it is possible to generate optical sectioned images with a step size (distance between optical sections; Wright and Wright 2002) as small as 1 μm under computer control.

Table 3.1 Experimental parameters used in this study.

Height × width × length of the microchannel	100 μm × 100 μm × 50mm
Flow rate	0.15 μl/min
Reynolds number	0.025
Particle diameter	1 μm
Particle concentration (PW)	0.1% solids
Particle concentration (HS 4% RBCs)	0.1% solids

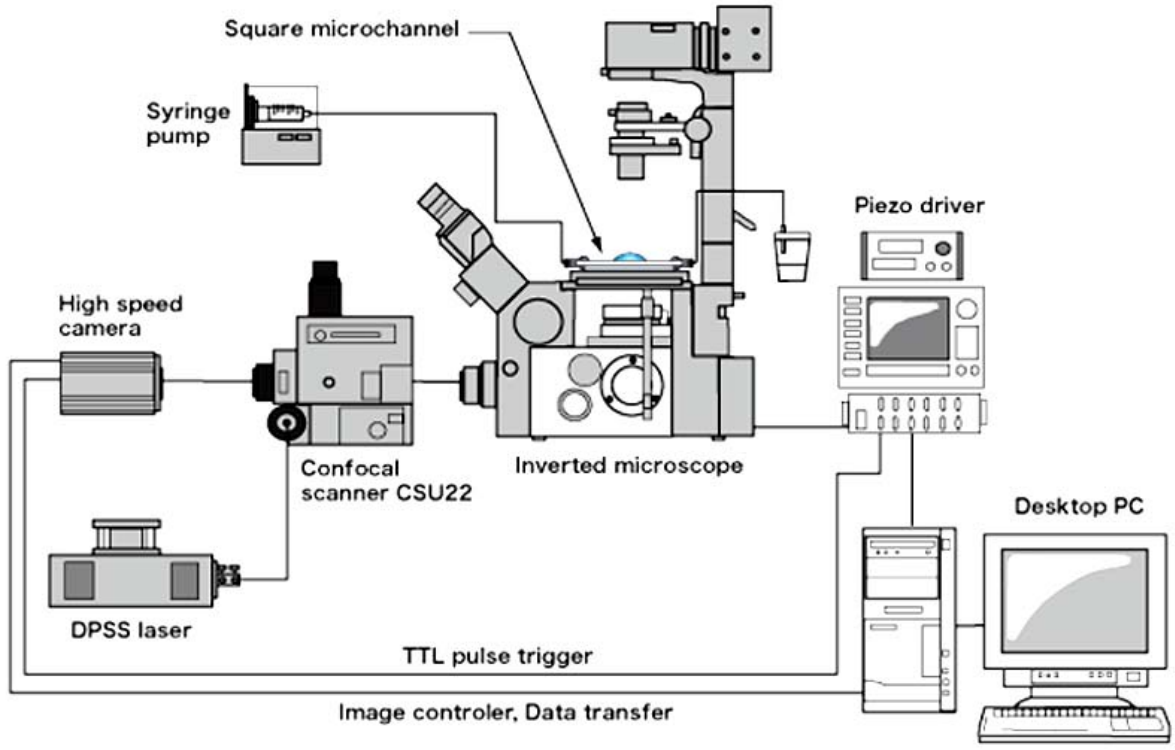

Figure 3.2 Experimental setup of the confocal micro-PIV system.

3.2.3.1 Spinning disk confocal microscope

In a conventional microscope, the entire depth or volume of the sample is illuminated continuously, which leads to the detection of out-of-focus emitted light, as well as light from the focal plane of interest. By contrast, with a confocal microscope, the sample is scanned using one or more very small spots that illuminate only the plane of focus at one time. In this way, the presence of suitably positioned confocal pinholes that act as a spatial filter, removes

out-of-focus emitted light, improving the lateral and axial spatial resolution. This spatial filter is the key to create optical sectioning planes along the depth of the microchannel. Typically, the confocal microscope is combined with a laser light source and scanning system in order to generate the entire field. By repeating a series of scans for multiple focal planes, we can obtain a 3D image of the specimen (Pawley 1989, Inoue 2002, Wright 2002, Park et al. 2004). However, conventional confocal microscopes use a point-scanning confocal system, which requires several seconds to generate a full-frame image. This is sufficient for scanning static specimens, but is very slow for studying microfluidics phenomena, such as blood flow. One way to overcome this speed limitation is to use a spinning disk confocal microscope, which uses a spinning disk or a Nipkow disk with several thousand pinholes usually arranged in a helical pattern. Since the disk spins very rapidly (1,800–5,000 rpm), it is possible to capture images in real time, which can be viewed directly or captured using a high-speed camera. In brief, the scanning method in the CSU units developed by Yokogawa Electric consists of two disks connected axially: the upper disk has 20,000 micro-lenses and the lower one, known as a Nipkow disk, has 20,000 matching pinholes 50 μm in diameter. The excitation light that first passes through the micro-lenses is focussed onto the corresponding pinhole and then illuminates the focal plane. Fluorescent light emitted from the focal plane is captured by the objective lens and focussed back along the same path onto the Nipkow disk containing the pinhole array. The pinholes remove the out-of-focus light and a dichromatic mirror located between the two disks reflects the treated emitted light from the focal plane onto a high-speed camera to build the image (see Figure 3.3). As the disks spin very rapidly, thousands of spots of light are scanned simultaneously across the focal plane within a very short time. This produces a very clean image for every video frame and can be viewed directly by eye (Inoue 2002, Tanaami et al. 2002, Wright 2002). The first CSU unit developed by Yokogawa was the CSU10, which operates with a fixed disk speed of 1,800 rpm and can acquire up to 120 full frame images every second (Inoue 2002, Tanaami et al. 2002, Park et al. 2004). However, this scanning rate limits the application of this type of confocal microscope to studying high-speed flows. To overcome this temporal resolution limitation, Yokogawa recently developed a new scanning unit known as the CSU22, in which the rotation speed of the Nipkow disk can be set from 1,800 to 5,000 rpm, making it possible to acquire confocal images at up to 2,000 frames per second (Inoue 2002, Tanaami et al. 2002). Another very remarkable innovation is the incorporation of a high-speed objective lens actuator allowing the accurate capture of full-frame optical sectioned images along the depth of the microchannel (*z*-axis). Note that this new function has submicron *z*-direction resolution and can be controlled via computer. In our

experiment, we used this outstanding new scanning system to investigate blood fluid mechanics.

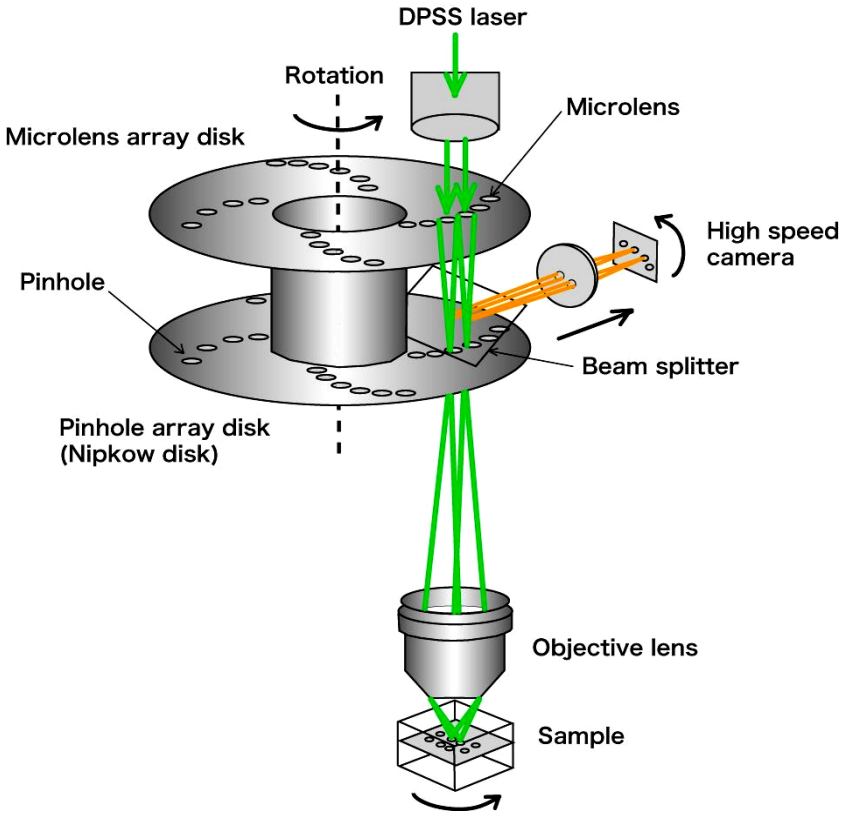

Figure 3.3 Principle of the spinning disk confocal microscope.

3.2.4 Spatial resolution and optical slice thickness of the confocal micro-PIV system

As noted, the spatial filtering performed by the pinhole apertures enables optical sectioning. This optical sectioning capability enabled us to obtain a series of optical sections at different focal planes, which provides 3D information about the spatial structure of the specimen (see Figure 3.4). It is generally agreed that the quality and accuracy of this information depends on the optical section thickness and on the distance between optical sections (step size). According to Wright (2002) and Willhelm et al. (2003), the optical section thickness should be smaller than the step size. In this way, when using a confocal micro-PIV system, it is crucial not only to determine the lateral and axial image resolution, but also the optical slice thickness. Note that for a conventional micro-PIV system, out-of-plane is usually associated with the depth of the field (Meinhart et al. 2000, Nguyen and Wereley 2002, Shinohara et al. 2004), while in the confocal micro-PIV, it is related to the optical slice thickness. A more detailed comparison of conventional and confocal micro-PIV systems can be found elsewhere (Park et al. 2004).

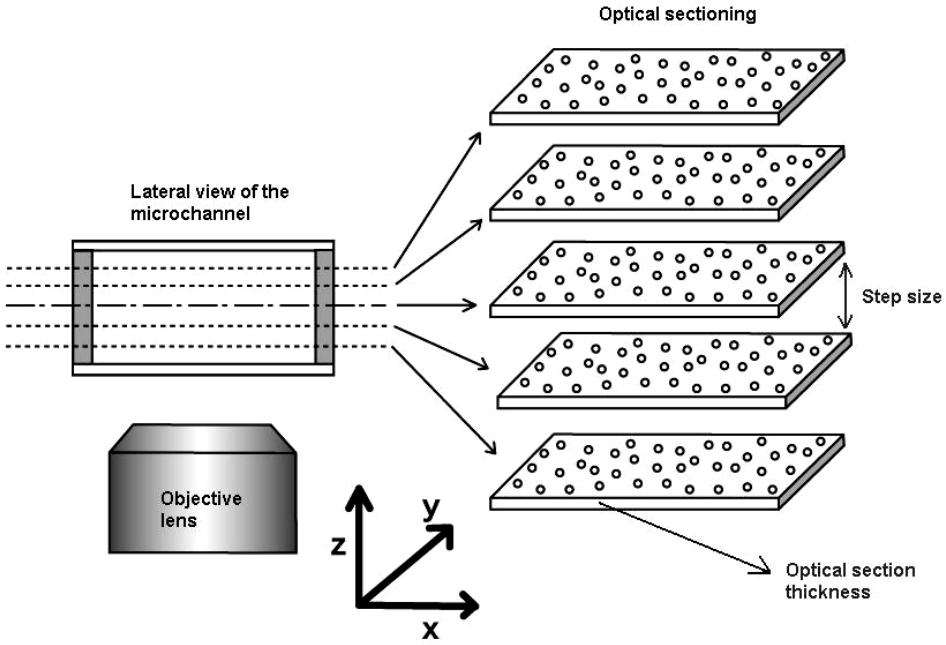

Figure 3.4 The principle of optical sectioning used for PIV measurements.

Confocal microscopy is a well established technique for many biomedical research applications mainly because of its exclusive, unique optical sectioning capability. As a result, several researchers have developed analytical expressions for spatial resolution using confocal microscopes, including Inoue (1989), Webb (1996), and Willhelm et al. (2003). One way to obtain lateral resolution, axial resolution, and optical slide thickness is to use the concept of resolution probability proposed by Willhelm et al. (2003). Tables 3.2 and 3.3 show the optical parameters used in this study and the estimated spatial resolution and optical slice thickness determined using the equations presented in Appendix A. A full description of the equations presented in Appendix A can be found in Willhelm et al. (2003).

Table 3.2 Optical parameters used in this study.

λ_{ex} excitation wavelength	532 nm
λ_{em} emission wavelength	612 nm
Refraction index (n)	1
Magnification (M)	20×
Numerical aperture (NA)	0.75
Airy unit (AU)	0.865
Pinhole diameter (PD)	50 μm
Modified pinhole diameter (MPD)	2.5μm

Table 3.3 Spatial resolution and optical slice thickness of the confocal micro-PIV system.

Lateral resolution (R_l)	0.36 μm
Axial resolution (R_a)	1.4 μm
Optical slice thickness (OST)	4.97 μm

From the estimated results shown in Table 3.3, it is possible to verify that the confocal system used in this study can achieve a high spatial resolution. The optical slice thickness (OST) can be reduced substantially by increasing the magnification objective (M), NA, and *n*. For example, by using an oil immersion 60×–0.9 NA objective lens, it is possible to obtain an OST less than 1 μm. In our study, we used a dry 20×–0.75 NA objective lens because it has a higher working distance and provides a larger field of view, allowing stronger irradiance onto the light detector. As a result, it was possible to cover the entire width of our microchannel with high spatial resolution and obtain adequate quality images along the depth of the square microchannel.

3.3 Results

3.3.1 Performance of the confocal micro-PIV

The confocal micro-PIV system was first evaluated by comparing the experimental results with a well established analytical solution for steady flow through a long, straight, rigid rectangular microchannel, *i.e.*, Poiseuille flow. We compared the experimental results using the confocal micro-PIV with a described analytical solution (Bruus 2004) for a rectangular microchannel.

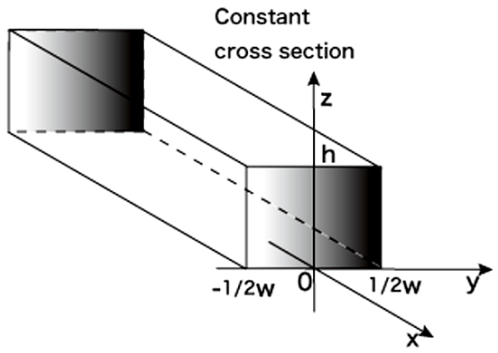

Figure 3.5 Main parameters of the rectangular microchannel.

By solving the Navier–Stokes equation with a constant pressure gradient along the rectangular microchannel (see Figure 3.5) and considering no-slip boundary conditions at the wall, the velocity field can be expressed as:

$$u_x(y,z)=\frac{48Q}{\pi^3 hw}\frac{\sum_{n,odd}^{\infty}\frac{1}{n^3}\left[1-\frac{\cosh(n\pi\frac{y}{h})}{\cosh(n\pi\frac{w}{2h})}\right]\sin(n\pi\frac{z}{h})}{\left[1-\sum_{n,odd}^{\infty}\frac{192h}{n^5\pi^5 w}\tanh(n\pi\frac{w}{2h})\right]} \qquad (3.1)$$

This equation is extremely useful when the flow rate is known, as in this study. Thus, analytical solutions were determined by considering the flow rate produced by the syringe pump in our experiment. A short derivation of Equation 1 is presented in Appendix B. A full description of this analytical solution can be found in Bruus (2004).

The experimental results in the centre plane ($z = hz/2$) of the microchannel were determined using the RT3D system, which has submicron z-direction resolution. Note that the origin of the z-axis (lower plate) was set to where the fluorescent particles appeared to be almost static.

Figure 3.6 compares the theoretical estimates using Equation 1 and the average fluid velocities of 20 PIV image pairs for a period 0.4 s. The PIV measurements were obtained with an exposure time of 4995 μs, magnification factor (pixels/μm) of 0.85, and time interval of 20 ms between two images. These results were obtained for the middle plane (50 μm height) of the microchannel. As Figure 3.6 shows, the averaged velocity data obtained from the confocal micro PIV measurements and the analytical solution were in close agreement, with errors less than 3%. In addition, Figure 3.6 confirms that a parabolic Poiseuille flow develops along the square microchannel.

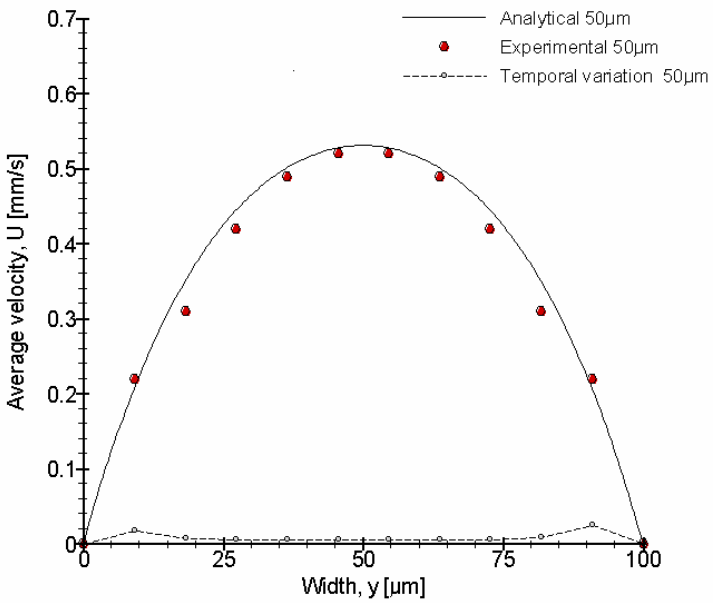

Figure 3.6 Comparison of the experimental data and analytical solution at the centre plane (50 μm height, Re = 0.025).

As noted, the confocal micro-PIV system has the unique capability of acquiring a series of optical sections along the z-axis. To analyse the three-dimensional optical sectioning ability of the confocal system, we acquired images at several distances from the focal plane. As the theoretical optical slice thickness is approximately 5 μm, by using a step size of 15 μm we

ensured that there was no overlap between the optically sectioned images. Figure 3.7 shows the average velocity data for several optical sectioned images along the *z*-axis.

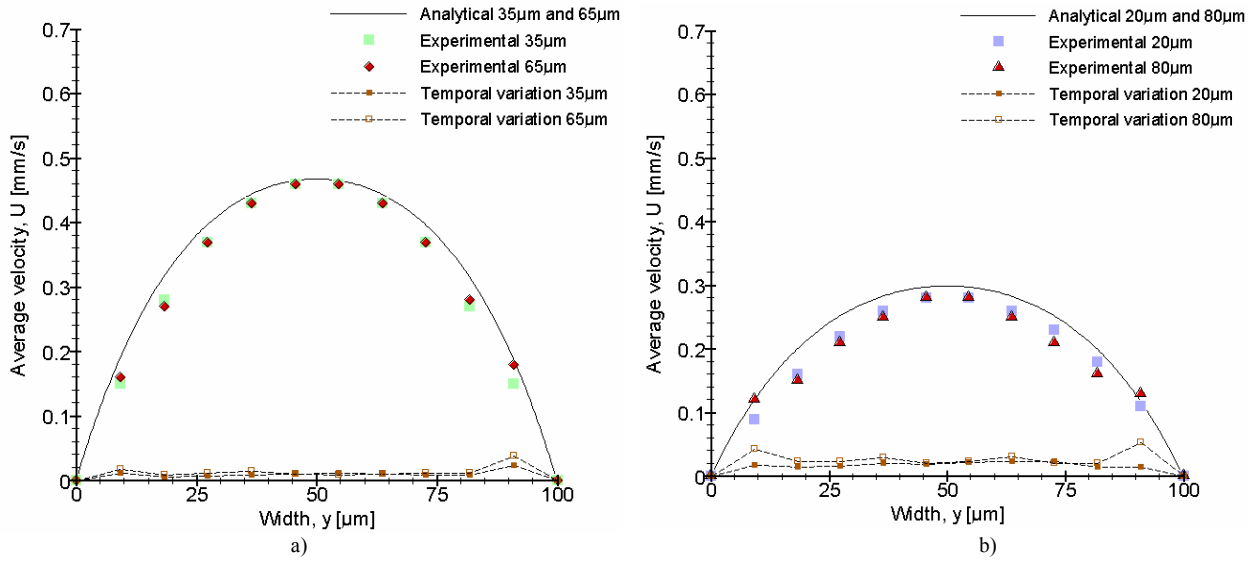

Figure 3.7 Comparison of the experimental data and analytical solution for several optically sectioned images along the *z*-axis: a) comparison at $z = 35$ µm and $z = 65$ µm; b) comparison at $z = 20$ µm and $z = 80$ µm.

The results shown in Figure 3.7a show close agreement (errors less than 6%) with some marginal deviation. At locations closer to the wall and farther from the focal plane (*xy* planes located 30 µm from the centre plane), the deviations were greater, with errors from 10 to 13%.

To evaluate the measurement accuracy over time, the temporal variance of the averaged velocities (U) is shown in Figures 3.6 and 3.7. Around the middle plane, the temporal variation was almost constant, with values of 2 to 4% of the time-averaged velocity. These results demonstrate the ability of our confocal system to obtain highly accurate measurements at the centre of the microchannel. Conversely, near the wall, the temporal variation was much greater, with values around 0.021 mm/s, which correspond to about 12% of the time-averaged velocity. This high variation demonstrates the difficulty in obtaining accurate measurements closer to the wall due to background noise present in the recorded images.

The analytical solution, for a Newtonian fluid with low Re, within a square microchannel is characterized by one-dimensional flow. By considering the centre of the microchannel as the reference axis, the *xy* planes located the same distance from the centre plane must have exactly the same velocities profile. In Figure 3.7, there is fairly good agreement between the average velocity profiles in the symmetric *xy* planes located 15 µm ($z = 35$ µm and $z = 65$ µm) and 30 µm ($z = 20$ µm and $z = 80$ µm) from the centre plane.

3.3.2 Comparison of velocity profiles of pure water vs blood cells suspension

As previously noted, besides examining pure water, we studied a physiological fluid containing 4% suspended RBCs. This nonhomogeneous fluid was used to evaluate the potential of the confocal micro-PIV system for investigating the flow behavior of complex fluids, such as *in vitro* blood flow.

An example of a recorded image (halogen illumination source) of the physiological fluid is presented in Figure 3.8a. Figure 3.8b displays a confocal image (laser-emitted light) used to calculate the velocity field of this nonhomogeneous fluid. Figure 3.8 shows the ability of the confocal system to obtain images using only the fluorescent particles within the plasma flow.

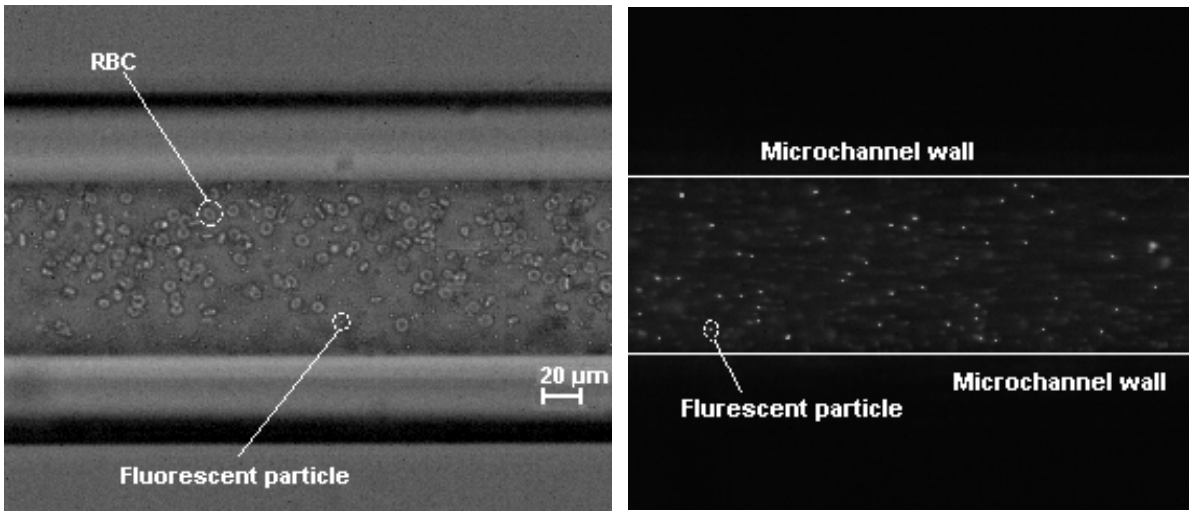

a) b)

Figure 3.8 a) An image of the physiological fluid used in this experiment with halogen illumination. The fluorescent particles are observed as very small points and RBCs as dark-grey rings. b) Confocal image of the same physiological fluid in which just the fluorescent particles are visualised.

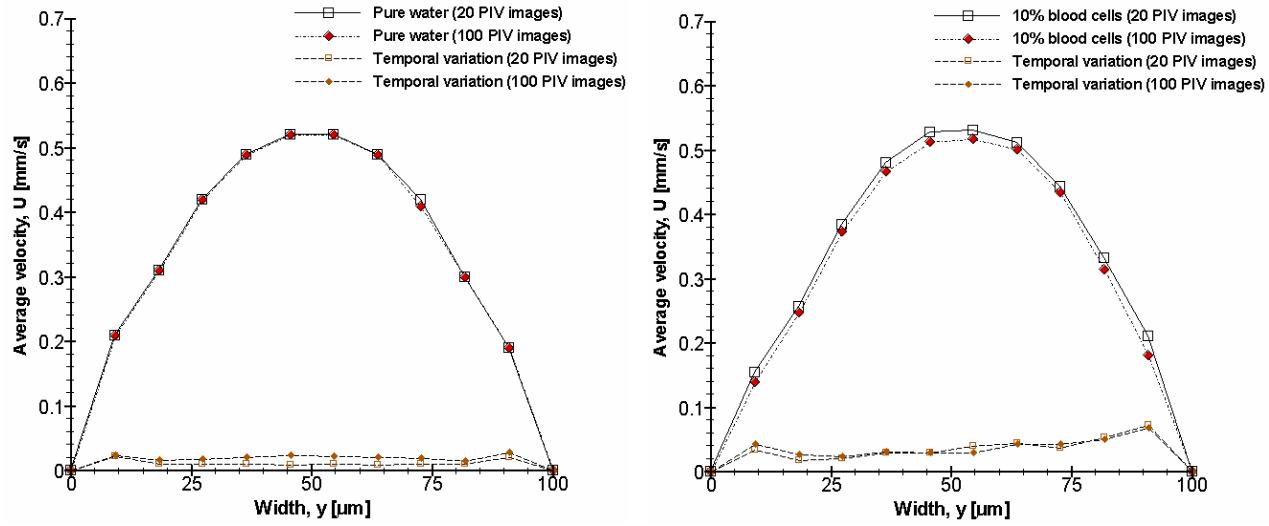

a) b)

Figure 3.9 Comparison between 20 and 100 PIV images pairs: a) pure water; b) 4% RBCS suspension.

To compare the velocity profiles of pure water and a 4% of RBCs suspension, it is important to determine the suitable number of PIV image pairs required to analyse the behavior of both fluids. Figure 3.9a shows the average velocity profiles of pure water for 20 and 100 PIV image pairs with a time delay of 5 ms. For pure water, it is clear that there is almost no difference between the two average velocity profiles, implying that 20 PIV image pairs are sufficient to obtain a reliable description of the flow of a homogeneous fluid, such as pure water. By contrast, when we made an identical comparison using a nonhomogeneous fluid containing 4% of RBCs, we have found a slight difference between the average velocity profiles obtained from 20 and 100 image pairs (see Figure 3.9b). As a result, we believe that 100 PIV image pairs with a delay of 5 ms gives a more reliable description of the flow behavior of the nonhomogeneous fluid used here. Since our main interest is to use the outstanding ability of the confocal system to acquire images in several planes along the microchannel depth, obtaining more than 100 PIV images in the middle plane will increase the recording video time and compromise the measurements in other planes. Hence, for comparing the average velocities profiles of both fluids, we decided to use 20 PIV image pairs for pure water and 100 PIV image pairs for the cell suspension with 5 ms interval between each pair of images. Figure 3.9 also compares the temporal variation calculated from the instantaneous velocities of both fluids. The evident increase in the temporal variation of the cell suspension indicates that there are some hydrodynamic disturbance effects on the flow behavior of the trace particles caused mainly by the presence of blood cells in the plasma.

As a first result, Figure 3.10 shows the velocity vector fields of pure water and Hanks solution containing 4% of RBCs, for different *xy* planes spaced at 15 μm depth intervals (*z*-direction).

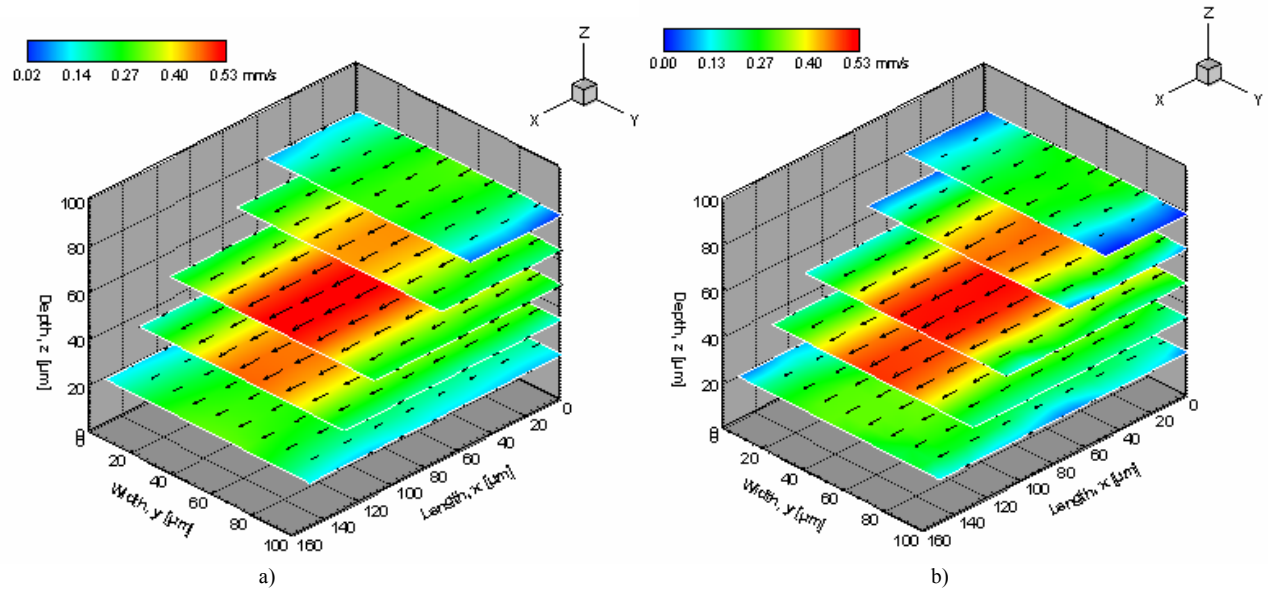

a) b)

Figure 3.10 Velocity vector fields at different z positions of a) pure water and b) a 4% suspension of RBCs.

From Figure 3.10a, the velocity profiles of pure water in several horizontal planes (*xy* axis) clearly show that the flow is stable and fully developed in this region. Moreover, there is a close correspondence between the velocity patterns in symmetric *xy* planes located 15 and 30 μm from the centre plane. As expected, the fluid velocity was greatest at the centre of the microchannel, while the velocities were low in regions close to the walls. Examining the velocity profiles of the physiological fluid (see Figure 3.10b), small deviations between the symmetric planes were observed. This becomes much clearer on analysing the 3D profiles shown in Figure 3.11.

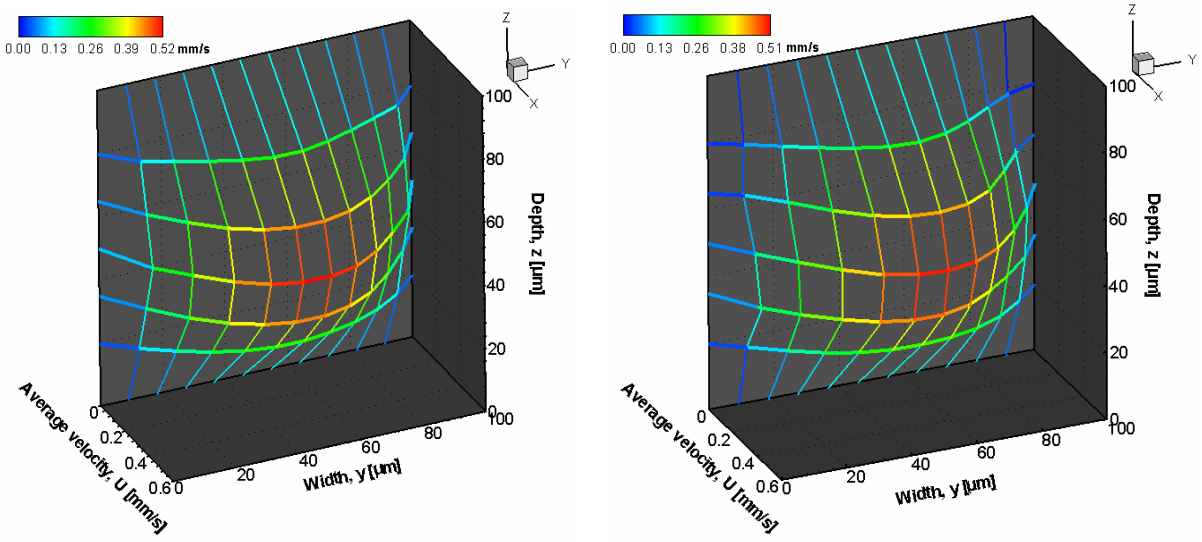

a) b)

Figure 3.11 Three-dimensional representation of optical sectioning velocity profiles of a) pure water and b) a 4% RBCs suspension. The 3D profiles were generated from several optical sectioned images along the *z*-axis measured using the confocal micro-PIV system.

Although ensemble-averaged velocity measurements provide more accurate results in a homogeneous fluid (Santiago et al. 1998, Meinhart et al. 1999, Nguyen and Wereley 2002), when analysing a nonhomogeneous fluid, some details of the flow behavior could be lost during the ensemble process. This is very clear on comparing the instantaneous velocity fields in the middle plane of both pure water and the cell suspension, as shown in Figure 3.12. Although the instantaneous velocities from pure water have a nearly constant parabolic profile, the instantaneous velocities from the cell suspension show some irregularities in the velocity profile. Figure 3.12b clearly shows the effect of the blood cells on the instantaneous velocity distribution of the plasma flow. These results are in agreement with the increase in the temporal variation of the cell suspension, as shown in Figure 3.9b.

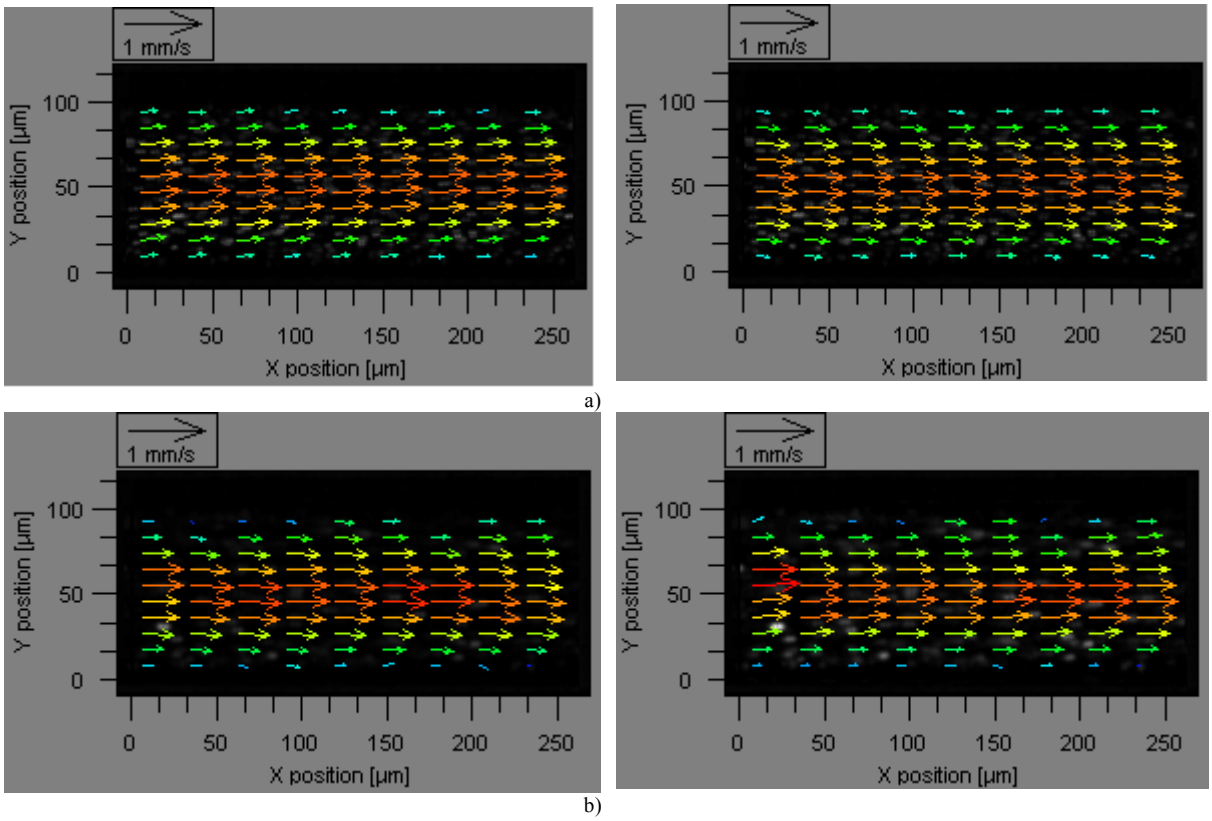

Figure 3.12 Instantaneous velocities of two PIV images pairs with a time delay of 5ms: a) pure water; b) 4% RBCs suspension.

3.4 Discussion

Using a homogeneous fluid, Park et al. (2004) recently showed the main advantages of confocal micro-PIV over conventional micro-PIV. In this study, we show the ability of the confocal micro-PIV system to obtain detailed measurements of a nonhomogeneous fluid. Furthermore, the new Nipkow disk of the Yokogawa CSU-22 incorporated in the confocal system allowed us to measure the velocity of a blood cell suspension, obtaining values of up to 0.52 mm/s.

The confocal micro-PIV measurements using pure water as the working fluid were in good agreement with the analytical solution. However, at locations closer to the wall and farther from the focal plane, the errors were slightly larger than 10%. We believe that this is mainly attributable to the increased degree of defocussing as one moves out of the ideal focus plane and to "second-order effects," such as the surface roughness of the wall. Despite the slightly greater deviation near the wall, the good agreement between the micro-PIV measurements and the predicted results for the centre planes shows that the flow behavior within 100 µm microchannels obeys macroscale flow theory, which reinforces the recent findings of Meinhart et al. (1999) and Devasenathipathy et al. (2003). Our results also reinforce the data

obtained by Park et al. (2004) for a circular microtube. In addition, our results are the first to show that the velocity profiles in symmetric *xy* planes agree fairly well with the predicted Poiseuille profiles. Thus, we conclude that the confocal micro-PIV system has the potential to generate 3D optical sections with high resolution within a range of 100 μm.

Besides the good agreement with the theoretical predictions, we also showed that our confocal system has high measurement accuracy at the centre of the microchannel, with maximum temporal variation up to 4% of the time average velocity. However, an increase in the temporal variation was observed near the wall of the microchannel. The main causes of this higher temporal variation are the increased image noise and the large particle diameter used in our experiment. We believe that the measurements close to the wall can be improved markedly by using 200 nm diameter seeding particles (Meinhart et al. 1999). Note that we used 1 μm diameter particles mainly to avoid possible Brownian motion associated with the low Re we used.

The combination of optical and experimental parameters used to investigate the behavior of the flow of a fluid containing suspended blood cells was fairly good for obtaining quantitative measurements, especially at the centre of the microchannel. It was possible to obtain confocal images using only the fluorescent particles within the plasma, while the blood cells were not captured because they had different emission wavelengths. The clear visualisation of flowing particles within the cell suspension is mainly attributable to the ability of the system to obtain extremely thin, in-focus images using its unique spatial filtering capability, which improves particle image contrast and decreases the background noise from the focal plane of interest (Park et al. 2004).

Comparing the instantaneous velocity fields of both fluids, we observed small fluctuations in the velocity profiles from the cell suspension, caused mainly by the presence of blood cells within the plasma flow. These fluctuations are in agreement with the increased temporal variance of the cell suspension. However, from the ensemble-averaged velocity measurements of the physiological fluid we used, the deviations were very slight compared to pure water. These results suggest that a 4% suspension of blood cells has a relatively small effect on the plasma flow and that this physiological fluid behaves as a Poiseuille flow. This behavior mainly results to the low haematocrit (~ 4%) we used. For example, it was not possible to observe a plasma layer along the flow, which is one of the main factors contributing to the

rheological behavior of blood flow in the microcirculation (Mchedlishvili and Maeda 2001, Lipowsky 2005). Our results concur with a recent study by Sugii et al. (2005) who reported that *in vitro* blood with a low haematocrit (21%) behaves as a typical Newtonian fluid. However, their work was limited to 2D measurements in the middle of the microchannel. As Figures 3.10 and 3.11 show, using the confocal micro-PIV system, it was possible to obtain fairly accurate velocity measurements in several *xy* planes along the *z*-direction and obtain more detailed information about the blood flow behavior. Using a conventional micro-PIV system, Park et al. (2004) also obtained measurements along the depth of the microchannel; however, their measurements were less accurate than the confocal micro-PIV measurements. The lower accuracy using conventional micro-PIV is believed to be mainly due to the inability of conventional microscopes to obtain true sliced images.

In a recent study, Park et al. (2004) used a confocal micro-PIV system with a temporal resolution of up to 120 frames/s. This low temporal resolution has limited the applicability of their system in microfluidics. By contrast, our system using the new scanning unit CSU-22 from Yokogawa allows us to obtain images at up to 2,000 frames/s, which corresponds to a time interval of 0.5 ms between a pair of images. Although this temporal resolution can be achieved using pure water, the images recorded using a blood cell suspension were too dark to be processed. The reason for this limitation is mainly due to the small fraction of illuminating light that makes through to moving pinholes to the blood cell suspension fluid. However, by decreasing the temporal resolution to 200 frames/s, the incident illumination light that passes through the pinholes was enough to successfully measure velocities up to 0.52 mm/s. As the velocities in the microcirculation are usually from 0.2 to 10 mm/s (Caro et al. 1978, Fung 1997) our confocal system is a very suitable measurement technique for studying microcirculation phenomena, especially in capillaries where the velocities are usually less than 1 mm/s. Note that, for higher velocity ranges, the coventional micro-PIV system seems to be the most appropriate measurement technique. Some examples are the studies performed by Sugii and his co-workers (Sugii et al. 2002, 2005).

It is evident from our results that the disturbance effect caused by 4% RBCs in the plasma flow is relatively small. We are now attempting to use the confocal micro-PIV system to investigate the *in vitro* behavior of blood with different haematocrits and are facing some difficulties, mainly due to the complex task of controlling the haematocrit through the microchannel. By combining our microchannel with a soft lithography technique, we expect

to create a bypass flow circuit at the inlet port, which will give a constant haematocrit throughout the microchannel.

Finally, although this system has the unique capability to acquire images at several distances from the focal plane, the 3D representation of the axial velocity still requires further study because the velocities along the *z*-direction are determined from linear relationships between the different optical sectioning velocity profiles. The 3D velocity profiles could be improved by combining our experimental data with numerical methods.

3.5 Conclusions

This study is the first attempt to obtain detailed measurements of a blood cell suspension fluid using a confocal micro-PIV system. This emerging technology combines a conventional PIV system with a spinning confocal microscope, which provides a high spatial resolution and 3D flow information. To evaluate the performance of our confocal micro-PIV system, we investigated the behavior of two different fluids within a square microchannel in several horizontal planes. The measured velocity profiles of pure water agree well with predicted Poiseuille profiles, indicating that microchannels with dimensions on the order of 100 μm obey macroscale flow theory. Moreover, the measurements of a physiological fluid containing 4% suspended RBCs demonstrated the ability of this system to obtain confocal images using only the fluorescent particles within the plasma, while the RBCs were not detected due to their different emission wavelength. Although we clearly observed small fluctuations in the instantaneous velocities fields on comparing pure water to a 4% RBCs suspension, when the ensemble-averaged velocities were compared, the local hydrodynamic disturbance effect caused by the blood cells may be rather small to create "microturbulences" within the plasma flow. In addition, the results obtained from the confocal micro-PIV system not only show the ability of this system to measure velocities up to 0.52 mm/s in a blood cell suspension, but also the potential for generating 3D profiles that allow us to obtain detailed information on the flow behavior within a 100 μm square microchannel. This study showed that the confocal micro-PIV system is a very suitable technique for investigating *in vitro* blood flow in the microcirculation.

CHAPTER 4

BLOOD FLOW IN A SQUARE MICROCHANNEL: THE EFFECT OF THE HAEMATOCRIT ON INSTANTANEOUS VELOCITY PROFILES

4.1 Introduction

The velocity profiles of blood flow *in vivo* and *in vitro* have been measured using several techniques, including double-slit photometry (Gaehtgens et al., 1970; Baker and Wayland, 1974), video microscopy and image analysis (Bugliarello et al., 1963; Tangelder et al., 1986; Parthasarathi et al.,1999), laser-Doppler anemometry (Einav et al., 1975; Born et al., 1978; Cochrane et al., 1981; Uijttewaal et al., 1994, Golster et al., 1999), and particle-measuring methods (Sugii et al., 2002, 2005; Nakano et al., 2003, 2005; Jeong et al., 2006). Nevertheless, no general consensus yet exists concerning the actual velocity profile in microvessels. While some studies have reported parabolic profiles (Baker and Wayland, 1974; Golster et al., 1999; Sugii et al., 2005), others have suggested blunt profiles (Bugliarello et al., 1963; Tangelder et al., 1986; Nakano et al., 2003); still others have reported blunt profiles at extremely low velocities and diameters and parabolic profiles at diameters exceeding 100 μm (Gaehtgens et al., 1970; Cochrane et al., 1981). Thus, further research is needed on the influence of flow parameters on the blood flow velocity profiles in microvessels.

Due to its outstanding spatial filtering technique and multiple point light illumination system, confocal micro-PIV (Tanaani et al., 2002; Park et al., 2004, 2006; Kinoshita et al., 2005; Lima et al., 2006) has become accepted as a reliable method for measuring velocity profiles with high spatial resolution. Very recently, we demonstrated the ability of confocal micro-PIV to measure both homogeneous and nonhomogeneous fluids (Lima et al., 2006). The present study compared the instantaneous and ensemble velocities profiles of pure water and blood flow *in vitro*. The velocity profiles of both pure water and *in vitro* blood with two different haematocrits (9%Hct and 17%Hct) were acquired in the centre plane of a 100 μm square microchannel.

4.2 Materials and methods

4.2.1 Working fluids and microchannel

This study examined three working fluids: pure water (PW) and physiological saline (PS) containing 9% (9Hct) or 17% (17Hct) human red blood cells (RBCs). All the fluids were seeded with 0.15% (by volume) 1-μm-diameter red fluorescent solid polymer microspheres (R0100; Duke Scientific, Palo Alto, CA, USA). The blood used was collected from a healthy adult volunteer (aged 32 years old), and ethylenediaminetetraacetic acid (EDTA) was added to prevent coagulation. The RBCs were separated from the bulk blood by centrifugation (1500 rpm for 20 min) and the plasma and buffy coat were removed by aspiration (see Figure 4.1). The washing and centrifuging with PS was repeated twice. The remaining RBCs were then resuspended in PS to make up the required RBC concentration by volume. The haematocrit of the two RBC suspensions used in this study was about 9% (9Hct) and 17% (17Hct), respectively. All the blood samples were stored hermetically at 4ºC until the experiment was performed at room temperature (25–27ºC). All procedures in this experiment were carried out in compliance with the Ethics Committee on Clinical Investigation of Tohoku University.

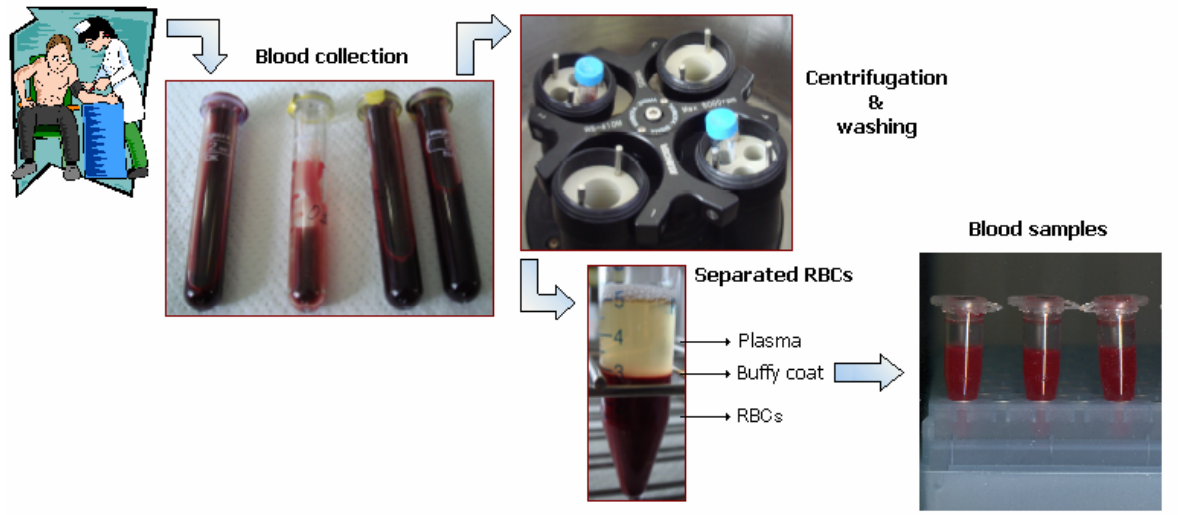

Figure 4.1 Preparation of the blood samples (adapted from Mannai 2006).

In this study, we used a 100 μm square borosilicate glass microchannel fabricated by Vitrocom (Mountain Lakes, NJ, USA), which was mounted on a slide glass immersed in glycerol that had the same refractive index. A square microchannel was selected to minimise possible refraction of the laser beam at the walls of the microchannel. Using a glass tube, the refraction arising from the curved walls would be more pronounced and might degrade the measured velocity fields.

4.2.2 Experimental setup

The confocal micro-PIV system we used consisted of an inverted microscope (IX71; Olympus, Tokyo, Japan) combined with a confocal scanning unit (CSU22; Yokogawa Corp., Tokyo, Japan) and a diode-pumped solid-state (DPSS) continuous wave (CW) laser (Laser Quantum, Stockport, UK) with an excitation wavelength of 532 nm. A high-speed camera (Phantom v7.1; Vision Research, Wayne, NJ, USA) was connected to the outlet port of the CSU22. The microchannel was placed on the stage of an inverted microscope and the flow rate (Q) of the working fluids was kept constant at 0.15 μl/min using a syringe pump (KD Scientific, Holliston, MA, USA), corresponding to a Reynolds number of 0.025.

The laser beam was illuminated from below the microscope stage through a 20× objective dry lens with a numerical aperture (NA) equal to 0.75. Satisfactory illumination was achieved by seeding 1 μm diameter fluorescent particles that absorb green light (absorbance peak 542 nm) and emit red light (emission peak 612 nm). The light emitted from the fluorescent flowing particles passes through a colour filter into the CSU22 scanning unit, where it is reflected onto a high-speed camera using a dichromatic mirror to record the PIV images.

In order to obtain adequate quality images for processing with the PIV software (PivView; PivTec GmbH, Göttingen, Germany), we captured images with a resolution of 640 × 480 pixels and 12-bit greyscale, at a rate of 200 frames/s, with an exposure time of 4995 μs, and a time interval (Δt) of 5 ms and 10 ms between two images. All the PIV measurements were performed for a period of approximately 0.5 s in order to obtain both instantaneous and ensemble averaged velocities. After recording the images, they were digitised and transferred to a computer for evaluation using Phantom camera control software (PH607). The PIV images of the flowing particles were processed and the flow velocity was determined using PivView version 2.3 (Rafael et al., 1998). The images were evaluated using a cross-correlation method in which the time between two images was set to 5 ms and 10 ms for all working fluids. Using a multiple-pass interrogation algorithm with a 24 × 16 pixel interrogation window (50% overlap), which corresponds to a spatial resolution of 28.24 × 18.83 μm, it was possible to obtain the corresponding instantaneous and ensemble velocity fields. A full description and evaluation of the confocal micro-PIV system used in this study can be found in Lima et al. (2006).

4.3 Results and discussion

4.3.1 Ensemble velocity profiles

Most previous studies have determined the velocity profiles of flowing blood by measuring the time-averaged velocity field. Figure 4.2a and 4.1b show the averaged velocity of 100 (Δt = 5ms) and 50 (Δt = 10ms) ensemble PIV images, respectively. These images were recorded at the same time period of approximately 0.5 s. Figure 4.2 also compares the PIV measurements with an analytical solution for steady flow through a long, straight, rigid square microchannel (see Lima et al., 2006 for more details).

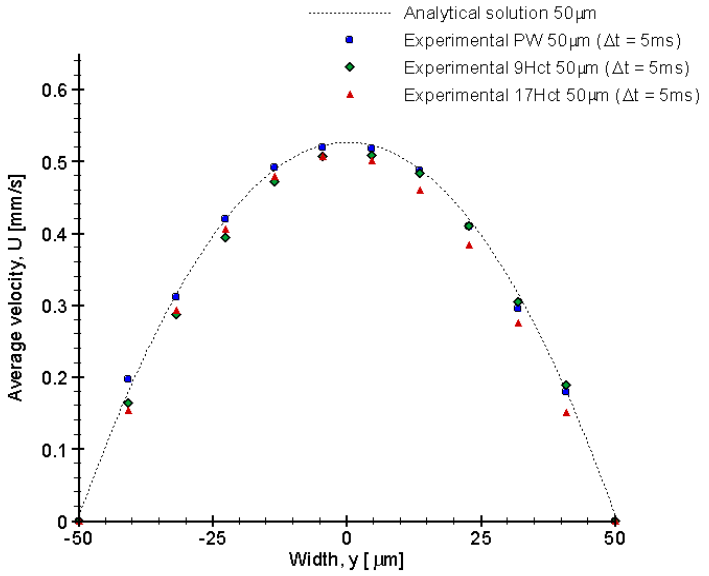

a)

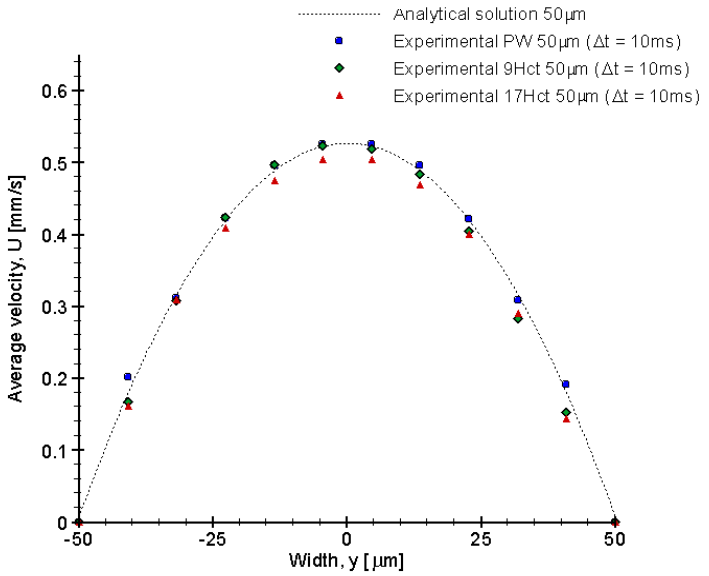

b)

Figure 4.2 Averaged ensemble velocity profiles for six different series of confocal micro-PIV measurements in the central plane (50 µm) of (a) pure water (PW) and *in vitro* blood with haematocrit 9% (9Hct) and 17% (17Hct) for Δt = 5ms; (b) pure water (PW) and *in vitro* blood (9Hct and 17Hct) for Δt = 10ms.

Comparing the ensemble velocity profiles of all fluids (see Figure 4.2), we observed small deviations (< 5%) for both Δt = 5ms and Δt = 10ms, especially in the central region of the velocity profile. Using the t-test analysis we found no significant difference between the working fluids and the analytical solution at 98% confidence interval. Hence, these results imply that the ensemble-averaged velocity profiles of *in vitro* blood with haematocrits up to 17% flowing within a 100 μm square microchannel do not change significantly from a parabolic shape. These results agree with Baker et al. (1974) and Sugii et al. (2005). Furthermore, from the ensemble-averaged velocity profiles for both Δt = 5ms and Δt = 10ms the average deviation was estimated to be 2% for PW and 17%Hct and 5% for 9%Hct. On comparing the results from both Δt we found no significant difference between Δt = 5ms and Δt = 10ms at 98% confidence interval. These results suggest that for both cases it is possible to obtain reliable ensemble-averaged velocity profiles for all the working fluids used in this study.

4.3.2 Instantaneous velocity profiles and root mean square (RMS)

A remarkable advantage of the PIV measuring technique over conventional methods, such as double-slit photometry or laser-Doppler anemometry, is its ability to obtain detailed information on the fluid flow behaviour from the evaluation of the instantaneous velocity fields. Although these velocity fields are extremely important for flows with high Re in which turbulent flow fields are likely to occur (Meinhart et al., 2000b; Bates et al., 2001; Heise et al., 2004), we believe that instantaneous velocities are also crucial for evaluating several phenomena in steady flows, especially for complex fluids containing suspended blood cells in plasma. In this way, Figures 4.3–4.4 show the first time series of the instantaneous velocity profiles of pure water and *in vitro* blood with two different haematocrits at Re 0.025 for Δt = 10ms.

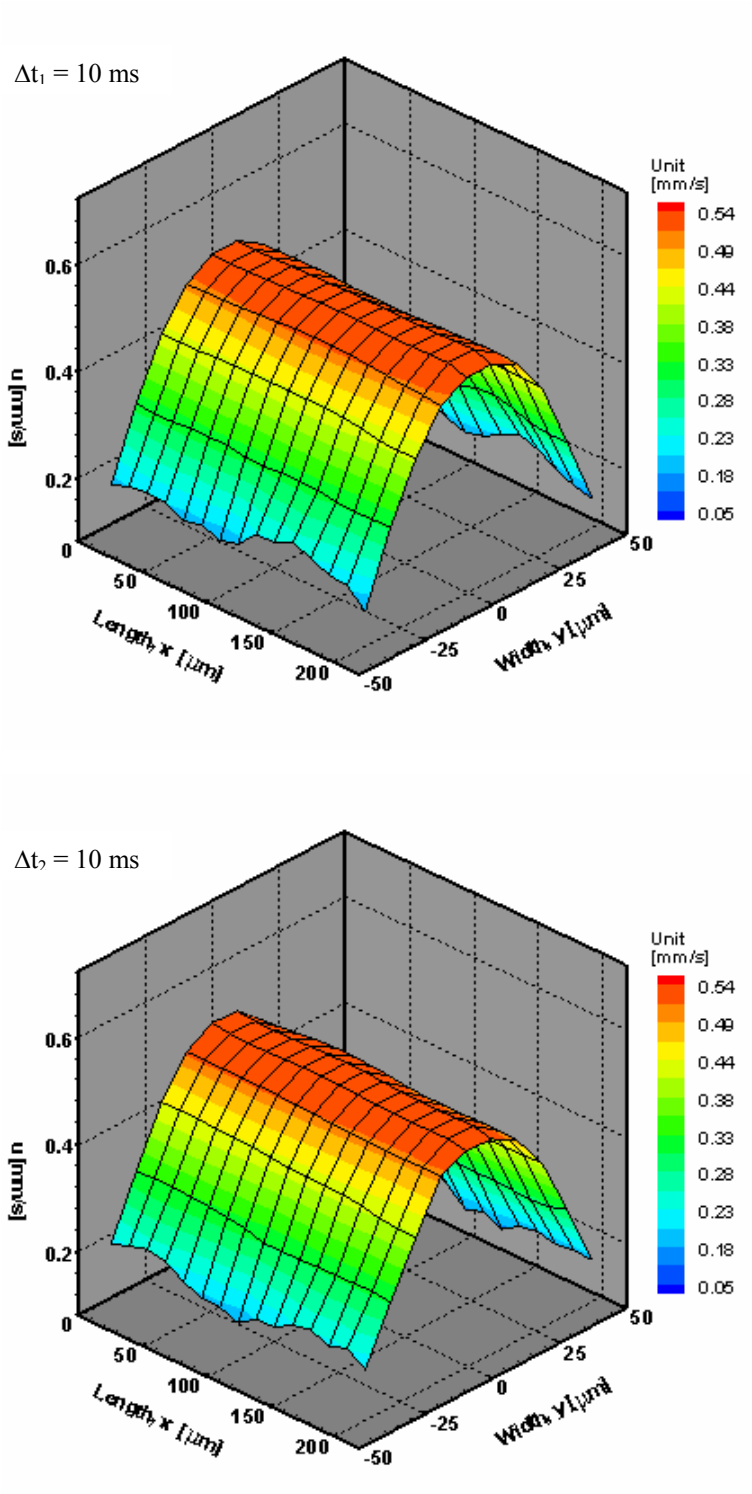

Figure 4.3 Two examples showing series of instantaneous velocity profiles of pure water (PW) in the central plane (50 μm) of the microchannel for Δt = 10 ms. Note that, x, y represent respectively measured length and full width of the microchannel whereas u represents the axial velocity of the working fluid along the central plane of the microchannel.

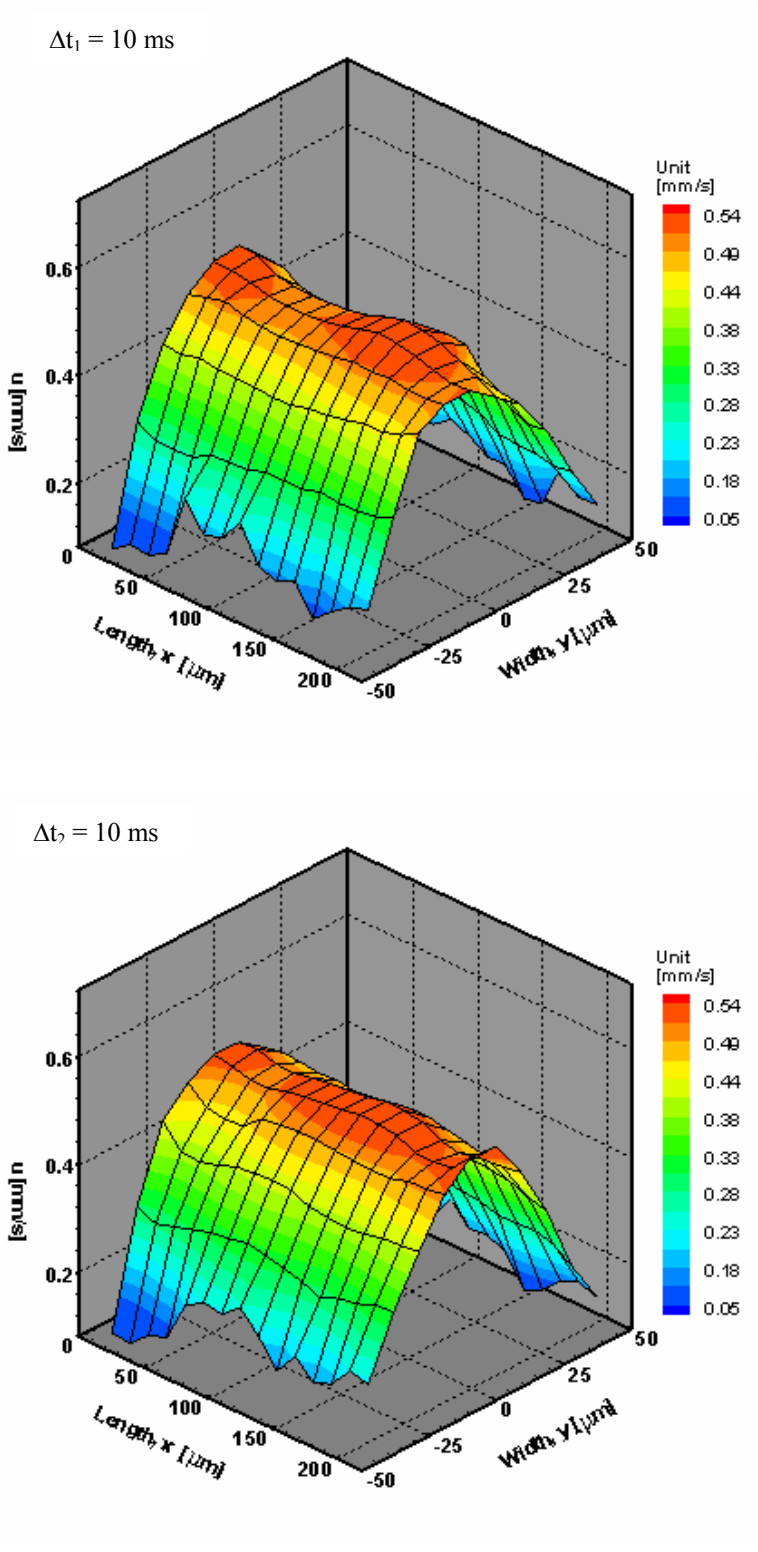

Figure 4.4 Two examples showing series of instantaneous velocity profiles of *in vitro* blood with a 9% (9Hct) haematocrit in the central plane of the microchannel for Δt = 10 ms.

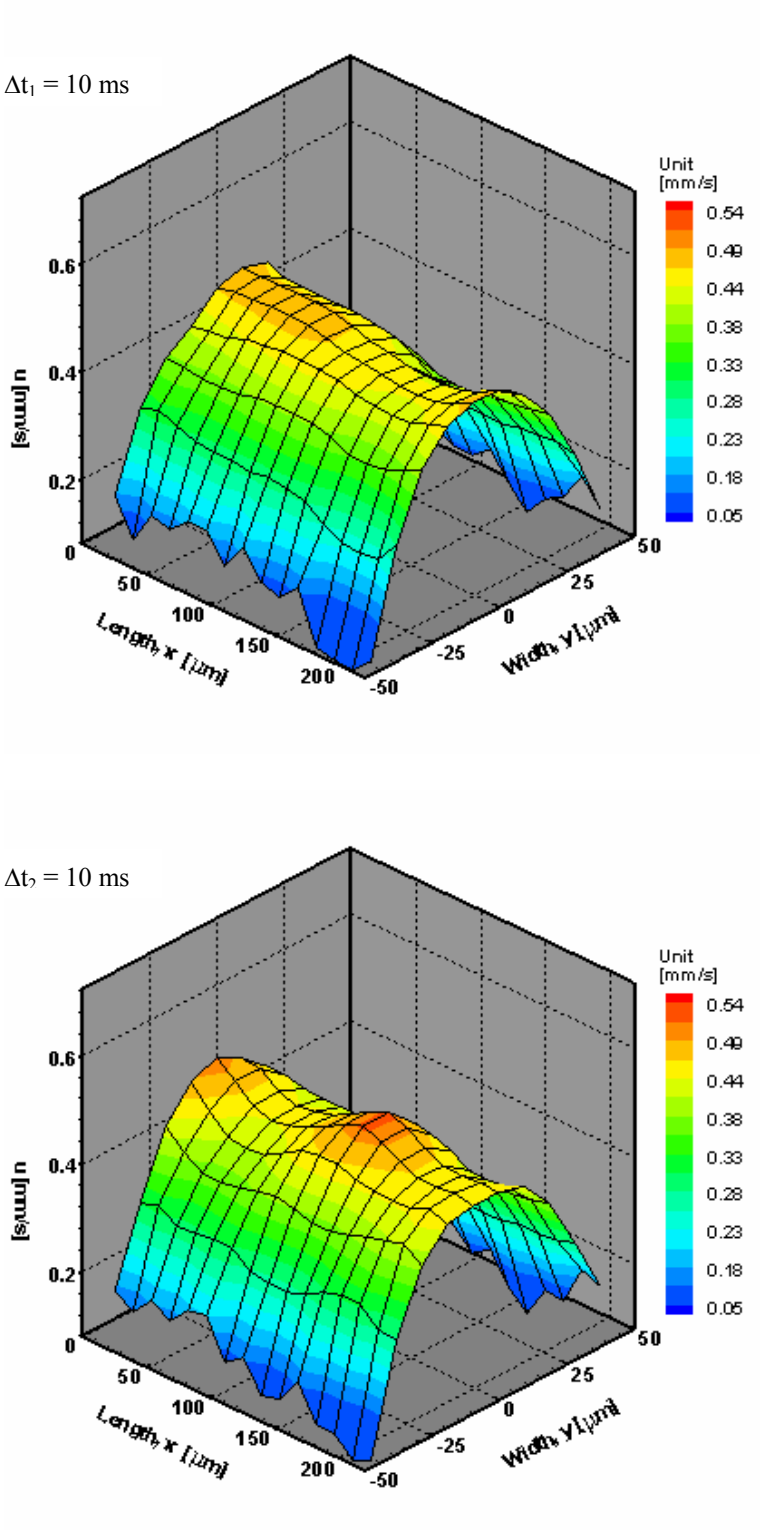

Figure 4.5 Two examples showing series of instantaneous velocity profiles of *in vitro* blood with a 17% (17Hct) haematocrit in the central plane of the microchannel for Δt = 10 ms.

In the conventional micro-PIV, most of the noise in the instantaneous velocity measurements is mainly due to the out-of-focus particle images, Brownian motion and low particle image density (Santiago et al., 1998; Nguyen and Wereley, 2002). The standard method to improve

the accuracy of the conventional micro-PIV measurements is by ensembling series of instantaneous velocities. However, very recently it was shown that confocal micro-PIV, due to its optical sectioning effect provided by the spinning disk, can improve significantly the background noise even when using high particle concentration, i. e., 0.1% by volume (Park et al., 2004, 2006; Lima et al., 2006). Furthermore by using trace particles with 1 μm diameter it is possible to minimize some possible Brownian motion effect (Santiago et al., 1998). As a result, we believe that confocal micro-PIV can provide reliable instantaneous velocity fields, especially for homogenous fluids and *in vitro* blood with low heamatocrit (Hct ≤ 9%) (see section 4.3.3).

On comparing the instantaneous velocity fields in the middle plane of pure water and *in vitro* blood (see Figures 4.3–4.5), it is possible to observe that the instantaneous velocities from pure water have a nearly constant parabolic profile, whereas the instantaneous velocities from both *in vitro* blood show some irregularities on the velocity profiles. However, these instantaneous velocity profiles are only qualitative observations which needed to be quantified in order to understand the possible causes of the fluctuations encountered on the *in vitro* blood instantaneous velocity profiles (see Figures 4.4 and 4.5).

In an attempt to elucidate the possible causes of these findings we have calculated the Root Mean Square (RMS) which can be determined from the ensemble averaging of the instantaneous velocity measurements. To calculate the RMS we first need to determine the standard deviation of both u and v components of the velocity at each grid point for a series of N frames by using the following equations:

mean velocity components :

$$\overline{u} = \frac{1}{N}\sum_{i=1}^{N} u_i \ , \qquad (4.1) \qquad \overline{v} = \frac{1}{N}\sum_{i=1}^{N} v_i \ , \qquad (4.2)$$

standard deviation of u and v components :

$$\sigma_u = \sqrt{\frac{\sum_{i=1}^{N}(u_i - \overline{u})^2}{N-1}} \ , \qquad (4.3) \qquad \sigma_v = \sqrt{\frac{\sum_{i=1}^{N}(v_i - \overline{v})^2}{N-1}} \ . \qquad (4.4)$$

After calculating both σ_u and σ_v, RMS can be estimated by

$$RMS = \sqrt{\sigma_u^2 + \sigma_v^2} \ . \qquad (4.5)$$

In Figure 4.6 the averaged RMS values for the three working fluids at two different Δt are plotted as a function of the microchannel width.

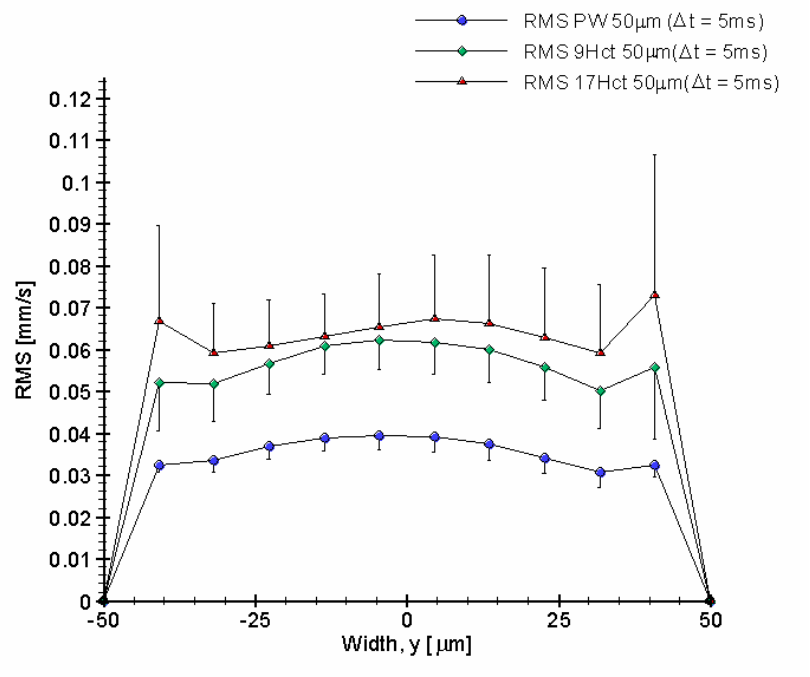

a)

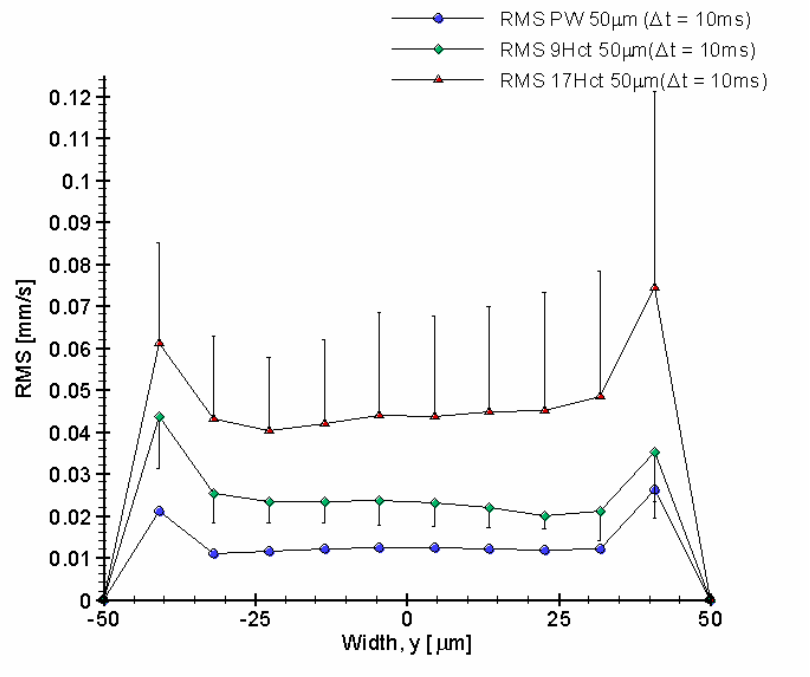

b)

Figure 4.7 Comparison of the RMS values for pure water (PW) and *in vitro* blood with haematocrits of 9% (9Hct) and 17% (17Hct) with (a) Δt = 5ms , (b) Δt = 10ms.

On comparing the RMS values with different Δt it is possible to observe that by increasing the time interval between two images the RMS decreases of about 50% for PW and 9% Hct and 25% for 17% Hct. Therefore, using Δt = 10 ms the accuracy of the instantaneous velocity

measurements are improved implying that the correspondent RMS values may represent a more reliable qualitative information about the time-dependent behaviour of the flow. Moreover, on comparing the RMS values from all the working fluids we have found that there is a significant difference between PW, 9% Hct and 17% Hct at 90% confidence interval, except for some values near the wall (see Figure 4.6). Despite the inclusion of some bias errors in the RMS values (see section 4.3.3), these results show clearly that the RMS increases with the haematocrit. We believe that the RMS values are strongly related to the fluctuations encountered in the instantaneous velocity profiles shown in Figures 4.4–4.5. The reasons for these small fluctuations are still not completely clear, however from the visualization of the RBCs motion through the microchannel, both rotational and tumbling motion and also the interaction between the neighbouring RBCs seem to be important factors to take into account. An ongoing study to clarify the effect of the RBCs on the plasma flow is currently under way.

It should be noted that for heamatocrits of about 17% we have observed some small random "plasma pockets" without particles in the PIV images which have created velocity vectors with small magnitudes due mainly to the light scattered and absorbed from the high concentration of RBCs within the plasma flow. Therefore, the RMS values for Hct = 17% contains quantitative information about not only the effect of the RBCs on the plasma flow but also some bias errors (see section 4.3.3). One way to overcome this limitation is by increasing the particles concentration within the plasma or by using a rectangular microchannel with low aspect ratio which creates an uniform distribution of RBCs (See chapter 5).

4.3.3 Measurement noise and accuracy of the confocal micro-PIV system

Past studies have already evaluated the accuracy of the confocal micro-PIV system to measure both homogenous and non-homogenous fluids (Park et al. 2004, 2006, Lima et al. 2006). However neither of them has investigated the influence of the light scattered and absorbed from the RBCs on the instantaneous velocity measurements. An approach to evaluate this effect is by calculating the Signal-to-Noise Ratio (SNR) for the working fluids used in this study. The measured SNR was defined as the highest peak image intensity divided by average background intensity in the predefined interrogation window. Figure 4.7 shows representative correlation planes for the working fluids using both confocal and conventional micro-PIV whereas Figure 4.8 shows the correspondent averaged SNR. Note that the conventional micro-PIV measurements were obtained for pure water under identical specified flow

conditions by using an epifluorescent microscope equipped with a mercury lamp and colour filters.

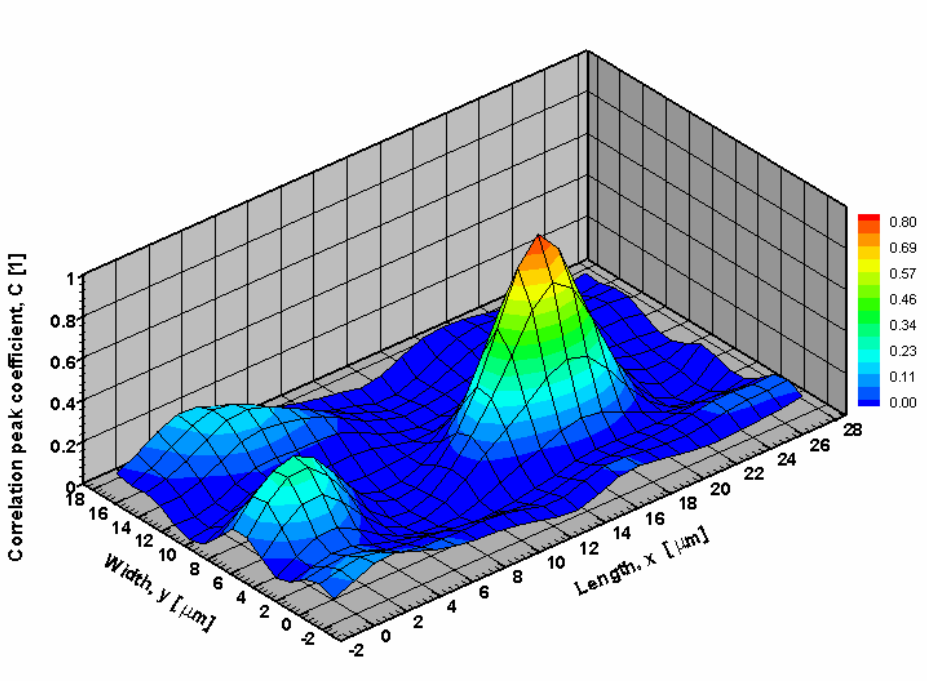

a)

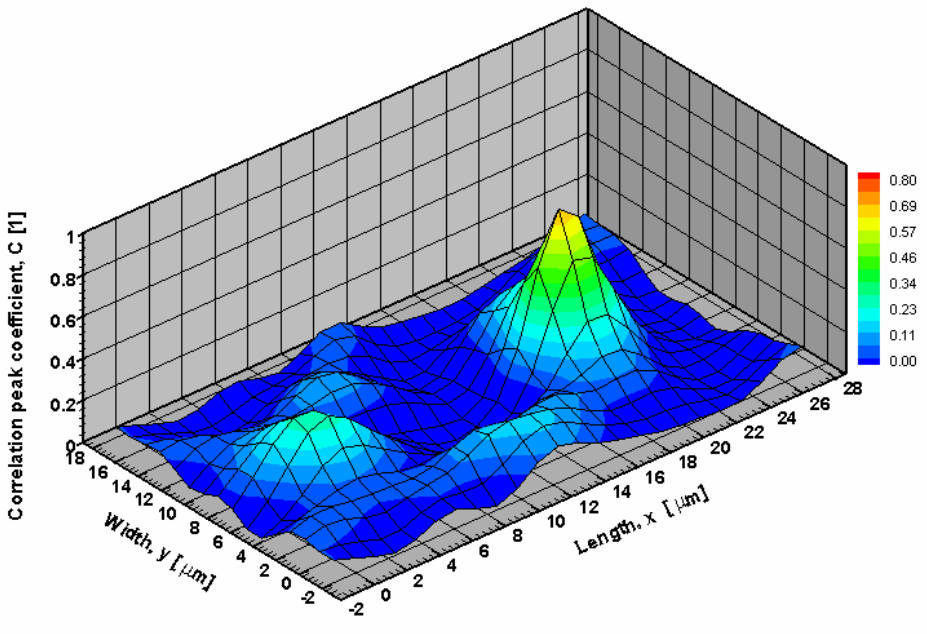

b)

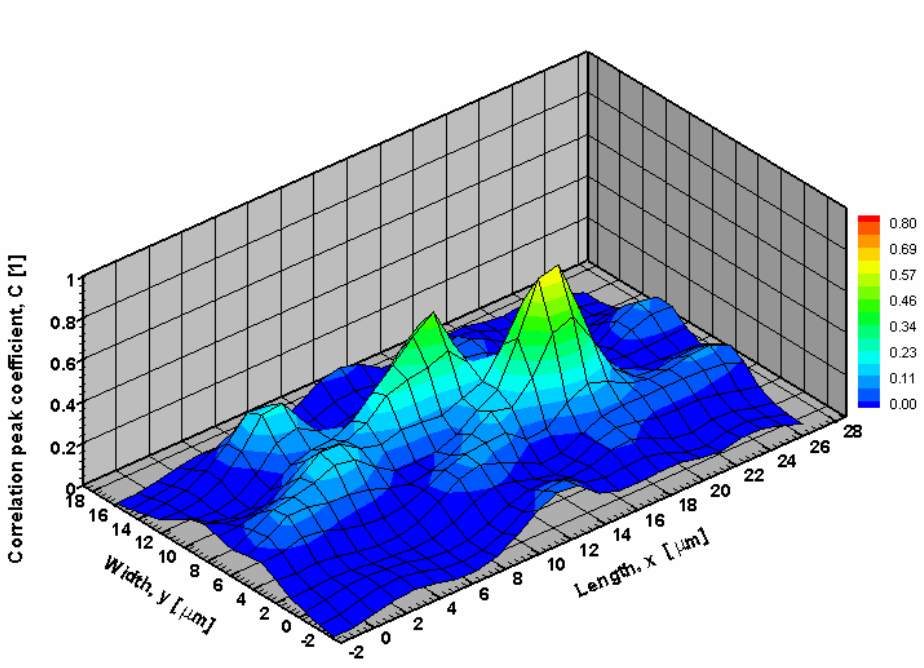

c)

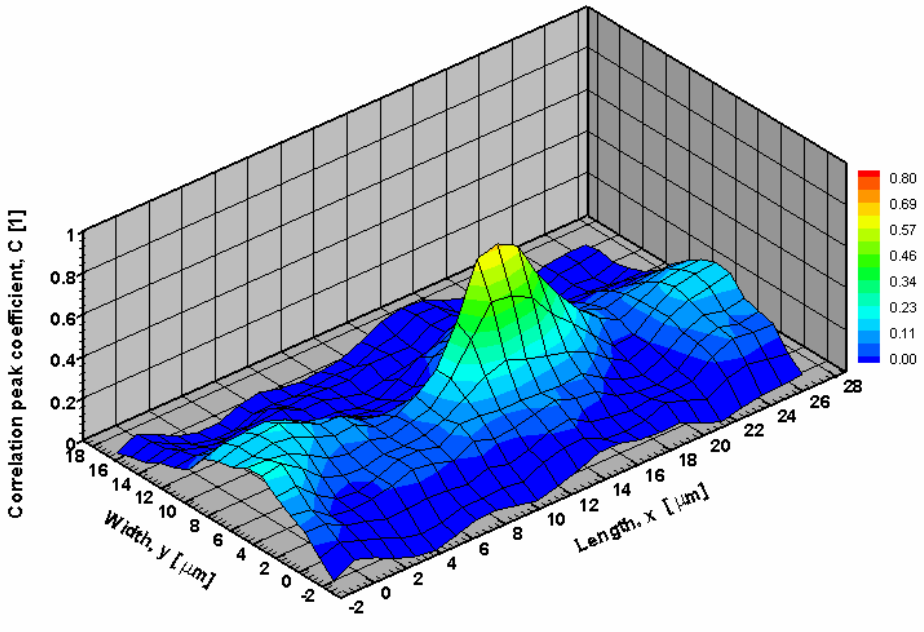

d)

Figure 4.7 Representative correlation planes for (a) pure water (PW), (b) *in vitro* blood with Hct = 9%, (c) *in vitro* blood with Hct=17% using a confocal system and (d) PW using a conventional micro-PIV technique. The x and y axis correspond to the interrogation window (28.24 × 18.83 μm) used to obtain both instantaneous and ensemble velocity fields.

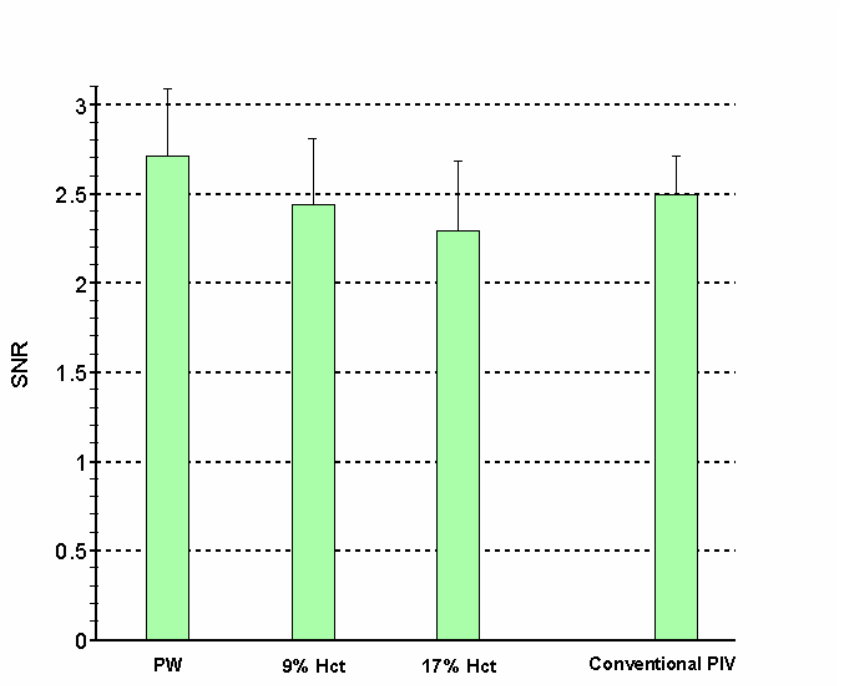

Figure 4.8 Comparison of the Signal-to-Noise Ratio (SNR) for PW, *in vitro* blood with haematocrits of 9% (9Hct) and 17% (17Hct) using a confocal system and PW using a conventional micro-PIV technique. The measured values of the SNR are expressed as the means ± standard deviation.

From Figure 4.7 it is possible to observe that for the case of the confocal system the correlation coefficient peak (C) for pure water is the highest with a value of about 0.8. By increasing the Hct the main peak tends to become weak (0.7 for 9%Hct and 0.6 for 17%Hct) due to the reduction of the number of particle pairs within the interrogation window. Nevertheless, the main peak for *in vitro* blood is still bigger than the noisy peaks. Furthermore, it is also possible to observe a decrease of the SNR with the increase of the Hct (see Figure 4.8).

Several researchers in microfluidics have performed successful measurements on both pure water (Santiago et al. 1998) and *in vitro* blood (Sugii et al. 2005) by using a conventional micro-PIV. Accordingly, we have decided to compare the SNR of pure water for both confocal and conventional micro-PIV system. The images obtained from the confocal system showed a much clearer image definition of the particles in comparison with the conventional system. We believe that the improvement on the image quality provided by the confocal system reflects the highest SNR shown in Figure 4.8. Nevertheless, the particle images with SNR values in the order of 2.5 seem to have adequate quality to obtain reliable velocity fields by using conventional correlation interrogation techniques. Thus, *in vitro* blood with 9% Hct seems to have enough SNR to generate reliable instantaneous velocity fields. For the case of Hct = 17% it is still possible to obtain instantaneous velocities vectors however some outliers

can be produced due mainly to the light scattered and absorbed from the high concentration of RBCs. In this way the instantaneous velocities fields for *in vitro* blood with 17% Hct blood still require further investigations. One way to overcome the limitation of having lower particle concentration is by using the particle tracking velocimetry method (Ravnic et al. 2006).

4.4 Conclusions

In this study, we determined both ensemble and instantaneous velocity profiles for *in vitro* blood (haematocrit up to 17%) flowing through a 100 μm square microchannel. Although the ensemble velocity profiles were markedly parabolic, some fluctuations in the instantaneous velocity profiles were found to be closely related to the increase in the haematocrit. The present study shows clearly that the RMS values increase with the haematocrit implying that the presence of RBCs within the plasma flow strongly influences the measurements of the instantaneous velocity fields. The possible reasons for the RMS increase are the motion and interaction of RBCs and the light scattered and absorbed from the RBCs. This latter cause seems to be more predominant at Hct = 17%. As a result, for 17% Hct improvements on the Signal-to-Noise Ratio are required to further enhance the measurement performance of the instantaneous velocities.

CHAPTER 5

BLOOD FLOW IN A RECTANGULAR PDMS MICROCHANNEL

5.1 Introduction

Blood is not a homogeneous fluid, but one composed mainly of a suspension of red blood cells (RBCs) in plasma. In addition, the non-continuum behaviour of blood flow through microvessels leads to complex flow mechanics, which are not yet clearly understood (Goldsmith and Turitto 1986, Secomb 1995, Mchedlishvili & Maeda 2001). Because several important physiological and pathological phenomena occur in the microcirculation, velocity profiles have been intensively studied both *in vivo* (Einav et al. 1975, Tangelder et al. 1986, Golster et al. 1999, Parthasarathi et al. 1999, Nakano et al. 2003) and *in vitro* (Gaehtgens et al. 1970, Baker & Wayland 1974, Born et al. 1978, Cochrane et al. 1981, Gaehtgens 1987, Uijttewaal et al. 1994, Alonso et al. 1995, Moger et al. 2004, Kim & Lee 2006, Lima et al. 2007) using several blood flow measuring techniques. Both *in vivo* and *in vitro* experiments have played important roles in our understanding of several phenomena in the microcirculation. Although several comprehensive reviews about blood flow behaviour in microvessels have been published (Caro et al. 1978, Chien et al. 1984, Secomb 1995, Mchedlishvili & Maeda 2001, Pries & Secomb 2003), much remains unknown about the physiological and pathological phenomena occurring in the microcirculation.

Historically, the most commonly used experimental techniques to study blood flow in the microcirculation have been double-slit photometry (Gaehtgens et al. 1970, Baker & Wayland 1974), video microscopy and image analysis (Bugliarello et al. 1963, Tangelder et al. 1986, Goldsmith and Turitto 1986, Gaehtgens 1987, Alonso et al. 1995, Parthasarathi et al. 1999, Tsukada 2000), and laser-Doppler anemometry (Einav et al. 1975, Born et al. 1978, Cochrane et al. 1981, Uijttewaal et al. 1994, Golster et al. 1999). However, with these techniques, both spatial resolution and velocity accuracy are unsatisfactory.

In recent years, due to advances in computers, optics, and digital image processing techniques, it has become possible to combine a conventional particle image velocimetry (PIV) system (Adrian 1991, Raffael et al. 1998) with an inverted epifluorescent microscope (Santiago et al. 1998, Koutsiaris et al. 1999). As a result, this combination, known as a micro-PIV, has greatly increased the resolution of conventional PIV. Because of the success of the micro-PIV in measuring accurate velocity fields of homogeneous fluids in microfluidic devices (Nguyen & Wereley 2002), the technique has been recently used to investigate blood flow behaviour in both microchannels and microvessels (Nakano et al. 2003, Bitsch et al. 2005, Vennemann P. et al. 2006).

Although the conventional PIV technique has proven useful in measuring blood flow velocities in microvessels, the entire flow field is illuminated and consequently the out-of-focus emitted light can result in high levels of background noise, which degrades the measured velocity fields (Meinhart et al. 2000, Nguyen & Wereley 2002). One way to minimise the depth-of-focus effect is using a confocal micro-PIV (Tanaami et al. 2002, Kinoshita et al. 2005, Lima et al. 2006) or confocal laser scanning microscopy (CLSM) micro-PIV (Park et al. 2004, 2006). This technique combines the conventional PIV system with a spinning disk confocal microscope (SDCM), which has the ability to obtain in-focus images with an optical thickness less than 1 μm (optical sectioning effect). Park et al. (2004, 2006) compared confocal micro-PIV with conventional micro-PIV and demonstrated that the former had improved particle image contrast and definition, allowing more accurate velocity measurements (see Table 1). As a result, by combining SDCM with a conventional PIV system, it is possible to achieve a PIV system with high spatial resolution able to generate velocity profiles at several optically sectioned planes along the microchannel depth.

Table 5.1 The lateral and axial resolutions of both conventional and confocal microscopes and optical slice thickness of confocal microscopes (Willhelm et al. 2003, Park et al. 2004).

Optical resolutions	Conventional microscopy		Confocal microscopy (SDCM)	
	40×	10×	40×	10×
Lateral resolution (μm)	0.418	1.047	0.331	0.829
Axial resolution (μm)	1.831	11.444	1.268	9.323
Optical slice thickness (μm)	Not definable		2.820	26.701

Progress in microfabricated technologies has attracted the attention of the biomedical research community to the development of diagnostic, microfluidic devices (so-called bio-systems or a lab-on-a-chip) (Sutton et al. 1997, Gomez et al. 2001, Beebe et al. 2002, Gifford et al. 2003, Minas et al. 2004, Toner and Irimia 2005, Faivre et al. 2006) capable of providing useful

information about the general health status of patients. However, most of the information provided by blood analysis in microchannels is based on conventional visual observations on the area and volume of the RBCs (Sutton et al. 1997, Gifford et al. 2003). We believe that the acquisition of quantitative blood flow measurements may also provide relevant information for the diagnosis of disease and the treatment of patients.

Recently, we demonstrated the ability of the confocal micro-PIV to measure both pure water and diluted suspensions of blood cells in a glass square microchannel (Lima et al 2006); however, glass microchannels are not ideal to study the flow properties of blood at microscopic level mainly due to fabrication problems and physicochemicals factors (Maeda 1996). First, glass-to-glass sealing is difficult because direct bonding needs extremely smooth and flat surfaces, and indirect bonding fills the channels with adhesives, sols, and metals. Second, the fabrication of microchannels on glass is limited in depth and width. Moreover, the most suitable objective lenses for the confocal micro-PIV system have limited working distances (up to 0.5 mm), which requires special considerations in microchannel design. Besides the fabrication limitations, several physical and biochemical factors contribute to the flow behavior of blood cells through microvessels. Glass microchannels differ from microvessels in several ways such as elasticity of the wall, the flow channel is always straight and long and the inner surface of the microchannel does not accommodate living endothelial cells. Hence, the results from classical in vitro experiments (Chien et al. 1984, Pries and Secomb 2003) that have used rigid straight glass microchannels needed to carefully reexaminated by using more sophisticated microchannels and measuring techniques.

Because of these limitations with glass microchannels, it is important to develop a microfluidic device closely representative of the *in vivo* microvascular environment using a reliable microfabrication technique compatible with the state-of-the-art flow measuring techniques, such as a confocal micro-PIV system. By using a soft lithography technique it is possible to generate extremely precise, reproducible and versatile rectangular microchannels. Although, rectangular microchannels may not be the best models to simulate *in vivo* microvessels geometry, many phenomena of blood flow behavior through this kind of microchannels exhibits certain features characteristic with those investigated in living microvessels (Shevkoplyas et al. 2003, Toner and Irimia 2005, Faivre et al. 2006). Furthermore, experiments with this kind of microchannels enable not only precise control of experimental parameters but also to obtain accurate measurements. So far confocal micro-PIV

measurements of *in vitro* blood flow, with heamatocrits (Hct ~ 20%) close to the *in vivo* environment, in a rectangular polydimethysiloxane (PDMS) microchannel, have not been published. Thus, as a first step towards integrating a confocal micro-PIV with a PDMS microchannel, measurements should be first performed in a simple straight rectangular microchannel.

In this study, we investigated the ability of our confocal micro-PIV system to measure the velocity profiles of physiological saline (PS) and *in vitro* blood at a normal Hct in a rectangular (300 μm wide, 45 μm deep) PDMS microchannel, which was fabricated by soft lithography. In particular, we compare the behaviour of PS and *in vitro* blood flow (20% Hct) in a rectangular microchannel with a low aspect ratio. The results presented are also a verification of the applicability of the confocal micro-PIV to obtain detailed measurements of blood flow with Hcts similar to actual Hcts encountered in microvessels.

5.2 Materials and methods

5.2.1 Fabrication of the PDMS microchannel

PDMS polymers have many useful properties, including good optical transparency and biocompatibility, easily reversible sealing to glass, elasticity, replication of fine and complex geometries, permeable to gases, thermally stable, and low cost (Duffy et al. 1998, Chang et al. 2003, Mata et al. 2005, Kaji et al. 2006). Because of these properties, this material was suitable for studying several phenomena in the microcirculation by combining it with our confocal micro-PIV system.

The PDMS rectangular microchannel was developed using a soft lithographic technique. The main steps for fabricating the PDMS microchannel (Figure 5.1) were as follows. First, the photomask was designed using a CAD system, and made on an emulsion-coated glass substrate using a pattern generator (Nihon Seiko, Japan). Next, applying a photolithographic technique, a solid master was fabricated on a glass substrate with an ultrathick photoresist (SU-8 50; Kayaku MicroChem, Japan). In this process, by using a spin-coating technique, a thin layer of SU-8 photoresist was coated on a glass substrate and then patterned by UV exposure through the photomask. Using a SU-8 developer, it was possible to obtain the desired mold master. Then, metal wire posts were placed on the SU-8 mold master to create the connection channels to the input/output ports. The PDMS prepolymer was prepared by

mixing a commercial prepolymer and catalyzer (Silpot 184; Dow Corning, USA) at a weight ratio of 10:1. After removing the bubbles created during mixing in a vacuum, the PDMS mixture was poured into the mold master and baked on a hot plate for about 2 h at low temperature (60–80°C). Both master and PDMS were then cooled to room temperature and the PDMS was peeled from the master. The embedded metal wire posts were then pulled out of the PDMS. Finally, the PDMS was cleaned with ethanol and brought into contact with a clean glass, where a reversible seal formed spontaneously. For this particular study we found no need to make the PDMS hydrophilic by using a oxygen plasma treatment.

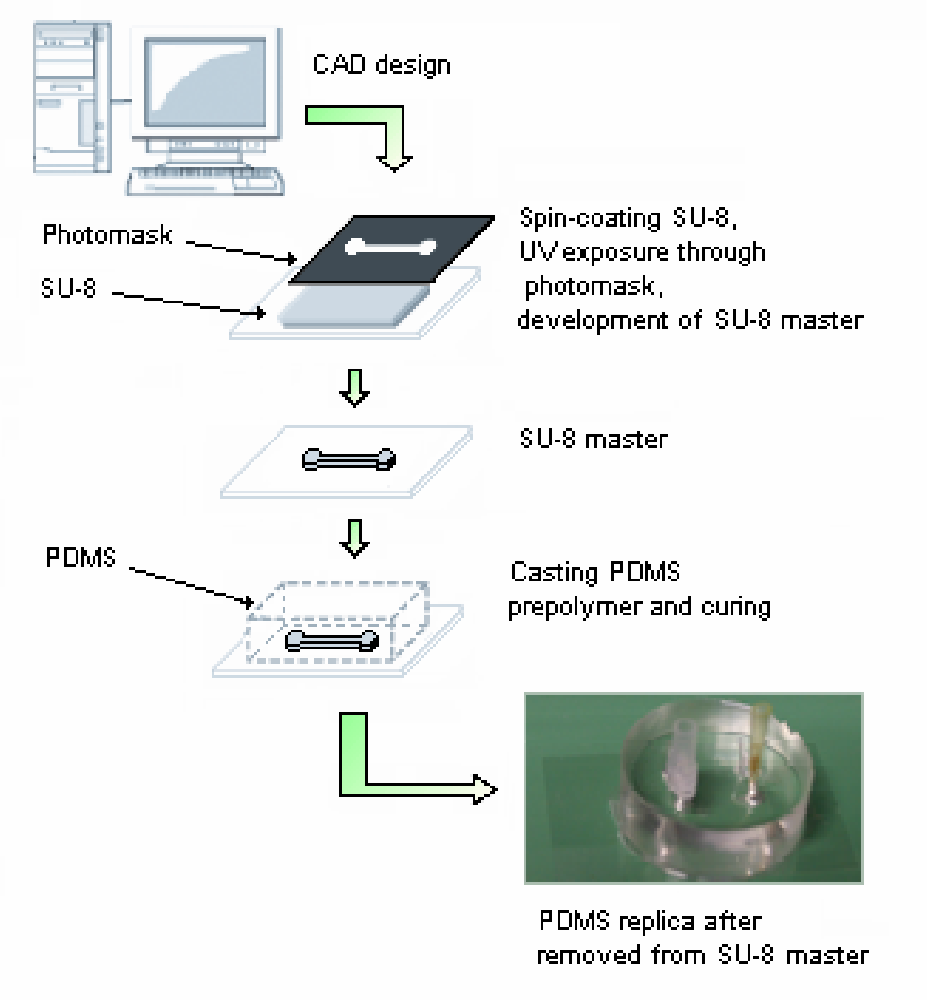

Figure 5.1 Main steps of the fabrication process.

The input/output ports were made by means of a 200 µl micro-pipette tip. This tip was inserted tightly into the connection channels where it exerts pressure on the PDMS and provides a liquidproof seal. Top tubes (2.1 mm outer diameter , 1.1 mm inner diameter) were also fitted tightly into the micro-pipette in order to deliver the working fluids from the syringe pump (see Figure 1). Due to the conical shape of the tip and low flow rates we did not observe

any fluid leakage during our experiments. Hence, we found no need to use additional bounding adhesives to avoid possible leakages from the microdevice.

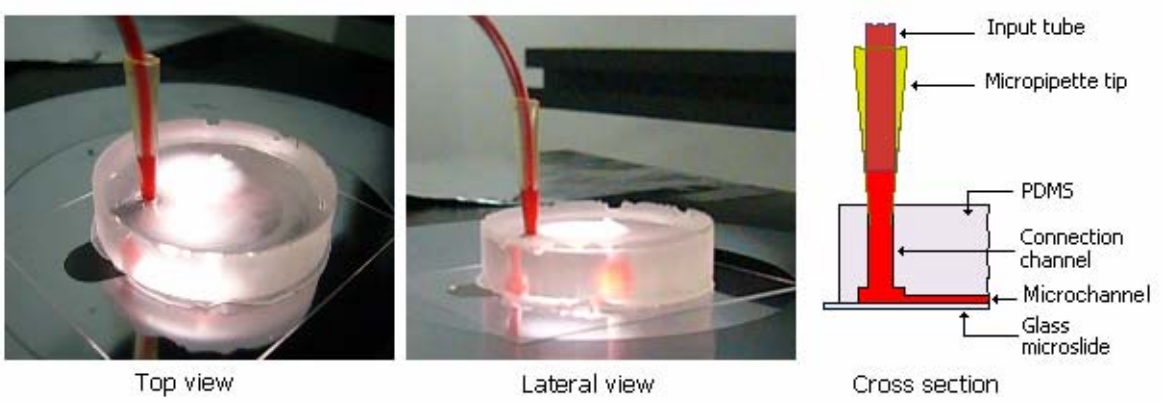

Figure 5.2 PDMS microdevice with the input port (a) top view, (b) lateral view, (c) schematic drawing of the cross section.

To evaluate the performance of the confocal micro-PIV system by comparing experimental data with a theoretical model, it is important to both qualitatively and quantitatively verify the actual final geometry of the PDMS microchannel. Thus, the depth profile of the microchannel was carefully measured using a surface profiler (P-10; KLA Tencor, USA). Figure 5.3 shows the average depth from eight different measurements along the PDMS microchannel. The average depth was found to be 45 μm ± 1 μm. In addition, by using a wide-field microscope the average width was found to be 300 μm ± 2 μm. Therefore, the measurement uncertainties for the depth and width of the microchannel were 2.2% and 0.7%, respectively. We also cut the PDMS microchannel transversely to measure the angle of the microchannel wall. We verified that the microchannel had a cross section that was nearly a perfect rectangular shape (300 μm wide, 45 μm deep). Figure 5.4 shows the cross section of the rectangular PDMS microchannel under an optical microscope.

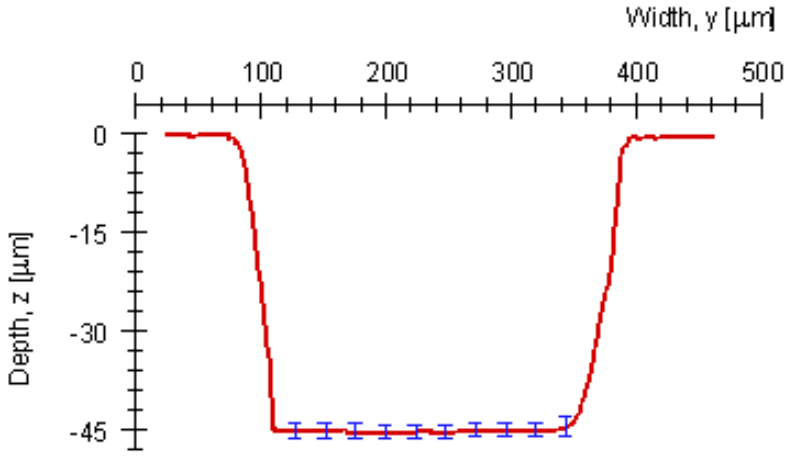

Figure 5.3 Average depth of the rectangular PDMS microchannel. The measured values of the depth are expressed as the means ± standard deviation.

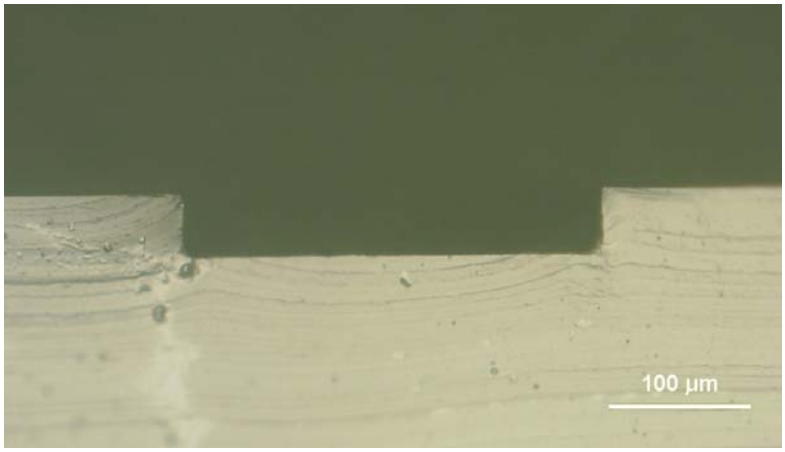

Figure 5.4 Cross section of the PDMS microchannel.

5.2.2 Sample preparation: working fluids and blood samples

Two working fluids were used in this study: physiological saline (PS) and *in vitro* blood (PS containing ~20% (by volume) human red blood cells (RBCs)). Fluids were seeded with 0.15% (v/v) 1-μm-diameter red fluorescent solid polymer microspheres (R0100; Duke Scientific, USA). For the *in vitro* blood, the fluorescent particles were first washed twice before seeding into the blood cell suspension.

Venous blood (~20 mL) was collected from a healthy, adult volunteer (aged 32 years old) to make six samples with ~20% (by volume) RBCs suspended in PS. To prevent coagulation of the blood cells during the experiment, ethylenediaminetetraacetic acid (EDTA) was added to the glass tube. The RBCs were separated from bulk blood by centrifugation (3000 rpm, 5 min) and aspiration of the plasma and buffy coat, and were then washed twice with PS. The washed RBCs were diluted with PS to make up the required RBC concentration by volume. The haematocrit of the RBC suspension was about ~20% (20% Hct) and the volume of each sample was 500 μL. Blood samples were stored at 4ºC until the experiment was performed at room temperature (25–27ºC). All procedures in this experiment were carried out in compliance with the Ethics Committee on Clinical Investigation of Tohoku University.

5.2.3 Confocal micro-PIV experimental setup

The confocal micro-PIV system used in this study is shown in Figure 5.5. A detailed description of the confocal system can be found elsewhere (Lima et al. 2006). In brief, the confocal system consisted of an inverted microscope (IX71; Olympus, Japan) combined with a confocal scanning unit (CSU22; Yokogawa, Japan), a diode-pumped solid-state (DPSS)

laser (Laser Quantum, UK) with an excitation wavelength of 532 nm, and a high-speed camera (Phantom v7.1; Vision Research, USA). The laser beam was illuminated from the bottom of the microscope stage through a dry 20× objective lens with a numerical aperture (NA) of 0.75. The light emitted from the fluorescent tracers flowing within the microchannel passed through a color filter into the scanning unit CSU22, where light was reflected by a dichromatic mirror onto a high-speed camera to record the PIV images.

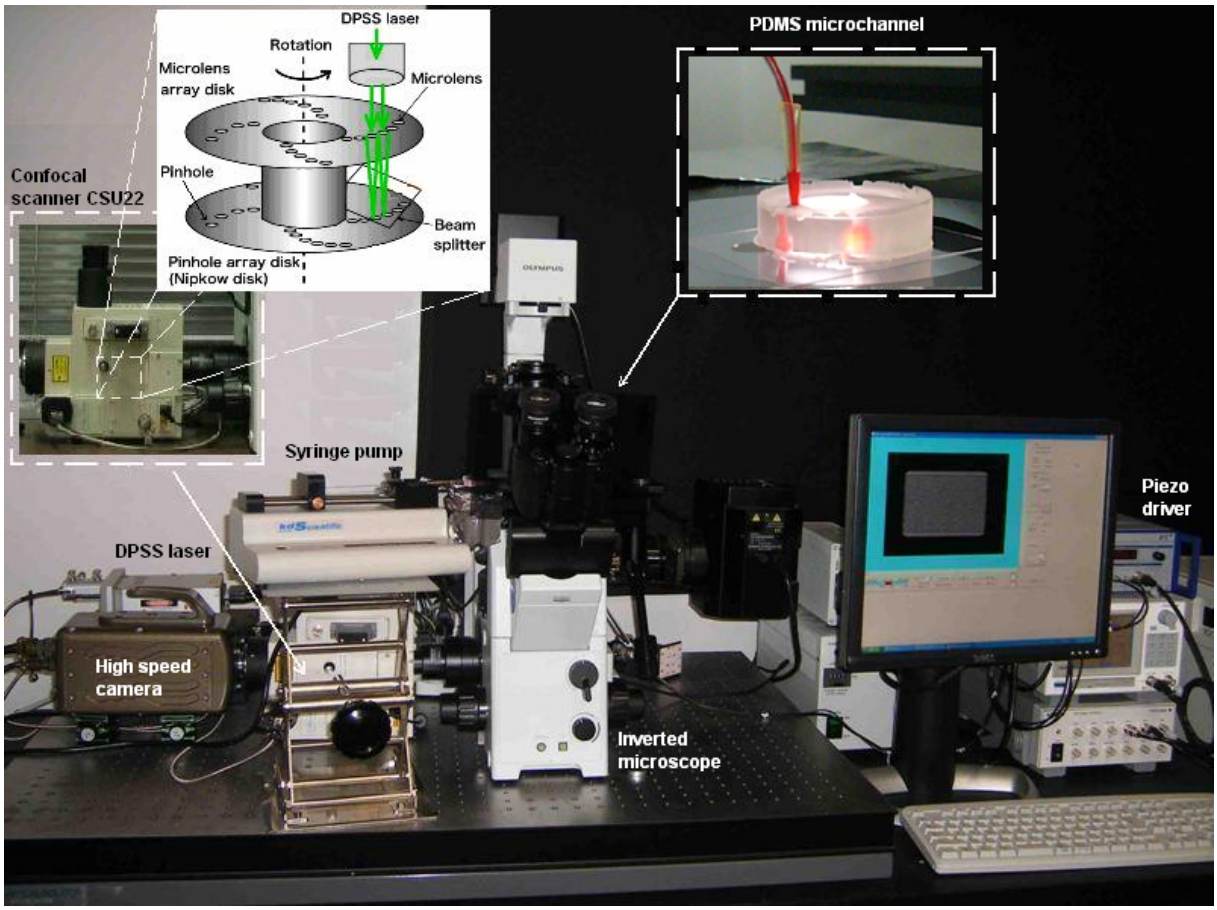

Figure 5.5 Confocal micro-PIV experimental setup.

The rectangular PDMS microchannel (300 μm wide, 45 μm deep, 10 mm long) was placed on the stage of an inverted microscope and using a syringe pump (KD Scientific, USA) a constant pressure-driven flow of 0.22 μL/min was maintained, corresponding to a Reynolds number (Re) of ~0.021 (based on the hydraulic diameter). A glass microsyringe (50 μL capacity) was used to obtain a flow rate as close as possible to a steady flow.

For the working fluids, the PIV images were first captured with a resolution of 640 × 480 pixels, at a rate of 200 frames/s with an exposure time of 4,995 μs and then recorded to a computer for evaluation, using the Phantom camera control software (PH607). Using a dry 20×/0.75 NA objective lens, the estimated thickness of the measurement plane (optical slice

thickness) was 4.97 μm. Moreover, by using a high-speed objective lens actuator with submicron *z*-direction resolution it was possible to accurately capture optically sectioned images along the depth (*z*-axis) of the PDMS microchannel.

The PivView version 2.3 (PivTec, Germany) software (Willert et al. 1996, Rafael et al. 1998) was used to process the images by an iterative cross-correlation method (Willert et al. 1996, Rafael et al. 1998), while an advanced correlation technique (multi-grid interrogation) was used to improve the accuracy of the particle image displacement. The cross-correlation evaluation with grid refinement has been previously described (Willert et al. 1996, Rafael et al. 1998). In brief, the cross-correlation method is a statistical analysis that determines the average displacement by comparing the positions of the tracer particles within an interrogation area in two consecutive images. The cross-correlation function $R_{fg}(x, y)$ can be defined as (Rafael et al. 1998, Nguyen & Wereley 2002):

$$R_{fg}(x,y) = \sum_{i=1}^{p}\sum_{j=1}^{q} f(i,j)g(i+x, j+y), \qquad (5.1)$$

where p and q are the dimensions (in pixels) of the interrogation area, and $f(i,j)$ and $g(i,j)$ represent the grey value distribution of the first and second image, respectively. The cross-correlation function correlates images of particles in two consecutive interrogation areas (particle image pair). The displacement of a particle image pair corresponds to the highest peak in the correlation plane. However, when small interrogation areas (usually less then 32 × 32 pixels) are used, random correlations can result in noisy peaks and can generate an erroneous velocity vector (outlier). To reduce measurement uncertainty and also to improve the signal-to-noise ratio, a multi-grid interrogation technique can be applied to the cross-correlation analysis (Rafael et al. 1998). The evaluation procedure of this advanced correlation technique is first based on a cross-correlation analysis at a relatively high correlation area (usually 32 × 32 pixels or more) in order obtain an accurate estimation of the displacement and then the process is repeated at each pass by refining the interrogation area. By using this procedure the displacement at a smaller interrogation area can be estimated with high accuracy and consequently high-resolution velocity vectors can be generated.

In our study, we used the iterative cross-correlation method, in which a multi-grid interrogation algorithm (grid refinement) was selected for evaluating the PIV image pairs. The initial interrogation area was 64 × 64 pixels whereas the final size was 24 × 32 pixel (50% overlapped) Furthermore, the least squares Gauss fitting algorithm was used for

detecting the peak on the correlation plane. Finally, the data were converted to the corresponding velocity fields using a magnification factor of 0.86 pixel/μm and pulse delay of 5 ms.

5.2.4 Ensemble averaged velocities

At steady flows, ensemble averaged velocities are known to improve the signal-to-noise ratio and consequently to generate more accurate velocity fields (Rafael et al. 1998, Meinhart et al. 2000). In this study, using the average velocity method, 100 instantaneous velocities measurements were ensemble-averaged to obtain the mean velocity field,$(\bar{U})$. This method first calculated the displacement field (peak detection) for each image pair and then the averaging operator was applied to all the instantaneous velocities measurements. The time-average mean velocity vector of the flow can be defined as

$$\vec{U} = \frac{\sum_{t=1}^{n} u_t}{n}, \qquad (5.2)$$

where n is the number of valid instantaneous velocity measurements. In this study, we evaluated 100 images with time intervals of 5 ms.

By calculating the u-component of the time-average mean velocity, it is possible to obtain the time-averaged velocity vector magnitude (U), which can be expressed as

$$U = \left|\vec{U}\right|. \qquad (5.3)$$

The time-averaged velocity vector magnitude for six different samples $(\overline{U})$ was defined as

$$\overline{U} = \frac{1}{m \times n} \sum_{i=1}^{m} \sum_{i=1}^{n} U \ , \qquad (5.4)$$

where m is the number of samples used and n is the number of grid points along the x-direction.

5.3 Results

5.3.1 Physiological saline (PS)

To evaluate the performance of the confocal micro-PIV system in measuring the velocity fields of the working fluids through the PDMS rectangular microchannel, the experimental results for PS were compared to a well established analytical solution for steady flow through a long, straight, rigid rectangular microchannel, that of Poiseuille flow. The equation used to calculate the analytical velocity profile of the rectangular microchannel with y and z cross section is the following (Bruus 2004, Mortensen et al. 2005):

$$u_x(y,z) = \frac{48Q}{\pi^3 hw} \frac{\sum_{n,odd}^{\infty} \frac{1}{n^3}\left[1 - \frac{\cosh(n\pi \frac{y}{h})}{\cosh(n\pi \frac{w}{2h})}\right]\sin(n\pi \frac{z}{h})}{\left[1 - \sum_{n,odd}^{\infty} \frac{192h}{n^5\pi^5 w}\tanh(n\pi \frac{w}{2h})\right]}, \qquad (5.5)$$

where u_x is the fluid velocity in the x-direction, y and z are the directions normal to the flow, w and h are the width and depth of the microchannel, respectively, and Q is the flow rate.

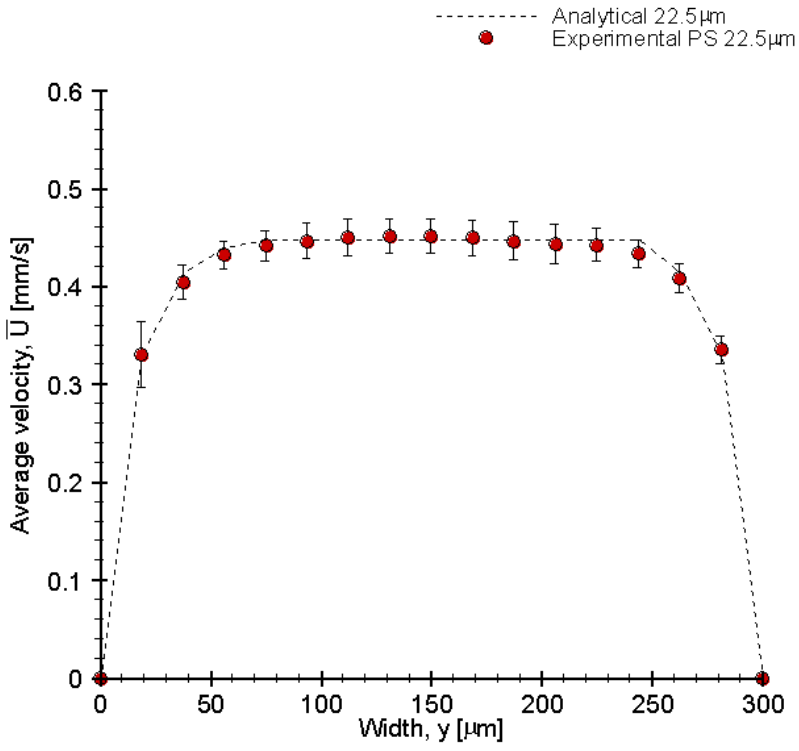

Figure 5.6 Comparison of experimental data and the theoretical model in the central plane (22.5 µm). The error bars represent the standard deviation of six measurements using Student's t-test with a 95% confidence interval.

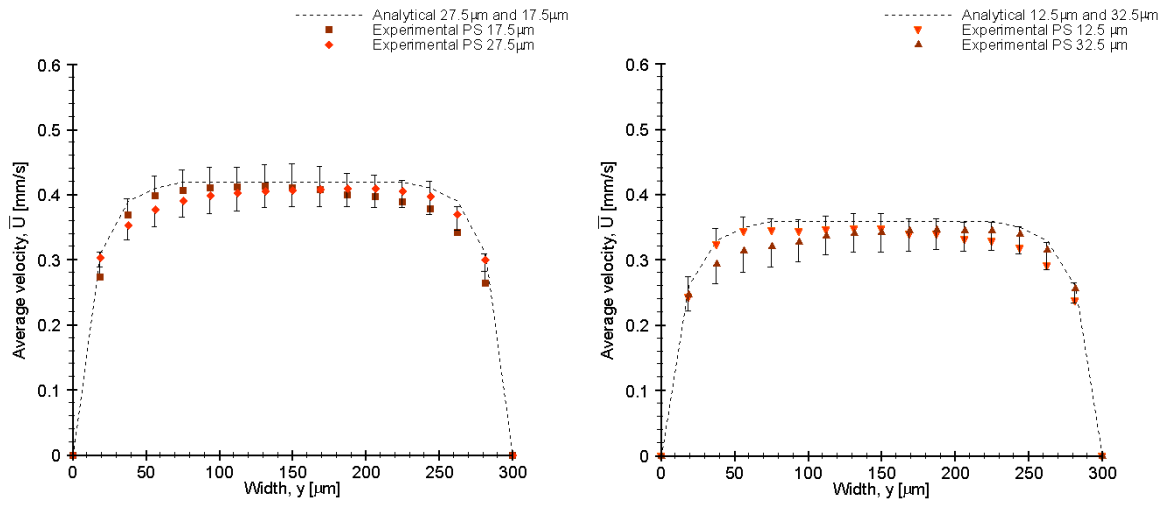

a) b)

Figure 5.7 Comparison of the experimental data and the theoretical model for optically sectioned images at a) z = 17.5 µm and z = 27.5 µm; b) z = 12.5 µm and z = 32.5 µm.

Figures 5.6 and 5.7 compare the theoretical estimates using Equation 5.5 and the average fluid velocities of 100 PIV image pairs for several optically sectioned planes along the microchannel depth. The PIV measurements were obtained with an exposure time of 4995 µs, magnification factor (pixels/µm) of 0.86, and time interval of 5 ms between two images.

Generally, the experimental results shown in Figures 5.6 and 5.7 were in good agreement with the analytical solution, especially the results at the middle plane (z = 22.5 µm), where we found errors less than 5% (Figure 5.6). As one moves out of the middle plane, the deviations start to increase and at locations close to the wall, the errors are around 7% (Figure 5.7).

5.3.2. Blood flow

5.3.2.1. Ensemble-averaged velocity profiles

In addition to examining PS, we studied the behaviour of *in vitro* blood (RBCs in PS, 20% Hct) through the rectangular PDMS microchannel. An example of a recorded image (halogen illumination source) of the *in vitro* blood flow is presented in Figure 5.8a. Figure 5.8b displays an image with both RBCs (halogen illumination) and fluorescent particles (laser-emitted light). The latter image could be used to calculate the velocity fields of the *in vitro* blood flow.

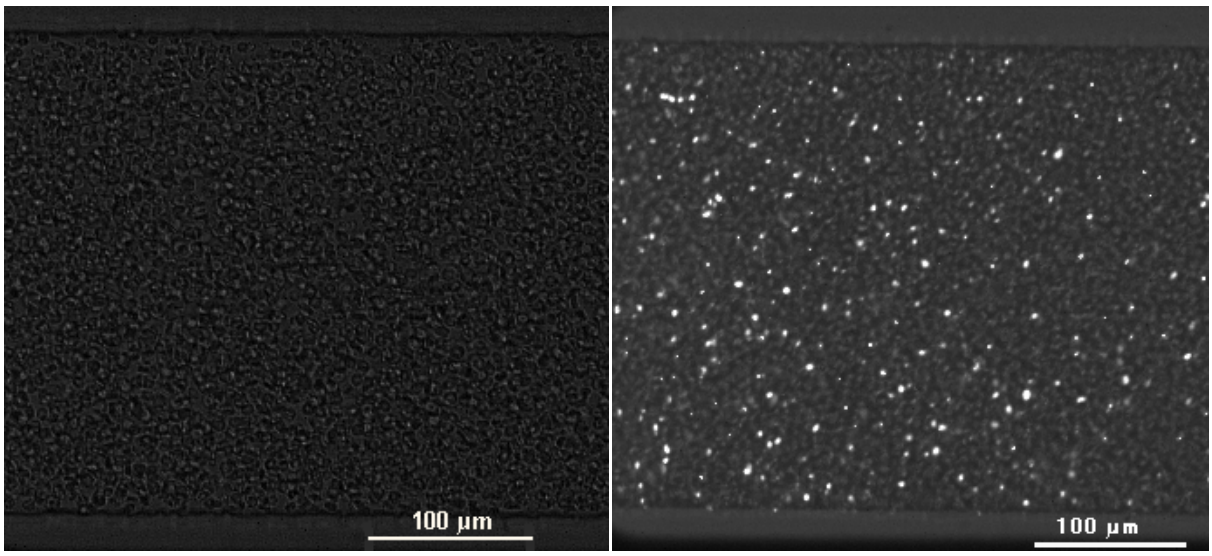

a) b)

Figure 5.8 a) An image of *in vitro* blood (20% Hct) flow with halogen illumination. The RBCs are observed as dark grey rings. b) Image of the same fluid in which both fluorescent particles and RBCs are visualised.

Figures 5.9 and 5.10 compare the mean velocity profiles of 100 ensemble image pairs for PS and *in vitro* blood (20% Hct), from six different measurements recorded at different *x*–*y* planes, spaced at 5 µm depth intervals (*z*-direction). Both results were obtained under the same experimental conditions (Re = 0.021).

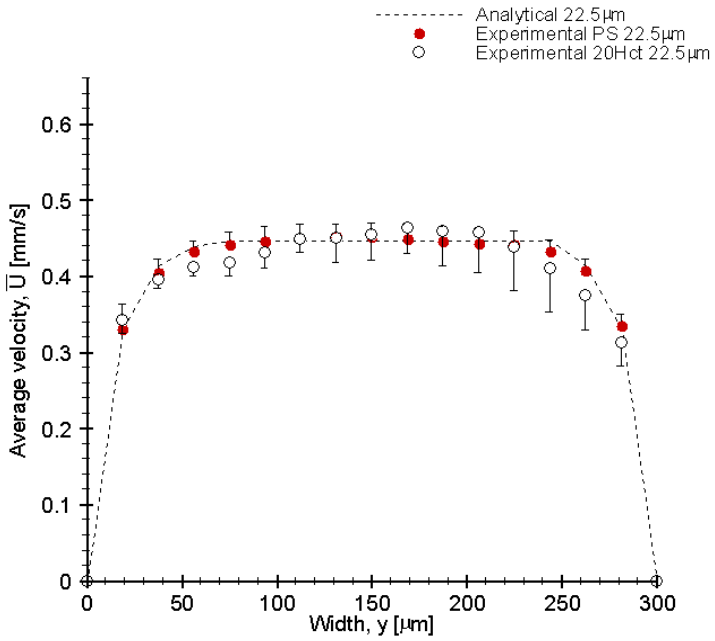

Figure 5.9 Comparison of ensemble-averaged velocity of PS and *in vitro* blood in the central plane (22.5 µm).

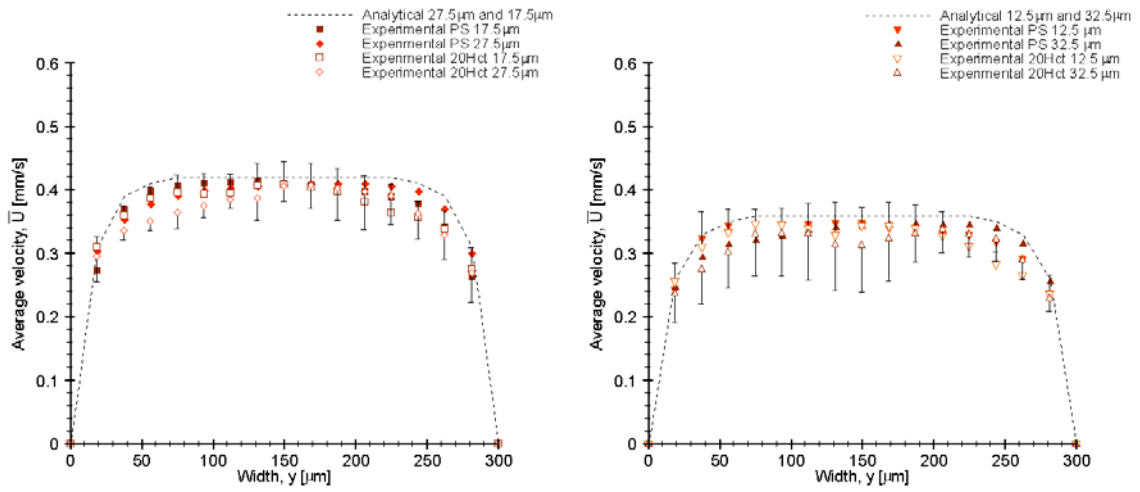

a) b)

Figure 5.10 Comparison of ensemble-averaged velocity of PS and *in vitro* blood at a) z = 17.5 µm and z = 27.5 µm; b) z = 12.5 µm and z = 32.5 µm.

From Figures 5.9 and 5.10, the velocity profiles of the PS fluid in several horizontal planes (x–y axis) clearly show that the flow is stable and fully developed. In addition, Figures 5.9 and 5.10 also show that for PS fluid, the shape of the mean velocity profile is markedly blunt in the middle region. However, examining the average velocity profiles of the *in vitro* blood, small deviations between the fluids were observed, especially in the regions near the walls. These small perturbations along the width of the microchannel become much clearer on analysing the 3-D profiles shown in Figure 5.11. From Figure 5.11a indicates that the PS velocity profile along the z-direction had a smooth parabolic shape, whereas the *in vitro* blood flow (Figure 5.11b) was characterised by a velocity profile containing several small disturbances along the z-direction.

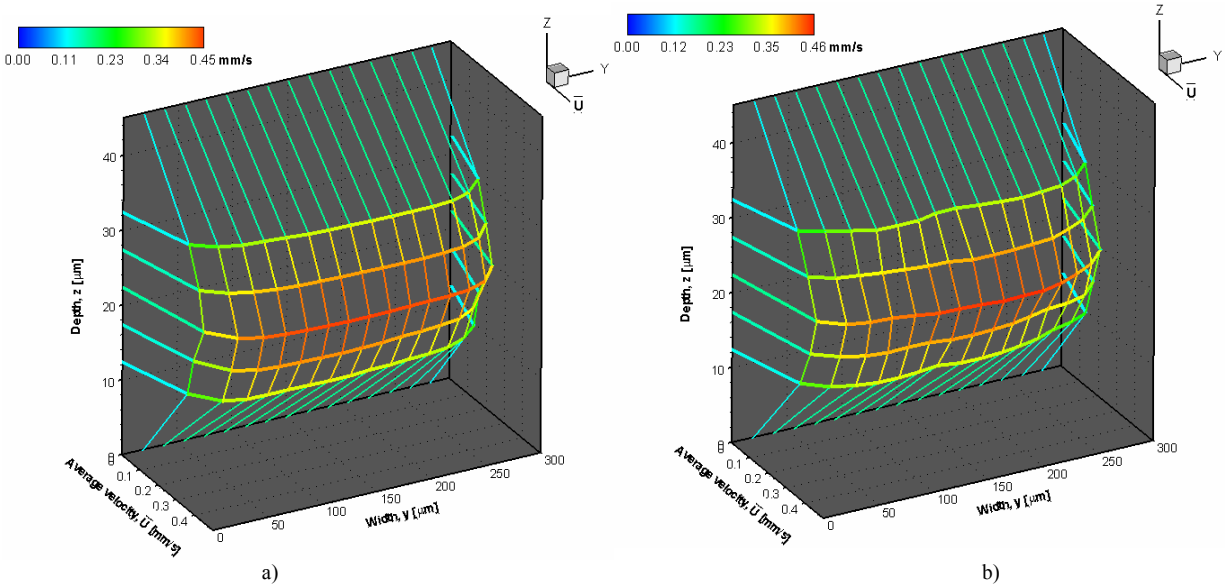

a) b)

Figure 5.11 Three-dimensional representation of optical sectioning velocity profiles of a) PS and b) *in vitro* blood.

5.3.2.2 Ensemble velocity profiles in the middle plane

It is generally agreed that the ensemble average velocity process improves the reliability and accuracy of PIV measurements because of the improvement in the signal-to-noise ratio and the reduction of measurement errors associated with the Brownian motion of the tracer particles and some possible "bottleneck" effects of the syringe pump. Furthermore, our experimental confocal PIV results with the PS fluid compared to the theoretical model (Figure 5.6) showed the best agreement in the middle plane of the microchannel ($z = 22.5$ µm) because of a reduction in several effects resulting from the microchannel wall (interaction between particle and wall, roughness of the wall, *etc.*). The PIV measurements in the middle plane seemed to generate results closer to the true velocity profile present in the rectangular PDMS microchannel. In this study, six samples of 100 PIV image pairs at the middle plane were analysed for both PS and *in vitro* blood (20% Hct). Figures 5.12 and 5.13 show the time-averaged velocity profiles (U) along a certain length (150 µm) from two different representative samples for PS and *in vitro* blood, respectively.

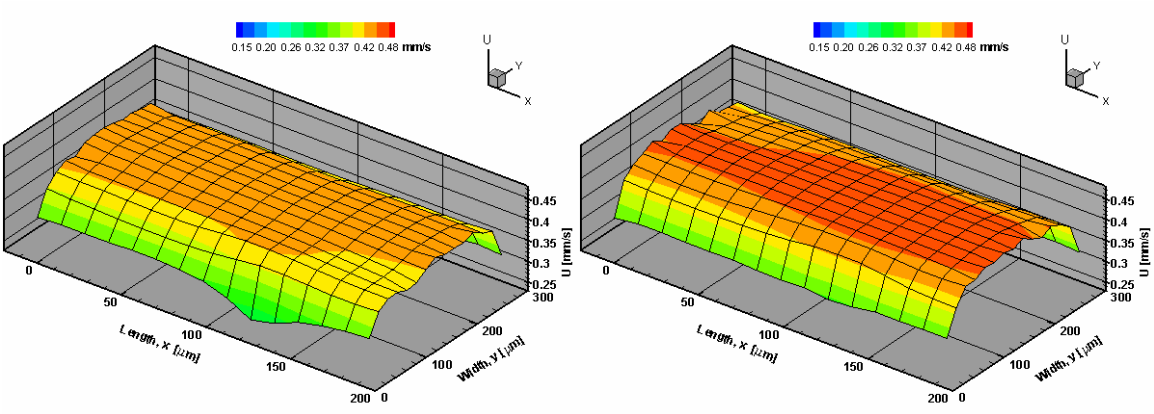

a) sample 1 b) sample 2

Figure 5.12 Ensemble velocity profiles (U) of two representative samples in the middle plane for PS

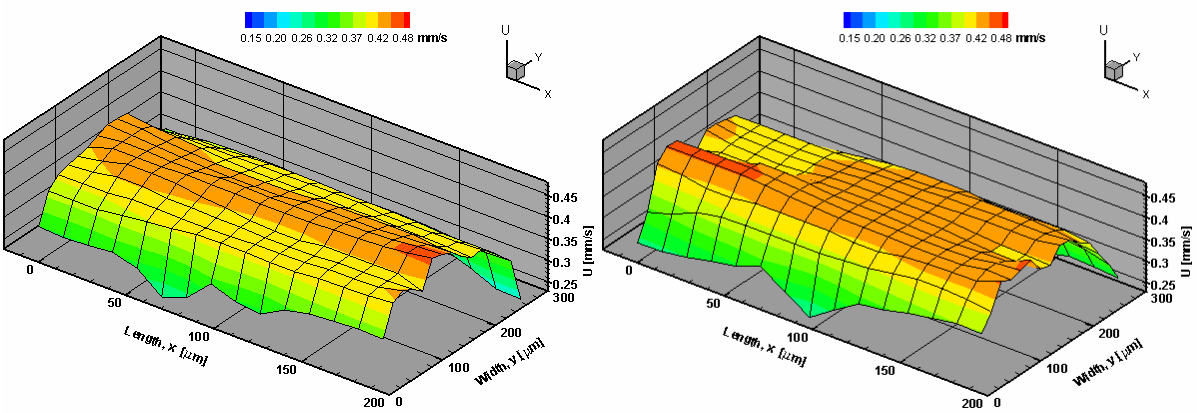

a) sample 1 b) sample 2

Figure 5.13 Ensemble velocity profiles (U) of two representative samples in the middle plane for *in vitro* blood.

Figure 5.12 shows that when using PS fluid, a markedly smooth, flat profile tended to develop along the rectangular microchannel. However, for the *in vitro* blood flow, small perturbations in the shape of the ensemble velocity profiles were observed (Figure 5.13). These qualitative observations can play an important role in providing reliable information on the time-averaged flow behaviour over a specific period of interest.

5.3.2.3 RBC flow visualization

To determine possible causes of the perturbations in the velocity profiles of the *in vitro* blood flowing in the rectangular microchannel, RBC motion was visualized with halogen illumination from our confocal micro-PIV system. Figure 5.14 shows the dynamic behaviour of the RBCs in a rectangular microchannel with a low aspect ratio. Figure 5.14 also shows detailed consecutive halogen images captured at time intervals of 10 ms, when the motion of one particular RBC was followed.

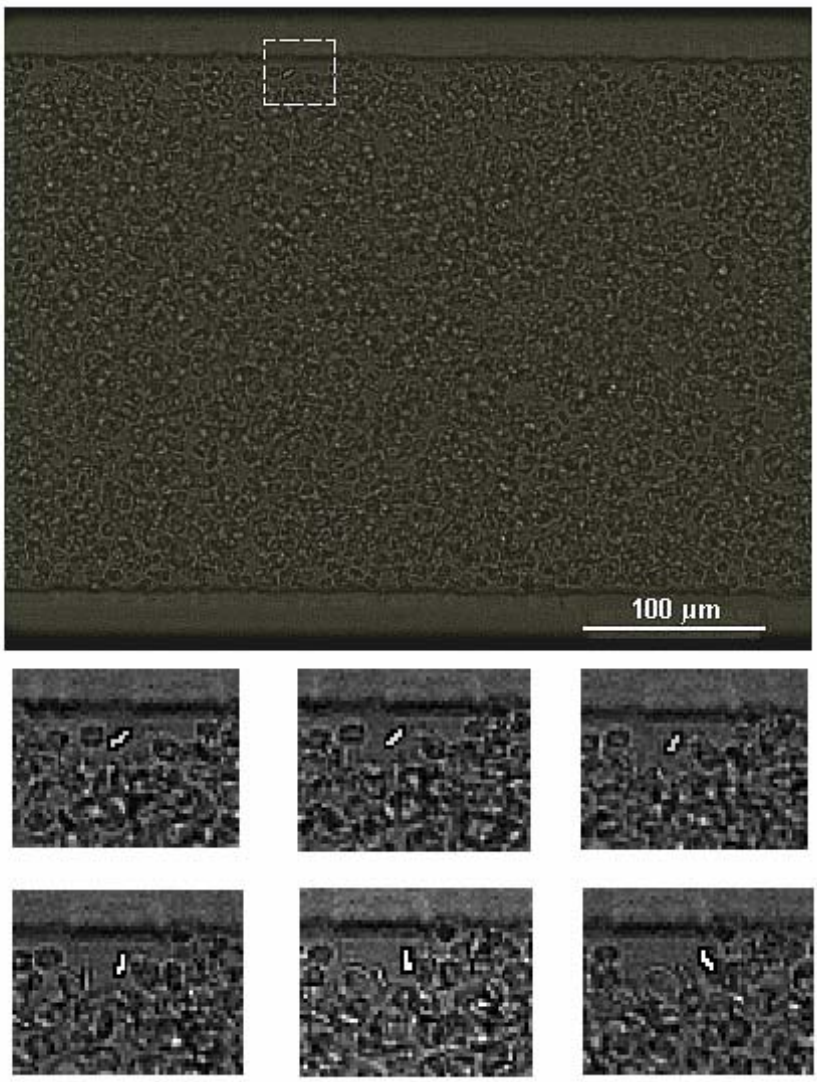

Figure 5.14 Motion of one RBC flowing in a rectangular microchannel with a low aspect ratio (h/w = 0.15). The RBC of interest has a bright grey color in its central region. All images were captured with a 20× objective lens.

During the capture of the images, we did not observe a plasma layer which may have been due to the geometry of the rectangular microchannel and PS suspension medium. Furthermore, in the central region of the microchannel (shear rate close to zero), the RBCs tended to move along with the flow with a regular rotational motion, retaining their biconcave shape. Near to the wall, where the shear rate increases significantly, both rotational and tumbling motions accompanied by membrane deformation were observed (see detailed consecutive images in Figure 5.14). Interactions between neighboring RBCs at different depth planes (boundary layers) were also observed along the full microchannel.

5.3.2.4 Plasma layer

The formation of a plasma-rich layer located between the RBC core and wall is well documented in the literature on glass microchannels with diameters less than 300 μm (Faharaeus and Lindqvist 1931, Chien et al. 1984, Maeda 1996, Pries and Secomb 2003). However, to our knowledge the effect of both geometry and suspension medium in a straight rectangular PDMS microchannel has not been investigated. In an effort to understand the causes for no observation of any plasma layer in our microchannel, firstly we have investigated the effect of the flow rate on the formation of the plasma layer. Figure 14 shows *in vitro* blood (~20% Hct in PS suspension medium) through the rectangular PDMS microchannel, for two different flow rates. The results illustrate that the RBCs flowing in this particular microchannel (300 μm wide, 45 μm deep) do not have tendency to migrate toward the centre axis for Re up to 0.1.

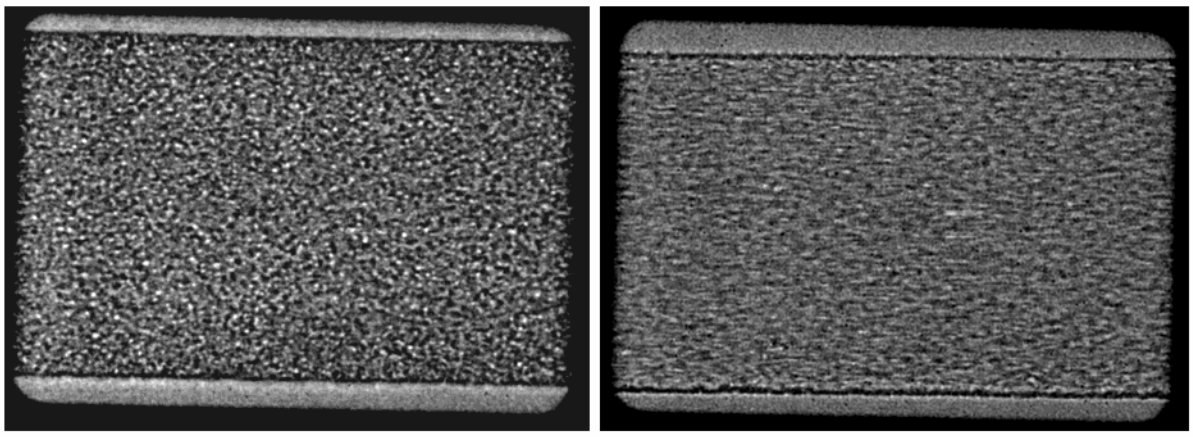

a) b)

Figure 5.15 Flow of RBCs (~20% Hct) suspended in PS through a rectangular PDMS microchannel 300 μm wide and 45 μm deep for a) Re ~0.02 b) Re ~0.1.

We next investigated the effect of the suspension fluid. In Figure 15 we show human RBCs (~20% Hct) suspended in dextran 40 (Dx-40, Otsuka Medicine) for Re up to 0.08. By using this high molecular suspension fluid, we eliminate the effects of sedimentation of the RBCs at low-shear rates. The qualitative results from Figure 15 show also no tendency for the RBCs to undergo axial migration.

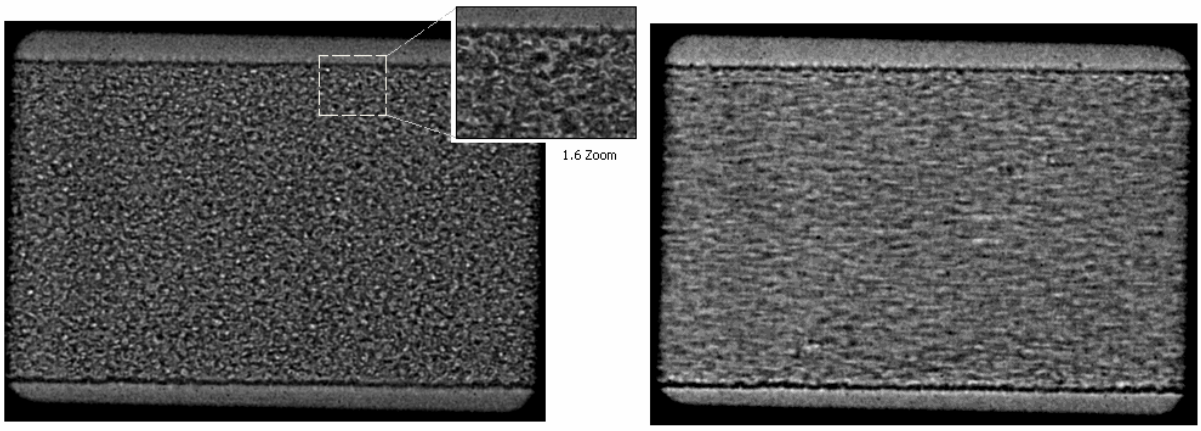

a) b)

Figure 5.16 Flow of RBCs (~20% Hct) suspended in dextran 40 (Dx-40) through a rectangular PDMS microchannel 300 μm wide and 45 μm deep for a) Re ~0.01 b) Re ~0.08.

Finally, we investigated the flow behavior of RBCs (~20% Hct) suspended in Dx-40 through a smaller PDMS microchannel (100 μm wide, 62 μm deep), for a Re ~0.03 (see Figure 16). In contrast to the previous results, the RBCs flowing through this PDMS microchannel have tendency to migrate toward the microchannel axis, promoting the formation of a plasma layer. Although we do not have extensive data on the influence of the width, it is nevertheless clear that the formation of the plasma layer is enhanced as the width becomes narrower.

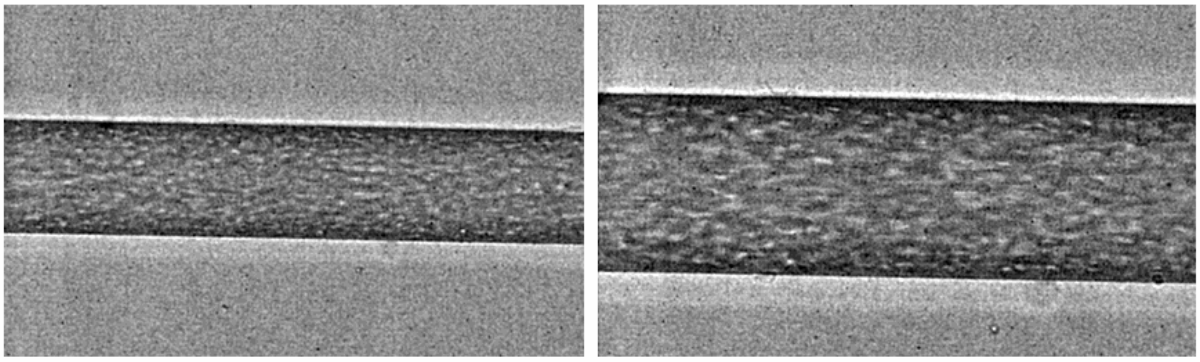

a) b)

Figure 5.17 Flow of RBCs (~20% Hct) suspended in dextran 40 (Dx-40) through a rectangular PDMS microchannel 100 μm wide and 62 μm deep for Re ~0.03 a) 20× objective lens b) 32× objective lens.

5.3.2.5 Physiological saline versus dextran 40

In Figure 5.18 we show fluorescent particles suspended in physiological saline (PS) and in dextran 40 (Dx-40). This qualitative results show that the particles have more tendency to aggregate each other when suspended in Dx-40. As a result, in this experiment we have decided to use PS as our working fluid.

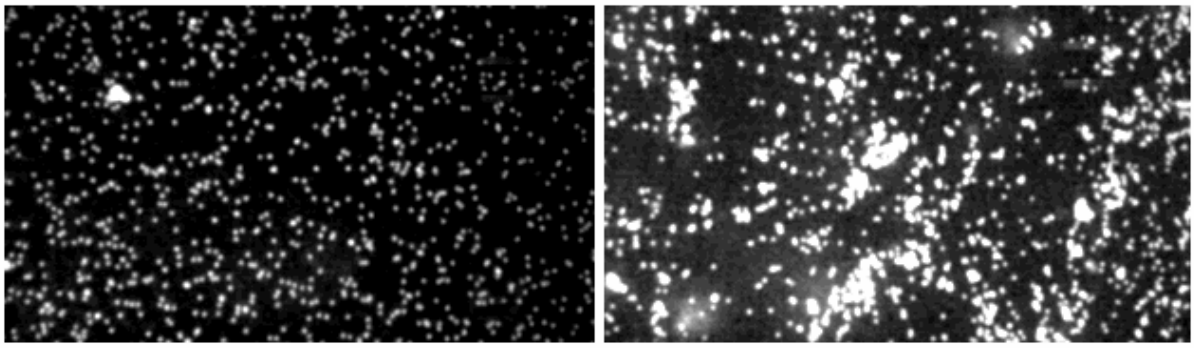

a) b)

Figure 5.18 Fluorescent particles suspended in a) physiological saline (PS) , b) dextran 40 (Dx-40).

5.4 Discussion

Flow behavior of PS and in vitro *blood through a PDMS microchannel*

In the present study, we determined the velocity profiles of PS fluid and *in vitro* blood (20% Hct) in a rectangular PDMS microchannel with a low aspect ratio (h/w = 0.15) using a confocal micro-PIV system. In the case of PS fluid, our results were in good agreement with the analytical solution around the central plane (z = 17.5 μm, z = 22.5 μm, and z = 27.5 μm). However, at locations closer to the wall, the errors were slightly larger than 7%. We believe that these larger errors were primarily attributable to "second-order effects," such as the surface roughness of the wall and background noise generated from particles adhering on the wall (bias effect). Although it is important to consider the data from all planes, we believe that the best results from the confocal system were presented in the middle plane. These results also demonstrated that around the central region, PS velocity profiles were markedly blunt, which is consistent with the characteristic behavior of a Newtonian fluid through a rectangular microchannel with a low aspect ratio.

By comparing the averaged ensemble velocity profiles of PS fluid and *in vitro* blood flow, we observed small deviations at all optically sectioned planes. These deviations were found to be larger at locations closer to the wall. Furthermore, the ensemble velocity profiles at the central

plane for the *in vitro* blood were not characterized by a flat profile in the central region; rather, the profile had small perturbations. The reasons for these small perturbations are still not completely understood. However, from the visualisation of the RBCs' motion through the rectangular microchannel, interactions between neighbouring RBCs seem to be an important factor to take into account. The abrupt increase in the shear rate in the vicinity of the wall likely plays an important role in the local disturbance effects caused by both rotational and tumbling motion of deformable RBCs within the fluid flow. Moreover, temporal variation in the haematocrit could be another factor contributing to the perturbations described above. From the six measurements (Fig. 5.13 shows two of six) performed at the centre plane at different time periods, all show random perturbations on the averaged ensemble velocity profiles. This suggests that the transverse motion of the RBCs fluctuates over time, consequently affecting the local apparent viscosity of the fluid. Effects such as Brownian motion, microelectrohydrodynamics, and bottlenecks (Tabeling 2001, Nguyen & Wereley 2002) seem unlikely to contribute significantly to the perturbations found in the *in vitro* blood velocity profiles because such perturbations were small when compared to the PS fluid profiles measured under the same experimental conditions. The present results suggest that the presence of deformable RBCs suspended within the plasma flow plays an important role on the hydrodynamic disturbance effect seen on the *in vitro* blood velocity profiles. Note that, these observations are consistent with several other measurements performed in glass microchannels (Goldsmith and Turitto 1986, Alonso et al. 1995, Lima et al. 2007). Further studies to clarify the presence of these fluctuations on the ensemble velocity profiles need to be conducted, not only using microchannels which closely mimic the actual human microvessels, but also using higher resolution objective lenses, such as 40× and 60×.

Plasma layer in a straight PDMS microchannel

It is well known that RBCs, in microvessels less than 300 μm (Faharaeus and Lindqvist 1931, Chien et al. 1984, Pries and Secomb 2003), tend to migrate towards the axis promoting the formation of a plasma layer adjacent to the vascular walls. In the present study we have used a PDMS microchannel with a width of 300 μm and depth 45 μm. For this particular microchannel no plasma layer was observed during our experiments. In order to understand the formation of the plasma layer in PDMS microchannels we have investigated the effect of different parameters on the formation of the plasma layer, including geometry, flow rate and suspending media. Under similar conditions, our results have showed that for a 300 μm wide microchannel no plasma layer was formed whereas for 100 μm width a thin plasma layer was

clearly observed. Thus, our qualitative results indicate that the geometry of PDMS microchannel is the main responsible for the formation of the plasma layer. In addition, our results also indicate that the plasma layer is enhanced as the width becomes narrower. This finding is consistent with a recent work performed on the flow of RBCs in model constrictions (Faivre *et al.* 2006).

PDMS versus glass microchannels

Several studies on blood flow in glass microchannels and in microvessels have yielded conflicting results with respect to flow resistance and deformability of RBCs (Pries at al. 1994, Suzuki et al. 1996). However, the observed *in vivo/in vitro* discrepancies have not yet been convincingly explained by using the research done in straight rigid glass microchannels. One possible way to overcome the limitations of the glass capillaries is by using PDMS microchannels. PDMS microchannels differ from glass capillaries in several ways (see also Table 5.2):

1. the permeability to gases, such as oxygen, has the unique advantage to culture living endothelial cells near to confluence (Borenstein et al. 2002, Shin et al. 2004) in closed microchannels, a task extremely difficult to achieve in glass capillaries. Very recently, a cellular micropatterning technique based on electrochemical method (Kaji et al., 2006) has also successfully cultured endothelial cells on the surfaces of PDMS microchannel;
2. PDMS is an elastomeric and biocompatible material. The typical ultimate tensile stress (UTS) for PDMS ranges from 3.9 MPa to 10.8 MPa (Mata et al. 2005), whereas the Young's elastic modulus (E) has a value of ~0.75MPa (Unger et al. 2000). The UTS and E of the blood vessels has values from 0.4 MPa to 1.4 MPa (Holzapfel et al 2005) and ~2.5 MPa (Steiger et al. 1989) respectively. The UTS and E is PDMS formulation dependent, by adjusting the ratio of the cross-linker (curing agent) and also the thickness of the wall, PDMS may be able to mimic more closely the geometric and structural properties of *in vivo* microvessels;
3. easy to replicate complex microvascular networks with submicron fidelity (McDonald et al. 2002, Shevkoplyas et al. 2003, Shin et al. 2004);
4. due to its spontaneous adhesion onto glass substrates, PDMS sealing does not need any complex bonding technique. Hence, PDMS microchannels besides offering optimum optical access for confocal systems, they can be reused several times because of its reversible bonding. Glass-to-glass sealing requires elaborate bonding processes such as direct, thermal compression or hydrofluoric bonding method, which are time consuming

and need very careful processing to obtain an acceptable yield. Using bonding interlayers such as silicon for anodic bonding, metal for fusion or eutectic bonding and spin-on-glass for thermal compression bonding are other options, however the interlayer are also deposited in the microchannel. In addition, all of these bonding methods need flat, smooth and clean surfaces, which requires a clean room facility.

5. possible to integrate into the PDMS device several functional components such as heaters, micromixers, micropumps, microvalves, temperature and pressure sensors, etc (Thorsen et al. 2002, Fujii 2002).

6. no need to use a refractive-index-matching liquid to minimize refraction from the walls. As a result, it is possible to use high magnification objective lenses (40×, 60×, 100×) with high NA, which have typically working distance from 100 to 200 μm. Consequently it is possible to obtain images with much higher resolution.

Table 5.2 Major advantages of PDMS microchannels over glass capillaries.

Physicochemical factors that affects blood flow behavior	**Glass capillaries**	**PDMS microchannels**	**Comments**
Ability to culture endothelial cells near to confluence	complex in closed microchannels	possible	Recently techniques have been developed to culture endothelial cells near to confluence in PDMS microchannels[1, 2, 3]. To the best of our knowledge, no work has reported culture cells near to confluence in closed glass microchanels. This is only possible by using parallel plate flow chambers[4].
Mechanical properties, ultimate tensile stress (UTS) Young's elastic modulus (E)	rigid material (UTS ~300 MPa to 900 MPa)[5] (E ~70 GPa)[5]	flexible material (UTS ~3.9 MPa to 10.8 MPa)[6] (E ~0.75 MPa)[7]	PDMS microchannels may be able to mimic the deformability of *in vivo* microvessels (UTS ~ 0.4 MPa to 1.4 MPa[8], E ~2.5 MPa[9]). PDMS allows large deflections with small actuation forces[7].
Geometry of the flow channel	any kind of geometry using photolithography, but limited in cross section, especially aspect ratio	any kind of geometry	Presently it is possible to fabricate rectangular PDMS microchannels with complex geometries[10]. Fabrication of microchannels in PDMS is simple, rapid and has high replication fidelity. In contrast, fabrication in glass increases the time, complexity, and cost of the fabrication process[11].

References : [1] Borenstein et al. 2002, [2] Shin et al. 2004, [3] Kaji et al. 2006, [4] Brown 2000, [5] Rika nenpyo 1996, [6] Mata et al. 2005, [7] Unger et al. 2000, [8] Holzapfel et al. 2005, [9] Steiger et al. 1989, [10] Shevkoplyas et al. 2003, [11]McDonal et al. 2002.

In addition, by using a soft lithography technique it is possible to fabricate easily precise and reproducible rectangular microchannels at low cost, because the master mold is reusable. Rectangular PDMS microchannel with a low aspect ratio seems to be appropriate to perform confocal micro-PIV measurements of *in vitro* blood with Hcts close the actual *in vivo* Hct in microcirculation. However, this geometry may not reflect the actual physiology of the microcirculation. Hence, very recently we have successfully fabricated straight circular PDMS microchannels by using a wire casting technique (see Appendix C). The fabrication of circular PDMS microchannels with complex geometries still remains a big challenge. Recently, Borenstein and his co-workers (2002, 2004) are developing a precise alignment technique to produce true cylindrical channels. However, the complexity of the alignment procedure, time-consuming and the thickness of the two matching PDMS templates containing the semicircular microchannels, may limit its practical applications onto confocal systems.

Nevertheless the limitations of PDMS microchannels, it is clear that this kind of microdevices exhibit features more close to the actual physiological conditions of the *in vivo* microvessels when compared with glass capillaries. Although PDMS microdevices are promising to mimic the *in vivo* microvascular environment, many challenges remain. First, the current PDMS fabrication processes need to be improved in order to produce precise circular microchanels with thin walls less than 200 μm to obtain accurate measurements by means of confocal systems. Second, PDMS collapsible microchannels need to be developed in order to mimic the deformability of blood vessels more closely. Finally, it is also imperative to evaluate if the current cell culture techniques used in PDMS microchannels create a microvascular environment closely representative of the *in vivo* situation.

Ongoing development

The *in vitro* research performed with classical glass microchannels has revealed several astonishing phenomena happening in microcirculation. Some examples are the Fahraeus effect and Fahraeus-Lindqvist effect (Chien et al. 1984). However, recently several studies on flow resistance (Pries at al. 1994) and RBCs deformation (Suzuki et al. 1996) have shown quantitative difference between the results in microvessels and in glass microchannels. The reason for these differences still remains unclear mainly because glass microchannels differ from microvessels in several aspects, such as elasticity and geometry of the microchannel and biological effect by the endothelial inner surface. We believe that these limitations

encountered in glass microchannels can be overcome by using a PDMS microchannel (see Table 2). Nevertheless, before moving to a more elaborated PDMS microchannel, we must first understand the flow behaviour of blood in simple geometry similar to the one used in the present study. To fully exploit the potential of this combined system, we are working to develop a synergetic biochip to mimic the *in vivo* environment. By using an innovative cellular micropatterning technique based on electrochemical method (Kaji et al., 2006), we expect to culture endothelial cells on the surfaces of the PDMS microchannel to near confluence. In addition, by combining this microdevice with the confocal system, we will be able to identify and quantitatively measure cellular and molecular events occurring between the blood cells and endothelium. As a longer range goal, we believe that this ongoing research will lead to new insights into the complicated microcirculation phenomena such as the role of the glycocalyx on the blood flow behaviour and the thrombogenesis process.

Because of their outstanding properties, rectangular PDMS microchannels are gaining popularity in biomedical research. In addition to providing the ability to investigate a variety of phenomena in the microcirculation (Takayama *et al.* 1999, Fujii 2002, Shevkoplyas *et al.* 2003), this kind of microfluidic device may be useful as a "lab-on-a-chip," a clinical diagnostic instrument. However, until now, precise measurements of blood flow behavior through this kind of microchannel has not been performed. In the present study, we demonstrated that by combining the rectangular PDMS microchannel with a confocal micro-PIV system it is possible to obtain both qualitative and quantitative information about the complex biophysical behaviour of *in vitro* blood flow at a mesoscopic level. Thus, we believe that the present combination has potential as a powerful tool to investigate several phenomena in the microcirculation.

5.5 Conclusions

We applied a confocal micro-PIV system to examine PS and *in vitro* blood flowing in a rectangular PDMS microchannel with a low aspect ratio. For PS, the flattening of the velocity profiles was in good agreement with an established analytical solution for this kind of microfluidic device. However, when we assessed the flow of *in vitro* blood (20% haematocrit), small fluctuations were observed in the velocity profiles at optically sectioned planes along the *z*-axis. Blood flow measurements performed at the centre plane of the microchannel clearly show small fluctuations on averaged ensemble velocity profiles. The reasons for the encountered "microturbulences" are not entirely clear, but our qualitative observations

indicate that interactions between neighbouring RBCs, the high shear rate generated in the vicinity of the walls, and temporal fluctuations in the haematocrit may play important roles in the hydrodynamic disturbance effects encountered in the blood velocity profiles. However, due to the variety of complex phenomena occurring at the microscale level, further studies are needed to clarify the presence of these fluctuations on the ensemble velocity profiles.

The measurements presented in this study clearly showed that confocal micro-PIV can be effectively integrated with a PDMS microchannel to obtain blood velocity profiles along the full depth of the microchannel because of its 3-D optical sectioning capability. This study also demonstrated that the combination of confocal micro-PIV systems with PDMS microchannels can play an important role in not only assessing existing theories, models, and computer simulations of the microcirculation, but also in the development of an accurate biochip device for various biomedical applications, such as patient diagnosis and monitoring, drug delivery, and cancer cell detection.

CHAPTER 6

MICROHAEMODYNAMIC MEASUREMENTS IN CONCENTRATED SUSPENSIONS OF ERYTHROCYTES USING A CONFOCAL MICRO-PTV SYSTEM

6.1 Introduction

Human blood is a complex fluid composed of deformable cells, platelets and proteins suspended in an aqueous solution called plasma. Phenomena of blood flow in microcirculation depend on several combined effects such as cell deformability, flow shear rates, vessel wall together with microscale biochemical and physiological factors. Since the availability of microscopic technique, scientists start investigating the flow behavior of blood in the microcirculation. One of the first main observations on the non-Newtonian behavior of the blood flowing in capillaries was done by Fahraeus and Lindqvist (Fahraeus and Lindqvist 1931). They found that when blood flows in capillaries less than 300 μm its apparent viscosity decreases with the capillary diameter in contrast to the Poiseuille law. However, some explanations on this finding was only provided in the 70's by microscopic observations (Schmid-Schonbein and Wells 1969, Chien 1970, Goldsmith 1971a, Goldsmith 1971b, Fischer et al. 1978). The most acceptable explanation relies on the formation of a cell-free layer (plasma layer) near the wall due to the tendency of the red blood cells (RBCs) to migrate towards the center of the capillary. After these observations, extensive research on flow properties of blood was performed in both diluted and concentrated suspension of blood cells by using several measuring techniques such as double-slit photometry (Gaehtgens et al., 1970; Baker and Wayland, 1974), video microscopy and image analysis (Bugliarello et al. 1963, Tangelder et al., 1986; Parthasarathi et al. 1999, Goldsmith 1971a, Goldsmith 1971b, Goldsmith and Karino 1977, Gifford et al. 2003, Suzuki et al. 1996, Alonso et al. 1995, Fischer et al. 1978), laser-Doppler anemometry (Einav et al. 1975, Born et al. 1978, Cochrane et al. 1981, Uijttewaal et al. 1994, Golster et al. 1999), and particle-measuring methods (Bitsch et al. 2005, Vennemann P. et al. 2006, Sugii et al. 2006, Kim and Lee 2006, Lima et al. 2007). Although the studies on the microhaemodynamic behavior of single red blood cells in diluted suspensions are reaching to a mature state, for highly concentrated suspensions still

not completley understood, partly due to technical limitations. The main limitation in measuring high concentrations of RBCs derives mainly from the attenuation of the incident light by hemoglobin absorption and RBCs light scattering. Thus, although the recent advances in microscopy, there still is a lack of understanding on the blood flow phenomena at a microscopic level.

Along the years Goldsmith and his colleagues have performed series of experiments on the flow behavior of blood cells in glass capillaries. An excellent review on their findings can be found in Goldsmith and Turitto 1986. Their results have provided the best insight to several microrheological phenomena happening at highly suspended blood cells. However, some disadvantages are also argued. In their research transparent ghost cells suspensions are used in order to avoid light absorption by the hemogoblin. It is well known that the hemogoblin strongly influences the mechanical properties of the RBC membrane. By removing the hemogoblin from the RBC, the membrane mechanical properties may have suffer appreciable modifications and consequently the rehological behaviour of the RBC may also differ from a normal RBC (Caro et al. 1978, Mason and Goldsmith 1979, Nash and Meiselman 1983, Shiga et al. 1990). In addition, by using a conventional microscope the entire flow region is illuminated and consequently the out-of-focus emitted light results in high levels of background noise, which degrades the flow measurements (Meinhart et al. 1999, Conchello and Lichtman 2005). Hence, there is a need for a new method able to obtain accurate measurements in concentrated suspensions of RBCs not only to obtain more accurate quantitative results but also to gain further insight into the complex microhaemodynamic phenomenon of blood in microcirculation.

Recently, considerable progress in the development of confocal microscopy and the advantages of this technique over conventional microscopy (Pawley 1990, Inoue and Inoue 2002, Wright and Wright 2002, Conchello and Lichtman 2005) have led to a new technique known as confocal micro-PIV (Tanaami et al. 2002, Park et al. 2004, Kinoshita et al. 2005, Lima et al. 2006). This method combines the conventional PIV system with a spinning disk confocal microscope (SDCM). By combining its outstanding spatial filtering technique with a multipoint illumination system, this technique has the ability to obtain in-focus images with optical thickness less than 1 μm (optical sectioning effect). As a result, this technique provides a superior spatial resolution which improves the image contrast and definition, allowing the measurement of several microrheology phenomenon in concentrated suspension

of RBCs. Very recently, we have used our confocal system combined with a cross-correlation technique in order to obtain detailed information on the velocity profiles for the flow of in vitro blood with haematocrit (Hct) up to 17% (Lima et al. 2007). Although at low Hcts (Htc < 9%) it was possible to obtain accurate measurements for bigger Hcts, the errors on the velocity fields tend to increase, due mainly to the low concentration of trace particles that exists on the captured images. Therefore, in order to measure microrhelogical behavior of blood with high Hcts, it is crucial to combine our confocal system with single particle method (SPT). To our knowledge, the present study provides for the first time confocal micro-PTV measurements on the microrheology behavior in highly concentrated suspensions of erythrocytes.

The present study demonstrates the ability of our confocal micro-PTV system to obtain detailed qualitative and quantitative information on the flow behavior of blood through glass capillaries. This approach not only eliminates the problems and concerns of the methods used in the past but also provides additional detailed description on the RBC motion not obtainable by other conventional methods. Due to the optical sectioning ability, the present work provides for the first time quantitative information on the blood cells interactions occurring during flow. Such information is extremely important to elucidate the blood transport mechanisms and associated diseases such as thrombosis and atherosclerosis.

6.2 Materials and methods

6.2.1 Preparation of blood cells labeling

This study examined four working fluids: dextran 40 (Dx-40, Otsuka Medicine) containing 3% (3Hct), 15% (15Hct) or 35% (35Hct) of human RBCs, and Dx-40 containing 20% (20Hct) of RBCs and 2% white blood cells (WBCs). Both RBCs and WBCs were labeled with lipophilic carbocyanime derivative, chloromethylbenzamido (CM-Dil, C-7000, Molecular Probes). This cell tracker was selected mainly because of its strong photostable fluorescence, excellent cellular retention and minimal cytotoxicity (see Figure 6.1).

Venous blood was collected from a healthy adult volunteer (aged 33 years old), and ethylenediaminetetraacetic acid (EDTA) was added to prevent coagulation of blood cells. The RBCs were separated from the bulk blood by centrifugation (1500 rpm for 20 min) and the plasma and buffy coat were removed by aspiration. The washing and centrifuging with

physiological saline (PS) were repeated twice. The washed RBCs were diluted with PS to make several samples with haematocrits of ~ 40% by volume. All the blood samples were stored hermetically at 4ºC until the labeling was performed. The procedure for labeling both RBCs and WBCs was the following:

1. centrifuge blood sample with 40%Hct at 2000 rpm for 5 min;
2. remove all the PS and add 200 μl of fresh PS and also 10μl of cell tracker CM-Dil, C-7000 (50 μg diluted with 200 μl ethanol, Ex.553nm-Em.570);
3. mix gently and incubate the blood cells for 30 min. at 37ºC and then for an additional time at 4ºC for 1-2h;
4. add approximately 500μl of washing solution (PS) and mix gently;
5. centrifuge the solution at 2000 rpm for 5 min to remove any excess dye;
6. resuspend the washed solution in Dx40 to make up the required RBCs or WBCs concentration by volume.

Due to possible losses of blood cells during the labeling process, the heamatocrict of each sample was always measured by using a heamatocrit centrifuge (Kubota 3220, Japan) prior the experiment. Note that the WBCs were obtained by using a lymphoprep tube (Axis-Shield, Norway) and by following the separation procedure recommended by the manufacturer. By using this approach the fluorescently labeled RBCs were around 10% of the total volume of blood cells (40%Hct). All procedures in this experiment were carried out in compliance with the Ethics Committee on Clinical Investigation of Tohoku University.

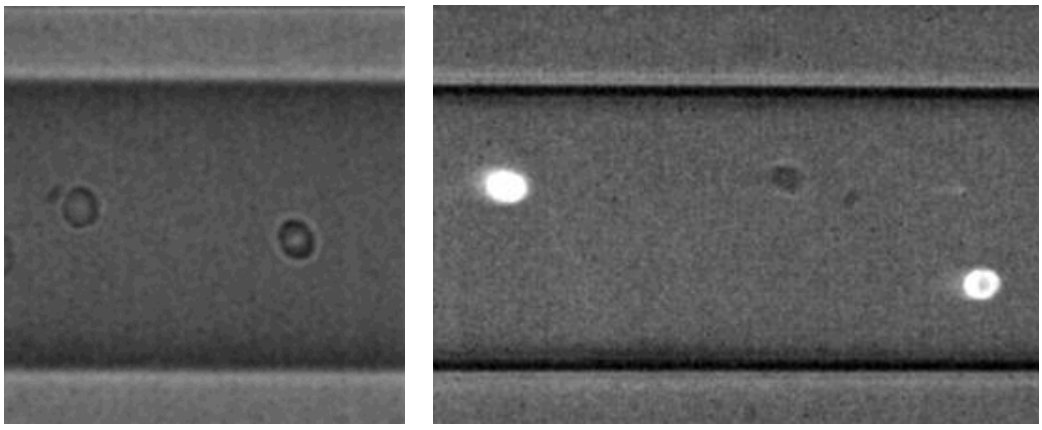

Figure 6.1 Halogen and confocal images of labeled RBCs.

6.2.2 Glass microchannel

In this study, we used a 100 μm circular borosilicate glass microchannel fabricated by Vitrocom (Mountain Lakes, NJ, USA). The capillary was mounted on a slide glass

approximately 80 μm thick, which was immersed in glycerol that had the same refractive index, so that the refraction from the walls of the microchannel was minimized.

6.2.3 Experimental setup

The confocal micro-PTV system used in our experiment consists of an inverted microscope (IX71, Olympus, Japan) combined with a confocal scanning unit (CSU22, Yokogawa, Japan) and a diode-pumped solid state (DPSS) laser (Laser Quantum Ltd, England) with an excitation wavelength of 532 nm. Moreover, a high-speed camera (Phantom v7.1, U.S.A.) was connected into the outlet port of the CSU22 (see Figure 6.2). The glass capillary was placed on the stage of the inverted microscope where the flow rate of the working fluids was kept constant by means of a syringe pump (KD Scientific Inc., U.S.A.). By using a thermo plate controller (Tokai Hit, Japan) the surrounding temperature around the capillary was 36ºC±1.

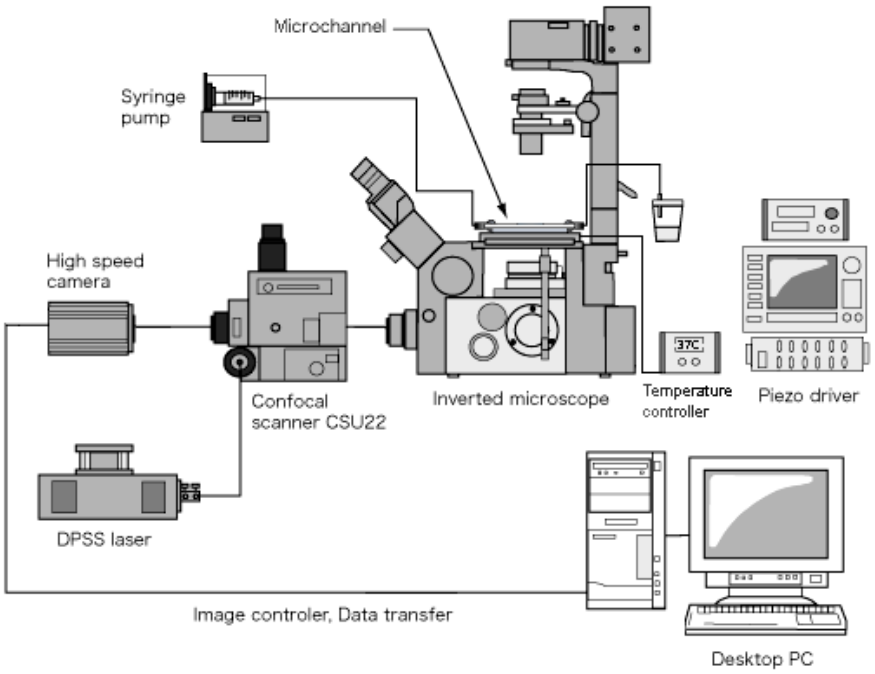

Figure 6.2 Confocal micro-PTV experimental set-up.

The laser beam illuminated the glass capillary from below the microscope stage through a dry 40× objective lens with a numerical aperture (NA) of 0.9. Satisfactory illumination was achieved by labeling both RBCs and WBCs, which absorb green light (excitation peak 553 nm) and emit yellow light (emission peak 570 nm). The light emitted from the flowing blood cells passes through a colour filter into the CSU22 scanning unit, where a dichromatic mirror reflects it onto a high-speed camera to record the confocal images. The optical sectioned

images were performed at several positions along the z-axis by using a piezo driver system and RT3D signal controller software from the Yokogawa corporation (see Figure 6.3). The optical slice thickness (OST) was 2 μm based on geometric–optical analysis criteria (Willhelm et al. 2003, Lima et al. 2006).

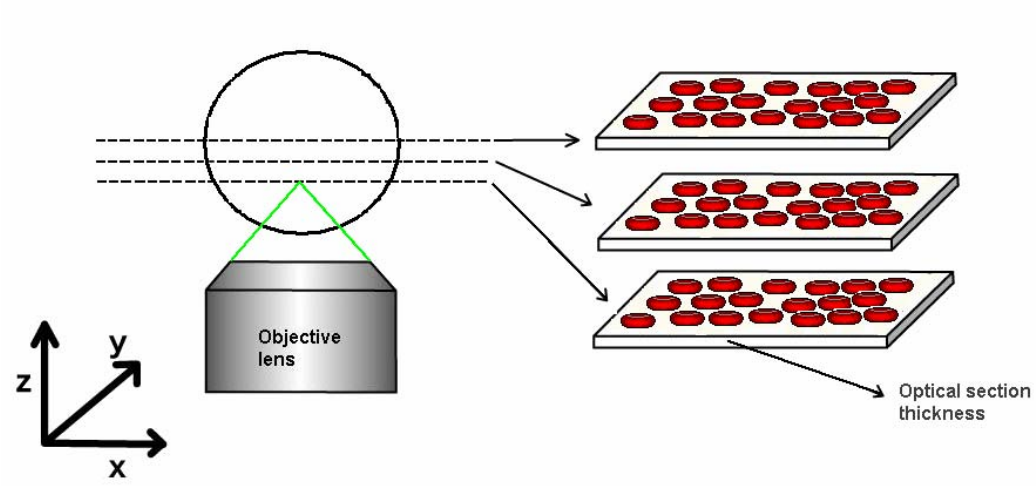

Figure 6.3 Diagram showing the ability of the confocal system to generate optical sectioned images along the z-axis.

The series of xy confocal images were captured with a resolution of 640×480 pixels, 12-bit grayscale, at a rate of 100 frames/s with an exposure time of 9.4 ms. The recorded images were evaluated in the Image J (NIH) (Abramoff et al. 2004) by using the manual tracking MTrackJ (Meijering et al. 2006) plugin. The labeled RBCs lying on the focus plane appear as spots with high intensity. The selected RBCs were then manually tracked through successive images by using the intensity-weighted mean position of pixels having a value above a certain threshold (bright centroid). By using this method, it was possible to track accurately the labeled RBCs even when two cells were closely together, which is the case of cell-cell interactions. After obtaining series of x and y positions, the data were exported to a C code to calculate several physical quantities such as velocity, radial displacement and radial dispersion coefficient .

6.3 Results

To analyse the ability of the confocal micro-PTV system to track RBCs, the motions of labeled RBCs were followed at several Hcts (3% to 35%). For the calculation of the radial dispersion coefficient (D_{yy}), measurements were performed at a series of optical sections along the *z*-axis. However to investigate complex microrhelogical events in flowing blood (such as interaction and orientation of blood cells) all measurements were performed near the

wall of the microchannel (z = 20 μm) with Hct = 20%. The region near the wall has gain interest during the years due mainly to the lack of understanding of the mass transport mechanisms responsible to the thrombogenesis process (Wootton and Ku 1999, Miayazaki and Yamaguchi 2003).

6.3.1 Blood flow visualization

RBCs and WBCs flow with 20% Hct

The interactions of blood cells in flowing blood and also their orientations were measured *in vitro* blood with 20% Hct at Re = 0.007. Examples of recorded images both in centre and bottom plane are presented in Figure 6.4. In Figure 6.4a it is possible to observe very clearly the plasma layer formed during our experiments. In Figure 6.4b, which is an image containing both halogen and laser light, it is possible to see both labeled and non-labeled RBCs. Figures 6.4c and 6.4d are both confocal images used to track the blood cells. Note that in Figure 6.4d the brightness and contrast of the image were adjusted in order to better visualize both RBCs and WBCs.

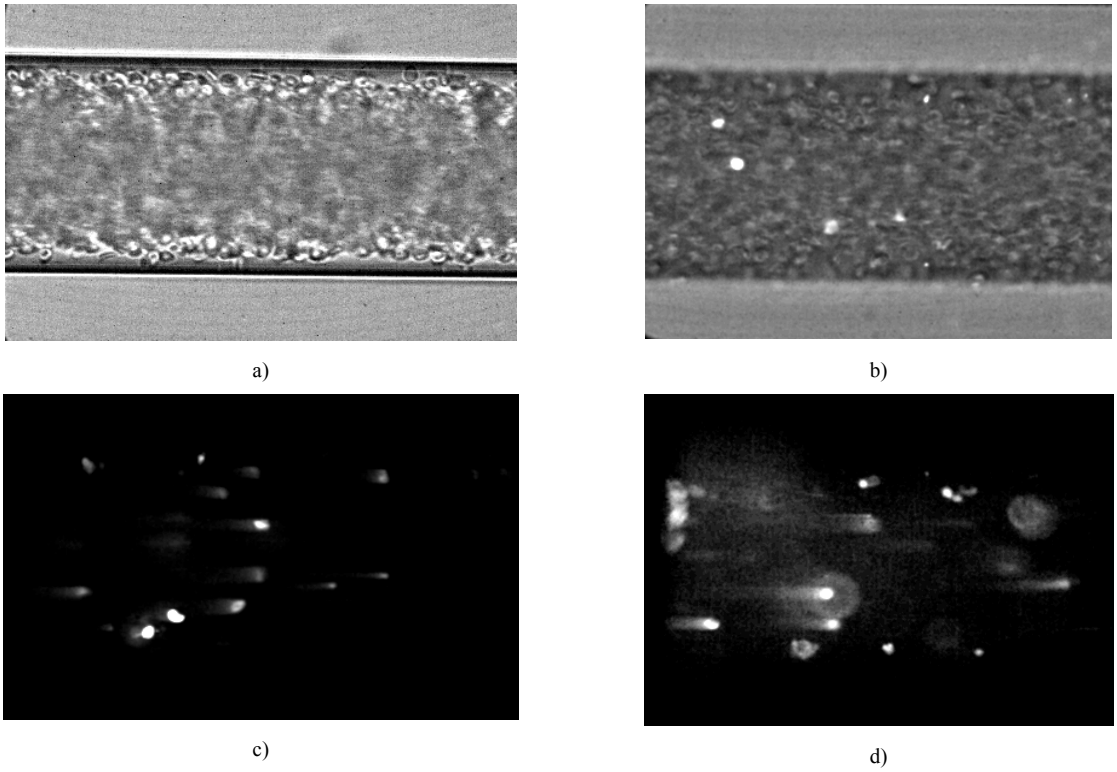

Figure 6.4 a) An image of the in vitro blood used in this experiment with halogen illumination recorded in centre plane. b) An image with both labeled RBCs (bright spots from laser-emitted light) and non-labeled RBCs (halogen illumination source) recorded at bottom plane (z = 20 μm). c) A confocal image used to track RBC motions. d) A treated confocal image to visualize both RBCs and WBCs.

RBCs flow at several Hcts around middle plane

The RBCs in flowing blood exhibit randomlike transverse motion which depends on the Hct. The radial dispersion of the labeled RBCs were measured in centre plane at several Hcts (3%, 15% and 35%) at a Re = 0.005. Figure 6.5 shows recorded images with both labeled and non-labeled RBCs at several Hcts. It is very clear from these images that plasma layer tends to decrease by increasing the Hct.

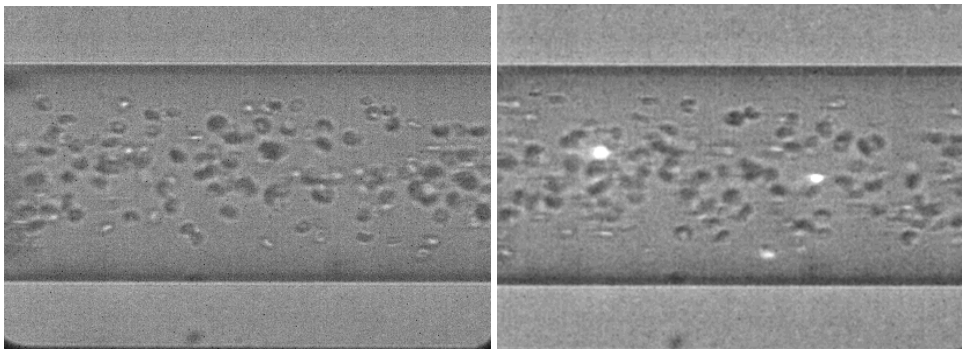

a) 3Hct

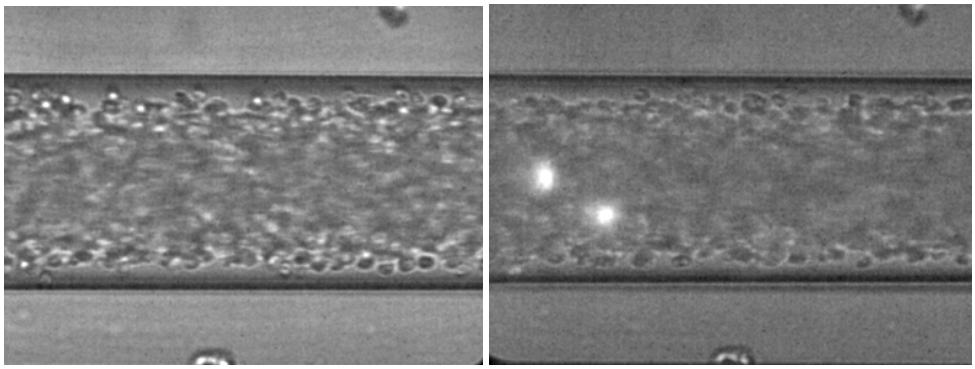

b) 15 Hct

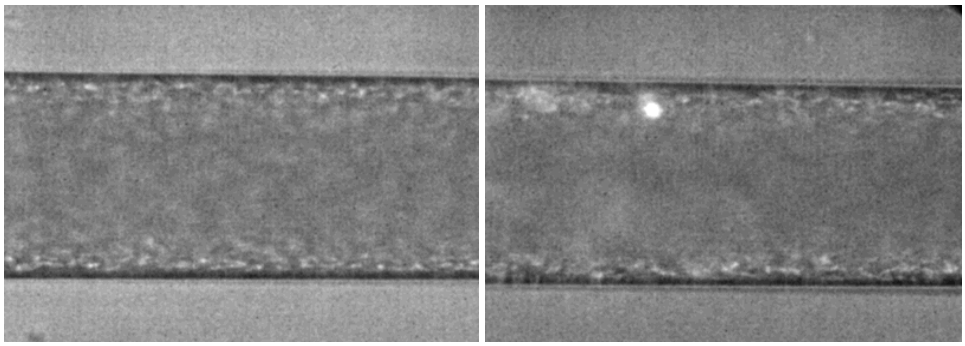

c) 35Hct

Figure 6.5 Halogen and confocal images in the middle plane of *in vitro* blood with (a) 3% Hct, (b) 15% Hct (c) 35% Hct. The non-labeled RBCs are observed as dark-grey rings, whereas labeled RBCs are observed as bright rings.

6.3.2 Blood microrheology behavior near the wall

In vitro blood with 20%Hct was used to evaluate the ability of the proposed confocal system to investigate microrheology behavior of erythrocytes flowing in croweded environment at Re = 0.007. The microrhelogy phenomenon studied was RBC-RBC and RBC-WBC hydrodynamic interaction and RBC orientation with and without interaction. Several representative examples are presented below. The hydrodynamic interaction is often quantified by the radial displacement (ΔR), given by:

$$\Delta R(t) = \left| R(t) - R(0) \right| \quad (6.1)$$

where R(0) is the initial radial displacement and R(t) is the cumulative radial displacement for a defined time interval.

RBC-RBC interactions in flowing blood

The effect of the hydrodynamic interactions on the motion of RBCs depend on multi-physic factors, such as shear rate, deformability, plasma layer and wall constriction. Four examples of RBC-RBC interaction nearby the plasma layer are presented below with $\dot{\gamma}$ from 16 s^{-1} to 20 s^{-1}.

Figure 6.6 shows the typical streamlines of two-RBC interactions nearby the plasma layer at $\dot{\gamma} \sim 16$ s^{-1}. This figure shows clearly the radial disturbance effect enhanced by the collision of a neighboring RBC. This disturbance effect is quantified in Figure 6.7.

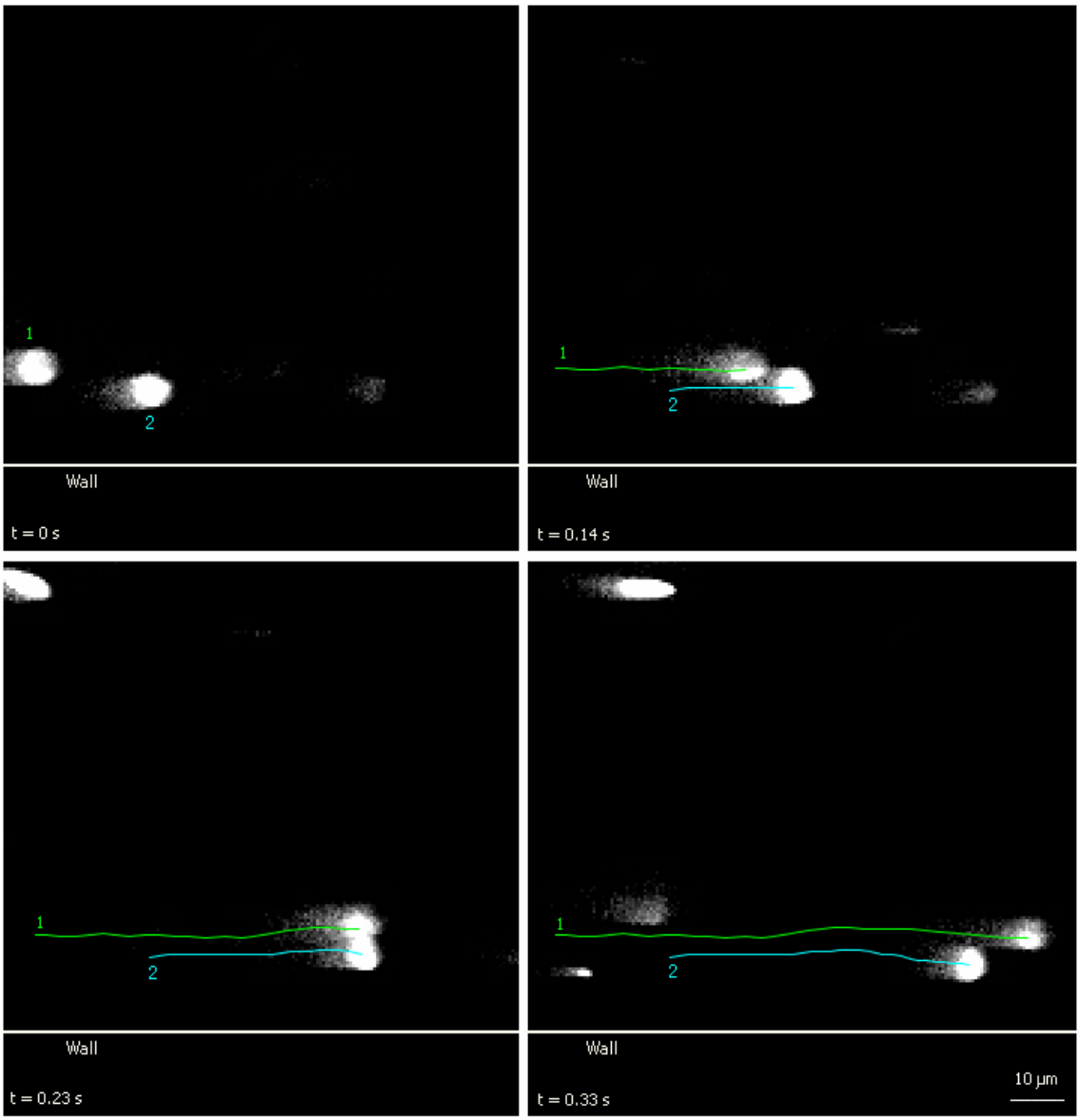

Figure 6.6 Two-RBC interactions at different times intervals (Re = 0.007; $\dot{\gamma}$ ~ 16 s^{-1}).

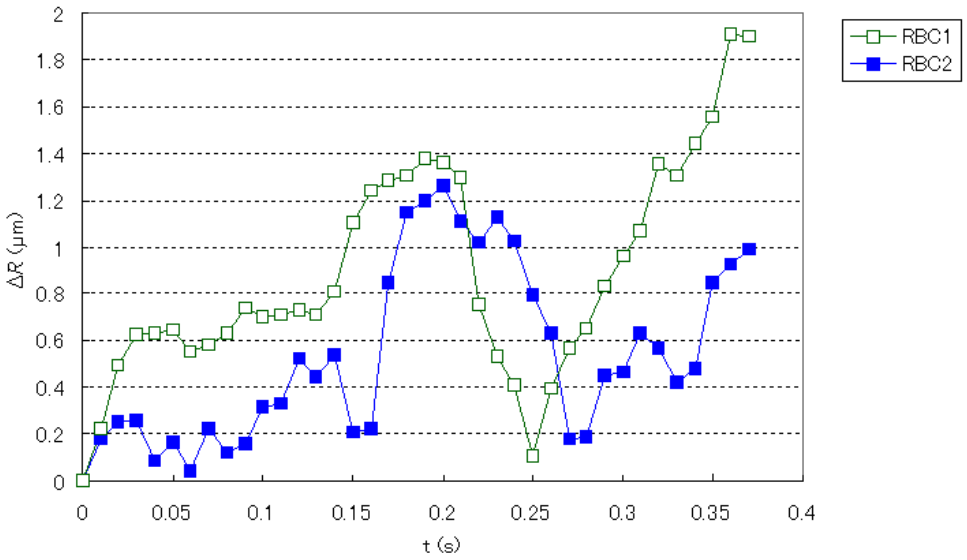

Figure 6.7 Radial displacement (ΔR) of two-RBC interactions at different times intervals.

From Figure 6.7, it is possible to observe that at t = 0.19s the radial displacement (ΔR) of the RBCs increases from 2 to 6 times of its initial radial displacement. For the case of RBC1, the ΔR continues to increase due not only to current interaction but also to other possible interactions with neighboring cells.

Figure 6.8 shows the streamline of a RBC (RBC4) interacting with two different RBCs in a period of time less than 0.2 s. From Figure 6.9, it is possible to observe that the radial displacement increases at t = 0.25s (first interaction) and then it decreases until t = 0.4s where it increases again due to another RBC interaction (second interaction). Note that for the case of RBC3 after the interaction (t = 0.18 s) the radial displacement tends to decreases gradually. This phenomenon is due to stokes flow regime (Re = 0.007) where the viscous force is dominant. These results suggest that after the interaction the RBCs tend to return to its initial streamline. However in dense suspensions this event rarely happens because of collision with another neighboring RCB.

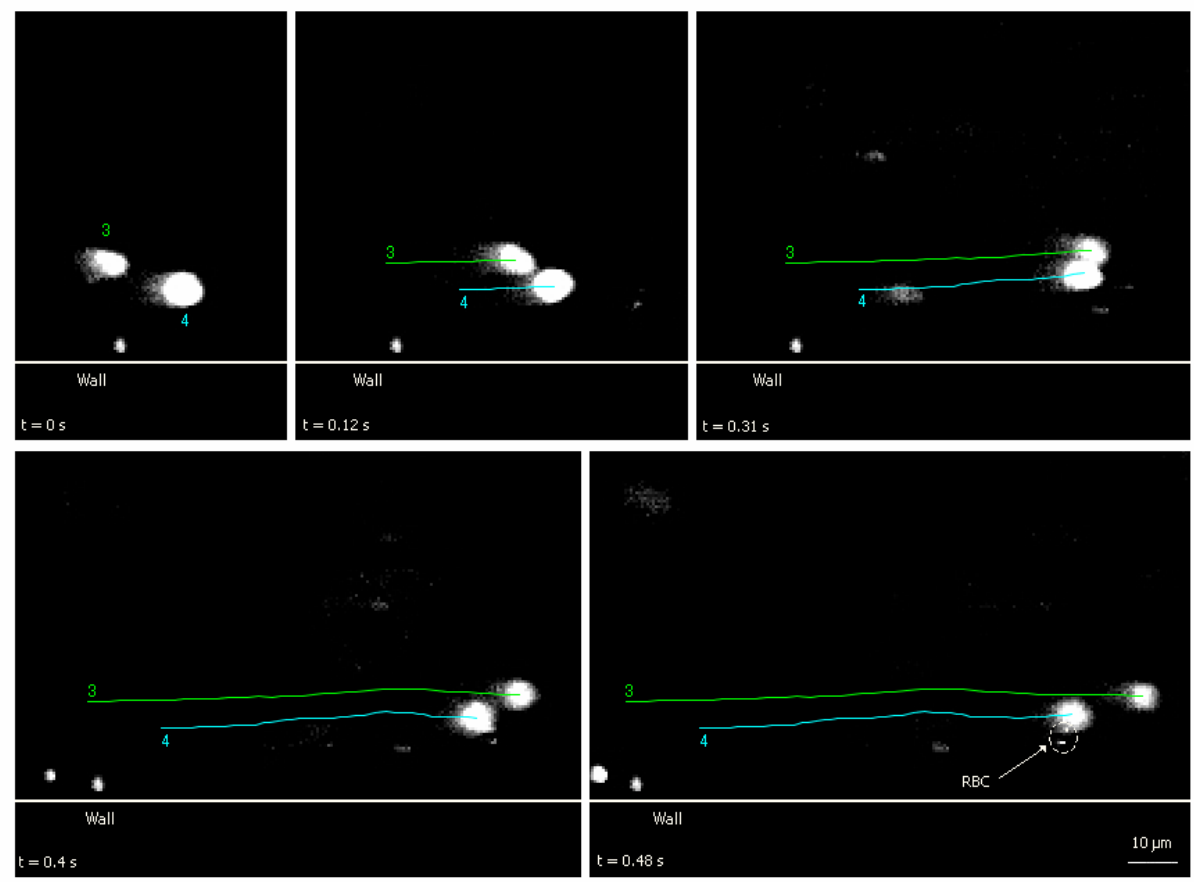

Figure 6.8 Multi-RBC interactions at different times intervals (Re = 0.007; $\dot{\gamma}$ ~ 16 s^{-1}).

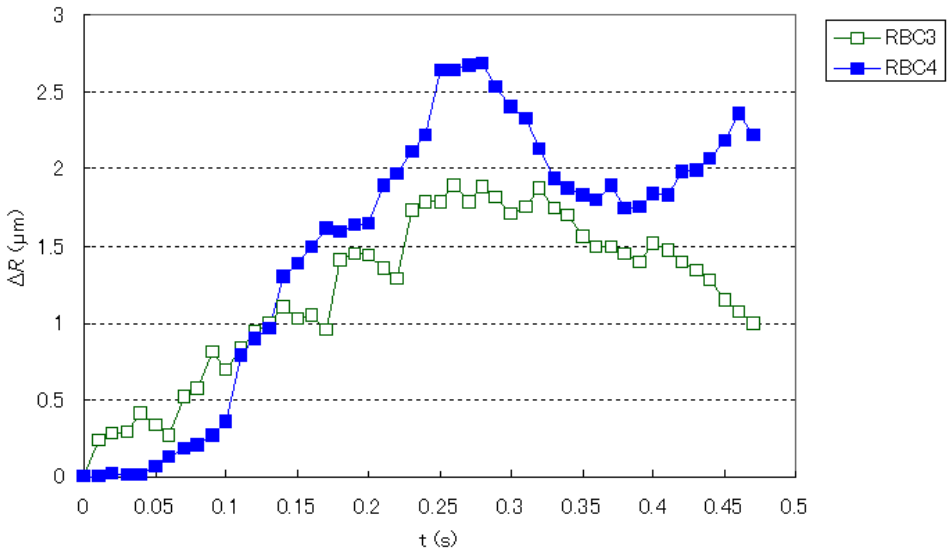

Figure 6.9 Radial displacement (ΔR) of multi-RBC interactions at different times intervals.

Figure 6.10 shows the streamline of two RBCs interacting close to the microchannel wall. Note that RBC6 is rolling along the wall. Figure 6.11 shows clearly that there is no radial displacement peak for RBC6, but rather a constant displacement especially for t > 0.25s. These results suggest that the trajectories of RBCs rolling on the wall surface do not suffer a strong hydrodymanic effect from the RBCs interacting in its neighboring. In contrast, RBC5 has suffered an increase on the radial displacement of about 2 μm. Note that the ΔR of this RBC tends to decrease gradually until its initial ΔR. This effect is obviously due to the presence of a plasma cell free layer that exists near the wall.

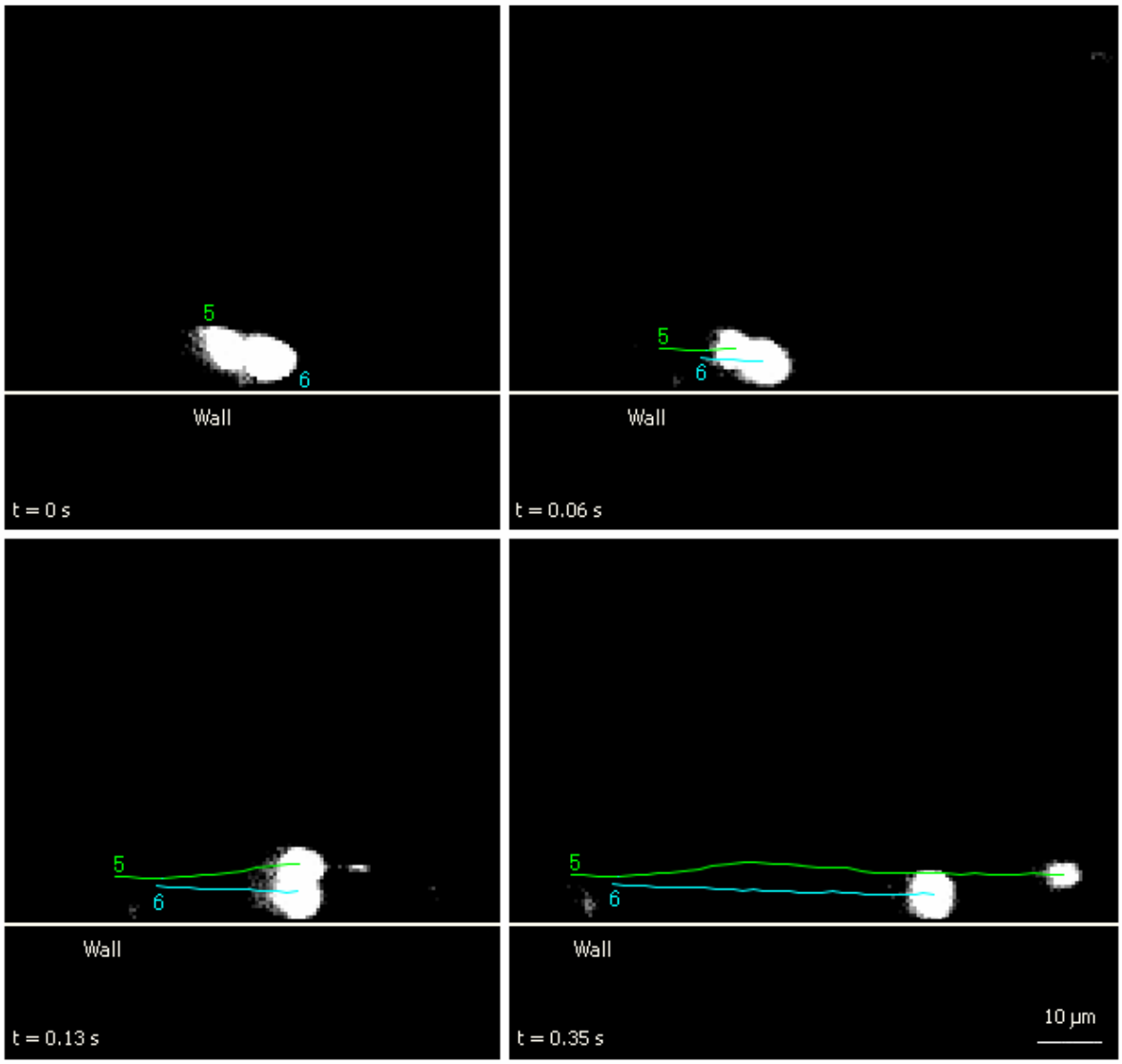

Figure 6.10 Two-RBC interactions close to the wall at different times intervals (Re = 0.007; $\dot{\gamma}$ ~ 20 s^{-1}).

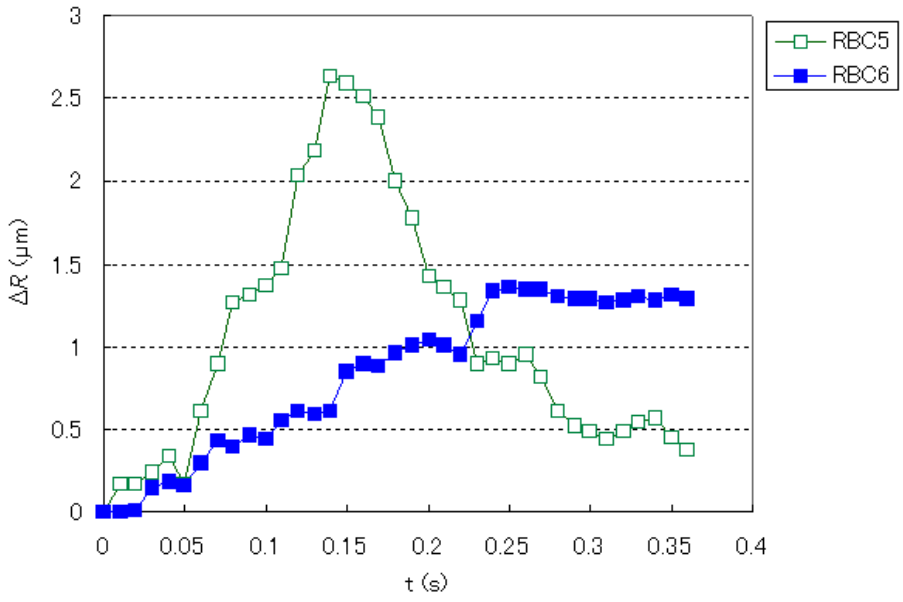

Figure 6.11 Radial displacement (ΔR) of two-RBC interactions close to the at different times intervals.

In Figure 6.12, it is possible to observe a cell (RBC7) located within the plasma layer with axial migration from the wall. However, this inward migration is inverted when it interacts with the RBC8 (t = 0.26) located in the crowded boundary region of the plasma layer. As a result, the radial displacement of RBC7, for this particular example, decreases due to the interaction with RBC8 at t = 0.26s (see Figure 6.13).

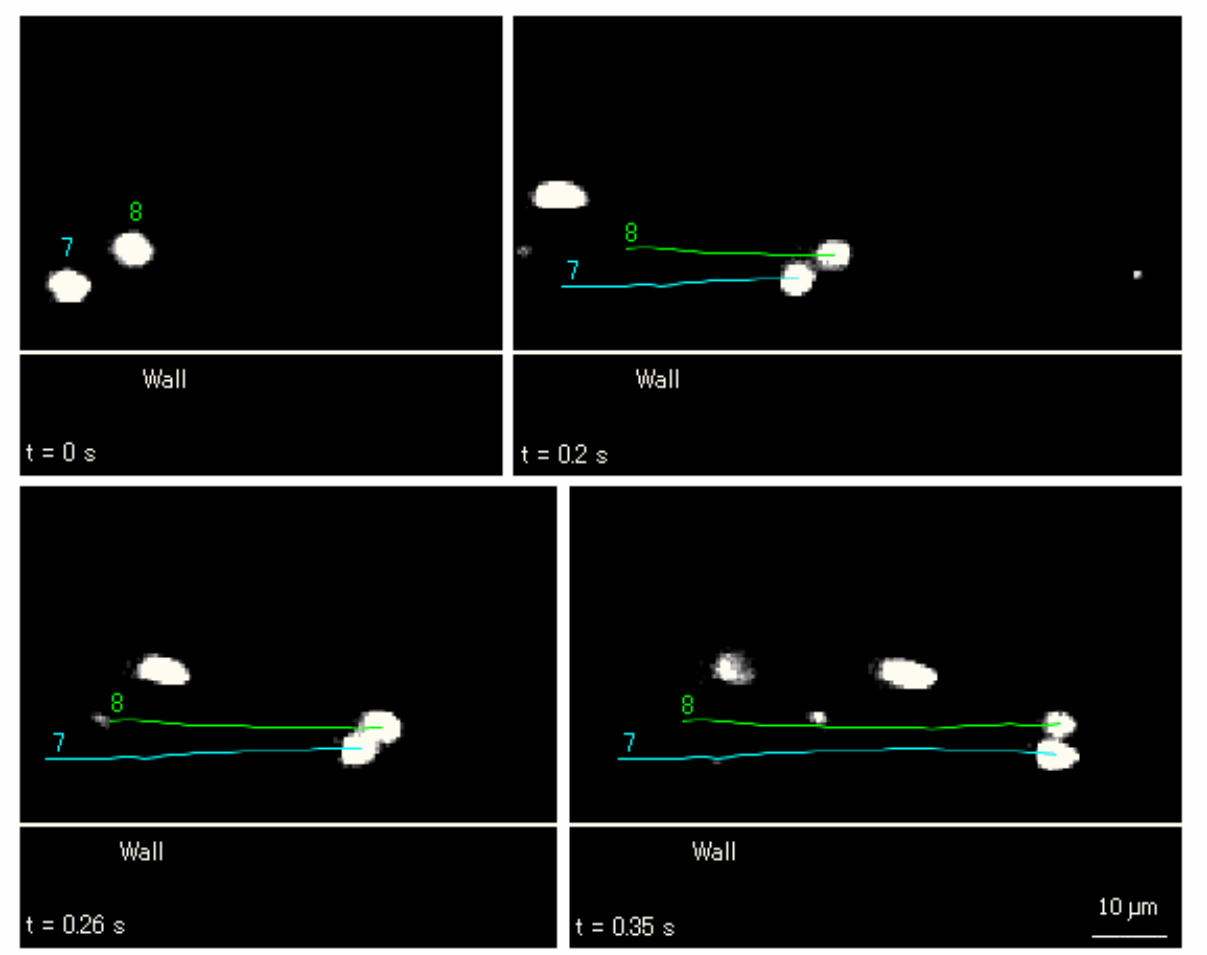

Figure 6.12 Two-RBC interactions close to wall at different times intervals (Re = 0.007; $\dot{\gamma}$ ~ 16 s^{-1}).

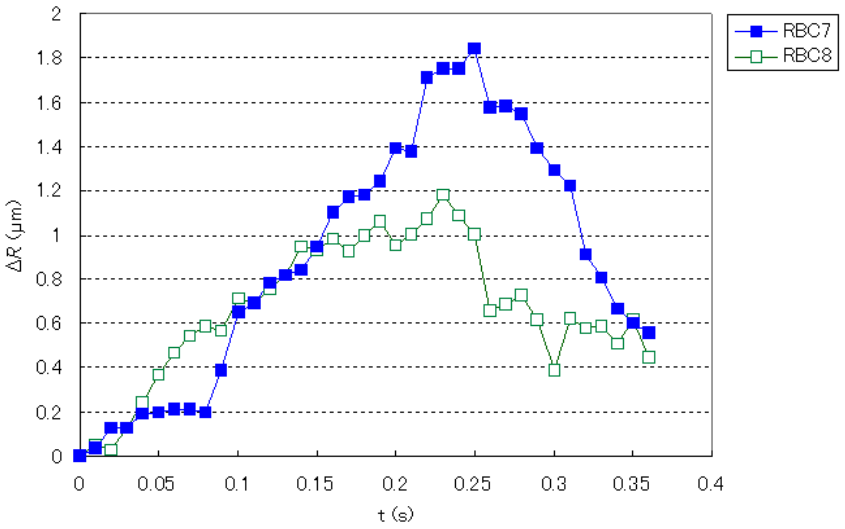

Figure 6.13 Radial displacement (ΔR) of two-RBC interactions close to the wall at different times intervals.

Figure 6.14 shows the radial displacement of two RBCs (RBCint1 and RBCint2) that have interacted with a neighboring RBC. Additionally, it is also shown the ΔR of two RBCs (RBCnoInt1 and RBCnoInt2) with any appreciable interaction at 3% Hct. These results show clearly the fluid-dynamical interaction effect on the motion of RBCs flowing in concentrated suspension of blood cells. For the selected RBCs, the radial displacement has increased of about 2 μm due to the hydrodynamic interaction.

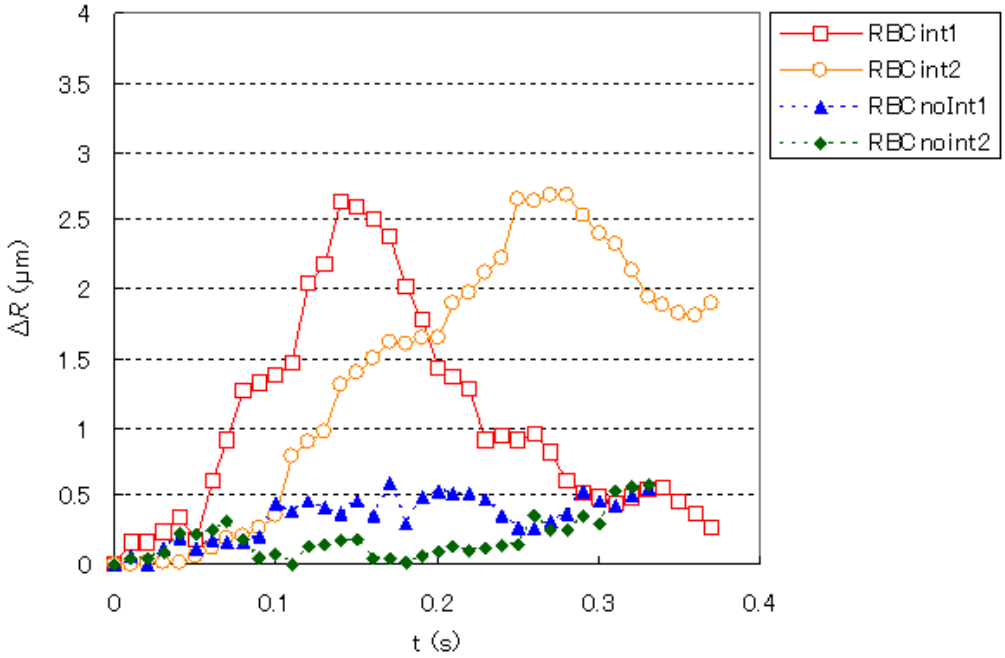

Figure 6.14 Comparison of the radial displacement (ΔR) between RBCs with interactions and RBCs with no interactions at low Hct (3%Hct).

RBC-WBC interactions in flowing blood

The hydrodynamic interaction effect of WBC on the motion of RBCs was also measured. Two examples are shown in Figures 6.15 and 6.16. Figure 6.15 shows a RBC interacting with centre upper part of a WBC. Note that the RBC is located in the in-focus plane (high intensity) whereas the WBC is under the in-focus plane (lower intensity). Although the WBC is not on in-focus plane due to its size (usually 2 times a RBC) and geometry, the motion of the RBCs are disturbed by its presence in the flow. For the other example the path of a RBC interacting with the left side of the WBC was measured. The radial displacement for both RBCs is presented in Figure 6.17.

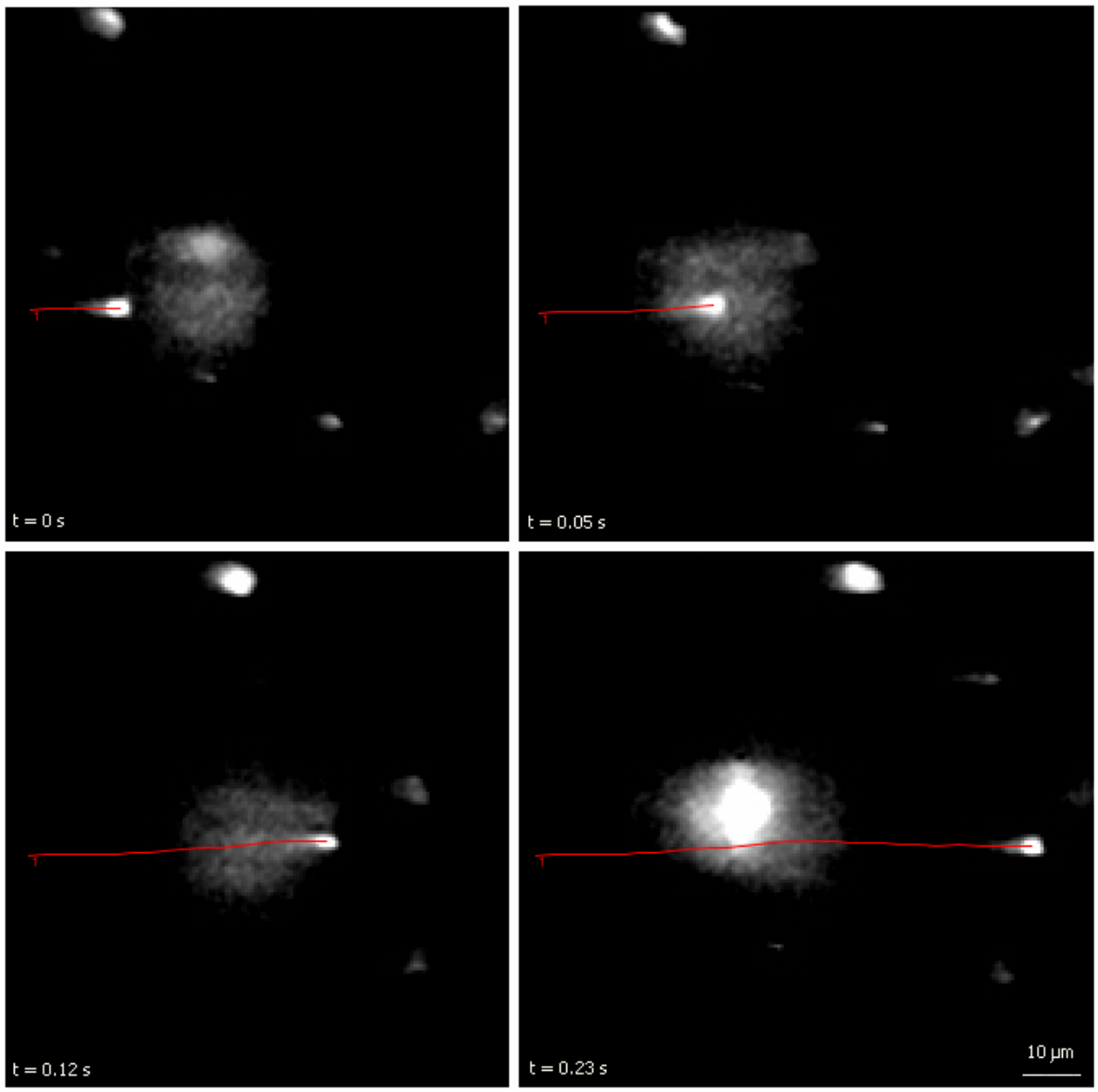

Figure 6.15 RBC-WBC interaction at different time intervals (Re = 0.007; $\dot{\gamma}$ ~ 16 s^{-1}).

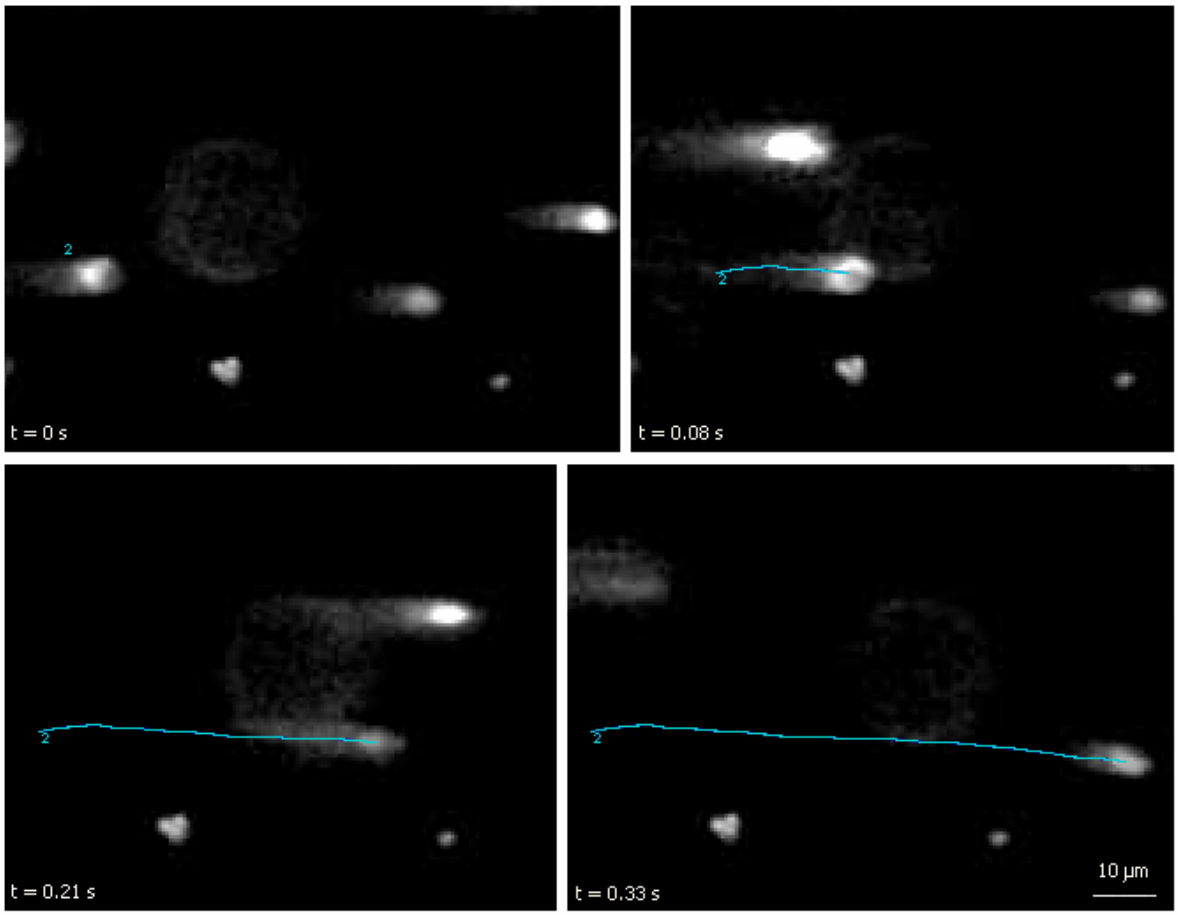

Figure 6.16 Lateral RBC-WBC interaction at different time intervals (Re = 0.007; $\dot{\gamma}$ ~ 16 s^{-1}).

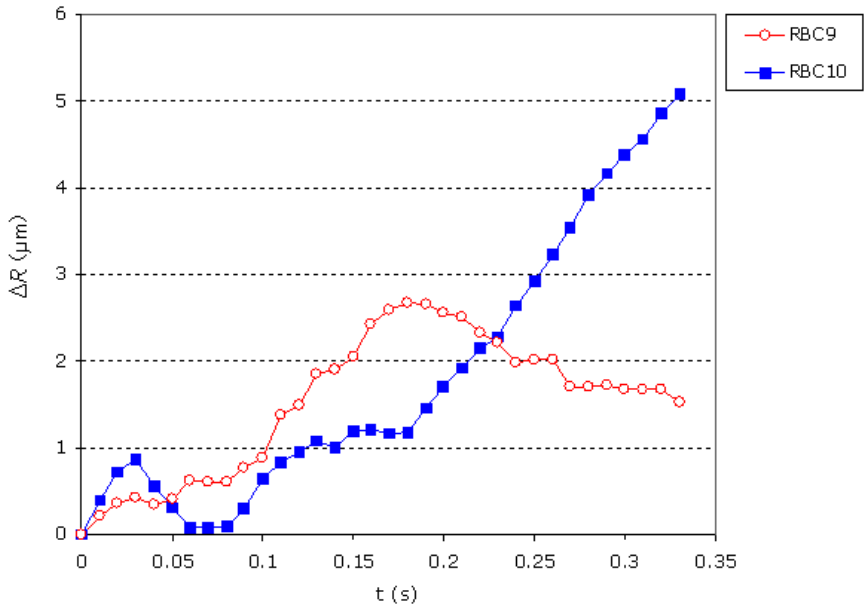

Figure 6.17 Radial displacement (ΔR) of RBC-WBC interactions at different time intervals.

From Figure 6.17, it is possible to observe that for both cases the radial displacement increases when the collision with a WBC occurred. However, the displacement seems to be increased considerably when the RBC interacts on the side of WBC. According to our

observations, when the RBC interacts around the centre of WBC, the displacement seems to be bigger along the z direction (depth of the microchannel). Although it is possible to visualize this three-dimensional displacement, presently our system is not able to quantify it.

Orientation of RBC in flowing blood

Although the orientation of RBCs was extensively studied in diluted suspensions, such is not the case for highly concentrated suspensions. In this section, the orientation of two RBCs with and without interaction was measured. By adjusting the image contrast, it was possible to measure both translational and rotational motion. The translational motion was measured at the centre of the RBC whereas the rotational was measured along the membrane as shown in Figures 6.18 and 6.19.

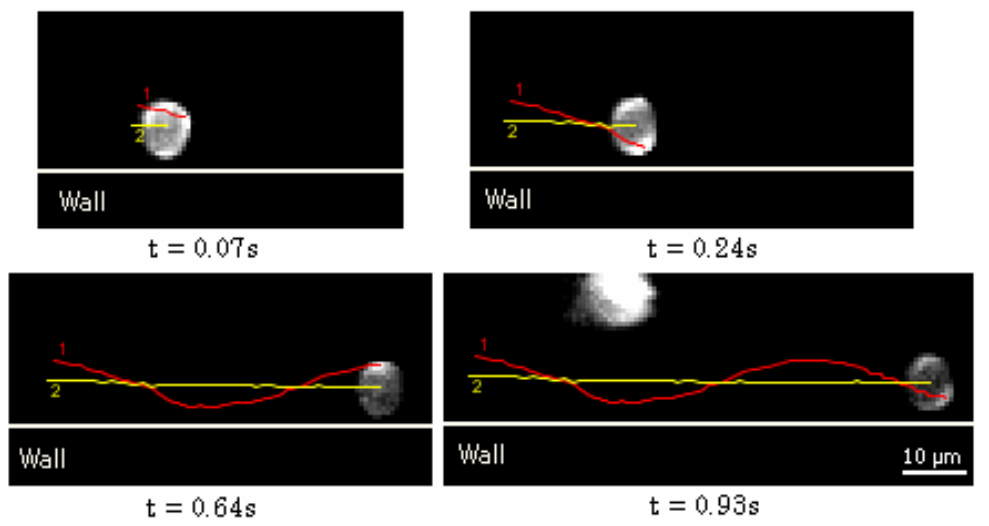

Figure 6.18.Translational and rotational motion of RBC without interaction (Re = 0.007; $\dot{\gamma}$ ~ 20 s^{-1})..

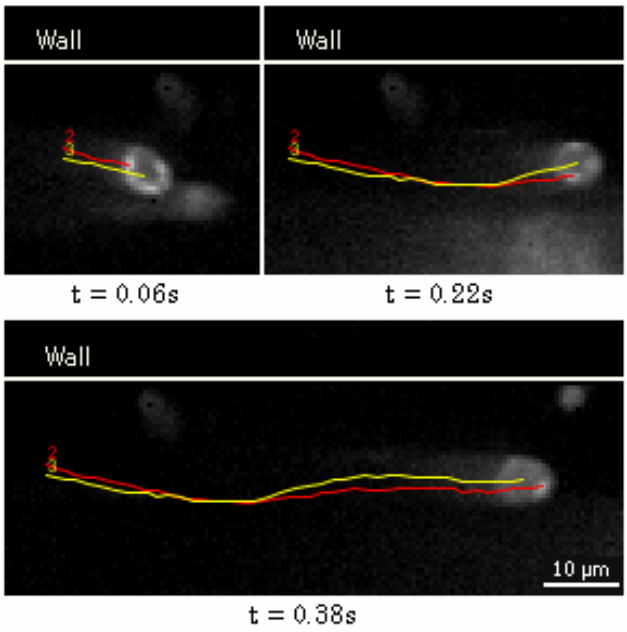

Figure 6.19 Translational and rotational motion of RBC with interaction (Re = 0.007; $\dot{\gamma}$ ~ 18 s^{-1}).

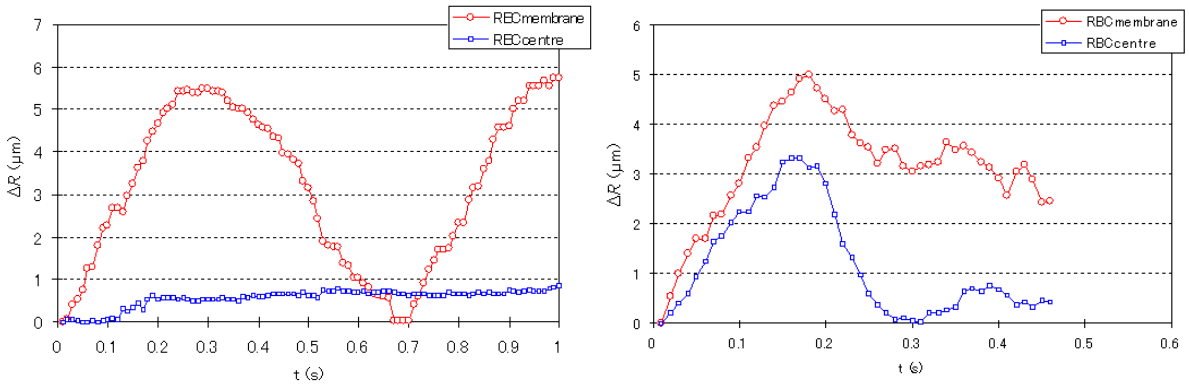

a) b)

Figure 6.20 Radial displacement (ΔR) of both translational and rotational motion of a RBC a)without interaction ; b) with interaction.

The RBC without interaction was measured along the surface of the wall. This RBC did not suffer any interaction with a neighboring RBC so that its translational radial displacement was almost constant. Moreover, as it is possible to observe in Figures 6.18 and 6.20a, the RBC rotates as biconcave disc in a clockwise direction with periodically varying angular velocity. In contrast, the RBCs that interact with neighboring cells both translational and rotational motion change dramatically. These RBCs no longer rotate in regular and periodically way but rather in an erratic way.

6.3.3 Radial disperson of labeled RBCs at different Hcts

The randomlike transverse motions of RBCs can be analysed by using a radial dispersion coefficient (D_{yy}) (Goldsmith and Turitto 1986), given by:

$$D_{yy}(t) = \frac{1}{N}\sum_{i=1}^{N}\frac{\left\langle \left(R_{i,y}(t) - R_{i,y}(0)\right)^2 \right\rangle}{2t} \qquad (2)$$

where $\langle (R_{i,y}(t)-R_{i,y}(0))^2 \rangle$, t and N are the mean square displacement, time interval and number of measured RBCs.

For the present study, *in vitro* blood with several Hct was used at Re = 0.005. The paths of hundreds labeled RBCs were measured not only in the centre plane but also at other focal planes located at 35 μm and 20 μm from the bottom of the capillary. Figure 6.21 shows the typical radial displacement of RBCs at different in-focus planes for three different concentrations of RBCs, i. e., 3% Hct, 15% and 35% Hct. The RBC dispersion coefficient at the centre plane (D_{yy}^{c}) for several Hcts is shown in Figure 6.22 whereas the D_{yy} at three different in-focus planes is shown in Figure 6.23.

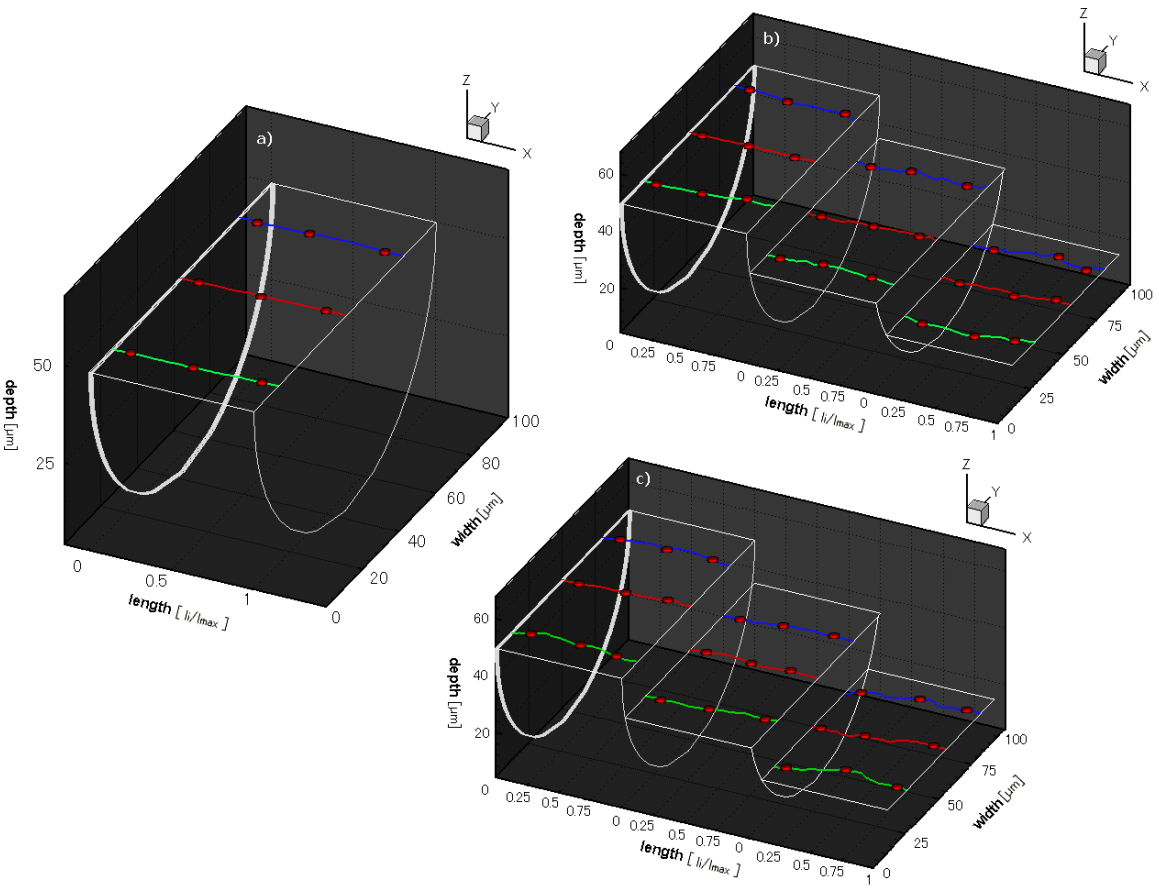

Figure 6.21 Radial displacement (ΔR) of labeled RBCs at different in-focus planes for a) 3%Hct, b) 15%Hct, c) 35% Hct (Re = 0.005).

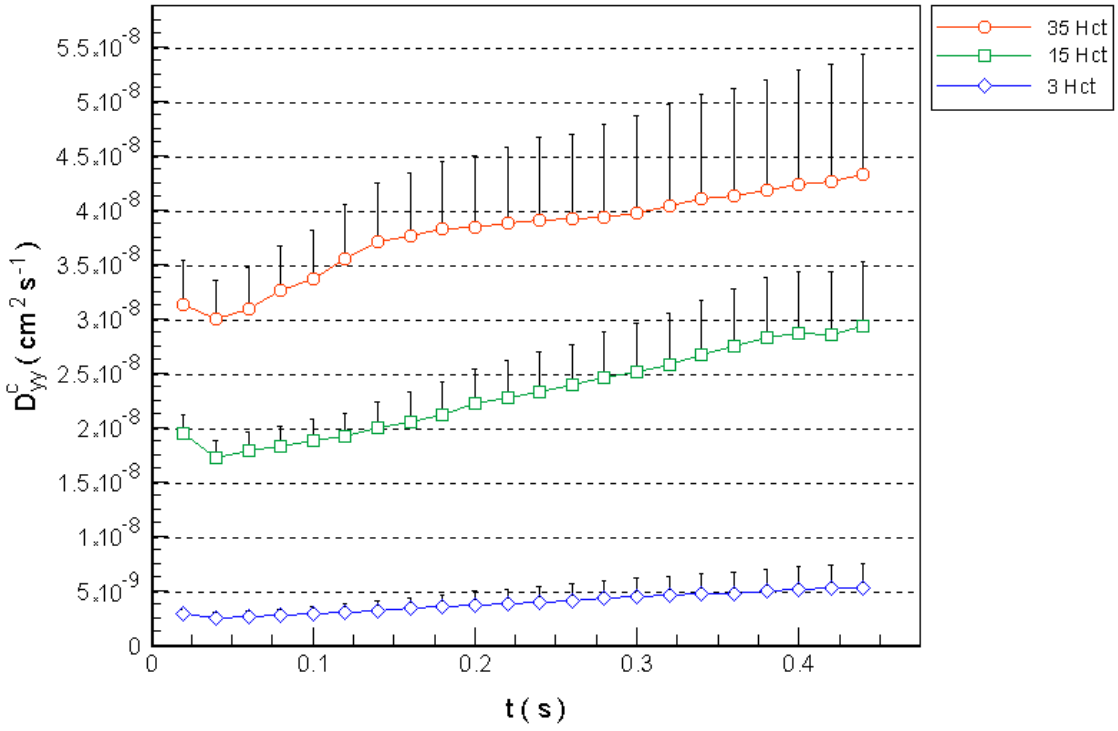

Figure 6.22 RBC radial dispersion coefficient at the centre plane (D^c_{yy}) for 3% Hct, 15% Hct and 35% Hct (Re = 0.005). The measured values are expressed as the means ± standard deviation by using t-test analysis at 95% confidence interval.

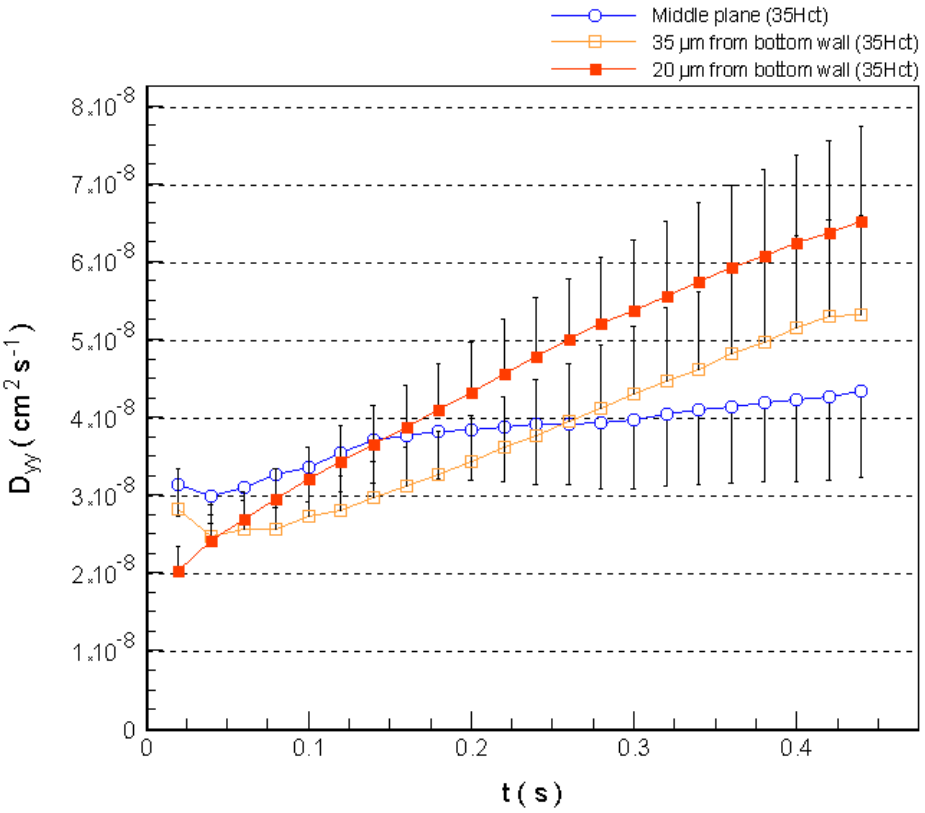

a)

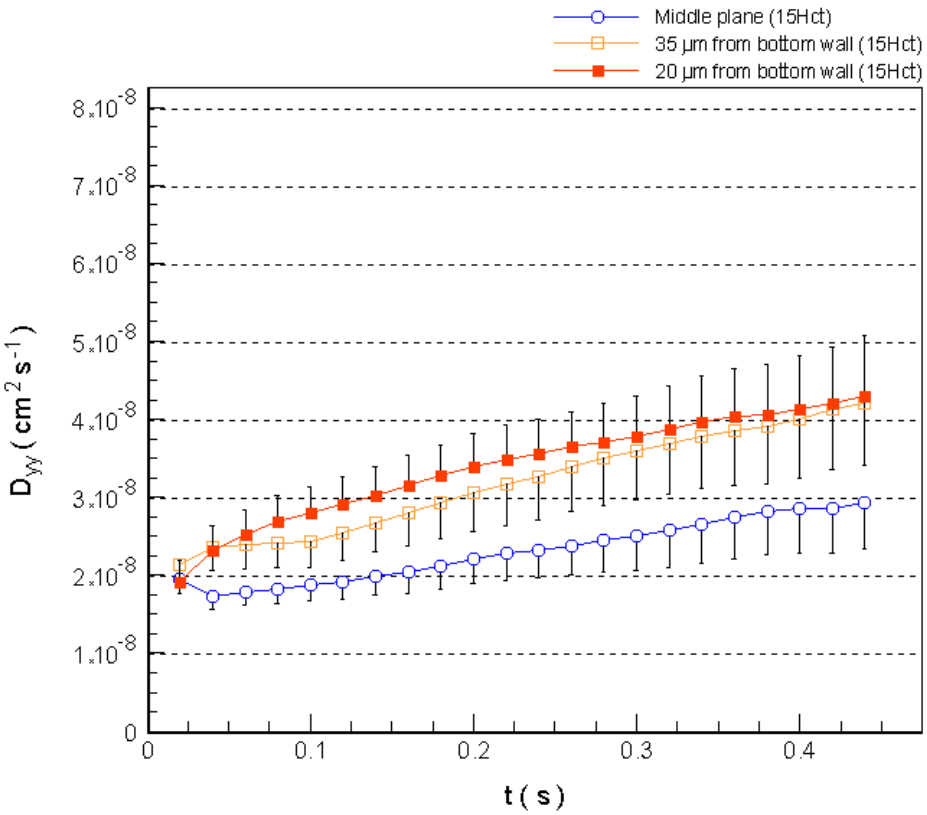

b)

Figure 6.23 RBC radial dispersion coefficient (D_{yy}) at different in-focus planes for a) 35% Hct, b) 15% Hct (Re = 0.005). The measured values are expressed as the means ± standard deviation by using t-test analysis at 95% confidence interval.

The results from Figure 6.22 shows clearly that the radial dispersion coefficient increases with the Hct implying that the RBCs at dense concentrations exhibit higher erratic radial displacement due to collisions with neighboring RBCs. As already mentioned our system has the ability to measure the motion of RBCs at several in-focus planes and as result it was possible to calculate the correspondent radial dispersion coefficient. The results presented in Figure 6.23 shows that the D_{yy} tends to increase as one moves away from the tube axis. These results suggest that the velocity gradients induced by the wall has a strong influence on the RBCs erratic radial displacements as shown in Figure 6.21.

6.4 Discussion

Along the years, several researchers have found temporal fluctuations in the blood velocity profiles in microvessels. Most of the results were performed at a macro and mesoscale levels which have leed to some controversies. We believe that it is crucial to investigate the cause of this phenomenon at cellular level. The data presented in this study demonstrates the ability of the proposed confocal micro-PTV system to obtain further insight onto the complex flow behavior of blood in microcirculation.

Blood cells interactions in flowing blood

The limitation of the present experimental optical techniques to investigate blood flow properties at a microscopic level has leed to some numerical studies on cell-cell interaction (Liu et al. 2004, Dzwinel et al. 2003, Ishikawa 2006, Tsubota 2006). However, in order to validate these numerical studies experimental results on the interactions between cells are essential. The present study provides for the first time both quantitative and qualitative evidence on cell-cell hydrodynamic interaction in flowing blood. The measurements were possible due to the unique ability of the confocal systems to obtain thin in-focus planes (2 μm for the present study). Thus, this system can provide the paths of two or more blood cells interacting in the same focal plane.

The hydrodynamic interactions of RBCs in concentrated suspensions are dependent on multi-physics hemodynamics such as shear rate ($\dot{\gamma}$), plasma layer and RBC deformability. We have presented four typical RBC-RBC interaction in flowing blood. Generally, when there is a cell interaction, the radial displacement tends to increase to a maximum peak and then the cell

begins to return towards its initial position. However, most of the times it never returns to the initial position as an interaction with another neighboring cell is likely to occur. Two interesting phenomenon happening within the plasma layer are presented in Figures 6.10 and 6.12. For the first case our results show that when a RBC is rolling on the surface of the microchannel, an interaction does not cause a significant increase on its radial displacement (see Figure 6.11). This behavior indicates that the lubrication force between the RBC and the wall is bigger than the hydrodynamic force caused by the interaction. The second phenomenon happens around the boundary of the plasma layer with the crowded suspension where there is a competition for the centre position. Although the RBC7 (see Figure 6.12) has a tendency to migrate towards the center of the tube, this migration is inverted due to a hydrodynamic interaction caused by a RBC flowing in the crowded region. It is well known that there is a formation of a plasma layer in capillaries but this layer is not a complete cell free layer as shown in our results. Our results suggest that a RBC flowing in the plasma layer is subjected to both axial and lateral migration which generate an undulated trajectory. This phenomenon may play an important role not only on the increase of the apparent blood viscosity but also on the blood mass transport of cells and proteins to tissues and thrombus.

Generally, when a RBC interacts with a neighboring RBC its radial displacement tends to deviates at least 2% from its original path. Due to multibody collisions, the RBC streamlines are continuously diverted and consequently the hydrodynamic interactions introduce disturbances to the blood flow at a microscopic level. The shear rates ($\dot{\gamma}$) used in this study was from ~16 s^{-1} to ~20 s^{-1},considering Poiseuille flow. As a result, we did not observe any RBCs aggregation in our experiments, which is consistent with other experimental observations (Goldsmith and Marlow 1979, Chien 1970). Moreover, the use of Dextran 40 may also contribute for reducing the tendency of RBC to aggregate.

During our experiments most of WBCs were flowing near the bottom wall of the capillary. In the present study, two representative RBCs-WBCs interactions were analysed (see Figures 6.15 and 6.16). Note that some measurements of cells paths were performed with faint images (slightly out-of-focus cells). Our results suggest that the WBC hydrodynamic effect on the trajectory of the RBC is dependent on its contact angle. For instance, the radial displacement of RBC1 increases of about 2 μm (see Figure 6.15) by interacting with the upper centre periphery of the WBC, while the radial displacement of RBC2 (see Figure 6.16) increases dramatically (> 4 μm) when it interacts with its lateral surface.

Orientation of RBCs in flowing blood

Due to the shear rate used in our experiment (~16s^{-1} to ~20s^{-1}), we did not observe any considerable deformation of the RBCs especially around the plasma layer. However, we have observed that the degree of the deformation seems to increase as the RBCs migrate towards the centre of the capillary. At this region, due to high concentration, RBCs have tendency to squeeze as they pass through each other. Our study presents two remarkable examples on the RBCs orientation at low shear rates (~18s^{-1} to ~20s^{-1}). By using the proposed technique, we have measured both translational and rotational motion of a RBC with and without interaction. As shown in Figures 6.18 and 6.19, the RBCs with hydrodynamic interactions rotate erratically in contrast to the cells rolling along the wall surface without any interaction. This finding may be relevant to obtain further insight onto the oxygen transport mechanism in microcirculation.

RBCs Radial disperson coefficient

The present study provides quantitative data on radial fluctuations of RBCs at different Hcts and in-focus planes. Our results show clearly that the RBCs radial dispersion coefficient increases with the Hct (see Figure 6.22). It is also very clear that the RBCs that flow near the wall have higher radial dispersion. These results reinforce the evidence that both Hct and velocity gradient induced by the wall play an important role on the blood flow properties which influences the resistance to blood flow in microvessels.

In previous studies, Goldsmith and his colleagues (1971, 1986) have calculated the radial dispersion coefficient by using a fluid containing 39% of ghost cells. Their values are slightly higher when compared to the present results, especially near the wall where the difference can reach almost one order of magnitude. This discrepancy may be due to the use of RBCs without hemogoblin which could affect their rheological properties. Moreover, the out-of-focus effect may have also contributed to perform measurements on RBCs lying away from the in-focus plane of interest. Hence, the previous *in vitro* studies performed with wide-field microscopes may needed careful reexamination.

Main advantages and limitations of the proposed confocal micro-PTV

One of the main advantages of the proposed confocal micro-PTV system is the ability of the spinning disk confocal microscope (SDCM) to reduce the background noise from the out-of-focus planes. By using a conventional microscope, the intensity of the RBCs within the out-of-focus planes does not change with the distance from the in-focus plane so that the estimated depth of field (Meinhart et al. 2000a) is often 4 times higher than the size of tracer RBCs. In contrast, by using a SDCM, the brightness of the RBCs decreases dramatically, especially at distances very close (1 μm) to the in-focus plane. This dramatic improvement of the background noise rejection provides greater contrast of the tracer RBCs and permits the generation of true thin optical sections (2 μm for current study). Hence, SDCM systems can provide accurate measurements on the paths of single RBCs or multi-RBC interactions flowing in the same focal plane, task not possible by using a conventional microscope.

One of the main limitations by the use of the SCDM is on the blood flow rate able to obtain accurate measurements. This limitation is mainly due to losses of the incident illumination induced by the spinning disk pinholes. One way to overcome this limitation is to increase the pinhole size, however both optical sectioning and spatial resolution will be compromised.

6.5 Conclusions

We have applied a confocal micro-PTV system to measure the motion of individual RBCs through a 100 μm capillary. The fluorescent labeled RBCs exhibited similar flow characteristics encountered *in vivo* microvessels implying that the *in vitro* blood used in the present study may represent an adequate model to study the flow behavior of RBCs through microchannels.

The ability of the confocal system to generate thin in-focus planes has allowed the measurement of several microscale phenomena on the flow behavior of RBCs. To our knowledge, the present study shows for the first time both qualitative and quantitative measurements in flowing blood at concentrated suspensions of: cell-cell hydrodynamic interaction, RBC orientation and RBC radial dispersion at different depths. In general our results show evidence that the plasma layer enhance the collisions between neighboring RBCs which influence the motion and flow behavior of the cells. Our results provide clear evidence that the multibody collisions promote fluctuations on both translational and rotational motion

of RBCs. These results not only confirm earlier observations but also provide new insights into the complex behavior of RBCs flowing in a crowded environment.

The proposed confocal micro-PTV system proves to be a powerful technique to obtain the paths of two or more blood cells interacting in the same focal plane, a task not possible by using a micro-PIV system equiped with a conventional microscope. Hence, the presented approach not only eliminates the problems and concerns of the methods used in the past but also provides additional detailed description on the RBC motion not obtainable by other conventional methods. We believe that this system will provide a powerful tool to obtain further insights into the complex flow properties of blood in the microcirculation with the expectation that a better understanding on the blood flow phenomena will make a contribution to the prevention, diagnosis, and treatment of vascular diseases.

CHAPTER 7

RADIAL DISPERSION OF RED BLOOD CELLS IN BLOOD FLOWING THROUGH GLASS CAPILLARIES: ROLE OF HEAMATOCRIT AND GEOMETRY

7.1 Introduction

The primary function of the red blood cells (RBCs) is to transport oxygen and carbon dioxide bound to the intracellular hemogoblin. In microcirculation, the flow behavior of RBCs plays also a crucial role in many physiological and pathological phenomena. For instance, the randomlike transverse motion and rotation of RBCs in shear flow is believed to play an important role to the thrombogenesis process. However, the role of the RBCs on the mass transport mechanism of cells and proteins to the thrombus is still not completely understood (Goldsmith and Turitto 1986, Wootton and Ku 1999, Miayazaki and Yamaguchi 2003). As a consequence, many studies have been performed on both rheological and microrheological behavior of RBCs flowing through glass capillaries (Chien et al. 1984, Goldsmith and Turitto 1986, Pries et al. 1992, Shiga et al. 1990, Mchedlishvili and Maeda 2001).

The majority of the researches on the RBCs microhemorhelogical behavior in shear flow was mainly done in diluted suspensions. By using video microscopy examination, the motion of single RBC was studied in detail by several researchers which have led to an almost mature knowledge on this topic (Goldsimth 1971, Fischer et al. 1978, Shiga 1990, Lominadze and Mchedlishvili 1999, Pries and Secomb 2003, Bitbol 1986, Suzuki et al. 1996, Abkarian et al. 2006). However, one of the biggest scientific challenges in this field is related to the behavior of the RBCs flowing in relatively high concentrations close to haematocrits (Hct) that exists in microvessels (Hct from 10% to 26%) (Fung 1997). Despite the relevance of this phenomenon on the blood mass transport, very few studies has been performed during the past years, partly due to the absence of adequate visualization techniques able to obtain both direct and quantitative measurements on multi-RBCs motions in concentrated suspensions. An extremely important work on this field was carried out by Goldsmith and his coworkers (Goldsmith 1971a, Goldsmith 1971b, Goldsmith and Karino 1977, Goldsmith and Marlow

1979, Goldsmith and Turitto 1986, Cokelet and Goldsmith 1990). By using a traveling microscope, they were able to study the behavior of RBCs in concentrated suspensions. However, in order to have adequate signal to noise ratio to permit the detection of tracer RBCs at Hct bigger than 10%, they have used ghost cells as models of erythrocytes. The preparation of ghost cells requires the rupture of the RBC membrane to allow the diffusion of the hemoglobin (Hb) into the surrounding fluid (hemolysis) (Caro et al. 1978, Burton 1966). The preparation procedure of the ghost cells and also the removal of the Hb may contribute to differences in the membrane mechanical properties between ghost RBCs and normal RBCs and consequently the dynamic behavior of RBCs might be affected (Caro et al. 1978, Goldsmith and Marlow 1979, Nash and Meiselman 1983). The controversy whether ghost cell suspensions is a good physical model for blood remains, mainly because there has not yet been experimental evidence on this question. Thus, it is important to re-examine the work of Goldsmith and his colleagues by using a physiological fluid containing normal RBCs. In this way, the present study introduces a new approach to measure the radial dispersion of labeled RBCs flowing in concentrated suspensions of normal RBCs.

Along the years, the main limitation in measuring high concentrations of normal RBCs has owed mainly on the attenuation of the incident light by hemoglobin absorption and RBCs light scattering. However, by combining a spinning disk confocal microscope (SDCM) with a laser, the emitted light intensity is significantly improved and as a result, it is possible to obtain adequate signal to noise ratio to detect the motion of the RBCs in concentrated suspensions (Tanaami et al. 2002, Park et al. 2004, Lima et al. 2006, 2007). Moreover, in contrast to the conventional microscope where the entire flow region is illuminated, the confocal systems have the ability to obtain in-focus images with optical thickness less than 1 μm (optical sectioning effect). As a result, confocal systems provide a superior spatial resolution which allows direct measurements on RBCs motion in concentrated suspension at several optically sectioned planes along the microchannel depth. In our recent work, we have used our confocal system combined with a cross-correlation technique (confocal micro-PIV) in order to obtain the velocity profiles of *in vitro* blood flowing through a 100 μm square microchannel. However, by using this combination, we were only able to obtain accurate measurements with Hcts up to 17%, mainly due to the low density of trace particles available on the captured images. However, in the present study we have integrated our confocal system with a single particle method (SPT) in order to measure the motion of individual RBCs at Hcts up to 35%.

The present work introduces a new approach (confocal micro-PTV) to obtain direct and quantitative detailed description of the flow behavior of RBCs in concentrated suspensions of normal RBCs. This approach eliminates the problems and concerns of the methods used in the past and provides additional detailed description on the RBC motion not obtainable by other conventional methods. The ability of our system to obtain thin in-focus planes along the microchannel allows us to obtain accurately the radial position of the RBCs and for this reason interaction between two labeled RBCs was also possible to be measured. The information provided by this study not only complements previous investigations on hemomicrorheology of RBCs but also shows the influence of both Hct and geometry on the RBCs radial dispersion. Such information is important for a better understanding on the blood mass transport mechanisms under both physiological and pathological conditions. The experiments were performed in 50μm and 100 μm glass capillaries at Reynolds numbers (Re) from 0.003 to 0.005, by using Hcts from 2% to 35%. Although it is possible to obtain measurements at several planes by using our confocal system, particular emphasis was devoted on the radial dispersion of RBCs located in middle plane.

7.2 Materials and methods

7.2.1 Working fluids and RBCs labeling

The present study examined several working fluids: dextran 40 (Dx-40, Otsuka Medicine) containing 2%±1 (2Hct), 3%±1 (3Hct), 8%±1 (8Hct), 9%±2 (9Hct), 15%±1 (15Hct), 23%±1 (23Hct), 24%±1 (24Hct), 32%±1 (32Hct), and 35%±1 (35Hct) of human RBCs. The Hcts correspond to the feed reservoir Hct and it was measured by using a heamatocrit centrifuge (Kubota 3220, Japan), always immediately before each experiment.

The RBCs were fluorescently labeled with a lipophilic carbocyanime derivative dye, chloromethylbenzamido (CM-Dil, C-7000, Molecular Probes) using a procedure previously described (see Chapter 6). In brief, the RBCs where separated from the bulk blood by centrifugation (1500 RPM for 20 min) and aspiration of the plasma and buffy coat and then washed twice with physiological saline (PS). The washed RBCs were then incubated in the dye solution for 30 min. at 37ºC and then for an additional time at 4ºC for 1-2h. The fluorescently labeled RBCs were washed to remove any excess dye and diluted with Dx40 to make up the required RBCs concentration by volume. This dye was well retained by the

RBCs and had a strong light intensity (excitation: 553nm, emission: 570nm) which have allowed the visualization of labeled RBCs in concentrated suspensions. It should be noted that the RBCs labeling was performed immediately before each experiment. All procedures in this experiment were carried out in compliance with the Ethics Committee on Clinical Investigation of Tohoku University.

7.2.2 Glass microchannels

In this study, we used a 100-μm and a 50-μm circular borosilicate glass microchannel fabricated by Vitrocom (Mountain Lakes, NJ, USA). The capillary was mounted on a slide glass with a thickness of 80±20 μm and was immersed in glycerol in order to minimize the refraction from the walls.

7.2.3 Experimental setup

The confocal micro-PIV system used in this study consists of an inverted microscope (IX71; Olympus, Japan) combined with a confocal scanning unit (CSU22; Yokogawa, Japan), a diode-pumped solid-state (DPSS) laser (Laser Quantum, UK) with an excitation wavelength of 532 nm and a high-speed camera (Phantom v7.1; Vision Research, USA). The glass capillaries were placed on the stage of the inverted microscope and by using a syringe pump (KD Scientific, USA) a pressure-driven flow was kept constant (Re from 0.003 to 0.005). Moreover, by using a thermo plate controller (Tokai Hit) the temperature surrounding the capillary was 36ºC±1.

The laser beam was illuminated from below the microscope stage through a dry 40× objective lens with a numerical aperture (NA) equal to 0.9. The light emitted from the fluorescent flowing RBCs passes through a color filter into the scanning unit CSU22, where by means of a dichromatic mirror, is reflected onto a high speed camera to record the confocal images. The confocal images were captured in middle of the capillary with a resolution of 640×480 pixels, 12-bit grayscale, at a rate of 100 frames/s with an exposure time of 9.4 ms. A manual tracking plugin (MTrackJ) (Meijering et al. 2006) of an image analysis software (Image J, NIH) (Abramoff et al. 2004) was used to track the label RBCs. By using this software, the bright centroid of the selected RBC was automatically computed through successive images so that it was possible to track accurately the labeled RBCs even when two cells were close together, which is the case of cell-cell interaction. The x and y-axis coordinate data for the individual

positions of each RBC were then exported to an appropriate C program (see Appendix D) able to calculate several physical quantities such as velocity, radial displacement and radial dispersion coefficient. A full description of the confocal micro-PTV/PIV system used in this study can be found in Chapter 3.

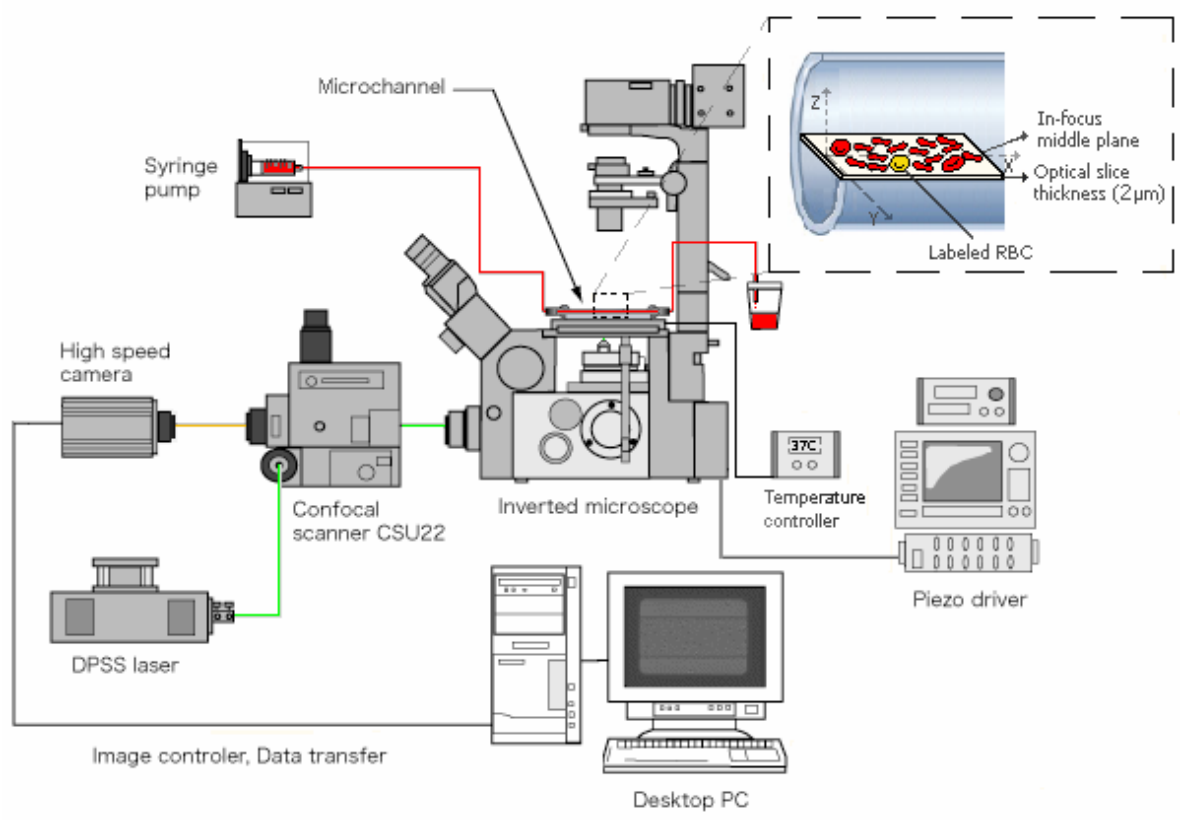

Figure 7.1 Schematic diagram of the confocal micro-PTV system and optical sectioned in-focus plane in the centre of the capillary.

The optical sectioned images were performed at several positions along the z-axis by using a piezo driver system and RT3D signal controller software from the Yokogawa corporation. The optical slice thickness (OST) was 2 μm based on geometric–optical analysis criteria (Willhelm et al. 2003, Lima et al. 2006)

7.2.4 RBC radial dispersion coefficient and displacement

The present study aims to obtain further insights on the RBCs flow behavior in glass capillaries. By using a confocal PTV system, the paths of hundreds labeled RBCs were measured mainly in the centre plane of two different capillaries 100 μm and 50 μm. In addition, to elucidate the effect of the heamatocrit on the motions of individual RBCs, several Hcts (from 2% to 35%) were analyzed by using Re from 0.003 to 0.005. Figure 7.2 shows a typical halogen and confocal image recorded in the middle plane of a 100 μm glass capillary with 15% Hct.

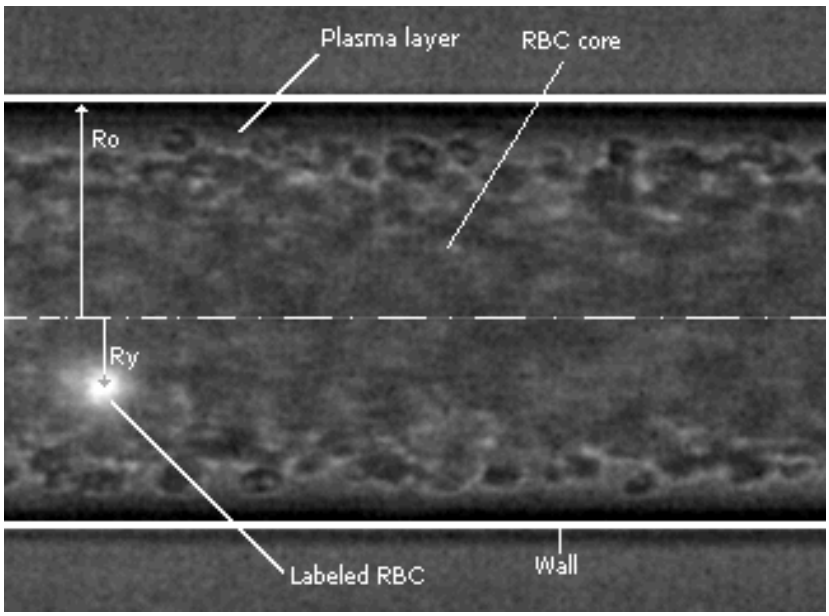

Figure 7.2 Coordinate system in the middle plane of a 100 μm capillary with 15% Hct. The image contains both halogen and laser light, that enables to see both labeled and non-labeled RBCs.

The detailed measurements on the motion of individual RBCs at a microscopic level are crucial to elucidate both mesoscopic and macroscopic blood flow properties. One accepted way to correlate the microscopic events to the macroscopic flow behavior is by calculating the radial dispersion coefficient (D_{yy}) (Goldsmith, 1971, Goldsmith and Turitto 1986). In the present study, we have analyzed the motions of RBCs by using a radial dispersion coefficient (D_{yy}) (Goldsmith and Turitto 1986), given by:

$$D_{yy}(t) = \frac{1}{N}\sum_{i=1}^{N}\frac{\left\langle \left(R_{i,y}(t) - R_{i,y}(0)\right)^2 \right\rangle}{2t} \qquad (7.1)$$

where $R_{i,y}(t)$-$R_{i,y}(0)$ is the radial distance traveled by individual RBC i over some time interval of length t and the radial squared displacement is averaged (indicated by ⟨⟩) over many such time intervals. The radial dispersion coefficient is then averaged over all RBCs (N) measured by the confocal system.

Besides the calculation of the radial dispersion coefficient (D_{yy}), the radial displacement (ΔR) of some representative microscopic events was also determined. The microscopic events, such as RBC-RBC and RBC-wall hydrodynamic interaction, were investigated by using a cumulative radial displacement (ΔR), given by:

$$\Delta R(t) = \left| R(t) - R(0) \right| \qquad (7.2)$$

where R(0) is the initial radial position of the RBC and R(t) is the cumulative radial displacement over time t.

7.3 Results

7.3.1 Blood flow visualization in a 100μm and 50μm capillary at several Hcts

The RBCs in flowing blood exhibit randomlike transverse motion which depends on the Hct and microchannel diameter. Figure 7.3 and 7.4 show recorded images with both labeled and non-labeled RBCs measured in centre plane of 100μm and 50μm capillary at several Hcts (form 2% to 35%) with Re from 0.003 to 0.005 (shear rates ($\dot{\gamma}$) from 3 to 25 s^{-1}).

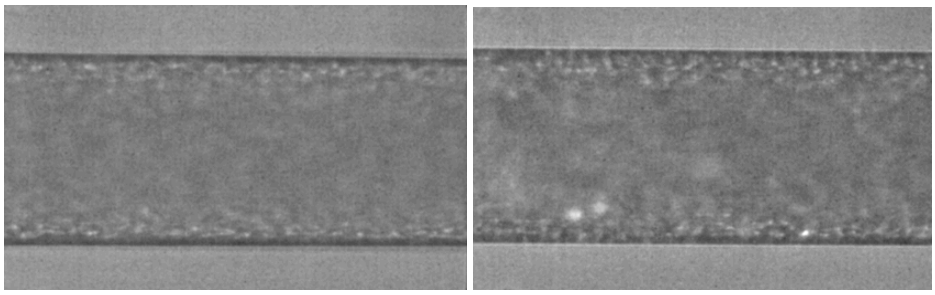

a) 35Hct

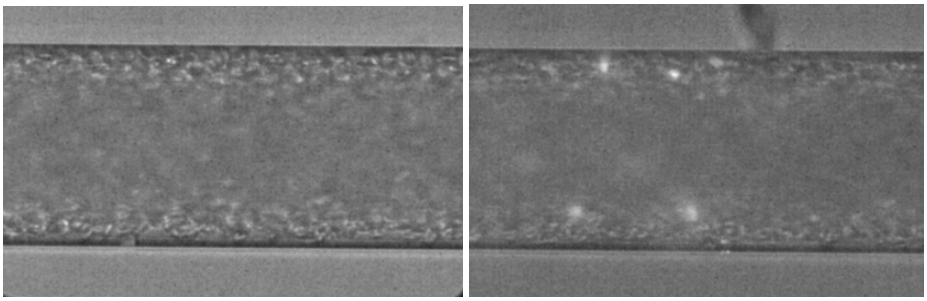

b) 24Hct

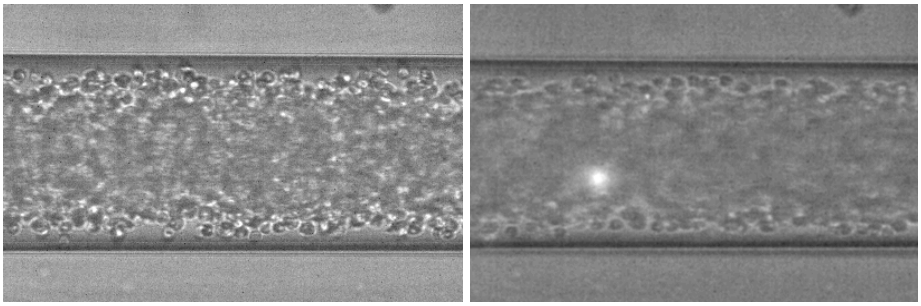

c) 15 Hct

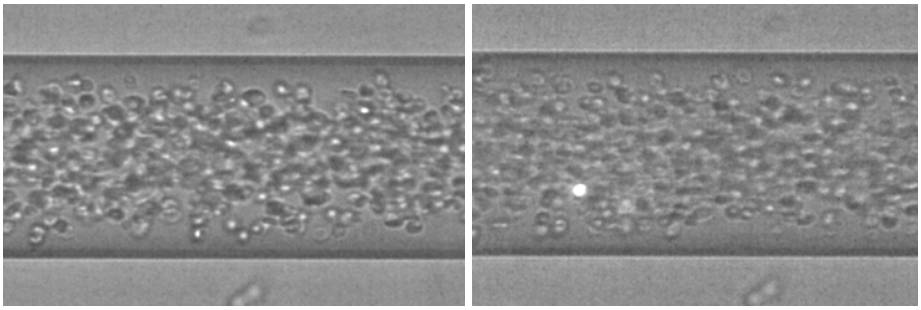

d) 9Hct

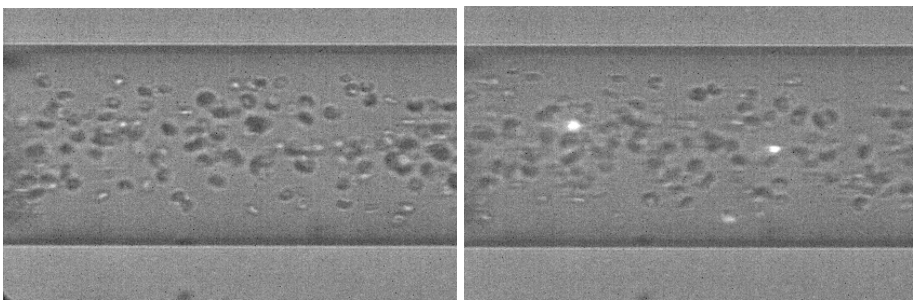

e) 3Hct

Figure 7.3 Halogen (left side) and confocal (right side) images in the middle plane of a 100μm glass capillary with a) 35% Hct, b) 24% Hct, c) 15% Hct, d) 9% Hct, e) 3% Hct. The non-labeled RBCs are observed as dark-grey rings, whereas labeled RBCs are observed as bright rings.

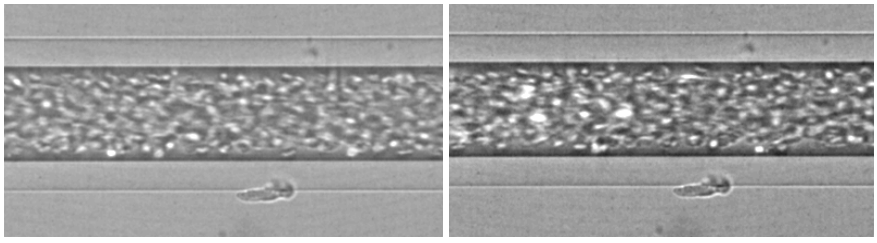

a) 32 Hct

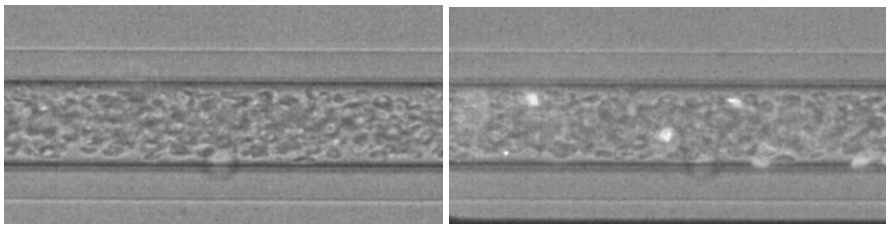

b) 23 Hct

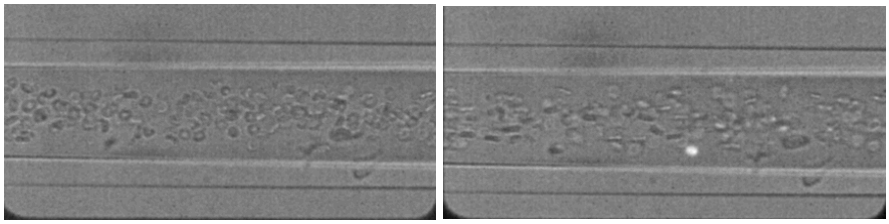

c) 8 Hct

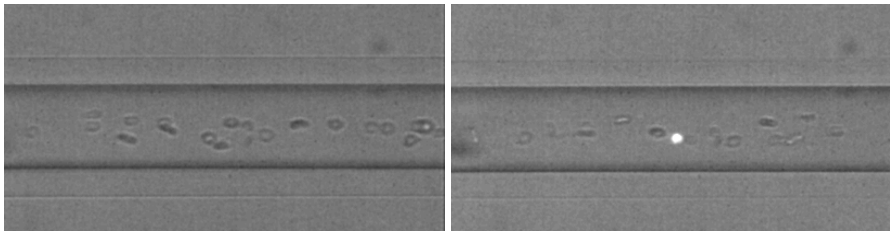

d) 2 Hct

Figure 7.4 Halogen (left side) and confocal (right side) images in the middle plane of a 50μm glass capillary with a) 32% Hct, b) 23% Hct c) 8% Hct, d) 2% Hct. The non-labeled RBCs are observed as dark-grey rings, whereas labeled RBCs are observed as bright rings.

It is very clear from Figure 7.3 and 7.4 that the Hct decreases with the microchannel diameter. These observations corroborates the well known Faharaeus effect (Chien et al. 1984). Moreover, it is also evident that the plasma layer tends to increase by decreasing the Hct. This

latter phenomenon is related to the Fahareues-Lindqvist effect (Fahareues and Lindqvist 1931). Although this phenomenon is still not completely understood (Caro 1979, Fung 1993), the most acceptable explanation is related to the tendency of the RBCs to migrate toward the microtube axis enhanced by the RBCs deformation and interations (Schmid-Schonbein and Wells 1969, Goldsmith 1971). A further consequence is that the apparent blood viscosity is reduced so that the flow resistance through the capillary also decreases.

7.3.2 Radial dispersion in a 100μm capillary at different Hcts

By measuring the radial displacement of labeled RBCs flowing through a 100μm capillary (Re ~ 0.005) for a known time interval, it was possible to calculate the correspondent dispersion coefficient (D_{yy}). Hundreds of RBCs were tracked for each Hct at the middle plane of the microchannel. Figure 7.5 shows the RBC averaged dispersion coefficient at the middle plane (D^c_{yy}) for several Hcts (3%Hct, 9%Hct, 15%Hct, 24%Hct and 35% Hct) whereas Figure 7.6 shows the RBC averaged D_{yy} located at different radial positions. Note that for this case the D_{yy} of RBCs was determined by dividing the recorded images into five equal areas on either side of the axis (see Figure 7.6a).

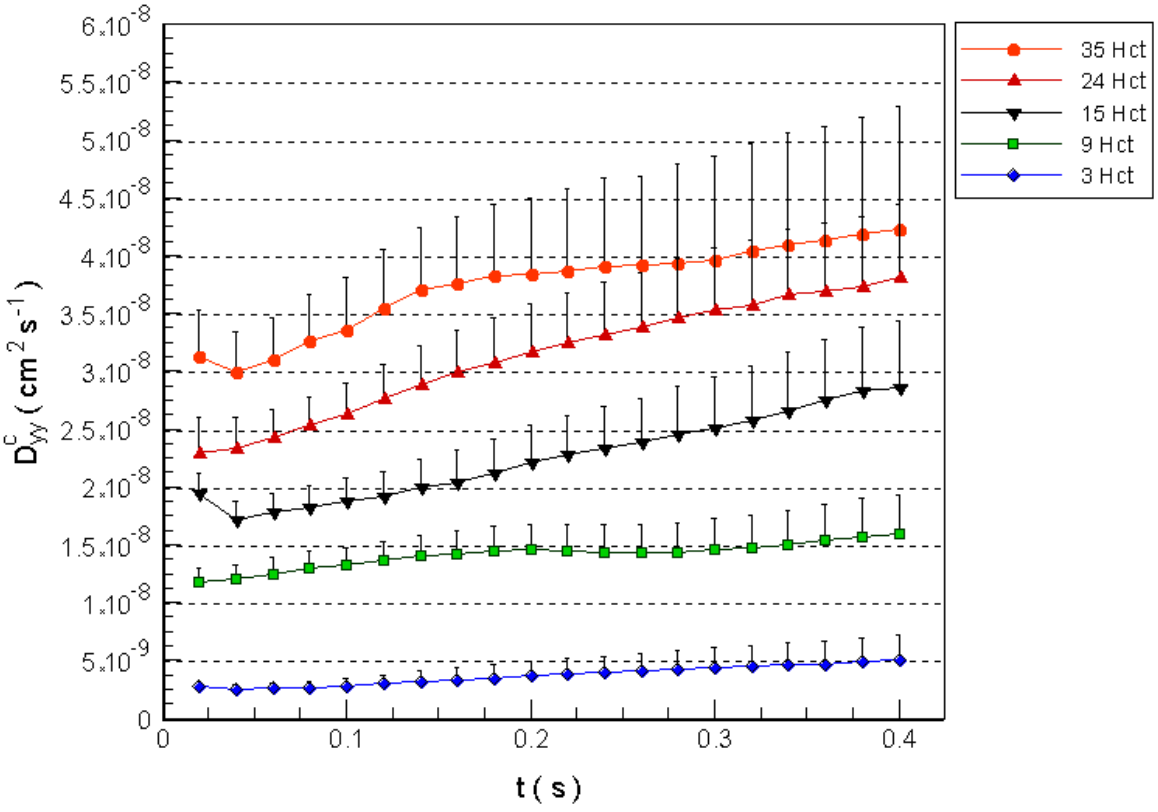

Figure 7.5 RBC dispersion coefficient at the middle plane (D^c_{yy}) for 35%Hct, 24%Hct , 15%Hct, 9%Hct and 3% Hct. The Re was ~0.005 and $\dot{\gamma}$ from ~2 s^{-1} to 12 s^{-1}. The measured values are expressed as the means ± standard deviation by using t-test analysis at 95% confidence interval.

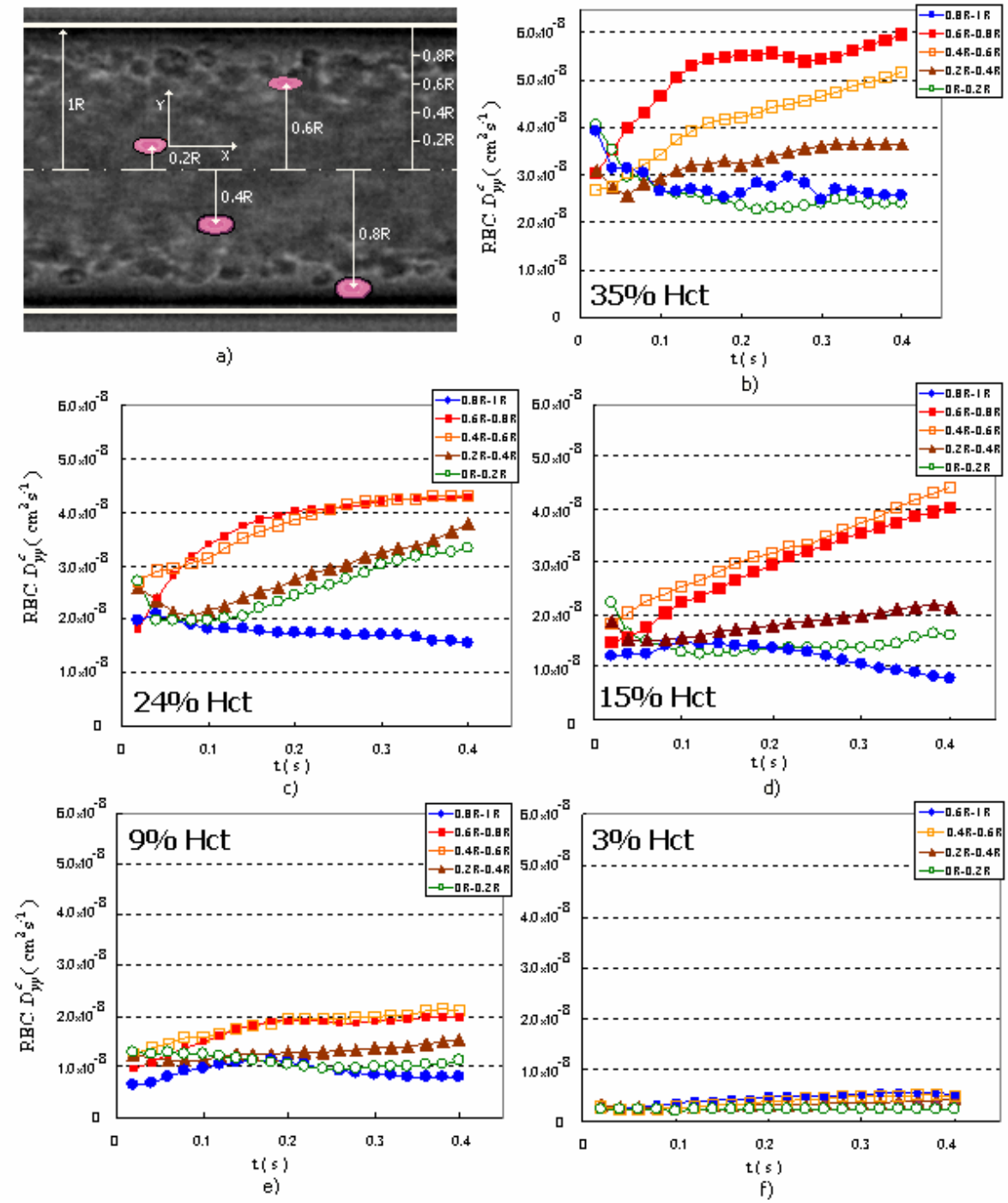

Figure 7.6 a) Schematic diagram of the different RBC position areas at the centre plane. RBC D^c_{yy} at different radial positions intervals for b) 35%Hct, c) 24%Hct, d) 15% Hct, e) 9%Hct, f) 3%Hct (Re ~ 0.005; $\dot{\gamma}$ from ~2 s^{-1} to 12 s^{-1}).

The results from Figure 7.5 show that the radial dispersion coefficient (D_{yy}) increases with the Hct. In addition, the RBC D_{yy} for Hcts from 24% to 35% have almost an order magnitude greater than the D_{yy} 3%Hct. These results clearly demonstrate that the RBCs at dense concentrations exhibit higher erratic radial displacement when compared with diluted suspensions of RBCs. In general, the results presented in Figure 7.6 shows that D_{yy} is the

greatest at radial positions between 0.4R to 0.8R. The D_{yy} near wall is the lowest mainly because of the RBCs that rolls along the wall with small radial displacements. However, for Hcts around 3%, the D_{yy} seems to increase proportionally with the radial position. In this case, it was extremely difficult to observe RBC flowing adjacent to the wall for the tendency of the RBCs to migrate to the tube axis at diluted solutions.

7.3.3 Radial dispersion in a 50μm capillary at different Hcts

Additional experiments through a 50μm capillary (Re ~ 0.003) were performed to evaluate the effect of the microtube size on the RBC radial dispersion coefficient (D_{yy}). Several Hcts (2% Hct, 8% Hct , 23% Hct and 32% Hct) were used in order to obtain further information on the role of Hct in the D_{yy}. Figure 7.7 shows the RBC averaged dispersion coefficient (D_{yy}) at several Hcts (2% Hct, 8% Hct , 23% Hct and 32% Hct) whereas Figure 7.8 shows the RBC averaged D_{yy} located at different radial positions. For this case, the D_{yy} of RBCs was determined by dividing the recorded images into four equal areas on either side of the axis (see Figure 7. 8a).

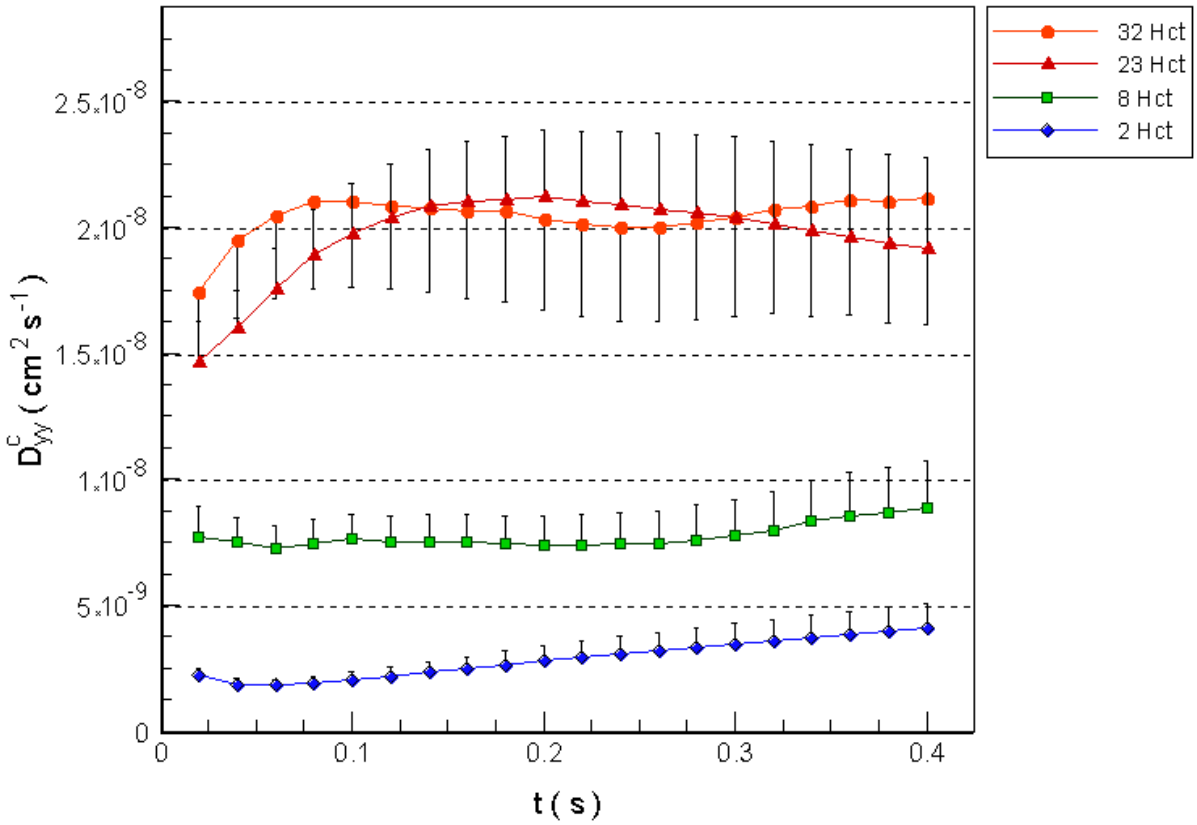

Figure 7.7 RBC D_{yy} at the middle plane (D^c_{yy}) for 32%Hct, 23%Hct , 8%Hct and 2% Hct. The Re was ~0.003 and $\dot{\gamma}$ from ~3 s^{-1} to 25 s^{-1}. The measured values are expressed as the means ± standard deviation by using t-test analysis at 95% confidence interval.

The first observation from these results is that the tube Hct has reduced considerably (Fahraeus) due to capillary size (see Figure 7.3 and 7.4). However, for convenience we will use the feed Hct as our reference Hct through out the discussion of the results.

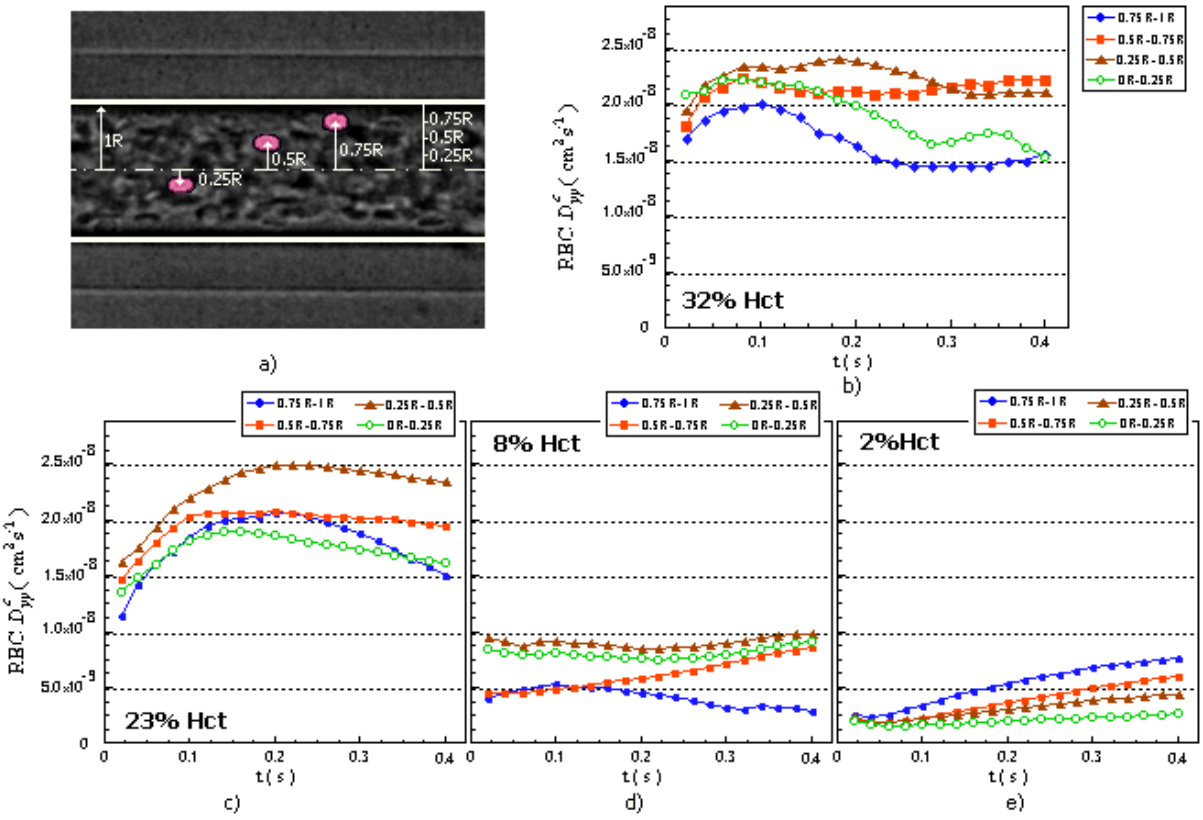

Figure 7.8 a) Schematic diagram of the different RBC position areas at the centre plane. RBC D^c_{yy} at different radial positions intervals for b) 32%Hct, c) 24%Hct, d) 8%Hct and 2% Hct (Re ~ 0.003; $\dot{\gamma}$ from ~3 s^{-1} to 25 s^{-1}).

The results from Figure 7.7 show that the radial dispersion coefficient (D_{yy}) increases up to a Hct of 23%, at which it levels off. It is interesting that D_{yy} reduces about 2 to 4 times when compared with D_{yy} obtained in a 100μm capillary. We believe that this reduction is due not only to the geometry constrain which limits the RBCs transverse motion but also due to the Fahraues effect. In Figure 7.8, the data suggest that for Hcts bigger than 8% the D_{yy} is the greatest at radial positions between 0.25R to 0.75R. At these radial positions we did not obtain any significant statistical difference. However, it is interesting to note that for Hcts higher than 8% the D_{yy} is always smaller at positions near the wall (0.75R to 1R). These latter results are consistent with the data previously reported in Figure 7.6. For Hcts of about 8% the RBCs density around the tube axis tends to decrease and consequently D_{yy} located at this region (0R to 0.25R) has tendency to increase. It is also worth saying that for diluted concentrations (2% Hct) the D_{yy} seems to increase approximately linearly with the radial

position and therefore with the shear rate. These results are in agreement with the data obtained in a 100µm capillary.

7.3.4 Effect of radial position on the RBCs radial dispersion

The wall boundary effect is believed to influence the RBCs radial displacements paths. Figure 7.9 and 7.10 show the D_{yy} as a function of the average radial position at several Htcs for both 100µm and 50µm capillary.

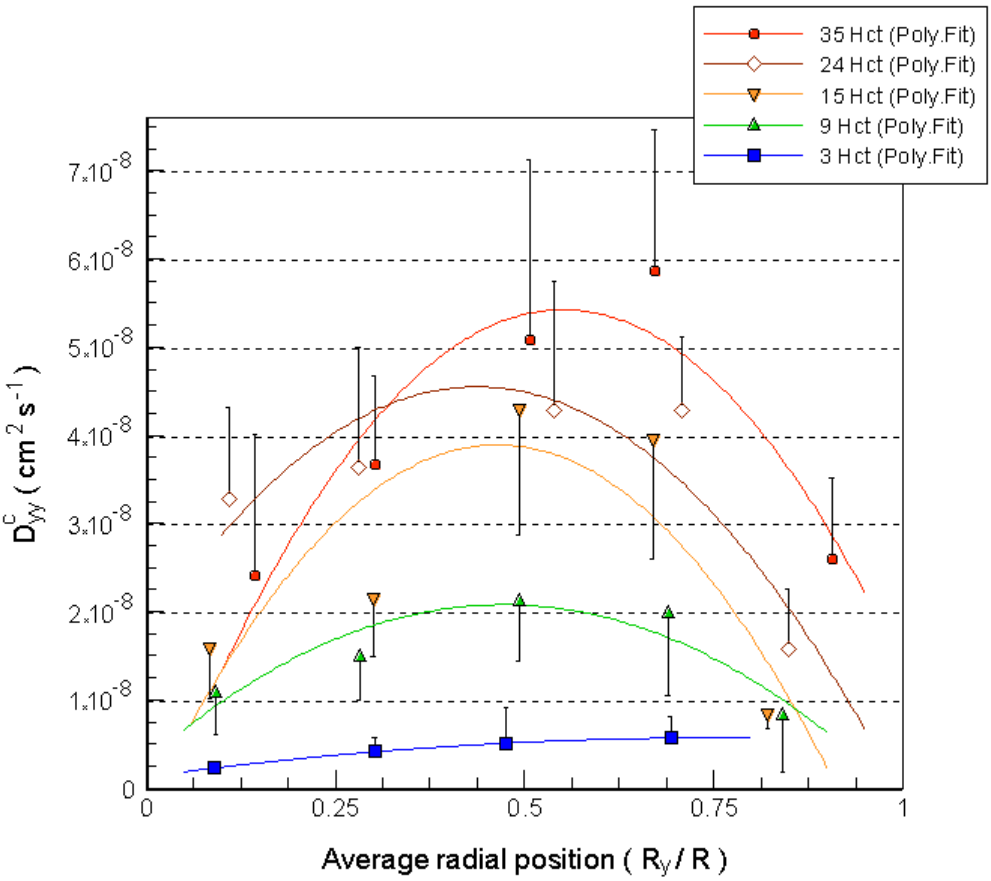

Figure 7.9 RBC D^c_{yy} as a function of the average radial position at several Htcs for 100µm capillary (Re ~ 0.005; $\dot{\gamma}$ from ~2 s^{-1} to 12 s^{-1}). The measured values are expressed as the means ± standard deviation by using t-test analysis at 90% confidence interval.

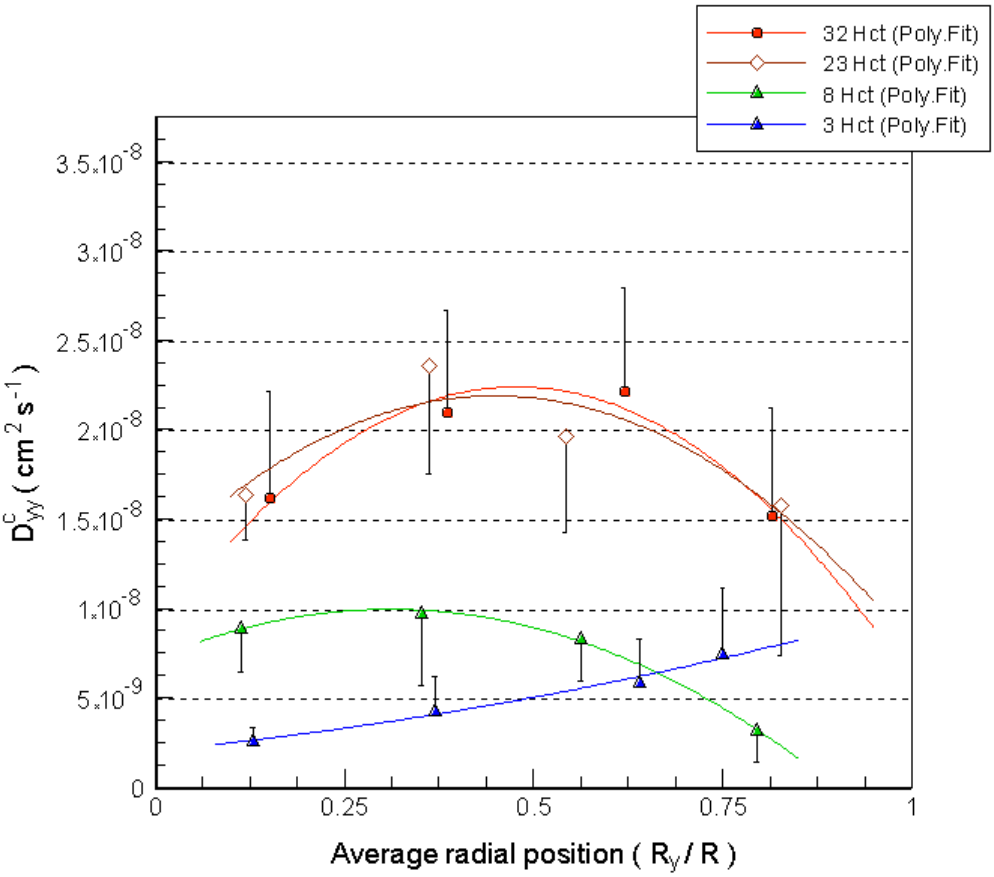

Figure 7.10 RBC D^{c}_{yy} as a function of the average radial position at several Htcs for 50μm capillary (Re ~ 0.005; $\dot{\gamma}$ from ~3 s^{-1} to 25 s^{-1}). The measured values are expressed as the means ± standard deviation by using t-test analysis at 90% confidence interval.

Although some results do not present significant statistical difference, it is interesting to observe that at high and moderate Hct the D_{yy} is the lowest around the centre and wall periphery of the capillary. In contrast, for diluted suspensions (Hct < 3%) D_{yy} tends to increase approximately linearly with the radial position.

7.3.5 Microscopic flow behavior of RBCs

It is well known that the radial dispersion coefficient (D_{yy}) can provide important information on both mesoscopic and macroscopic blood flow properties. The RBCs D_{yy} is a statistical quantity which reflects several micro-scale phenomena of the RBCs flow behavior, such as RBC-RBC interaction and RBC tendency for radial migration. In this way, it is also important to examine the motion of RBCs at a microscopic level. Several relevant micro-scale phenomena on flow behavior of RBCs at concentrated suspensions are presented below.

RBC ΔR within the plasma layer and adjacent to the wall

Figure 7.11 shows the effect of the radial position on the motion of four individual RBCs flowing through a 100µm and 50µm glass capillary, for a feed Hct of about 24%. The correspondent radial displacements (ΔR) are shown in Figure 7.12.

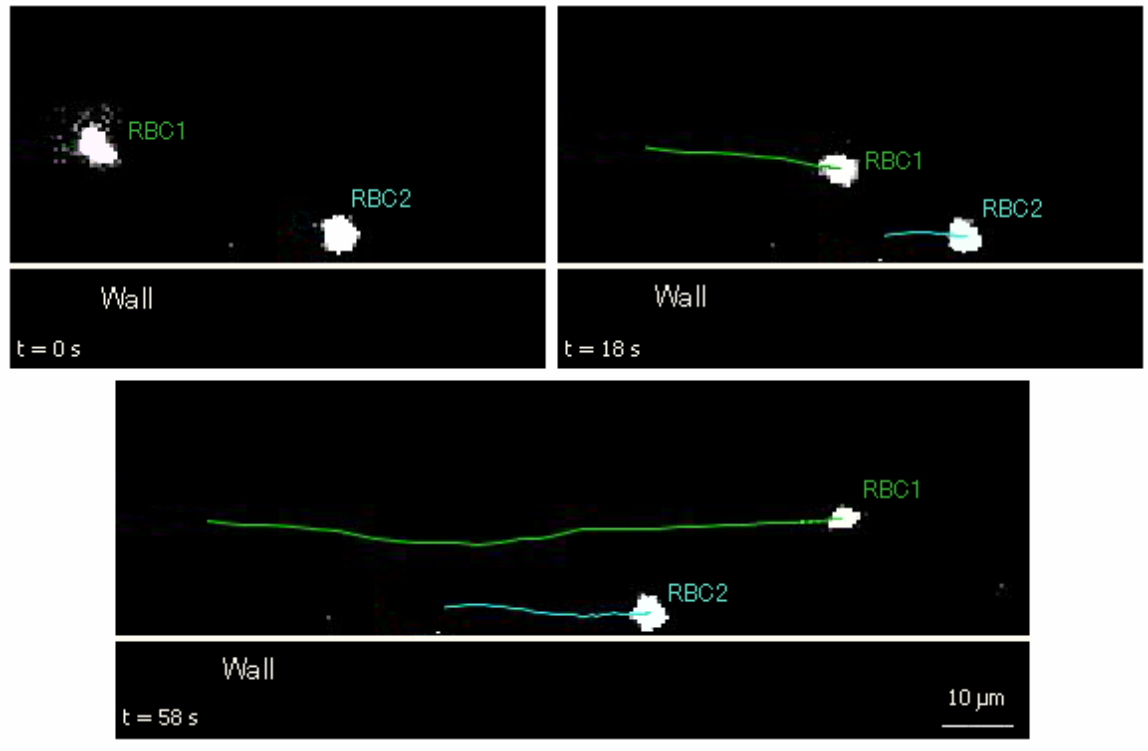

a)

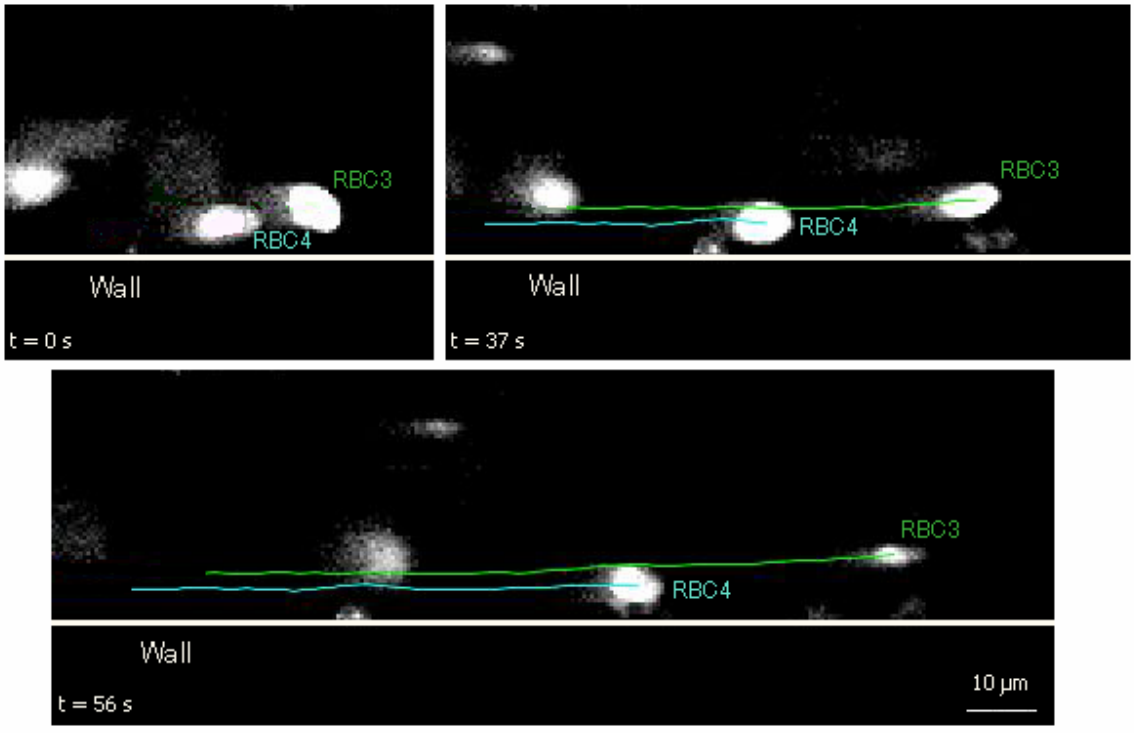

b)

Figure 7.11 The effect of the radial position on the motion of RBCs at a) 100µm (24Hct) and b) 50µm (23Hct) capillary. The Re for 100µm and 50µm was 0.005 and 0.003 respectively

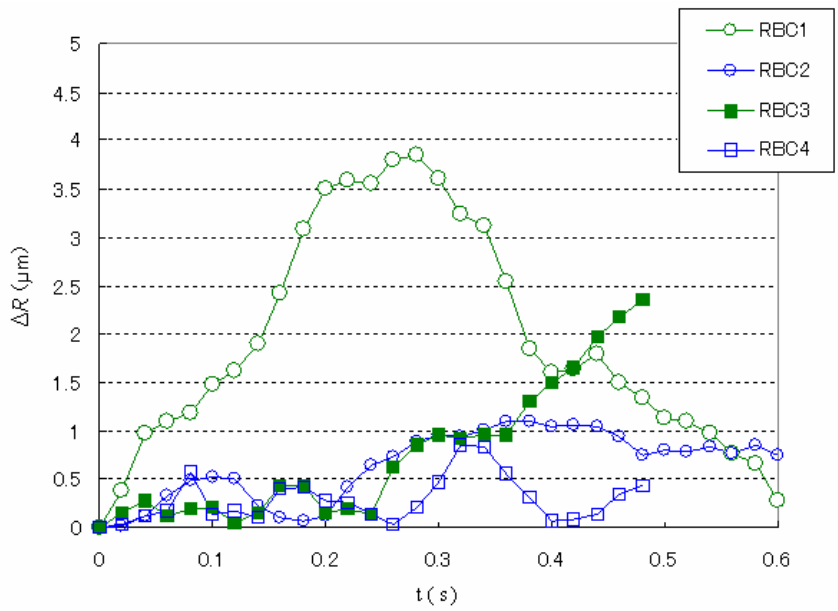

Figure 7.12. The role of the radial position on the radial displacement (ΔR) of tracer at 100μm and 50μm microtube. RBC2 and RBC4 are traveling adjacent to the wall whereas RBC1 and RBC3 are flowing within the plasma layer.

From Figure 7.12 it is possible to observe that radial displacement (ΔR) of the RBCs (RBC1, RBC3) flowing within the plasma layer is around 1 to 4 times higher than the RBCs (RBC2, RBC4) traveling adjacent to the wall of the microchannel. These microscopic observations reflect the low D_{yy} obtained at radial positions near the wall (0.8R to 1R). Therefore, although the shear rate is higher near the wall, the trajectories of the RBCs traveling on the wall do not exhibit strong radial dispersion. In contrast, the RBCs flowing within the boundary region of RBC core (0.6R to 0.8R) suffer multiple hydrodynamic interactions with neighboring RBCs. The random like transverse motions happening in this region are due not only to neighboring RBCs flowing with lower velocity but also to the collision with RBCs within the plasma layer, which tend to migrate away from the microtube wall. As a result, RBCs flowing at radial positions between 0.6R and 0.8R appear to undergo the largest radial displacements.

Radial displacement (ΔR) of two-RBC interactions

Figure 7.13 shows the streamlines of two RBCs interacting within the plasma layer (0.6R-0.9R), whereas the ΔR for each individual RBC is shown in Figure 7.14. The RBCs interaction was obtained at a 100μm glass capillary for a feed Hct around 24%.

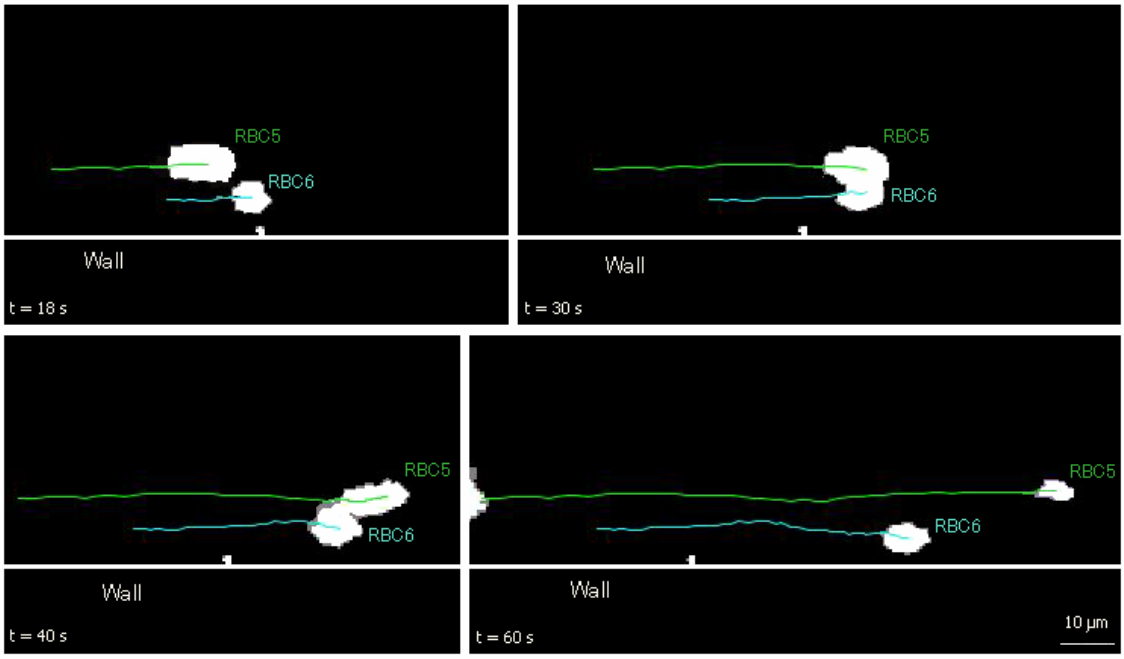

Figure 7.13 Two-RBC interactions at different time intervals at 100μm glass capillary (24Hct).

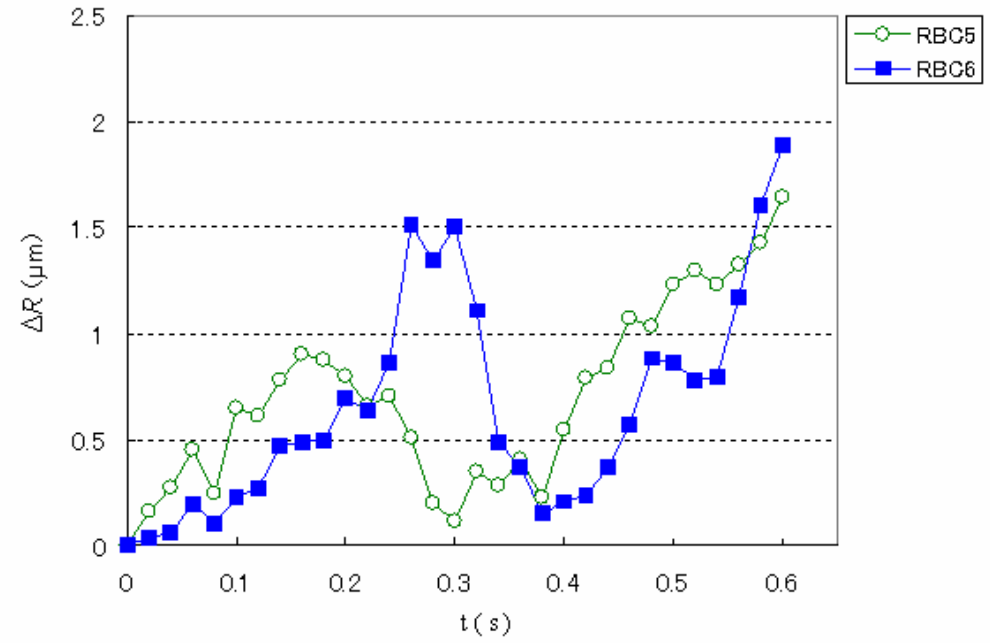

Figure 7.14 Radial displacement (ΔR) of two-RBC interactions at different time intervals.

In Figure 7.13, it is possible to observe a cell (RBC6) located within the plasma layer with tendency to migrate axially from the wall. However, this inward migration is inverted when it interacts with the RBC5 (t ~ 0.3s) located around the boundary of RBC core region. These results show clearly the fluid-dynamical interaction effect on the motion of RBCs flowing in concentrated suspension of blood cells. For this case, the RBC radial displacements have increased around 1 to 2 times of its initial path.

7.4 Discussion

Mass transport in blood flow is still not completely understood, partly because of the lack of experimental data on the flow properties of cells in concentrated suspensions. It is known that RBC motions play an important role in the mass transport mechanism (Goldsmith and Turitto 1986, Wootton and Ku 1999, Munn et al. 1996, Miayazaki and Yamaguchi 2003), which can be quantified by the radial dispersion coefficient (D_{yy}). The present study examines the effect of the haematocrit (Hct) and microtube geometry on RBCs D_{yy} by using a confocal micro-PTV system.

Effect of the Hct on the RBC radial dispersion

A previous study performed by Goldsmith and Marlow (1979) have measured the effect of volume concentrations (from 10% to 93%) on the radial displacements of tracer RBC in ghost cell suspensions. The present work extends their investigations by using labeled RBCs in normal cell suspensions and adds the effect of the Hct on the RBC radial dispersion coefficient at the centre plane (D_{yy}^{c}). Figure 7.15 illustrates the Hct effect on D_{yy}^{c} for both 100μm and 50μm glass capillaries. Note that D_{yy} presented in Figure 7.15 were averaged with respect to the last three values obtained in Figures 7.5 and 7.7. This procedure is frequently used to determine the diffusion coefficient. However, in our study the diffusion coefficient was not always completely constant at t = 0.4s so that we have decided to call it radial dispersion coefficient in accordance with other previous studies (Goldsmith 1971, Goldsmith and Marlow 1979, Goldsmith and Turitto 1986).

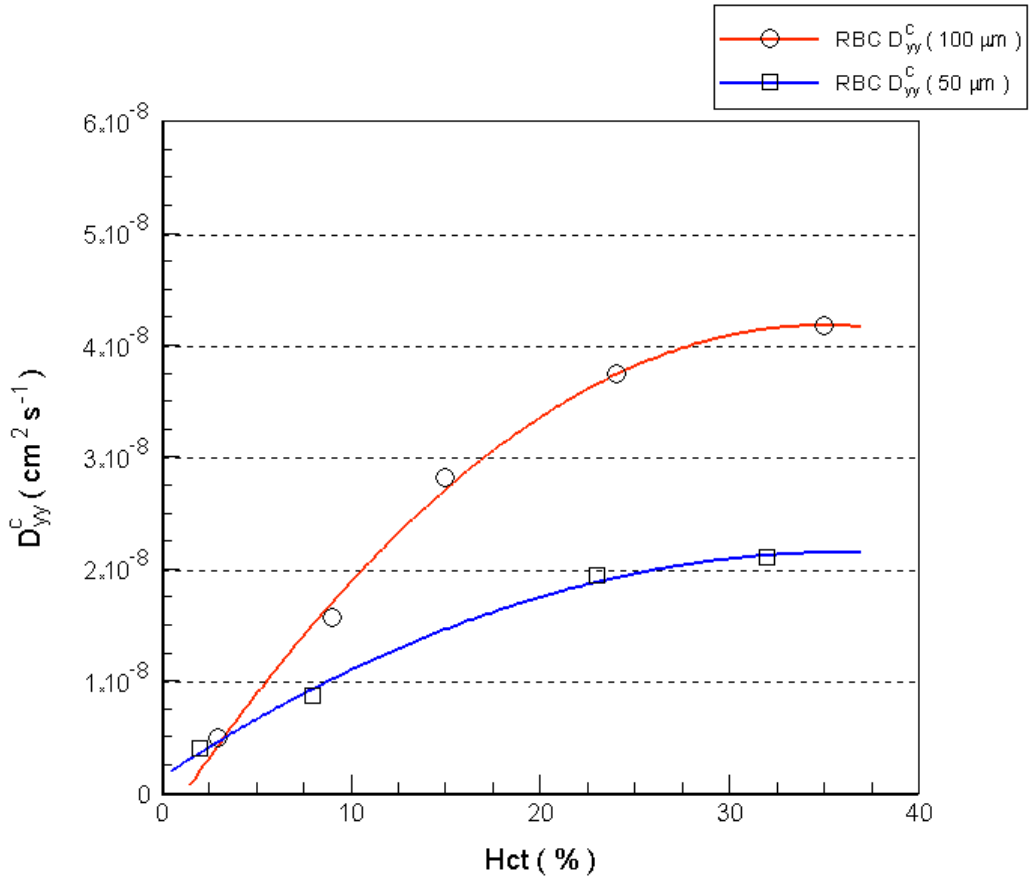

Figure 7.15 Effect of the Hct on the RBC D^c_{yy} at 100µm and 50µm glass capillary.

It is qualitatively evident that the RBC radial dispersion rises with the Hct but then at Hct around 25% it tends to levels off. These results suggest that the plasma layer plays an important role on the increase of RBCs transverse motion. Direct qualitative measurements at Hcts higher than 30% have shown almost no plasma layer. Moreover, previous results preformed by Goldsimth and coworkers (Goldsmith 1971, Goldsmith and Karino 1977, Goldsmith and Marlow 1979, Goldsmith and Turitto 1986) have observed that at Hcts bigger than 50% the radial displacements tend to decrease as extremely high concentration of ghost cells limit the amplitude of the RBCs radial movements. In accordance with these consistent results, the development of a plasma layer at Hcts lower than 30% and also the decrease of the local cell density surrounding the RBCs may be the main causes of the enhanced radial dispersion of the cells.

Effect of the microtube geometry on the RBC radial dispersion

Since the finding of the Faharaeus-Lindqvist effect (Faharaeus and Lindqvist 1931), many investigators have attempted to understand the main causes for the decrease of the apparent

viscosity as the diameter of microtube decreases (Chien 1970, Gaehtgens 1980, Chien et al. 1984, Goldsmith and Turitto 1986, Reike et al. 1987, Pries et al. 1992). The present work provides quantitative data of the effect of the microtube diameter on the RBC radial dispersion (see Figure 7.15 and Figure 7.16). The results form Figure 7.16 clearly demonstrate that RBC radial dispersion tend to decrease with the diameter. Obviously, the main reason is due to Hct reduction with the diameter (Faharaeus effect). However, we believe that the geometry constriction also limits the amplitude of the RBCs radial displacements, which leads to an attenuation of the RBC transverse motion. The present data seems to indicate that the reduction of RBC radial dispersion and hence the continuous multibody collisions may be linked to the decrease in apparent viscosity described by previous authors (Faharaeus and Lindqvist 1931, Reike et al. 1987, Pries et al. 1992).

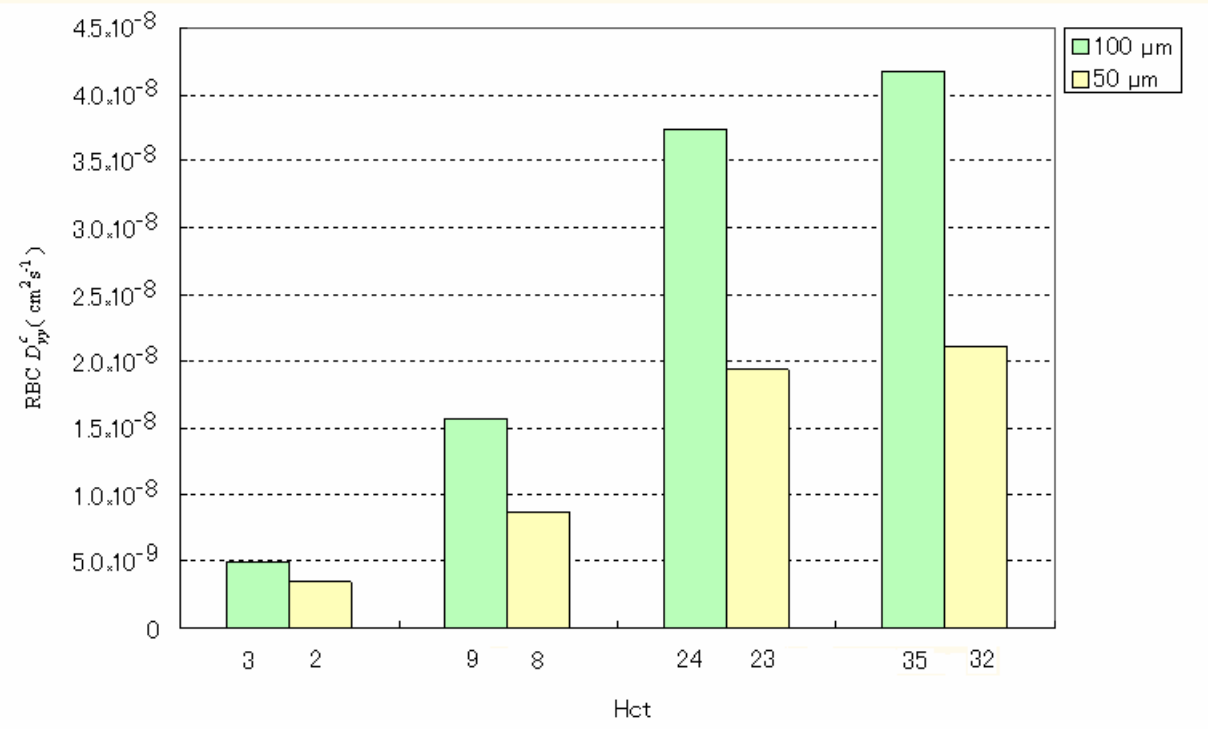

Figure 7.16 Effect of the microtube geometry on the RBC D_{yy}^{c} .

The RBC radial dispersion (D_{yy}) is also influenced by the radial position and correspondent shear rate. Generally, our results for moderate and higher Hct indicate that D_{yy}^{c} is the greatest at radial positions between 0.4R to 0.8R, whereas at locations adjacent to wall (0.8R to 1R) and around the middle of the capillary (0R to 0.2R), the paths of the tracer RBCs tend to exhibit lower erratic displacements normal to the direction of the flow. As already mentioned, the plasma layer seems to enhance continuous erratic radial displacements, which leads to an increase of multibody interactions. In contrast, the paths of the RBCs traveling in apparent contact with the wall had the lowest radial dispersion. Visual observations as well

measurements on the radial displacement had shown that even interactions with neighboring RBCs with higher velocities did not cause significant increase on radial displacement of the RBCs rolling on the wall surface of the microchannel. The reason for this phenomenon is not completely understood, however, the electrostatic attractive force and also the lubrification force between the RBC and the wall may play an important role in its flow behavior. Generally, our results reinforce early observations by Goldsmith and his colleagues (Goldsmith and Marlow 1979, Goldsmith and Turitto 1986), who reported that the radial displacements are greatest at radial distances between 0.5R and 0.8R.

Microhemodynamcis of RBCs

The unique ability of our confocal system to generate thin in-focus planes allows us to obtain detailed information not only on the RBC radial displacement but also on RBC-RBC interaction. Hence, the confocal system can provide the paths of two or more blood cells interacting in the same focal plane, a task not possible by using a conventional microscope. The present study provides for the first time both quantitative and qualitative evidence on RBC-RBC hydrodynamic interaction in concentrated suspensions. A representative example of two labeled RBCs interacting within the plasma layer is shown in Figure 7.13. For this case, we have observed that the amplitude of the RBC radial displacement have deviated around 1 to 2 times of its initial path. Generally, when there is a RBC interaction the radial displacement tends to increase to a maximum peak and then returning to its initial position. However, for moderate and high Hc,t the RBCs are subjected to continuous erratic radial displacements due to multibody collisions. The enhanced radial dispersion of the RBCs within the plasma layer leads to an increase on the collision frequency between the RBC and wall. We have observed that at diluted suspensions (Hct ~ 3%) there were no collisions with the microtube wall as they tend to migrate toward the axis. As the Hct increases the collision rates with wall tends also to increase. The fluctuations of the RBCs trajectories within the plasma layer and the consequent increase of the collisions rate with the vessel wall are believed to be an essential contributor to the thrombogenesis process (Munn et al. 1996, Miayazaki and Yamaguchi 2003).

Comparison with previous studies

To our knowledge, the past work that has provided most insights to the RBCs flow behavior in glass capillaries was carried out by Goldsmith and his coworkers (Goldsmith 1971a,

Goldsmith 1971b, Goldsmith and Karino 1977, Goldsmith and Marlow 1979, Goldsmith and Turitto 1986, Cokelet and Goldsmith 1990). Although there is an appreciable difference between the measuring techniques, qualitatively our results are consistent with the results performed by Goldsimth et al.. Figures 7.17 and 7.18 show that some of our findings correspond to that observed by previous researchers. However, it is also clear that the magnitudes of radial dispersion presented here are generally lower than the data obtained by Goldsmith el al..

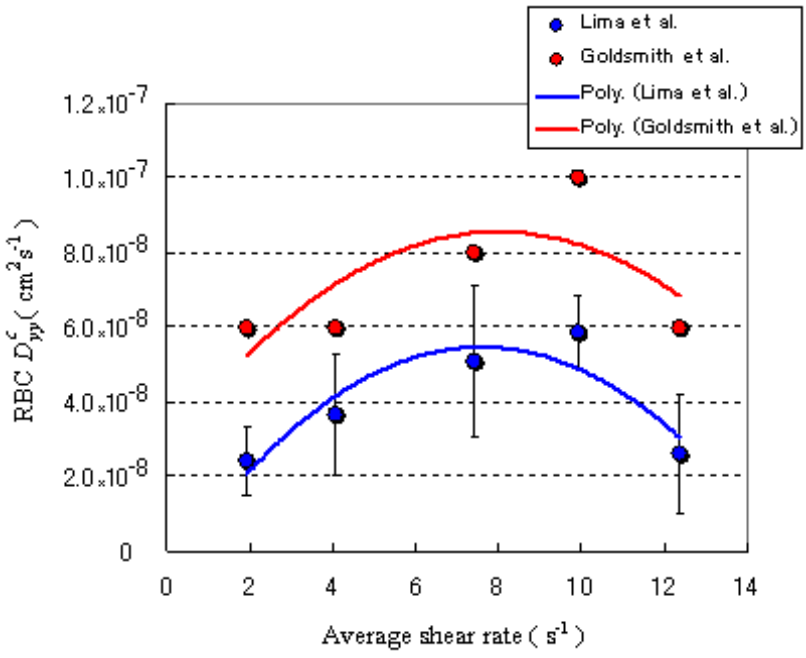

Figure 7.17 RBC D^c_{yy} as a function of the average shear rate ($\bar{\gamma}$). Our results were obtained with 35% Htc at a 100μm capillary whereas Golsmith et al. results were obtained with 40% Hct .

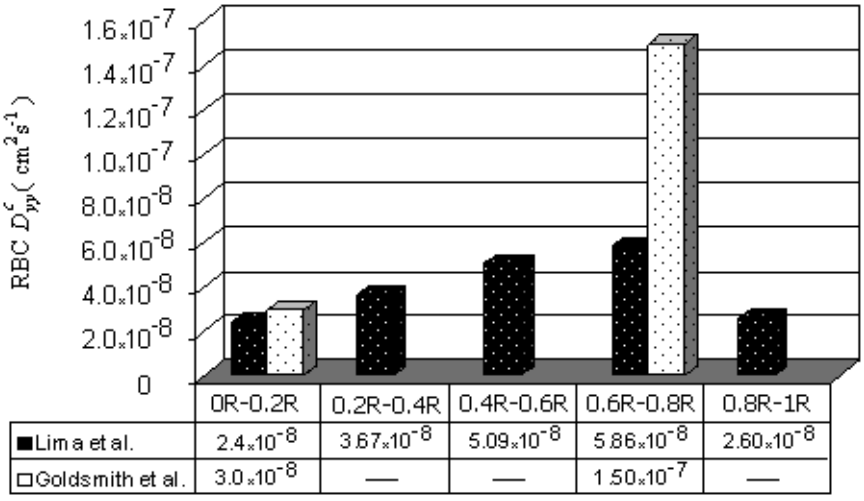

Figure 7.18 Comparison between the present results (35%Hct, 100 μm capillary) and data obtained by Golsmith et al. (39%Hct, 76.5 μm capillary) (Goldsmith 1971). (b) RBC D^c_{yy} as a function of the capillary depth.

As previously mentioned, Goldsmith and his coworkers have used ghost cells as models of erythrocytes in order to measure the RBCs motions at concentrated suspensions. According to Nash and Meiselman (1983), the preparation procedure of the ghost cells and also the removal of the hemoglobin (Hb) may contribute to the changes in the membrane mechanical properties of the ghost RBCs. According to their findings, ghost cells were faster to recover to its original cell shape when compared with normal RBCs. The ability of the ghost cells to deform more easily than normal cells may affect the RBCs dynamic behavior in shear flow. This phenomenon may be responsible for the higher RBC radial dispersion values obtained by Goldsmith et al..

Another possible cause for higher displacements may be due to the optical measuring technique used by Goldsmith et al.. It is well known that conventional microscopes detect cells in both in-focus and out-of-focus planes. As a result, by using a conventional microscope, they have measured not only the RBCs in the centre plane (in-focus plane) but also RBCs flowing in the neighboring planes (out-of-focus plane). As it is demonstrated in Figure 7.19, the radial dispersion increases by moving away from the centre plane. Thus, the out-of-focus RBCs may also have contributed to the higher radial dispersion values.

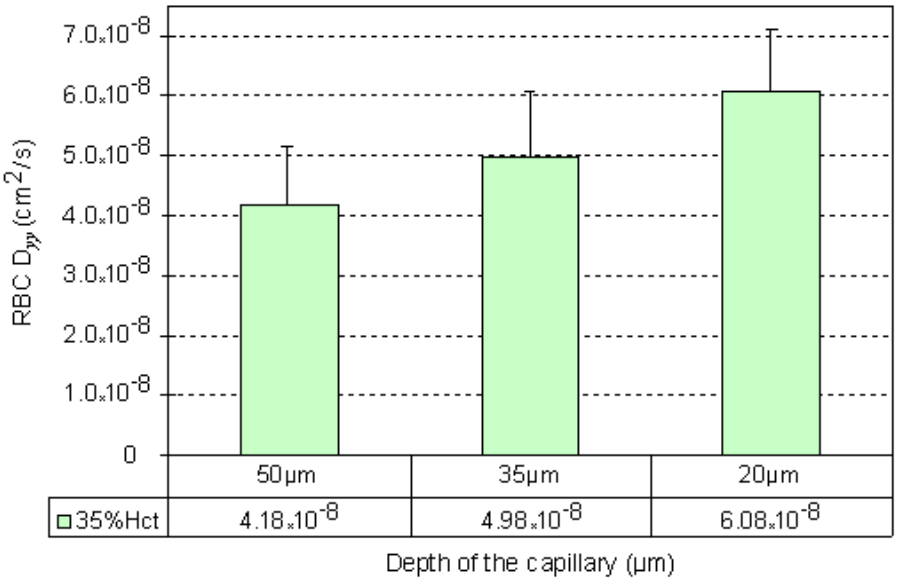

Figure 7.19 RBC D_{yy} as a function of the capillary depth.

7.5 Conclusions

Direct and quantitative detailed description of the flow behavior of labeled RBCs in both diluted and concentrated suspensions were studied under a confocal micro-PTV system. The experiments were performed in the middle plane of 50μm and 100 μm glass capillaries at low Reynolds numbers (Re from 0.003 to 0.005) by using Hcts from 2% to 35%. Several microscale phenomena of the RBCs flow behavior, such as RBC-RBC interaction and RBC tendency for radial migration, were analysed by using the RBCs radial dispersion coefficient (D_{yy}) approach. Hence, the present study examines the effect of the haematocrit (Hct) and microtube geometry on RBCs D_{yy}. Our results demonstrate that D_{yy} tends to increase with the Hct, however, at Hct of about 25% it tends to level off. These findings, which corroborates with past results, suggest that the development of the plasma layer and consequent decrease of the local cell density surrounding the RBCs may enhance the radial dispersion of RBCs. Generally, our results for moderate and higher Hct indicate that $D_{yy,}$ is the greatest at radial positions between 0.4R to 0.8R, whereas the paths of the tracer RBCs tend to exhibit lower radial displacements at locations adjacent to wall (0.8R to 1R) and around the middle of the capillary (0R to 0.2R). Although there is evidence that latter phenomenon is mainly due to the low shear rate and high RBCs concentrations in the centre of the microtube, the former phenomenon is still not completely understood. Our results on RBC-RBC interactions suggest that at regions near the wall the motions of RBCs are dominated not only by hydrodynamic forces but also by other additional forces such as electrostatic attractive forces and lubrification forces developed at the wall boundary layer.

The present work also demonstrates that D_{yy} tends to decrease with the diameter. This phenomenon is believed to be due to Hct reduction with the diameter (Faharaeus effect) and also to the geometry constrictions which naturally limit the amplitude of the RBCs radial displacements. Hence, this finding seems to indicate that the reduction of RBC radial dispersion and the continuous multibody collisions may be linked to the decrease in apparent viscosity with decreasing diameter (Faharaeus-Lindqvist effect).

The confocal micro-PTV system used in the present work proves to be a powerful technique to obtain detailed measurements on several micro-scale phenomena of the RBCs flow behavior, such as RBC-RBC interaction and RBC tendency for radial migration. This confocal system eliminates the problems and concerns of the methods used in the past and

provides additional detailed description on the RBC motion not obtainable by other conventional methods. It might therefore be interesting for future research to investage the blood mass transport mechanisms in detail under both physiological and pathological conditions.

CHAPTER 8

CONCLUSIONS AND FUTURE DIRECTIONS

This chapter summarizes the work presented in this thesis and suggests directions for further research work.

8.1 Conclusions of the thesis

The recent advances in computers, digital image processing techniques, and confocal microscopy have made it possible to combine both particle image velocimetry (PIV) and particle tracking velocimetry (PTV) system with a spinning disk confocal microscope (SDCM). In this thesis, a confocal micro-PIV/PTV system was used, for the first time, to investigate *in vitro* blood flow through microchannels.

This thesis is divided into two main parts. In the first part, which comprises Chapter 3, 4 and 5, a PIV cross-correlation technique was used to obtain the velocity profiles of the *in vitro* blood. In the second part of this thesis (Chapter 6 and 7), a low-image-density PIV technique, often known as particle tracking velocimetry (PTV) or as single particle tracking (SPT), was employed to study the microheamodynamics behavior of labeled RBCs in concentrated suspensions of normal RBCs. The summary and main conclusions of this dissertation are presented below.

In Chapter 3, validation studies were performed to evaluate the performance of a confocal micro-PIV system to measure both pure water and dilute suspensions of RBCs (~ 4% Hct) through a 100 μm square microchannel in several horizontal planes. Good agreement between the measured velocity profiles of pure water and an established analytical solution was obtained for steady flow in a long, straight square microchannel. Moreover, the measurements of a physiological fluid containing 4% suspended RBCs demonstrated the ability of this system to obtain confocal images using only the fluorescent particles within the plasma, while the RBCs were not detected due to their different emission wavelength. Although we clearly observed small fluctuations in the instantaneous velocities fields by comparing pure water

with a 4% RBCs suspension, when the ensemble-averaged velocities were compared, the local disturbance effect caused by the blood cells was not large enough to create major fluctuations on the blood plasma velocity profiles. These results suggest that instantaneous velocities may give additional information on the blood flow behavior at a microscale level. Furthermore, we have also demonstrated the ability of the confocal micro-PIV to generate 3D velocity profiles of a blood cell suspension fluid. Experimental 3D profiles of *in vitro* blood flow had not been previously reported.

The results of Chapter 3 inspired the study presented in Chapter 4. In this Chapter, we determined both ensemble and instantaneous velocity profiles for *in vitro* blood (haematocrit up to 17%) flowing through a 100-μm square microchannel. All the measurements were made in the middle plane of the microchannel at a constant flow rate and low Reynolds number (Re = 0.025). Although the ensemble velocity profiles were markedly parabolic, some fluctuations in the instantaneous velocity profiles were found to be closely related to the increase in the haematocrit. This study demonstrated for the first time that the RMS values increase with the haematocrit implying that the presence of RBCs within the plasma flow strongly influences the measurements of the instantaneous velocity fields. The possible reasons for the RMS increase are the motion and interaction of RBCs and the light scattered and absorbed from the RBCs. This latter cause seems to be more predominant at Hct = 17%. As a result, for 17% Hct improvements on the Signal-to-Noise Ratio are required to further enhance the measurement performance of the instantaneous velocities.

In the previous Chapters (Chapter 3 and 4), we demonstrated the ability of the confocal micro-PIV to measure *in vitro* blood in glass microchannels. Along the years, it was demonstrated that many microcirculation phenomena in living microvessels qualitatively agree with those investigated in glass microchannels. However, it is also evident that this classical microchannels differ from microvessels in several ways, such as elasticity of the wall, and the fact that the flow channel is always straight and long and the inner surface of the microchannel does not accommodate living endothelial cells. Hence, the results from classical *in vitro* experiments that have used rigid straight glass microchannels need to be carefully reexaminated by using more sophisticated microchannels. Therefore, in Chapter 5 we investigated the ability of our confocal micro-PIV system to measure the velocity profiles of both physiological saline (PS) and *in vitro* blood (20% Hct) in a rectangular (300 μm wide, 45 μm deep) polydimethysiloxane (PDMS) microchannel, which was fabricated by soft

lithography. Generally, the velocity profiles were found to be markedly blunt in the central region, mainly due to the low aspect ratio (h/w = 0.15) of the rectangular microchannel. Predictions using a theoretical model for the rectangular microchannel corresponded quite well with the experimental micro-PIV results for the PS fluid. However, for the *in vitro* blood with 20% haematocrit, small fluctuations were found in the ensemble velocity profiles. The reasons for the encountered "microturbulences" are not entirely clear, but our qualitative observations indicate that interactions between neighbouring RBCs, the high shear rate generated in the vicinity of the walls, and temporal fluctuations in the haematocrit may play important roles in the hydrodynamic disturbance effects encountered in the blood velocity profiles. In addition, the present study also demonstrated that confocal micro-PIV can be effectively integrated with a PDMS microchannel and used to obtain blood velocity profiles along the full depth of the microchannel because of its unique 3-D optical sectioning ability.

In Chapter 4, we showed that the confocal micro-PIV system is able to measure with good accuracy blood plasma with Hct up to 9%, in a 100-μm square microchannel. Unfortunately, for Hct bigger than 9%, the light absorbed by the RBCs contributes to diminish the concentration of tracer particles in the acquired confocal images. This low density images become more evident for Hct bigger than 20 %, which generates spurious errors in the velocity fields. For this reason, in Chapter 6, a Langragian approach was implemented to the confocal system in order to track individual tracer cells at high concentration suspensions of RBCs. Hence, in Chapter 6 a confocal micro-PTV system was employed, for the first time, in an effort to obtain detailed quantitative measurements on the motion of blood cells at both diluted and high suspensions of RBCs. We have successfully labeled both RBCs and WBCs and we have measured their motions through a 100 μm glass capillary. The ability of the confocal system to generate thin in-focus planes has allowed both qualitative and quantitative measurements in flowing blood at concentrated suspensions (up to 35% Hct) of: cell-cell hydrodynamic interaction, RBC orientation and RBC radial dispersion at different depths. Detailed measurements on the flow properties of individual RBCs in concentrated suspension of normal RBCs had not been previously reported. Such information is extremely important to elucidate the blood transport mechanisms and associated diseases such as thrombosis and atherosclerosis. We believed that the proposed confocal micro-PTV system will provide a powerful tool to obtain further insight onto the complex flow behavior of blood in microcirculation.

The comparison of the results between Chapter 4 and Chapter 6 showed that the *in vitro* blood using Dextran 40 and fluorescent labeled RBCs exhibited more similar flow characteristics encountered *in vivo* microvessels than the *in vitro* blood using physiological saline and fluorescent tracer particles (Chapters 3 to 5). These qualitative observations imply that the *in vitro* blood used in Chapter 6 and 7 represent a more adequate model to study the flow behavior of RBCs through microchannels.

The final application presented in this thesis is based on the findings presented in Chapter 6. Hence, in Chapter 7 detailed description of the flow behavior of labeled RBCs in both diluted and concentrated suspensions (Hcts up to 35%) were studied under a confocal micro-PTV system. In this study the RBCs radial dispersion coefficient (D_{yy}) was calculated in the middle plane of a 50μm and 100 μm glass capillaries at low Reynolds numbers (Re from 0.003 to 0.005). The results demonstrated that RBCs D_{yy} tends to increase with the Hct but at Hct of about 24% it tends to level off. This finding suggests that at moderate Hcts the development of the plasma layer and consequent decrease of the local cell density surrounding the RBCs may enhance the radial dispersion of RBCs. In addition, we have also reported that D_{yy} is greatest at radial positions between 0.4R to 0.8R, whereas at locations adjacent to wall (0.8R to 1R) and around the middle of the capillary (0R to 0.2R) the paths of the tracer RBCs tend to exhibit lower radial displacements. The results obtained on RBC-RBC interactions suggest that at regions near the wall the motions of RBCs are dominated not only by hydrodynamic forces but also by other additional forces such as electrostatic attractive forces and lubrification forces which may be the dominant cause for the low D_{yy} encountered near the wall. In addition, in Chapter 7 we have also demonstrated that RBCs D_{yy} tends to decrease with the diameter. This phenomenon is believed to be due to Hct reduction with the diameter (Faharaeus effect) and also to geometry constrictions which limit the amplitude of the RBCs radial displacements. Hence, this finding seems to indicate that the reduction of RBC radial dispersion and hence the continuous multibody collisions may be linked to the decrease in apparent viscosity with decreasing diameter (Faharaeus-Lindqvist effect).

One of the key conclusions drawn from this thesis is that confocal systems that comprise a spinning disk confocal microscope (CSU-22) prove to be the most suitable technique to obtain detailed measurements on blood flow behavior through microchannels. The presented research demonstrated for the first time that confocal systems eliminate the problems and

concerns of the experimental techniques used in the past and provide additional detailed description on the RBC motion not obtainable by other conventional methods. For example, this study has demonstrated the ability of confocal systems not only to generate 3D velocity profiles of *in vitro* blood flow but also to obtain valuable additional information from the instantaneous velocities profiles often ignored by the micro-PIV research community. In addition, this work also represents the first experimental work able to quantify several microscopic phenomena in concentrate suspension of normal RBCs. Hence, we have demonstrated that the RBC dispersion coefficient is strongly dependent on the Hct. In closing, this thesis provides the basis not only to obtain further insights on the blood mass transport mechanisms under both physiological and pathological conditions but also to improve the existing theories, models, and computer simulations on the blood flow at both micro and macroscale levels.

8.2 Suggestions for further research

The research carried out in this thesis provides the basis for further research into several scientific challenges in the biomedical field. A few of the many possible research topics currently under way and to be addressed in the near future are:

1. **Effect of complex geometries** – In Chapter 5 we have successfully measured the blood flow through a straight rectangular PDMS microchannel. However, the *in vivo* microvascular networks are composed by short vessel segments with several branches and asymmetrical structures. The heterogeneity of the microvascular network may strongly influence the flow behavior of blood cells in microcirculation. A study into the mechanics of blood flow in both bifurcations and irregular geometries is currently under way.

2. **Circular PDMS microchannel** – The soft lithography technique has the ability to generate extremely precise, reproducible and versatile rectangular PDMS microchannels. Although, by using this technique, it is possible to mimic complex geometries similar to human blood arterioles and capillary networks, blood flow behavior through this kind of microchannels may exhibit different features characteristic with those investigated in living microvessels. Hence, it is imperative to develop a circular PDMS microchannel able to mimic *in vivo* environment. In Appendix C we present a simple method to manufacture circular PDMS

microchannels. By using these microchannels, we expect to culture living cells on their surfaces and consequently to provide experimental evidence on several microcirculation mysteries, such as the role of the glycocalyx on the flow behavior of blood.

3. **Comparison with computational methods** – Computational modeling is a powerful way to obtain detailed information on the mechanical behaviors of multiple RBCs. Recently, several numerical methods have been proposed to analyze microscale blood flows in microvessels (Yamaguchi et al. 2006). Some successful examples are the particle method (Tsubota et al. 2006) and the elastic RBC flow model (Wada and Kobayashi 2002, Tsubota et al. 2006c). We expect in the near future to compare the reported experimental results with the numerical methods mentioned above. This collaborative process between experimental and computational methods will contribute not only to improve the modeling of cell behavior but also to provide better understanding on several microcirculation phenomena.

4. **Hybrid 3D method** – In Chapter 3 and 5, we showed the ability of the confocal system to generate velocity fields at several xy planes along the microchannel depth (z axis). However, currently it is still not possible to measure the velocity of the tracer particles along the z direction. Hence, by integrating the experimental data from the confocal system with a numerical model based on the continuity equation, a fully three-dimensional (3D) velocity profile may be possible to be generated.

5. **Automatic tracking method** – Another area for further research is the improvement of the current automatic particle tracking methods. In this thesis a manual tracking method was used due to the inability of the automatic methods to track RBCs when they experienced collisions. Hence, a more reliable automatic tracking method needs to be developed to reduce the time-consuming and also to avoid the tedious work performed during the post-processing procedure.

6. **New CSU** – A novel design to improve the Nipkow disk scanning rate and also the losses of incident illumination need to be addressed. This new design will provide the possibility to study the blood behavior at higher velocity ranges.

7. ***In vivo* studies** – To apply the confocal system to study the flow behavior of RBCs in living microvessels is one of the biggest challenges in this field. We believe that present confocal system may be successfully applied to investigate the blood flow in capillaries. At these microvessels the Hct is usually less than 10% and the Re is often less than 0.01, which are within the same range of values used in this thesis.

FULL LIST OF PUBLICATIONS AND PROTOCOLS

Refereed journals

Lima, R., Wada, S., Tsubota, K., and Yamaguchi, T., 2006. Confocal micro-PIV measurements of three dimensional profiles of cell suspension flow in a square microchannel. Measurement Science and Technology 17, 797-808.

Lima, R., Wada, S., Takeda, M., Tsubota, K., and Yamaguchi, T., 2007. *In vitro* confocal micro-PIV measurements of blood flow in a square microchannel: the effect of the haematocrit on instantaneous velocity profiles. Journal of Biomechanics 40, 2752-2757.

Lima, R., Wada, S., Tanaka, S., Takeda, M., Ishikawa T., Tsubota, K., Imai, Y., and Yamaguchi, T., 2008. *In vitro* blood flow in a rectangular PDMS microchannel: experimental observations using a confocal micro-PIV system. Biomedical Microdevices, (in press).

Lima, R., Ishikawa, T., Imai, Y., Takeda, M., Wada, S., and Yamaguchi, T., Measurements of individual red blood cell motions under high hematocrit conditions using a confocal micro-PTV system. (submitted to Annals of Biomedical Engineering).

Lima, R., Ishikawa, T., Takeda, M., Imai, Y., Tsubota, K., Wada, S., and Yamaguchi, T., 2008. Radial dispersion of red blood cells in blood flowing through glass capillaries: role of heamatocrit and geometry, Journal of Biomechanics, (in press).

International conferences

Lima, R., Wada, S., Tsubota, K., and Yamaguchi, T., 2005. Analysis of velocity profiles of blood flow in microchannels using confocal micro-PIV and particle method, In: Proceedings of the II International Conference on Computational Bioengineering, IST, Portugal.

Lima, R., Wada, S., Tsubota, K., and Yamaguchi, T., 2005. Confocal micro-PIV velocity measurements of physiological fluids in a Rectangular microchannel, In: Proceedings (CD ROM) of the 3rd IASTED International Conference on Biomechanics - BioMech 2005, Spain.

Lima, R., Wada, S., Tsubota, K., and Yamaguchi, T., 2005. Velocity measurements of physiological flows in microchannels using a confocal micro-PIV System, In: Proceedings of the 16th JSME Conference on Frontiers in Bioengineering, Kusatsu Japan.

Lima, R., Wada, S., Takeda, M., Tsubota, K., and Yamaguchi, T., 2006. Confocal micro-PIV measurements of blood flow in microchannels, In: 5th World Congress of Biomechanics, Munich, Germany.

Lima, R., Wada, S., Tanaka, S., Takeda, M., Tsubota, K., Ishikawa, T., and Yamaguchi, T., 2006. Velocity measurements of blood flow in a rectangular PDMS microchannel assessed by confocal micro-PIV system. In: Proceedings of the World Congress on Medical Physics and Biomedical Engineering. Seoul, pp. 278-281.

Lima, R., Ishikawa, T., Takeda, M., Tanaka, S., Imai, Y., Tsubota, K., Wada, S., and Yamaguchi, T., 2007. Tracking Red blood cells in a circular PDMS Microchannel using a Confocal micro-PIV System, In: International Symposium of Future Medical Engineering based on Bio-nanotechnology, Sendai, Japan.

Lima, R., Ishikawa, T., Takeda, M., Tanaka, S., Imai, Y., Tsubota, K., Wada, S., and Yamaguchi, T., Measurement of erythrocyte motions in microchannels by using a confocal micro-PTV, (accepted as an oral presentation at ASME 2007 Summer Bioengineering Conference, Colorado, USA)

Lima, R., Ishikawa, T., Fujiwara, H., Takeda, M., Imai, Y., Tsubota, K., Wada, S., and Yamaguchi, T., Blood cell motions and interactions in microchannels, (accepted as an oral presentation at the Annual meeting of the Visualization Society of Japan, Tokyo, Japan)

Lima, R., Nakamura, M., Ishikawa, T., Tanaka, S., Takeda, M, Imai, Y., Tsubota, K., Wada, S., and Yamaguchi, T., Microscale flow dynamics of red blood cells in a circular microchannel, (accepted as an oral presentation at ECCOMAS Thematic Conference on Computational Vision and Medical Image Processing, Porto, Portugal).

Lima, R., Ishikawa, T., Fujiwara, H., Takeda, M., Imai, Y., Tsubota, K., Matsuki, N., Wada, S., and Yamaguchi, T., Measurement of multi-red blood cells interactions in blood flow by confocal micro-PTV, (submitted to the Third Asian Pacific Conference on Biomechanics, Tokyo, Japan)

Books, domestic conferences and papers as a co-author

Lima, R., Kitagawa, Y., Kamada, H., Tsubota, K., Wada, S., and Yamaguchi, T., 2005. A particle method (MPS) computer simulation: applications to the study of blood flow, In: Encontro 1 Biomecanica, Abrantes, Portugal.

Tsubota, K., Wada, S., Kamada, H., Kitagawa, Y., **Lima, R.,** and Yamaguchi, T., 2006, A particle method for blood flow simulation: application to flowing red blood cells and platelets, Journal of the Earth Simulator 5, 2-7.

Lima, R., Ishikawa, T., Tanaka, S., Takeda, M., Tsubota, K., Wada, S., and Yamaguchi, T., 2007. Velocity fields of blood flow in microchannels using a confocal micro-PIV system, In: Esashi, M., Ishi, K., Ohuchi, N., Osumi, N., Sato, M. and Yamaguchi, T. (Eds), Future Medical Engineering based on Bio-nanotechnology, ICP, 973-980.

Fujiwara, H., Ishikawa, T., **Lima, R.,** Takeda, M., Kaji, H., Matsuki, N., Nishizawa, M., and Yamaguchi, T., Observation of blood flow in a microchannel with stenosis by confocal micro-PIV, (submitted to the Third Asian Pacific Conference on Biomechanics, Tokyo, Japan)

Protocols

During the present research the following protocols were developed:

- label blood cells by using a lipophilic carbocyanime derivative, chloromethylbenzamido (see Chapter 6);
- fabrication of circular PDMS microchannels by using a wire casting technique (see Appendix C).

REFERENCES

Abkarian M., Magalie Faivre M., Stone H., 2006. High-speed microfluidic differential manometer for cellular-scale hydrodynamics. PNAS 103 (3), 538-542.

Abramoff, M., Magelhaes, P., Ram, S., 2004. Image Processing with Image J, Biophotonics International 11 (7), 36-42.

Adrian, R., 1991. Particle-imaging techniques for experimental fluid mechanics. Annu. Rev. Fluid Mech. 23, 261-304.

Alonso, C., Pries, A., Kiesslich, O, Lerche D., Gaehtgens, P., 1995. Transient rheological behaviour of blood in low-shear tube flow: velocity profiles and effective viscosity. Am. J. Physiol. 268, H25-H32 .

Amos, W., White, J., 2003 How the confocal laser scanning microscope entered biological research Biology of the ceel 95, 335-342.

Baker M., Wayland H., 1974. On-line volume flow rate and velocity profile measurement for blood in microvessels. Microvascular Research 7 131-143

Bates, C., O`Doherty, D., Williams, D., 2001. Flow instabilities in a graft anstomosis: a study of instantaneous velocity fields. Proc. Instn. Mech. Engrs. Part H 215, 579-587.

Beebe, D, Mensing, G., Walker, G., 2002. Physics and applications of microfluidics in biology. Annu. Rev. Biomed. Eng. 4, 261-286.

Bitbol, M., 1986. Red blood cell orientation in orbit C = 0. Biophysical Journal 49, 1055-1068.

Bitsch, L. Olesen, C. Westergaard, H. Bruus, H. Klank, J. Kutter, 2005. Micro particle-image velocimetry of bead suspensions and blood flows. Experiments in Fluids 39, 505-511.

Borenstein J., Terai H., King, K., Weinberg E., Kaazempur-Mofrad M., Vacanti J., 2002. Microfabrication Technology for Vascular Tissue Engineering. Biomedical Microdevices 4 (3), 167-175.

Born G., Melling A., Whitelaw J., 1978. Laser Doppler microscope for blood velocity measurement. Biorheology 15, 163-172

Bourdon, C., Olsen, M., Gorby, A., 2004. Power-filter technique for modifying depth of correlation in microPIV experiments. Experiments in Fluids 37, 263–271.

Brown, D., Larson, R., 2001. Improvements to parallel plate flow chambers to reduce reagent and cellular requirements, BMC Immunology, 2-9.

Brown, T., 2000. Techniques for mechanical stimulation of cells in vitro: a review. Journal of Biomechanics 33, 3-14.

Bruus, H., 2004. Theoritical microfluidics. Lecture notes, MIC Department of Micro and Nanotechnology Technical, University of Denmark, Denmark.

Bugliarello G., Hayden J., 1963. Detailed characteristics of the flow of blood *in vitro*. Trans. Soc. Rheol. 7, 209-230.

Burton, A., 1966. Physiology and Biophysics of the circulation, Year Book Medical Publishers.

Caro, C., Pedley, T., Schroter, R., Seed W., 1978. The mechanics of the circulation, Oxford University Press.

Chang, W., Akin, D., Sedlak, M., Ladisch, M., Bashir, R., 2003. Poly(dimethylsiloxane) (PDMS) and silicon hybrid biochip for bacterial culture. Biomedical Microdevices 5 (4), 281-290.

Chien, S., 1970. Shear dependence of effective cell volume as a determinant of blood viscosity. Science 168, 977-979.

Chien, S., Usami, S., Skalak, R., 1984. Blood flow in small tubes In: Handbook of Physiology – The cardiovascular system IV, 217-249.

Chiu J., Chen C., Lee P., Yang C., Chuang H., Chien S., Usami S., 2003. Analysis of the effect of distributed flow on monocytic adhesion to endothelial cells. Journal of Biomechanics 36, 1883-1895.

Cochrane T., Earnshaw J., Love A., 1981. Laser Doppler measurement of blood velocity in microvessels. Med. & Biol. Eng. & Comput. 19 589-596

Cokelet, G., Goldsmith H., 1990. Decreased hydrodynamic resistance in the two-phase flow of blood through small vertical tubes at low flow rates. Circulation Research 68 (1), 1-17.

Conchello J., Lichtman, J., 2005. Optical sectioning microscopy. Nature Methods 2, 920 - 931

Devasenathipathy S., Santiago J., Wereley S., Meinhart C., Takehara K., 2003. Particle imaging techniques for microfabricated fluidic systems. Experiments in Fluids 34, 504-514.

Duffy C., McDonald J., Schueller O., Whitesides G., 1998. Rapid prototyping of microfluidic systems in poly(dimethylsiloxane). Anal. Chem. 70, 4974-4984.

Dzwinel, W., Boryczko K., Yuen D., 2003. A discrete-particle model of blood dynamics in capillary vessels. J Colloid Interface Sci. 258(1), 163-173.

Einav S., Berman R., Fuhro P., DiGiovanni P., Fine S., Fridman J., 1975. Measurement of velocity profiles of red blood cells in the microcirculation by laser Doppler anemometry (LDA). Biorheology 12, 207-210.

Fahraeus, R., Lindqvist, T., 1931. The viscosity of the blood in narrow capillary tubes. Am. J. Physiol. 96, 562-568.

Faivre, M., Abkarian, M., Bickraj, K., Stone, H., 2006. Geometrical focusing of cells in a microfluidic device: an approach to separate blood plasma. Biorheology 43 147-159.

Fischer T., Stohr-Lissen M, Schmid-Schonbein, H., 1978. The red cell as a fluid droplet: tank tread-like motion of the human erythrocyte membrane in shear flow. Science 202, 894-896.

Fujii, T., 2002. PDMS-based microfluidic devices for biomedical applications, Microelectronic Engineering 61-62, 907-914.

Fujiwara, H., 2007. Interaction of two red blood cells in a circular microchannel. Graduation Report, PFSL, Department of Bioengineering and Robotics, Tohoku University, Japan (in Japanese).

Fung ,Y., 1993. Biomechanics – Mechanical properties of living tissues. second edition, Springer-Verlag,, New York.

Fung, Y., 1997. Biomechanics – Circulation.. second edition, Springer-Verlag, New York.

Gaehtgens P., 1980. Flow of blood through narrow capillaries; rheological mechanisms determining capillary hematocrit and apparent viscosity, Biorheology 17, 183-189.

Gaehtgens P., 1987. Tube flow of human blood at near zero shear. Biorheology 24, 367-376.

Gaehtgens P., Meiselman H., Wayland H., 1970. Velocity profiles of human blood at normal and reduced hematocrit in glass tubes up to 130 μ diameter. Microvascular Research 2 13-23

Giddens D., Zarins C., Glagov S., 1993. The role of fluid mechanics in the localization and detection of atherosclerosis. Journal of Biomechanical Engineering 115, 588–594.

Gifford S, Frank M, Derganc J, Gabel C, Austin R, Yoshida T., Bitensky W, 2003. Parallel microchannel-based measurements of individual erythrocyte areas and volumes. Biophysical Journal 84, 623-633.

Goldsmith H., 1971a. Red cell motions and wall interactions in tube flow, Federation Proceedings 30 (5), 1578-1588.

Goldsmith H., 1971b. Deformation of human red cells in tube flow, Biorheology 7, 235-242.

Goldsmith H., Karino T., 1977. Microscopic considerations: the motions of individual particles. Annals New York Academy of Sciences 283, 241-255.

Goldsmith, H., Marlow, J., 1979. Flow behavior of erythrocytes. II. Particles motions in concentrated suspensions of ghost cells, Journal of Colloid and Interface Science 71 (2), 383-407.

Goldsmith, H., Turitto, V., 1986. Rheological aspects of thrombosis and haemostasis: basic principles and applications. ICTH-Report-Subcommittee on Rheology of the International Committee on Thrombosis and Haemostasis. Thromb Haemost. 55(3), 415–435.

Golster H., Linden M., Bertuglia S., Colantuoni A., Nilsson G., Sjoberg F., 1999. Red blood cell velocity and volumetric flow assessment by enhanced high-resolution laser Doppler imaging in separate vessels of hamster cheek pouch microcirculation. Microvascular research 58, 62-73.

Gomez, R., Bashir, R., Sarikaya, A., Ladish, M., Sturgis, J., Robison, J., Geng, T., Bhunia, A., Apple, H., Wereley, S., 2001. Microfluidic biochip for impedance spectroscopy of biological species, Biomedical Microdevices, 3 (3), 201-209.

Heise M., Schmidt S., Kruger U., Ruckert R., Rosler S., Neuhaus P., Settmacher U., 2004. Flow pattern and shear stress distribution of distal end-to-side anastomoses. A comparison of instantaneous velocity fields obtained by particle image velocimetry. Journal of Biomechanics 37, 1043-1051.

Holzapfel G., Sommer G., Gasser C., Regitnig P., 2005. Determination of layer-specific mechanical properties of human coronary arteries with nonatherosclerotic intimal thickening and related constitutive modeling. Am. J. Physiol Heart Circ. Physiol. 289, H2048-H2058.

Ichihara, A., Tanaami, T., Isozaki, K., Sugiyama, Y., Kosugi Y., Mikuriya K., et al., 1996. High-speed confocal fluorescent microscopy using a Nipkow scanner with microlenses for 3-D imaging of single fluorescent molecule in real time. Bioimages 4 (2), 57-62.

Inoue, S. 1989. Foundations of confocal scanned imaging in light microscopy. Handbook of biological confocal microscopy, Plenum Press, 1-14

Inoue, S., Inoue, T., 2002. Direct-view high-speed confocal scanner: the CSU-10. Cell Biological Applications of Confocal Microscopy, Academic Press, 87-127.

Ishikawa, T., Simmonds, M., Pedley, T., 2006. Hydrodynamic interaction of two swimming model micro-organisms. Journal of Fluid Mechanics 568, 119-160.

Jeong, J. H., Sugii, Y., Minamiyama, M., Takeuchi, H., Okamoto, K., 2006. Interaction between liposomes and RBC in microvessels in vivo. Microvascular Research 73, 39-47.

Kaji, H., Kawashima, T., Nishizawa, M., 2006. Patterning cellular motility using an electrochemical technique and a geometrically-confined environment. Langmuir 22, 10784-10787.

Kaji, H., Hashimoto, M., Kawashima, T., Abe, T., Nishizawa, M., 2007. An electrochemical microsystem for manipulating living cells, In: Esashi, M., Ishi, K., Ohuchi, N., Osumi, N., Sato, M. and Yamaguchi, T. (Eds). Future Medical Engineering based on Bio-nanotechnology, ICP, 3-14.

Kim G B, Lee S J, 2006. X-ray PIV measurements of blood flows without tracer particles. Experiments in Fluids 41, 195-200.

Kinoshita H., Oshima M., Kaneda S., Fujii T., 2005. Confocal micro-PIV measurement of internal flow in a moving droplet. In : Proceedings of the 9thICMSCLS. Boston, Massachusetts, 629-631

Klank H, Goranovic G, Kutter J, Gjelstrup H, Michelsen J, Westergaard C, 2002. PIV measurements in a microfluidic 3D-sheathing structure with three-dimensional flow behaviour. Journal of Micromechanics and Microengineering, 12, 862-869.

Koutsiaris A, Mathioulakis D, Tsangaris S, 1999. Microscope PIV for velocity-field measurement of particle suspensions flowing inside glass capillaries. Measurement Science and Technology 10, 1037-1046.

Kroll M, Hellums J, Mcintre L, Schafer A, Moake J., 1996. Platelets and shear stress. Blood 88 (5), 1525-1541.

Lee J., 2000. 1998 Distinguished lecture: biomechanics of the microcirculation, an integrative and therapeutic perspective. Annals of Biomedical Eng. 28, 1-13.

Levick, J., 2003. An Introduction to Cardiovascular Physiology, fourth ed., Arnold.

Lima, R., Wada, S., Tsubota, K.,Yamaguchi, T., 2006. Confocal micro-PIV measurements of three dimensional profiles of cell suspension flow in a square microchannel. Measurement Science and Technology 17, 797-808.

Lima, S. Wada, M. Takeda, K. Tsubota and T. Yamaguchi, 2007. *In vitro* confocal micro-PIV measurements of blood flow in a square microchannel: the effect of the haematocrit on instantaneous velocity profiles. Journal of Biomechanics, 40, 2752-2757.

Lipowsky H., 2005. Microvascular rheology and hemodynamics. Microcirculation 12, 5-15.

Liu, Y., Zhang, L., Wang, X., Liu, W., 2004. Coupling of Navier-Stokes equations with protein molecular dynamics and its application to hemodynamics. International Journal of Numerical Methods in Fluids 46 (12), 1237-1252

Lominadze D., Mchedlishvili G., 1999. Red blood cell behavior at low flow rate in microvessels. Microvascular Research 58 (2), 187-189.

Maeda, N., 1996. Erythrocyte rheology in microcirculation. Japanese Journal of Physiology 46, 1-14.

Mannai, A, 2006. Microbifurcations and red blood cells flow, Research Internship Report, PFSL, Department of Bioengineering and Robotics, Tohoku University Japan.

Mata, A., Fleischman A., Roy S., 2005. Characterization of polydimenthylsiloxane (PDMS) properties for biomedical micro/nanosystems. Biomedical Microdevices 7(4), 281-293.

McDonald J., Whitesides G., 2002. Poly(dimenthysiloxane) as a material for fabricating microfluidic devices. Accounts of Chemical Research 35 (7), 491-499.

Mchedlishvili, G., Maeda, N., 2001. Blood flow structure related to red cell flow: a determination of blood fluidity in narrow microvessels. Japanese Journal of Physiology 51, 19-30.

Meijering E., Smal I., Danuser G., 2006. Tracking in Molecular Bioimaging, IEEE Signal Processing Magazine, 23 (3), 46-53.

Meinhart C, Wereley S, Santiago J., 1999. PIV measurements of a microchannel flow. Experiments in Fluids 27, 414-419.

Meinhart C, Wereley S., Gray H., 2000a Volume illumination for two-dimensional particle image velocimetry. Measurement Science and Technology 11, 809-814.

Meinhart C., Wereley S., Santiago J., 2000b. A PIV algorithm for estimating time-averaged velocity fields. Journal of Fluids Engineering 122, 285-289

Miyazaki, H. and Yamaguchi, T., 2003. Formation and destruction of primary thrombi under the influence of blood flow and von willebrand factor analysed by a D. E. M., Biorheology 40, 265-272.

Mielnik M., 2005. Micro–PIV and its application to some BioMEMS related microfluidic flows. Doctoral Thesis, Department of Energy and Process Engineering, Norwegian University of Science and Technology, Norway.

Minas G, Martins J, Ribeiro J, Wolffenbuttel R., Correia J., 2004. Biological microsystem for measuring uric acid in biological fluids. Sensors and Actuators 110, 33-38.

Moger J, Matcher S, Winlove C, Shore A., 2004. Measuring red blood cell flow dynamics in a glass capillary using Doppler optical coherence tomography and Doppler amplitude optical coherence tomography. Journal of Biomedical Optics 9(5), 982-994.

Mortensen, N, Okkels F., Bruus H, 2005. Reexamination of Hegen-Poiseuille flow: shape dependence of the hydraulic resistance in microchannels. Physical Review E 71, 1-4.

Munn, L., Melder R., Jain, R., 1996. Role of erythrocytes in leukocyte-endothelial interactions: mathematical model and experimental validation. Biophysical Journal 71, 466-478.

Nakano A., Sugii Y., Minamiyama M., Niimi H. 2003. Measurement of red cell velocity in microvessels using particle image velocimetry (PIV). Clinical Hemorheology and Microcirculation 29, 445-455.

Nakano, A., Sugii, Y., Minamiyama, M., Seki, J., Niimi, H. 2005. Velocity profiles of pulsatile blood flow in arterioles with bifurcation and confluence in rat mesentery measured by particle image velocimetry. JSME International Journal, C, 48(4) 444-452.

Nash, G., Meiselman, H., 1983. Red cell and ghost viscoelasticity. Effects of hemoglobin concentration and in vivo aging. Biophysical Journal 43, 63-73.

Nguyen N, and Wereley S 2002. Fundamentals and applications of microfluidics, Norwood, MA: Artech House.

Park J, Choi C, and Kihm K, 2004. Optically sliced micro-PIV using confocal laser scanning microscopy (CLSM). Experiments in Fluids 37, 105-119.

Park, J., Kihm, K., 2006. Use of confocal laser scanning microscopy (CLSM) for depthwise resolved microscale-particle image velocimetry (μ-PIV). Optics and Lasers in Engineering 44, 208-223.

Parthasarathi A., Japee S., Pittman R., 1999. Determination of red blood cell velocity by video shuttering and image analysis. Annals of Biomedical Engineering 27, 313-325

Pawley, J., 1989. Handbook of biological confocal microscopy, Plenum Press, New York.

Pries, A., Neuhaus, D., Gaehtgens P., 1992. Blood viscosity in tube flow: dependence on diameter and hematocrit.. Am J Physiol 263, H1770-H1778.

Pries, A., Secomb, T., 2003. Rheology of the microcirculation. Clinical Hemorheology and Microcirculation 29, 143-148.

Pries, A., Secomb, T., Gessner, T, Sperandio, M., Gross, J., Gaehtgens, P., 1994. Resistance to blood flow in microvessels in vivo. Circulation Research 75, 904-915.

Raffel M, Willert C., Kompenhans J., 1998. Particle image velocimetry: a practical guide, Springer-Verlag, Germany.

Ravnic, D., Zhang, Y., Tsuda, A., Pratt, J., Huss, H., Mentzer, S., 2006. Multi-image particle tracking velocimetry of the microcirculation using fluorescent nanoparticles. Microvascular Research 72, 27-33.

Reike, W., Gaehtgen, W., Johnson P., 1987. Blood viscosity in small tubes: effect of shear rate, aggregation, and sedimentation. Am. J. Physiol. 253, H540-H547.

Rika nenpyo, 1996. Chronological scientific tables, National Astronomical Observatory, Maruzen Co., Japan.

Santiago, J., Wereley, S., Meinhart C., Beebe D., Adrian R., 1998. A particle image velocimetry system for microfluidics. Experiments in Fluids 25, 316-319.

Sbalzarini, I., and Koumoutsakos, P.., 2005. Feature point tracking and trajectory analysis for video imaging in cell biology. J. Struct. Biol. 151(2), 182-195.

Schmid-Schonbein, H., Wells, R., 1969. Fluid drop-like transition of erythrocytes under shear. Science 165, 288-291.

Secomb, T., 1995. Mechanics of blood flow in the microcirculation, Symp. Soc. Exp. Biol. 49, 305-321.

Shevkoplyas S, Gifford S, Yoshida T, Bitensky M., 2003. Prototype of an in vitro model of the microcirculation, Microvascular Research 65, 132-136.

Shiga, T., Maeda N., Kon K., 1990. Erythrocyte rheology. Crit. Rev. Oncol. Hematol. 10, 9-48.

Shin M., Matsuda K., Ishii O., Terai H., Kaazempur-Mofrad M., Borenstein J., Detmar M., Vacanti J., 2004. Endothelialized networks with a vascular geometry in microfabricated poly(dimethylsiloxane). Biomedical Microdevices 6 (4), 269-278.

Shinohara K, Sugii Y, Arata A, Hibara A, Tokeshi M, Kitamori T, Okamoto K, 2004. High-speed micro-PIV measurements of transient flow in microfluidic devices. Measurement Science and Technology 15, 1965-1970.

Sinton D., 2004. Microscale flow visualization. Microfluid Nanofluid 1, 2-21.

Slaaf, D., Arts, T., Jeurens T., Tangelder G., Reneman R., 1984. Electronic measurement of red blood cell velocity and volume flow in microvessels, In: ChavenJ, Bitensky, L. (eds): Investigative Microtechniques in Medicine and Biology, New York, pp. 327-364.

Stanton A., 1999. Haemodynamics, wall mechanics and atheroma: a clinician`s perspective. Proc. Inst. Mech. Engrs, H 213,, 385-390.

Steiger H., Aaslid R., Keller S., Reulen H., 1989. Strength, elasticity and viscoelastic properties of cerebral aneurysms. Heart and Vessels 5 (1), 41-46.

Sugii Y, Nishio S, Okamoto K, 2002. In vivo PIV measurement of red blood cell velocity field in microvessels considering mesentery motion. Physiol. Meas. 23 ,403-416.

Sugii Y, Okuda R, Okamoto K, Madarame H, 2005. Velocity measurement of both red blood cells and plasma of in vitro blood flow using high-speed micro PIV technique. Measurement Science and Technology 16, 1126-1130.

Sutton N, Tracey M, Johnston I, Greenaway R, Rampling M, 1997. A novel instrument for studying the flow behaviour of erythrocytes trough microchannels simulating human blood capillaries. Microvascular Research 53, 272-281.

Suzuki, Y., Tateishi, N., Soutani M. and N., Maeda, 1996. Deformation of erythrocytes in microvessels and glass capillaries: effects of erythrocyte deformability. Microcirculation 3, 49-57.

Tabeling, P., 2001. Some basic problems of microfluidics. In: Proceedings of the 14th Australasian Fluid Mechanics Conference, Adelaide, Autralia.

Takayama S, McDonald J, Ostuni E, Liang M, Kenis P, Ismagilov R, Whitesides G, 1999. Patterning cells and their environments using laminar fluid flows in capillary networks. Proc. Natl. Acad. Sci. 96, 5545-5548.

Tanaani T, Otsuki S, Tomosada N, Kosugi Y, Shimizu M. Ishida H., 2002. High-speed 1-frame/ms scanning confocal microscope with a microlens and Nipkow disks. Applied Optics 41 (22), 4704-4708.

Tangelder G., Slaaf D., Muijtjens M., Arts T., Egbrink M., Reneman R. 1986. Velocity profiles of blood platelets and red blood cells flowing in arteriols of rabbit mesentery. Circulation Research 59, 505-514.

Thorsen T., Maerkl S, Quake S., 2002. Microfluidic large-scale integration. Science 298, 580-584.

Toner M., Irimia D., 2005. Blood on a chip. Annu. Rev. Biomed. Eng. 7, 77-103.

Tsubota, K., Wada, S., Yamaguchi, T., 2006a. Particle method for computer simulation of red blood cell motion in blood flow. Computer Methods and Programs in Biomedicine 83, 139-146.

Tsubota, K., Wada, S., Yamaguchi, T., 2006b. Simulation study on effects of hematocrit on blood flow properties using particle method. Journal of Biomechanical Science and Enginneering 1, 159-170.

Tsubota, K., Wada, S., Kamada, H., Kitagawa, Y., Lima, R., and Yamaguchi, T., 2006c, A particle method for blood flow simulation: application to flowing red blood cells and platelets, Journal of the Earth Simulator 5, 2-7.

Uijttewaal W., Nijhof E., Heethaar R., 1994. Lateral migration of blood cells and microspheres in two-dimensional Poiseuille flow: a laser Doppler study. Journal of Biomechanics 27, 35-42

Unger M., Chou H., Thorsen T., Scherer A., Quake S., 2000. Monolithic microfabricated valves and pumps by multilayer soft lithography. Science 288, 113-116.

Vennemann P., K. Kiger, R. Lindken, B. Groenendijk, S. Stekelenburg-de Vos, T. Hagen, N. Ursem, R. Poelmann, J. Westerweel, B. Hierk, 2006. In vivo micro particle image velocimetry measurements of blood-plasma in the embryonic avian heart. Journal of Biomechanics 39, 1191-1200.

Wada, S., Kobayashi, R., 2002. Simulation of the shape change of a red blood cell at the entrance of a capillary. In: Proceedings of the 4th World Congress of Biomechanics, Calgary, Canada.,

Waite L., 2005. Biofluid Mechanics in Cardiovascular Systems, McGraw-Hill, USA.

Webb R., 1996. Confocal optical microscopy, Rep. Prog. Phys. 59, 427-471.

Westerweel J, Dabiri D, Gharib M., 1997. The effect of a discrete window offset on the accuracy of cross-correlation analysis of digital PIV recordings. Experiments in Fluids 23, 20-28.

Wilhelm S, Grobler B, Gluch M, Heinz H., 2003. Confocal laser scanning microscopy: principles, Carl Zeiss, Germany.

Willert C, Raffel M, Kompenhans J, Stasicki B, Kahler C., 1996. Recent applications of particle image velocimetry in aerodynamic research. Flow Meas. Instrum. 7, 247-256.

Wootton, D., Ku D., 1999. Fluid mechanics of vascular systems, diseases, and thrombosis. Annual Review of Biomedical Engineering 1, 299-329.

Wright S, Wright D., 2002. Introduction to confocal microscopy. Cell Biological Applications of Confocal Microscopy, Academic Press, 1-85.

Yamaguchi, T., Ishikawa, T., Tsubota, K., Imai, Y., Nakamura M., Fukui T., 2006. Computational blood flow analysis – new trends and methods. Journal of Biomechanical Science and Enginneering 1, 29-50.

APPENDIX A - Spatial resolution and optical slice thickness of the confocal micro-PIV system.

The image formed by a point of light in the focal plane is not an ideal point object because the point is always distributed over a possible area within the image plane. As a result, the image properties of an optical system can be described using the point spread function (PSF), which represents the light intensity distribution on the image plane. This distribution has a higher probability at the centre (higher light intensity) and a lower probability at the outside (lower light intensity) (Willhelm et al. 2003).

Resolution can be defined as the ability to distinguish two point objects from each other (Wright and Wright 2002). In confocal microscopy, the pinhole plays an important role in calculating spatial resolution. Since the modified pinhole diameter (MPD) can be defined as the pinhole diameter (PD in μm) divided by the magnification (M), the airy unit (AU) can be obtained using the following equation (Willhelm et al. 2003, Park et al. 2004)

$$AU = \frac{1.22\lambda_{ex}}{NA} \qquad \text{(A1)}$$

where λ_{ex} is the wavelength of the illuminating laser light and NA is the numerical aperture of the microscopic objective lens. It is possible to determine the spatial resolution of the confocal system by applying the following criteria:

if MPD > 1.0 AU, apply geometric-optical analysis;
if MPD < 0.25 AU, apply wave-optical analysis (Willhelm et al. 2003).

The confocal microscope system used in our experiment used geometric–optical analysis, as the MPD (2.5 μm) was bigger than the AU value (0.865). Using geometric–optical analysis, it was possible to calculate the spatial resolution of the system by applying the following equations (Willhelm et al. 2003):

$$R_l = \frac{0.51\lambda_{ex}}{NA} \qquad \text{(A2)}$$

$$R_a = \frac{0.88\lambda_{ex}}{n - \sqrt{n^2 - NA^2}} \qquad \text{(A3)}$$

$$OST = \sqrt{\left(\frac{0.88\lambda_{em}}{n - \sqrt{n^2 - NA^2}}\right)^2 + \left(\frac{\sqrt{2}n \cdot MPD}{NA}\right)^2} \qquad \text{(A4)}$$

where R_l is the lateral resolution, R_a is the axial resolution, OST is the optical slice thickness, λ_{em} is the emission wavelength, and n the refractive index of the immersion liquid.

APPENDIX B - Analytical solution for laminar flow in a rectangular microchannel.

By solving the Navier–Stokes equation with a constant pressure gradient along the rectangular microchannel and considering no-slip boundary conditions at the wall, it is possible to obtain the following equation for the corresponding boundary conditions (Bruus 2004)

$$\left[\partial_y^2 + \partial_z^2\right] u_x(y,z) = \frac{\Delta p}{\mu L} \qquad \text{for} \qquad -\frac{1}{2}w < y < \frac{1}{2}w, \;\; 0 < z < h \tag{B1}$$

$$u_x(y,z) = 0 \quad \text{for} \qquad y = \pm\frac{1}{2}w, \;\; z = 0, \;\; z = h \tag{B2}$$

where u_x is the fluid velocity in the x-direction, y and z are the directions normal to the flow, w is the width of the microchannel, μ is the fluid viscosity, L is the length of the microchannel, and $\Delta p/L$ is the pressure gradient. Furthermore, by using a Fourier series along the z-direction, we obtain the following velocity field equation as function of location within the cross section of the microchannel and applied pressure gradient:

$$u_x(y,z) = \frac{4h^2\Delta p}{\pi^3 \mu L}\sum_{n,odd}^{\infty}\frac{1}{n^3}\left[1 - \frac{\cosh(n\pi\frac{y}{h})}{\cosh(n\pi\frac{w}{2h})}\right]\sin(n\pi\frac{z}{h}). \tag{B3}$$

Double integration of equation B3 over the cross section gives the corresponding flow rate (Q):

$$Q = \frac{h^3 w\Delta p}{12\mu L}\left[1 - \sum_{n,odd}^{\infty}\frac{192h}{n^5\pi^5 w}\tanh(n\pi\frac{w}{2h})\right] \tag{B4}$$

Finally, by combining equations B3 and B4, it is possible to obtain a very useful expression for calculating the velocity profile for the Poiseuille flow in a rectangular or square microchannel. In this way, the velocity field can then be expressed as

$$u_x(y,z) = \frac{48Q}{\pi^3 hw} \frac{\sum_{n,odd}^{\infty} \frac{1}{n^3} \left[1 - \frac{\cosh(n\pi \frac{y}{h})}{\cosh(n\pi \frac{w}{2h})} \right] \sin(n\pi \frac{z}{h})}{\left[1 - \sum_{n,odd}^{\infty} \frac{192h}{n^5 \pi^5 w} \tanh(n\pi \frac{w}{2h}) \right]} \qquad \text{(B5)}$$

APPENDIX C - Development of a circular PDMS microchannel to mimic *in vivo* microvessels.

Along the years, various experimental techniques have been performed in glass microchannels (Chien et al. 1984) in an effort to understand the blood flow behavior in microcirculation. The most remarkable phenomena observed in glass capillaries related to the flow characteristics of blood are known as Faharaeus effect and Faharaeus-Lindqvist effect. These two effects are strongly related to the microtube diameter and they were also observed *in vivo* experiments. Although glass microchannels present certain similarities to *in viv*o microcirculation, it is also clear that these kind of static microchannels differ from microvessels in several respects, such as: elasticity of microvessels, role of the irregularly shaped endothelial surface and effect of the branches and asymmetrical structure of microvessels. Thus, it was not surprising that several studies on blood flow in glass microtubes and in microvessels have yielded conflicting results with respect to flow resistance (Pries et al. 1994) and deformability of RBCs (Suzuki et al. 1996). In former case, they reported that the apparent viscosity was higher *in vivo* than in glass tubes weheras in the latter they have found that RBCs deform less in microvessels. However, the observed in *vivo/in vitro* discrepancies could not yet been convincingly explained. We believe that experimental studies in microchannels should be beyond static conditions. Hence, it is imperative to develop a dynamic microchannel closely representative of *in vivo* microvascular environment.

It is obvious that the quantitative conflicting results arisen from in *vivo/in vitro* experiments can not be explained by using the research done in straight rigid glass microchannels. One possible way to overcome the limitations of the glass capillaries is by using a soft lithography technique. This method has the ability to generate extremely precise, reproducible and versatile rectangular polydimethysiloxane (PDMS) microchannels. Although, by using this technique, it is possible to mimic complex geometries similar to human blood arterioles and capillary networks, blood flow behaviour through this kind of microchannels may exhibit different features characteristic with those investigated in living microvessels. Hence, it is imperative to develop a circular PDMS microchannel able to mimic *in vivo* environment and to use the state-of-the-art micro-visualization techniques, such as confocal micro-PIV. Table C1 summarizes both advantages and disadvantages of using glass capillaries, rectangular PDMS microchannel and circular PDMS microchannel.

Table C1 – The most relevant advantages and disadvantages of using glass capillaries, rectangular PDMS microchannel and circular PDMS microchannel.

Physicochemical factors that affects blood flow behavior	Glass capillaries	rectangular PDMS microchannel	circular PDMS microchannel
Geometry of the flow channel	any kind of geometry	any kind of geometry	simple geometries
Mechanical properties	Rigid	flexible	flexible
Ability to culture cells in the inner surface	not possible	possible	possible
Ability to study microcirculation pathogenesis phenomena	not possible	possible	possible

We report here a simple method to manufacture circular PDMS microchannels. We believe that this kind of microchannels will lead to new insights into several microcirculation phenomena such as the role of the glycocalyx on the flow behavior blood and the thrombogenesis process.

Materials and methods

Fabrication of the circular PDMS microchannel

The circular PDMS microchannels were fabricated by a wire casting technique. Generally, the fabrication process, which is outlined in Figure C1, was the following:

A. the master was first fabricated by using an acrylic based, a needle, screws, nuts and several washers or o-rings. The precision wires were inserted into the needle and then stretched by rotating the screw. Depending on the diameters of the wires, the materials used were stainless steel, polyester and aluminum (Riken);

B. the PDMS prepolymer was prepared by mixing a commercial prepolymer and catalyzer (Silpot 184; Dow Corning, USA) at a weight ratio of 10:1. The PDMS mixture was poured into the mold master and baked on a hot plate for about 2 h at low temperature (50–60°C). Both master and PDMS were then cooled to room temperature and the PDMS was peeled from the master ;

C. the PDMS containing the needle and the precision wire were then immersed in ethanol for a period of at least 5 hours at 4°C . This procedure is extremely important in order to allow a smooth extraction of the precision wire;

D. finally the needle and wire were pulled out gently and the inlet and outlet ports were embedded in the PDMS device.

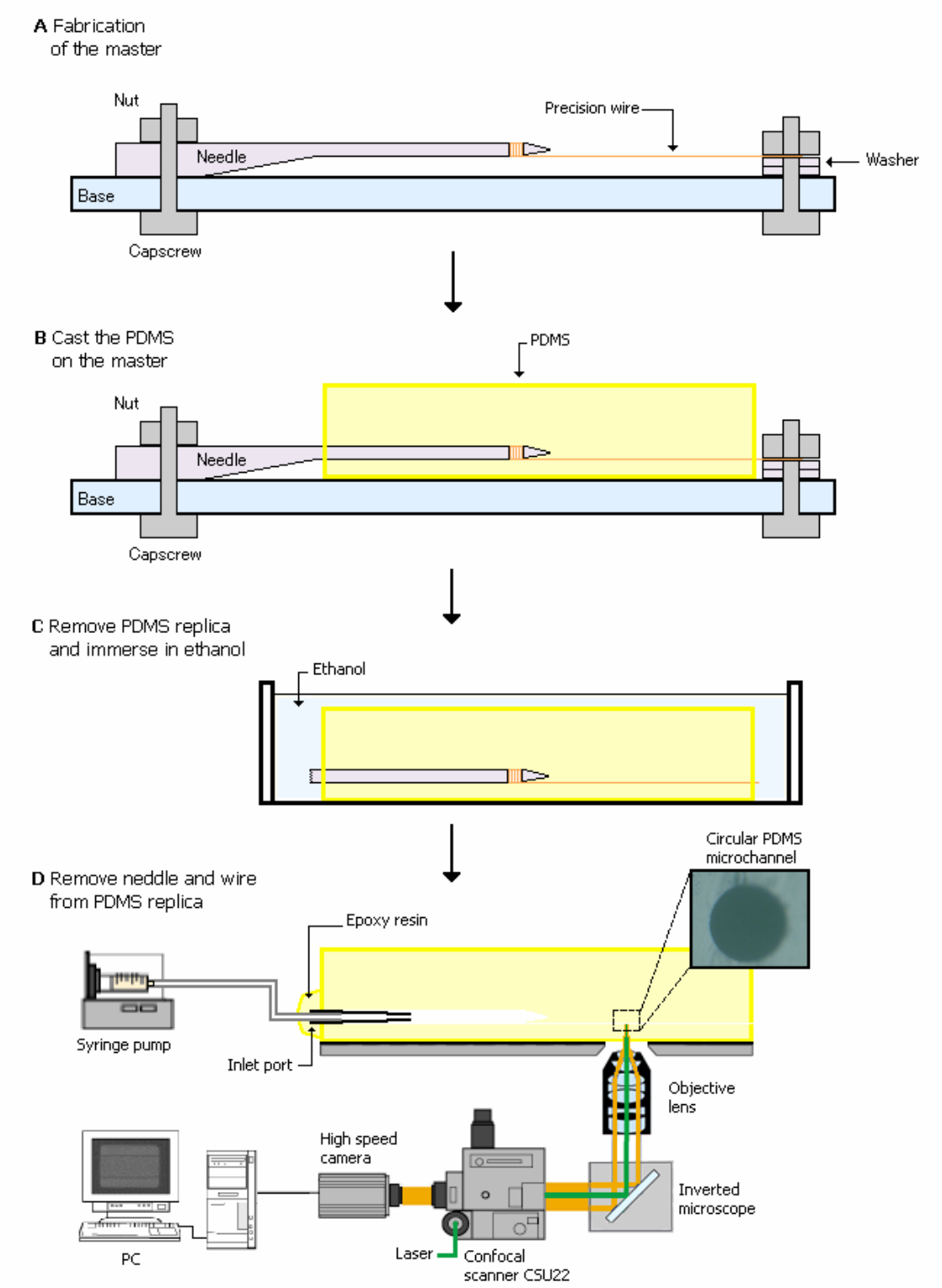

Figure C1. Schematic diagram describing the procedure to fabricate a circular PDMS microchannel and micro-visualization technique used to measure the blood flow through the microchannel.

Confocal micro-PTV

The confocal micro-PTV system used in the present study consists of an inverted microscope (IX71, Olympus, Japan) combined with a confocal scanning unit (CSU22, Yokogawa, Japan) and a diode-pumped solid state (DPSS) laser (Laser Quantum Ltd, England) with an excitation wavelength of 532 nm and a high-speed camera (Phantom v7.1, U.S.A.). The circular PDMS microchannel was placed on the stage of the inverted microscope where the flow rate of the working fluids was kept constant by means of a syringe pump (KD Scientific Inc., U.S.A.). By using a thermo plate controller (Tokai Hit), the microscope stage was set to 37ºC.

All the confocal images were recorded in the middle of the microchannels, using a piezo driver system and RT3D software from the Yokogawa corporation. The series of xy confocal images were captured with a resolution of 640×480 pixels, 12-bit grayscale, at a rate of 100 frames/s with an exposure time of 9.4 ms. The recorded images were transfered to the computer and then evaluated in the Image J (NIH) (Abramoff et al., 2004) by using the manual tracking MtrackJ plugin (Meijering et al., 2006). As a result, it was possible to track single RBCs through the middle plane of the microchannel. Detailed information about the experimental set-up, used in the present study, has already been described previously (Lima et al. 2006).

Results and discussion

Geometry of the microchannel

Figure C2 shows the cross section of three different PDMS microchannels. The diameters of the precision wires were 150 μm, 75 μm and 50 μm. From figure C2, it is possible to observe that the proposed fabrication process can produce transparent *in vitro*, real-scale models with diameters comparable to *in vivo* microcirculatory vessels.

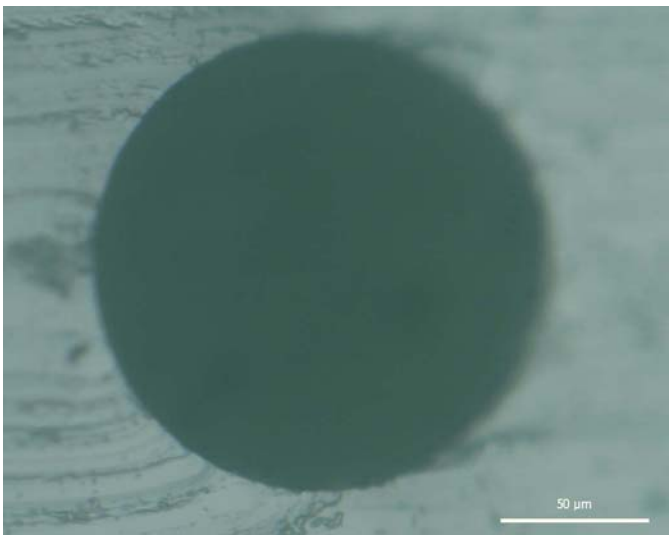

a)

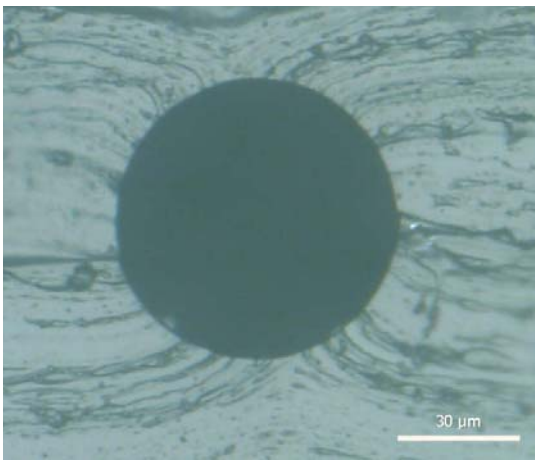

b)

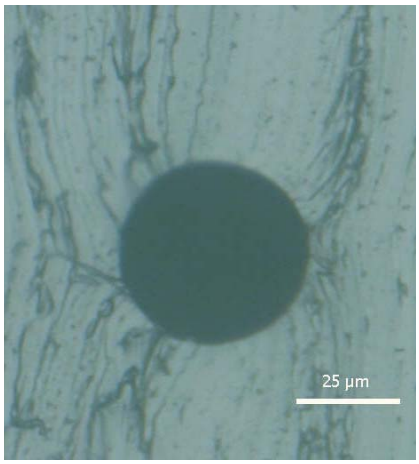

c)

Figure C2. Cross section of the PDMS microchannels with different diameters a) 150 µm b) 75 µm and c) 50 µm (wide field microscope with a magnification of 1000).

RBC flow visualization

By using the optical sectioning ability of the confocal system, it was possible to obtain series of optical sectioned images at the middle of microchannel. Figures C2 to C4 show images of both RBCs (halogen illumination) and labeled RBCs (laser-emitted light) at different Hcts together with the correspondent time position tracking of individual RBCs. The measurements were performed in the centre plane of a 75 µm circular PDMSmicrochanel.

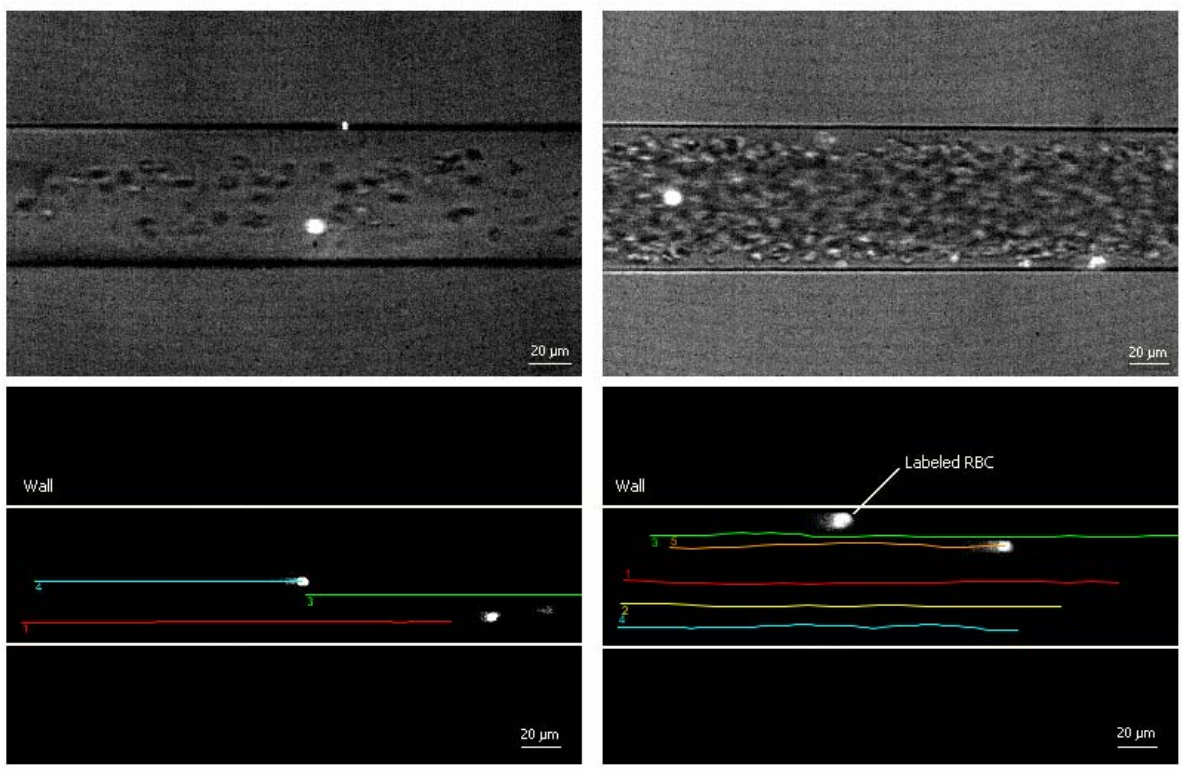

a) b)

Figure C3. Both normal and labeled RBCs (bright spot form laser-emitted light) with a) 2% Hct (20×, 1.6 zoom objective lens) and correspondent RBC paths displacement; b) 23% Hct (20×, 1.6 zoom objective lens) and correspondent RBC paths displacement.

Figures C3 demonstrates that the confocal system can be successfully integrated with the proposed fabrication technique. This combination will provide a powerful way of investigating several microcirculation phenomena and consequently it helps to understand the actual physiopathological phenomena in microvessls.

Ongoing development

Besides the ability to produce models with diameters comparable to *in vivo* microvessels, this kind of microchannels have others remarkable properties such as good optical transparency, biocompatibility and permeability to gases. This latter property makes these microchannels adequate to culture living cells on their surfaces, such as endothelial cells (Kaji et al., 2006, 2007).

The flow behavior of blood cells in microvessels is not only dependent on its vessel geometry but several other biochemical and biophysical factors may also contribute to the rheological characteristics of blood. Due to the inability of glass microchannels to culture living cells, several researchers have been using parallel plate flow chamber (Brown and Larson, 2001) to

investigate the cellular and molecular events occurring between the blood cells and endothelium. Unfortunately, the flow conditions provided by these microchannels differ from the flow in microvessles. As a result, there is a need of an *in vitro* blood flow system with characteristics close to *in vivo* microvessels, such as the proposed circular PDMS. Recently, Kaji and his colleagues (Kaji et al., 2006, 2007), by using an innovative cellular micropatterning technique based on electrochemical method, have successfully cultured endothelial cells on the surfaces of rectangular PDMS microchannel. An ongoing work to culture endothelial cells on the surfaces of the proposed circular PDMS microchannel is currently under way. By culturing endothelial cells within the microfluidic device, we expect to develop a flow system device that closely mimics the *in vivo* environment and also to identify and quantitatively measure cellular and molecular events occurring between the blood cells and endothelium.

APPENDIX D – C code to calculate RBC dispersion coefficient.

```
/*********************************************************/
/***   SPT, RBCs Dispersion coeficient, Rui Lima, PFSL, 2007    ***/
/*********************************************************/
/*******************         PART I         *********************/
/*********************************************************/
/******   RBCs tracking using Manual Tracking (MTrackj)  *****/
/** ##### Do not use this code for commercial activities ##### **/

#include <stdio.h>
#include <stdlib.h>
#include <math.h>

#define N1 10000
#define N2 10000

/***** main *****/
/*----------------------------------------------------------------*/

int main()
{
        FILE *fpi, *fpo, *fpo1;
    double t[N1];
        double f[N1];
        double x[N1];
        double y[N1];
        double t1d1[N2]; /* Track 1 */
        double t1d2[N2];
        double t1d3[N2];
        double t1d4[N2];
        double t1d5[N2];
        double t1d6[N2];
        double t1d7[N2];
        double t1d8[N2];
        double t1d9[N2];
        double t1d10[N2];
        double t1d11[N2];
        double t1d12[N2];
        double t1d13[N2];
        double t1d14[N2];
        double t1d15[N2];
        double t1d16[N2];
        double t1d17[N2];
        double t1d18[N2];
        double t1d19[N2];
        double t1d20[N2];
        double t1d21[N2];
        double t1d22[N2];
        double t1d23[N2];
        double t1a[N2];
        char fname[50];          /* file name */
        char dummy[256];         /* ignore file text */
        char dum1[256];
        char dum2[256];
        char dum3[256];
        int dmi1, dmi2, dmi3;           /* ignore file text */
        double dmd1, dmd2, dmd3, dmd4, dmd5, dmd6, dmd7, dmd8, dmd9, dmd10, dmd11;    /*ignore file text*/
        int i,j, nd, nt;
```

```
/*---------------------------------------------------------------------*/
/*****  Open data file   *****/

        printf("File name to open ?\n"); /* name of file to open */
        scanf("%s",&fname);

        printf("Number of Data ?\n"); /*max number of data to be processed, depends on the amount of RBCs
tracked*/
        scanf("%d",&nd);
        fpi = fopen(fname,"r");
        if(fpi==NULL){printf("%s cannot open\n");exit(1);}
        printf("%s open...\n",fname);

        fgets(dummy,256,fpi);
          for(i=0;i<nd;i++){ /* read y */

        fscanf(fpi,"%d %d %lf %lf %lf %lf %lf %lf %lf %s %s %s", &dmi1, &dmi2, &t[i], &f[i], &x[i],
&y[i], &dmd3, &dmd4, &dmd5, &dmd6, &dum1, &dum2,&dum3);
        }

        fclose(fpi);

/*****  Calculation of radial displacement Ry for a time increment for several tracks*****/

        printf("Output file name for SPT\n");
        scanf("%s",&fname);

        fpo = fopen(fname,"w");
        fprintf(fpo, "Track, y ,       -- t1 --    \n");

do {
        printf("RBC track number 1,2,3... (0 to exit) ?\n"); /* RBC track number to be processed */
        scanf("%d",&nt);

        if (nt==0){exit(1);}
        for (i=0;i<nd;i++){

        if  (t[i]==nt)
        {t1a[i]=y[i];}

        }
        for (i=0;i<nd;i++){
        t1d1[i]=(t1a[i]-t1a[i+1]);
        }
        for (i=0;i<nd;i++){
        t1d2[i]=(t1a[i]-t1a[i+2]);
        }
        for (i=0;i<nd;i++){
        t1d3[i]=(t1a[i]-t1a[i+3]);
        }
        for (i=0;i<nd;i++){
        t1d4[i]=(t1a[i]-t1a[i+4]);
        }
        for (i=0;i<nd;i++){
        t1d5[i]=(t1a[i]-t1a[i+5]);
        }
        for (i=0;i<nd;i++){
        t1d6[i]=(t1a[i]-t1a[i+6]);
        }
        for (i=0;i<nd;i++){
        t1d7[i]=(t1a[i]-t1a[i+7]);
```

```
}
for (i=0;i<nd;i++){
t1d8[i]=(t1a[i]-t1a[i+8]);
}
for (i=0;i<nd;i++){
t1d9[i]=(t1a[i]-t1a[i+9]);
}
for (i=0;i<nd;i++){
t1d10[i]=(t1a[i]-t1a[i+10]);
}
for (i=0;i<nd;i++){
t1d11[i]=(t1a[i]-t1a[i+11]);
}
for (i=0;i<nd;i++){
t1d12[i]=(t1a[i]-t1a[i+12]);
}
for (i=0;i<nd;i++){
t1d13[i]=(t1a[i]-t1a[i+13]);
}
for (i=0;i<nd;i++){
t1d14[i]=(t1a[i]-t1a[i+14]);
}
for (i=0;i<nd;i++){
t1d15[i]=(t1a[i]-t1a[i+15]);
}
for (i=0;i<nd;i++){
t1d16[i]=(t1a[i]-t1a[i+16]);
}
for (i=0;i<nd;i++){
t1d17[i]=(t1a[i]-t1a[i+17]);
}
for (i=0;i<nd;i++){
t1d18[i]=(t1a[i]-t1a[i+18]);
}
for (i=0;i<nd;i++){
t1d19[i]=(t1a[i]-t1a[i+19]);
}
for (i=0;i<nd;i++){
t1d20[i]=(t1a[i]-t1a[i+20]);
}
for (i=0;i<nd;i++){
t1d21[i]=(t1a[i]-t1a[i+21]);
}
for (i=0;i<nd;i++){
t1d22[i]=(t1a[i]-t1a[i+22]);
}
for (i=0;i<nd;i++){
t1d23[i]=(t1a[i]-t1a[i+23]);
}

/****** Input zero values into data file ******/

for (i=0;i<nd;i++){
  if(t1d1[i] > 20.0) t1d1[i]=0.0;
  if(t1d2[i] > 20.0) t1d2[i]=0.0;
  if(t1d3[i] > 20.0) t1d3[i]=0.0;
  if(t1d4[i] > 20.0) t1d4[i]=0.0;
  if(t1d5[i] > 20.0) t1d5[i]=0.0;
  if(t1d6[i] > 20.0) t1d6[i]=0.0;
  if(t1d7[i] > 20.0) t1d7[i]=0.0;
  if(t1d8[i] > 20.0) t1d8[i]=0.0;
  if(t1d9[i] > 20.0) t1d9[i]=0.0;
```

```
          if(t1d10[i] > 20.0) t1d10[i]=0.0;
          if(t1d11[i] > 20.0) t1d11[i]=0.0;
          if(t1d12[i] > 20.0) t1d12[i]=0.0;
          if(t1d13[i] > 20.0) t1d13[i]=0.0;
          if(t1d14[i] > 20.0) t1d14[i]=0.0;
          if(t1d15[i] > 20.0) t1d15[i]=0.0;
          if(t1d16[i] > 20.0) t1d16[i]=0.0;
          if(t1d17[i] > 20.0) t1d17[i]=0.0;
          if(t1d18[i] > 20.0) t1d18[i]=0.0;
          if(t1d19[i] > 20.0) t1d19[i]=0.0;
          if(t1d20[i] > 20.0) t1d20[i]=0.0;
          if(t1d21[i] > 20.0) t1d21[i]=0.0;
          if(t1d22[i] > 20.0) t1d22[i]=0.0;
     if(t1d23[i] > 20.0) t1d23[i]=0.0;
          }

/*****  Out put file  ******/

          for(i=0;i<nd;i++){ /* x */
          if(fabs(t[i]-(double)nt) < 1.0e-10)
          {
          fprintf(fpo," %1.1f %7.3f %7.3f %7.3f %7.3f %7.3f %7.3f %7.3f %7.3f %7.3f %7.3f %7.3f %7.3f
%7.3f %7.3f %7.3f %7.3f %7.3f %7.3f %7.3f %7.3f %7.3f %7.3f %7.3f %7.3f \n",
          t[i],y[i],fabs(t1d1[i]),fabs(t1d2[i]),fabs(t1d3[i]),fabs(t1d4[i]),fabs(t1d5[i]),fabs(t1d6[i]),fabs(t1d7[i]),
          fabs(t1d8[i]),fabs(t1d9[i]),fabs(t1d10[i]),fabs(t1d11[i]),fabs(t1d12[i]),fabs(t1d13[i]),fabs(t1d14[i]),
          fabs(t1d15[i]),fabs(t1d16[i]),fabs(t1d17[i]),fabs(t1d18[i]),fabs(t1d19[i]),fabs(t1d20[i]),fabs(t1d21[i]),fabs(t
1d22[i]),fabs(t1d23[i]));
          }
          }

} while(nt=!0);

          fclose(fpo);
}
```

```
/*************************************************************************/
/**********        SPT, RBCs dispersion, Rui Lima, PFSL, 2007         **********/
/*************************************************************************/
/*******************              PART II              **********************/
/*************************************************************************/
/****  Mean square radial displacement to calculate RBCs dispersion coef  ****/
/* ######      Do not use this code for commercial activities        ###### *****/

#include <stdio.h>
#include <stdlib.h>
#include <math.h>
#define N1 10000
#define N2 10000

/***** main *****/
/*---------------------------------------------------------------*/

int main()
{
        FILE *fpi, *fpo, *fpo1;
   double t[N1];
        double f[N1];
        double x[N1];
        double y[N1];
        double t1d1[N2]; /* Track 1 */
        double t1d2[N2];
        double t1d3[N2];
        double t1d4[N2];
        double t1d5[N2];
        double t1d6[N2];
        double t1d7[N2];
        double t1d8[N2];
        double t1d9[N2];
        double t1d10[N2];
        double t1d11[N2];
        double t1d12[N2];
        double t1d13[N2];
        double t1d14[N2];
        double t1d15[N2];
        double t1d16[N2];
        double t1d17[N2];
        double t1d18[N2];
        double t1d19[N2];
        double t1d20[N2];
        double t1d21[N2];
        double t1d22[N2];
        double t1d23[N2];
        double t1a[N2];
        char fname[50];          /* file name */
        char dummy[256];         /* ignore file text */
        char dum1[256];
        char dum2[256];
        char dum3[256];
        int dmi1, dmi2, dmi3;            /* ignore file text */
        double dmd1, dmd2, dmd3, dmd4, dmd5, dmd6, dmd7, dmd8, dmd9, dmd10, dmd11, sum1=0.0,
sum2=0.0, sum3=0.0, sum4=0.0, sum5=0.0, sum6=0.0, sum7=0.0, sum8=0.0, sum9=0.0, sum10=0.0, sum11=0.0,
sum12=0.0, sum13=0.0, sum14=0.0, sum15=0.0, sum16=0.0, sum17=0.0, sum18=0.0, sum19=0.0, sum20=0.0,
sum21=0.0, sum22=0.0, sum23=0.0,
avgt1d1, avgt1d2, avgt1d3, avgt1d4, avgt1d5, avgt1d6, avgt1d7,avgt1d8,avgt1d9,avgt1d10,avgt1d11,avgt1d12,
avgt1d13,avgt1d14,avgt1d15,avgt1d16,avgt1d17,avgt1d18,avgt1d19,avgt1d20,avgt1d21,avgt1d22,avgt1d23;
        int i,j, jtmp,  nd, nt, nt1, count = 0 ;
```

```
/*-----------------------------------------------------------------*/
/*****  Open data file   *****/

        printf("File name to open ?\n"); /* name of file to open */
        scanf("%s",&fname);
        printf("Number of total data (nd) ?\n"); /* max number of data to be processed, depends on amount of
RBCs tracked */
        scanf("%d",&nd);
        fpi = fopen(fname,"r");

        if(fpi==NULL){printf("%s cannot open\n");exit(1);}
        printf("%s open...\n",fname);
        fgets(dummy,256,fpi);

        for(i=0;i<nd;i++){ /* read y */

fscanf(fpi," %lf %lf %lf %lf %lf %lf %lf %lf %lf %lf %lf %lf %lf %lf %lf %lf %lf %lf %lf %lf %lf %lf %lf %lf
 %lf ", &t[i],&y[i],&t1d1[i],&t1d2[i],&t1d3[i],&t1d4[i],&t1d5[i],&t1d6[i],&t1d7[i],&t1d8[i],&t1d9[i],
&t1d10[i],&t1d11[i],&t1d12[i],&t1d13[i],&t1d14[i],&t1d15[i],&t1d16[i],&t1d17[i],&t1d18[i],&t1d19[i],
&t1d20[i],&t1d21[i], &t1d22[i], &t1d23[i]);
}
        fclose(fpi);

/*-----------------------------------------------------------------*/
/*****  Avg to calculate dispersion coef  ******/
/*****  Out put file for several tracks  ******/

        printf("Output file name for SPT\n");
        scanf("%s",&fname);

        fpo = fopen(fname,"w");
        fprintf(fpo, "Track, y ,       -- t1 --    \n");

do {
  sum1 = 0.0;  sum2 = 0.0; sum3 = 0.0; sum4 = 0.0; sum5 = 0.0; sum6 = 0.0; sum7 = 0.0; sum8 = 0.0; sum9 =
0.0; sum10 = 0.0; sum11 = 0.0; sum12 = 0.0; sum13 = 0.0;  sum14 = 0.0; sum15 = 0.0; sum16 = 0.0; sum17 =
0.0; sum18 = 0.0; sum19 = 0.0; sum20 = 0.0; sum21 = 0.0; sum22 = 0.0; sum23 = 0.0;
        printf("RBC track number 1,2,3...nt (0 to exit) ?\n"); /* RBC track number to be processed */
        scanf("%d",&nt);

if (nt==0){exit(1);}

/*****  Calculation mean square radial displacement (MSRD) *****/

        printf("Number of tracks for Avg?\n"); /* number of traks to calculate MSRD*/
        scanf("%d",&nt1);

        for (i=0;i<nd;i++){

        if(fabs(t[i]-(double)nt) < 1.0e-10)
          {
           sum1 += pow(t1d1[i], 2); /* sum1 = 0 + T1D1(1)^2 + T1D1(2)^2 ....*/
      }
}
        avgt1d1 = sum1/(double)nt1;

        for (i=0;i<nd;i++){
        if(fabs(t[i]-(double)nt) < 1.0e-10)
        {
        sum2+= pow(t1d2[i], 2);
        }
        }
```

```
avgt1d2 = sum2/((double)nt1-1);

for (i=0;i<nd;i++){
if(fabs(t[i]-(double)nt) < 1.0e-10)
{
sum3+= pow(t1d3[i], 2);
}
}
avgt1d3 = sum3/((double)nt1-2);

for (i=0;i<nd;i++){
if(fabs(t[i]-(double)nt) < 1.0e-10)
{
sum4+= pow(t1d4[i], 2);
}
}
avgt1d4 = sum4/((double)nt1-3);

for (i=0;i<nd;i++){
if(fabs(t[i]-(double)nt) < 1.0e-10)
{
sum5+= pow(t1d5[i], 2);
}
}
avgt1d5 = sum5/((double)nt1-4);

for (i=0;i<nd;i++){
if(fabs(t[i]-(double)nt) < 1.0e-10)
{
sum6+= pow(t1d6[i], 2);
}
}
avgt1d6 = sum6/((double)nt1-5);

for (i=0;i<nd;i++){
if(fabs(t[i]-(double)nt) < 1.0e-10)
{
sum7+= pow(t1d7[i], 2);
}
}
avgt1d7 = sum7/((double)nt1-6);

for (i=0;i<nd;i++){
if(fabs(t[i]-(double)nt) < 1.0e-10)
{
sum8+= pow(t1d8[i], 2);
}
}
avgt1d8 = sum8/((double)nt1-7);

for (i=0;i<nd;i++){
if(fabs(t[i]-(double)nt) < 1.0e-10)
{
sum9+= pow(t1d9[i], 2);
}
}
avgt1d9 = sum9/((double)nt1-8);

for (i=0;i<nd;i++){
if(fabs(t[i]-(double)nt) < 1.0e-10)
{
sum10+= pow(t1d10[i], 2);
```

```
    }
    }
    avgt1d10 = sum10/((double)nt1-9);

    for (i=0;i<nd;i++){
    if(fabs(t[i]-(double)nt) < 1.0e-10)
    {
    sum11+= pow(t1d11[i], 2);
    }
    }
    avgt1d11 = sum11/((double)nt1-10);

    for (i=0;i<nd;i++){
if(fabs(t[i]-(double)nt) < 1.0e-10)
    {
    sum12+= pow(t1d12[i], 2);
    }
    }
    avgt1d12 = sum12/((double)nt1-11);

    for (i=0;i<nd;i++){
if(fabs(t[i]-(double)nt) < 1.0e-10)
    {
    sum13+= pow(t1d13[i], 2);
    }
    }
    avgt1d13 = sum13/((double)nt1-12);

    for (i=0;i<nd;i++){
    if(fabs(t[i]-(double)nt) < 1.0e-10)
    {
    sum14+= pow(t1d14[i], 2);
    }
    }
    avgt1d14 = sum14/((double)nt1-13);

    for (i=0;i<nd;i++){
    if(fabs(t[i]-(double)nt) < 1.0e-10)
    {
    sum15+= pow(t1d15[i], 2);
    }
    }
    avgt1d15 = sum15/((double)nt1-14);

    for (i=0;i<nd;i++){
    if(fabs(t[i]-(double)nt) < 1.0e-10)
    {
    sum16+= pow(t1d16[i], 2);
    }
    }
    avgt1d16 = sum16/((double)nt1-15);

    for (i=0;i<nd;i++){
    if(fabs(t[i]-(double)nt) < 1.0e-10)
    {
    sum17+= pow(t1d17[i], 2);
    }
    }
    avgt1d17 = sum17/((double)nt1-16);

    for (i=0;i<nd;i++){
if(fabs(t[i]-(double)nt) < 1.0e-10)
```

```
        {
        sum18+= pow(t1d18[i], 2);
        }
        }
        avgt1d18 = sum18/((double)nt1-17);

        for (i=0;i<nd;i++){
        if(fabs(t[i]-(double)nt) < 1.0e-10)
        {
        sum19+= pow(t1d19[i], 2);
        }
        }
        avgt1d19 = sum19/((double)nt1-18);

        for (i=0;i<nd;i++){
    if(fabs(t[i]-(double)nt) < 1.0e-10)
        {
        sum20+= pow(t1d20[i], 2);
        }
        }
        avgt1d20 = sum20/((double)nt1-19);

        for (i=0;i<nd;i++){
    if(fabs(t[i]-(double)nt) < 1.0e-10)
        {
        sum21+= pow(t1d21[i], 2);
        }
        }
        avgt1d21 = sum21/((double)nt1-20);

        for (i=0;i<nd;i++){
    if(fabs(t[i]-(double)nt) < 1.0e-10)
        {
        sum22+= pow(t1d22[i], 2);
        }
        }
        avgt1d22 = sum22/((double)nt1-21);

        for (i=0;i<nd;i++){
    if(fabs(t[i]-(double)nt) < 1.0e-10)
        {
        sum23+= pow(t1d23[i], 2);
        }
        }
        avgt1d23 = sum23/((double)nt1-22);

        for(i=0;i<nd;i++){ /* x */
        if(fabs(t[i]-(double)nt) < 1.0e-10)
        {

        fprintf(fpo," %1.0f %7.2f %7.3f %7.3f %7.3f %7.3f %7.3f %7.3f %7.3f %7.3f %7.3f %7.3f %7.3f
%7.3f %7.3f %7.3f %7.3f %7.3f %7.3f %7.3f %7.3f %7.3f %7.3f %7.3f \n", t[i],y[i],fabs(avgt1d1),
fabs(avgt1d2),fabs(avgt1d3),fabs(avgt1d4),fabs(avgt1d5),fabs(avgt1d6),fabs(avgt1d7),fabs(avgt1d8),
fabs(avgt1d9),fabs(avgt1d10),fabs(avgt1d11),fabs(avgt1d12),fabs(avgt1d13),fabs(avgt1d14),
fabs(avgt1d15),fabs(avgt1d16),fabs(avgt1d17),fabs(avgt1d18),fabs(avgt1d19),fabs(avgt1d20),
fabs(avgt1d21),fabs(avgt1d22),fabs(avgt1d23));
        }
        }
        } while (nt=!0);
        fclose(fpo);
}
```